Stress in the liver: stereotypic genomic responses *in vitro* and *in vivo* involve inflammation and loss of metabolic functions

DISSERTATION

ZUR ERLANGUNG DES AKADEMISCHEN GRADES DES DOKTORS
DER NATURWISSENSCHAFTEN (DR. RER. NAT.)
DER CHEMISCHEN FALKULTÄT
DER TECHNISCHEN UNIVERSITÄT DORTMUND

VORGELEGT VON

AGATA WIDERA, M.Sc.

GEBOREN IN SOSNOWIEC, POLEN

DORTMUND 2014

1. GUTACHTER: PROF. DR. JAN G. HENGSTLER
2. GUTACHTER: PROF. DR. FRANK WEHNER

TAG DER DISPUTATION: 24.04.2014

Ich versichere hiermit, dass ich die vorliegende Dissertation selbstständig und ohne unzulässige fremde Hilfe erbracht habe. Ich habe keine anderen als die angegebenen Quellen und Hilfsmittel benutzt, sowie wörtliche und sinngemäße Zitate kenntlich gemacht.

Dortmund, 05.05.2014

_____	_____
Ort, Datum	Unterschrift

TABLE OF CONTENTS

SUMMARY

Hepatocyte *in vitro* systems represent a well-accepted tool in many fields of research. Despite their widespread use, research with primary hepatocytes remains challenging. Relevant for the field of *in vitro* studies, isolation and cultivation of hepatocytes induces massive transcriptional responses. To date, great efforts have been spent to control or attenuate alteration of hepatocytes *in vitro*. However, expression levels or activities comparable to the liver *in vivo* have rarely been achieved and the precise mechanisms controlling de-differentiation are still poorly understood.

To obtain a comprehensive overview of the expression alterations caused by various culture conditions and after radically different interventions, a time-resolved gene array analysis of mouse hepatocytes in sandwich and monolayer cultures was carried out. The results were compared to livers *in vivo* after treatment with carbon tetrachloride (CCl_4), lipopolysaccharide (LPS) or partial hepatectomy (PHx). Global gene expression profiling exposed profound alterations within the first 24 hours that orchestrate the cellular response of primary mouse hepatocytes *in vitro*. Time-resolved analysis revealed a strong and rapid expressional responses with the lowest total number of differentially expressed genes in sandwich cultures (n = 3296) compared to monolayer confluent and subconfluent cultures (n = 4002 and n = 4287, respectively). All cultivation systems - sandwich, monolayer confluent and subconfluent - expressed similar pattern of up-regulation for lipocalin-2 (Lcn2), metallothionein-2 (Mt2) and serum amyloid A3 (Saa3) and down-regulation of the bile salt export pump (Bsep), multidrug resistance-associated protein 2 (Mrp2) and cholesterol 7 alpha-hydroxylase (Cyp7a1). The sandwich system offers clear advantages over monolayers by maintaining a more stable profile of expressional changes and preserving more of the *in vivo*-like features.

Bio-statistical analysis identified a stereotypic gene expression response, which was similar for all the different types of stress tested: isolation by collagenase perfusion, intoxication with CCl_4 or lipopolysaccharide as well as after partial hepatectomy, namely an upregulation of inflammation and proliferation as well as a downregulation of metabolism-associated genes. Additionally, gene expression profiling showed that comparison of deregulated genes between all three *in vitro* and three *in vivo* models revealed a large overlap in their expression profiles, with lipocalin-2 being among the most up-regulated genes in all systems. The CCl_4 model shares the highest overlap with cultivation systems when comparing the total number of deregulated genes. In addition, genes *in vivo* that responded after one day of exposure to CCl_4, lipopolysaccharide or partial hepatectomy show a relatively large (<60%) overlap with *in vitro* deregulated genes at day one.

Metagene analysis of highly correlated gene clusters between the *in vitro* and *in vivo* models resulted in three biological motifs: proliferation, metabolism and inflammation. The ‘inflammation consensus cluster’ comprises 19 strongly up-regulated genes including the well-

known acute phase response genes Lcn2 and Saa3, which were more than 40-fold up-regulated after all interventions. The 'metabolism-consensus cluster' includes 28 strongly down-regulated genes with Bsep as a well-known lead gene. Transcription Factor Binding Site analysis of the promoter regions of deregulated transcripts identified hepatocyte nuclear factor 4α and -1α among the overrepresented transcription factors for the metabolism-associated genes and Sp1, Elk1, ETF for the inflammation and proliferation gene clusters.

Luminex screening showed rapid and strong activation of stress-associated signaling kinases during isolation of hepatocytes suggesting a new time frame for possible interventions. An inhibitor screening demonstrated a prominent role of c-Jun N-terminal kinases which when inhibited during liver perfusion or subsequent cultivation resulted in a strongly repressed inflammation response. In contrast, none of the tested inhibitors was able to rescue the profound repression of metabolism-associated genes, indicating that yet undiscovered pathways control this response.

Other interventions, such as the further purification of hepatocytes-enriched fraction from non parenchymal cell remnants or co-culture, use of different matrixes or the hepatocyte's own matrix in spheroids, did not ameliorate the overall gene expression response. However, the spheroid culture slightly improved the metabolism gene cluster compared to sandwich cultures, which may represent an advantage of the spheroid system.

A remarkable feature of the described stereotypical expression response is that its basic features were conserved across species including human. My study demonstrates that both human and rodent hepatocytes respond to the isolation procedure with a conserved stress response that includes features of inflammation and a decline in expression of metabolism-associated genes. However, there is a major quantitative difference and some alterations in human hepatocytes are only transient. This illustrates the need of a similarly comprehensive human study comprising isolated hepatocytes and liver tissue, both healthy and inflamed, *ex vivo*.

Elucidation of the molecular anatomy of gene expression patterns in stressed hepatocytes presented in my thesis suggests that the broadly applied hepatocyte *in vitro* systems do not represent a model system of the healthy liver but rather a critically inflamed state. In line with this knowledge, unveiling the molecular anatomy of gene expression also demonstrates that cultivated hepatocytes may be used to study pathological situations. For example, the gene expression changes observed in sandwich culture resemble those observed in inflamed liver tissue, such as after hepatectomy or in response to CCl_4 or lipopolysaccharide. In conclusion, my work identifies remarkable similarities between inflamed livers *in vivo* and cultivated hepatocytes, which opens new paths for mechanistic studies on liver inflammation and a more accurate use of hepatocyte *in vitro* systems.

ZUSAMMENFASSUNG

Obgleich kultivierte Hepatozyten bereits in vielen Forschungsgebieten Einsatz finden, stellt die Forschung über primäre humane Hepatozyten nach wie vor eine große Herausforderung dar. Bei *in vitro* Studien gilt zu berücksichtigen, dass sowohl die Isolierung als auch die Kultivierung von Hepatozyten bereits massive Veränderungen auf Transkriptionsebene induzieren. Bis heute ist unmöglich Veränderungen von Hepatozyten *in vitro* zu kontrollieren bzw. möglichst gering zu halten. Dabei sind Proteinexpression oder Enzymaktivitäten mit der *in vivo* Situation in der Leber selten vergleichbar und präzise Mechanismen, welche die Dedifferenzierung kontrollieren, nur wenig verstanden.

Um einen umfassenden Überblick über Expressionsveränderungen zu erhalten, welche durch diverse Kultivierungsbedingungen und durch grundlegende Eingriffe entstehen, wurden zeitaufgelöste Gene Array Analysen von primären Maus-Hepatozyten in Collagen Sandwich bzw. Collagen Monolayer Kultur durchgeführt. Diese Ergebnisse wurden verglichen mit *in vivo* Daten nach Tetrachlorkohlenstoff (CCl_4) bzw. Lipopolysaccharid (LPS) Behandlung beziehungsweise nach partieller Hepatektomie (PHx). Vollständige Genexpressionsprofile in primären Maus-Hepatozyten zeigten, dass innerhalb der ersten 24 Stunden umfangreiche Veränderungen auf zellulärer Ebene in Hepatozyten induziert werden. Zeitreihen von Hepatozyten *in vitro* zeigten eine starke und schnelle Expressionsantwort nach dem Ausplatieren. Dabei wurden in der Collagen Sandwich Kultur eine kleinere Zahl an exprimierten Genen beobachtet (3296 Gene) im Vergleich zu Collagen Monolayer konfluent (4002 Gene) bzw. Subkonfluent (4287 Gene). Alle Kultivierungssysteme – Collagen Sandwich, Monolayer konfluent und subkonfluent – zeigten ähnliche Expressionsmuster bezüglich der Induktion von Lipocalin-2 (Lcn2), Metallothionin-2 (Mt2) und Serum Amyloid A3 (SAA3), sowie die Herabregulation von Bsep (Bile salt export pump), Mrp2 (Multidrug resistance-associated protein 2) und der Cholesterol 7 alpha-Hydroxylase (Cyp7a1). Die Sandwich-Kultur bietet gegenüber der Kultivierung im Monolayer klare Vorteile. Sie ist deutlich stabiler gegenüber expressionellen Veränderungen und bewahrt zudem mehr *in vivo*-ähnliche Eigenschaften.

Biostatistischer Analysen zeigten eine stereotypische Genexpressionsantwort, welche für alle getesteten Arten von Zellstress ähnlich war: Isolatierung durch Perfusion mit Kollagenase, Vergiftung mit CCl_4 und LPS als auch partieller Hepatektomie. Besonders auffällig waren die Induktion von Entzündungsmarkern und Proliferation, als auch die Herabregulierung von metabolismusassoziierten Genen. Weiterhin zeigte ein Vergleich über alle herunterregulierten Gene der drei *in vitro* und drei *in vivo* Modelle eine große Überlappung der Genexpressionsprofile, wobei Lipocalin-2 das am stärksten induzierte Gen in allen Systemen war. Im Vergleich der Gesamtzahl der differenziert exprimierten Gene zeigte das CCl_4 Modell die größten Gemeinsamkeiten mit den Kultivierungssystemen. Weiterhin wiesen Gene *in vivo*, welche nach einem Tag CCl_4 oder LPS Exposition bzw. partieller Hepatektomie detektiert

wurden, eine recht große (>60%) Überlappung mit den *in vitro* deregulierten Genen nach einem Tag in Kultur auf.

Metagenanalysen von stark korrelierenden Gengruppierungen zwischen den *in vitro* und *in vivo* Modellen ergaben drei biologische Motive: Proliferation, Metabolismus und Entzündung. Die Gengruppierung „Entzündung" umfasst 19 stark heraufregulierte Gene, darunter bekannte Entzündungsmarker wie Lcn2 und SAA3, welche nach allen Interventionen mehr als 40-fach induziert waren. Der „Metabolismus" Konsensus Cluster beinhaltet 28 stark herunterregulierte Gene wie z.B. Bsep. Eine Analyse der Transkriptionsfaktorbindestellen innerhalb der Promotorregionen herunterregulierter Transkripte, identifizierte *hepatocyte nuclear factor 4*α und -1α (HNF4α bzw. HNF1α) als überrepräsentierte Transkriptionsfaktoren für die metabolismusassoziierten Gene und Sp1, Elk1 und ETF für die Gene des Entzündungs- und Proliferationsclusters.

Mittels Luminex Screening wurde eine starke und rasche Aktivierung von stressassoziierten Signalkaskaden während der Isolierung der Hepatozyten beobachtet, wodurch nur ein kurzes Zeitfenster für mögliche Interventionen optimal erscheint. Ein Inhibitorscreening hat ergeben, dass in diesem Zusammenhang c-Jun N-terminale Kinasen eine prominente Rolle spielen. Die Inhibierung von c-Jun Kinasen während der Leberperfusion bzw. während der anschließenden Kultivierung ergab eine stark unterdrückte Antwort der Entzündungsmarker. Dennoch konnte kein getesteter Inhibitor die massive Herabregulierung von metabolismusassoziierten Genen abschwächen, was darauf hindeutet, dass diese Antwort von bisher nicht bekannten Signalwegen kontrolliert wird.

Weitere Eingriffe, wie z.B. die weitere Aufreinigung von hepatozytenreichen Fraktionen von den restlichen nicht-parenchymalen Zellen oder Co-Kulturen, die Verwendung unterschiedlicher Matrizes oder auch die Kultivierung von Hepatozyten in Sphäroid konnten die allgemeine Genexpressionsantwort nicht verbessern. Dennoch konnte in Sphäroiden im Vergleich zur Collagen Sandwich Kultur eine leichte Optimierung innerhalb des „Metabolismus" Clusters beobachtet werden, was einen Vorteil des Sphäroid-Systems repräsentiert.

Eine bemerkenswerte Eigenschaft der beschriebenen stereotypischen Expressionsantwort ist, dass grundlegende Eigenschaften zwischen den einzelnen Spezies, inklusive Mensch, konserviert sind. Diese Studie zeigte, dass Hepatozyten vom Menschen als auch von Nagetieren auf den Isolierungsprozess mit einer konservierten Stressantwort reagieren, welche Eigenschaften von Entzündungsprozessen wiederspiegelt und zudem ein Absinken der Expression metabolismusassoziierter Gene mit sich bringt. Dennoch bestehen quantitativ enorme Unterschiede und manche Veränderungen in den menschlichen Expressionsprofilen sind nur vorrübergehend. Das veranschaulicht den Bedarf für gleichermaßen umfassende Studien für den Menschen, in welche sowohl isolierte Hepatozyten als auch Lebermaterial aus gesundem als auch entzündetem Gewebe *ex vivo* mit einbezogen werden sollten.

Die Darlegung der molekularen Anatomie von Genexpressionsmustern in gestressten Hepatozyten, welche in dieser Arbeit hier erläutert wird, zeigt deutlich, dass die gängig angewandten Hepatozyten *in vitro* Systeme keine Modellsysteme einer gesunden Leber repräsentieren, sondern vielmehr eines kritisch entzündeten Zustands. Unter Berücksichtigung dieses Wissens über die Details der Genexpression könnten die kultivierten Hepatozyten des weiteren auch zur Untersuchung von pathologischen Situationen herangezogen werden. Zum Beispiel ähneln die Genexpressionsveränderungen, welche im Sandwich System beobachtet werden, denen, die in entzündetem Gewebe auftreten, wie es z.B. nach partieller Hepatektomie oder ausgelöst durch CCl_4 und LPS der Fall ist. Zusammengefasst identifiziert diese Arbeit bemerkenswerte Ähnlichkeiten zwischen entzündeten Lebern *in vivo* und kultivierten Hepatozyten, was zum einen neue Wege für mechanistische Studien in entzündeter Leber, zum anderen aber auch eine präzisiere Verwendung von Hepatozyten *in vitro* Systemen eröffnet.

ACKNOWLEDGMENTS

The completion of my PhD degree was challenging and would not have been possible without the guidance, support, and wisdom from numerous people, only some of whom it is possible to give particular mention here.

First, I would like to express my sincere gratitude to **Prof. Dr. med. Jan G. Hengstler** for giving me the chance to work in his laboratory at the Leibniz Research Center for Working Environment and Human Factors (IfADo) in Dortmund, Germany. His guidance and gentle encouragment have tremendously contributed to my growth and development as a scientist.

I am deeply grateful to my PhD advisor and mentor **Prof. Dr. Patricio Godoy** for supporting me during these past three and a half years. He has been a visionary adviser who will always serve as my role model. Without his supervision and constant help, this dissertation would not have been possible.

In addition, I have been very privileged to get to know and collaborate with many other great people who directly contributed to my work, especially: **Dr. Gisela Campos Melo, Katharina Rochlitz, Regina Stöber** and **Larissa Puetter.** The tremendous kindness and understanding of **Dr. Gisela Campos Melo** had a great impact on me and will always be remembered and greatly appreciated. The energetic **Katharina Rochlitz** has been a pleasure to work with while supporting me with her technical excellence. Both, **Regina Stöber** and **Larissa Pütter**, were of fantastic help no matter the task or circumstance. For all these reasons and many, many more, I am eternally grateful.

My work has greatly benefited from all the successful collaborations. I take this opportunity to acknowledge **Wolfgang Schmidt-Heck** from the Hans-Knöll-Institute (HKI) in Jena for performing all the biostatistical analyses and for many of insightful discussions and suggestions.

I was also greatly influenced by scientific advice, helpful suggestions and kind encouragement from **Dr. Raymond "Uncle Ray" Reif**.

My sincere thanks go to **Dr. Rosemarie Marchan** for helping me with the English corrections, and most importantly for her lovely smile and kind encouragement.

I have greatly enjoyed the opportunity to work with or alongside my colleagues at IfADo:

Dr. Ahmed Ghallab	**Esmina Mjumjunov-Crncecic**	**Michaela Lesjak**
Alshimaa Adawy	**Georgia Günther**	**Dr. Seddik El Kariem Hammad**
Amnah Hofney Othman	**Dr. Iris von Recklinghausen**	**Dr. Joanna Stewart**
Bettina Büttner	**Dr. Jakia Amin**	**Sonia Vossbeck**
Brigitte Begher-Tibbe	**Kathrin Gianmoena**	**Amruta Vartak**
Dr. Cristina Cadenas	**Julius Göbel**	**Reham Hassan Reyad Khalil Alkashef**
Dennis Franckenstein	**Dr. Karolina Edlund**	**Doreen Werchau**

My time at IfADo was stongly enriched by the invaluable support you provided me during all these years. Thank you all!

My gratitude is also extended to **Mrs. Silke Hankinson** for her professionalism and irreplaceable help especially during my first weeks at IfADo.

My friends both near and far, deserve my most sincere appreciation for their continuing encouragement. I would like to express a heartfelt thanks to my best friends and former flatmates in Krakow: **Aleksandra Czechowska, Magdalena Kozioł, Anna Rutkowska, Katarzyna Piszczek, and Karolina Stefanowicz ("KROMA")** for their great support throughtout our Master's studies in Kraków, Poland. Special thanks go to **Naima Rüther, Petra Netter and Robert Witter ("Duden Girls" & "Dirty Talk")** for believing in me, most of all for your humor, and for the many precious memories along the way. Thank you.

Most importantly, I would like to thank my parents, **Krystyna and Jacek**, and my sister **Aleksandra** together with the rest of my **family** for their infinite love. Thank you for giving me the freedom to go my own way and supporting me in all my pursuits. I hope that this work makes you proud.

Przede wszystkim pragnę podziękować moim rodzicom, **Krystynie i Jackowi**, mojej siostrze **Aleksandrze** oraz **całej rodzinie** za ich bezgraniczną miłość i nieocenioną pomoc. Dziękuję, że daliście mi wybór, by iść własną drogą oraz za nieustannie okazywane mi wsparcie. Mam nadzieję, że moja praca jest dla Was powodem do dumy.

Thank you all - Vielen Dank an alle - Dziękuję Wam wszystkim!

ABBREVIATIONS

%	Percent
°C	Celsius degree
3 ”Rs”	Replacement, Reduction, Refinement
3D	Three-dimentional
ABC	ATP-binding cassette
ABCB4	Multidrug resistance protein 3
ABCG2	ATP-binding cassette sub-family G member 2
Akt	Protein Kinase B
AP1	Activator protein-1
APR	Acute phase response
APS	Ammonium persulphate
ATF	Activating transcription factor
BC	Bile canaliculi
BCA	Bicinchonic acid assay
bp	Base pairs
BSA	Bovine Albumin Fraction V
Bsep	Bile Salt Export Pump
C/EBP	Ccaat-enhancer-binding proteins
ca.	circa
Ca^{2+}	Calcium ion
CAR	Constitutive androstane receptor
CCl3*	Trichloromethyl free radical
CCl3OO*	Trichloromethylperoxy radical
CCl_4	Carbon tetrachloride
CD26	Cluster of differentiation
CMC	Collagen monolayer confluent
CMS	Collagen monolayer subconfluent
CO2	Carbon dioxide
CRP	C-reactive protein
CS	Collagen Sandwich culture
Ct	Ct value
CYP2e1	Cytochrome P450 enzyme 2e1
Cyp7a1	Cytochrome P450 enzyme 7a1
CYPs	Cytochrome P450 superfamily
d	Day(s)
DAG	Diacylglycerol
DAPI	4‘,6-Diamidin-2-phenylindol
DBP	D-binding protein
DEG(s)	Differentially expressed gene(s)
DEPC	Diethylpyrocarbonate
Dest.	Distilled
DILI	Drug-induced liver injury
DMEM	Dulbecco’s Modified Eagle’s Medium
DMSO	Dimethyl Sulfoxide
DNA	Deoxyribonucleic acid
DPPIV	Dipeptidyl peptidase-4
DTT	DL-Dithiothreitol
e.g.	For example
ECL	Enhanced Chemiluminescence
ECM	Extracellular matrix
EDTA	Ethylenediaminetetraacetic acid
EGF	Epidermal growth factor
EGTA	Ethylene glycol tetraacetic acid

EMT	Epithelial to mesenchymal transition
ERK	Extracellular Signal-Regulated Kinase
EtOH	Ethanol
FBS	Fetal bovine serum
FCS	Fetal calf serum
FDR	False discovery rate
FH	Fresh hepatocytes
FXR	Farnesoid X receptor
g	Standard gravity
g	Gram
GAPDH	Glyceraldehyde 3-phosphate dehydrogenase
Gly	Glycine
GO	Gene Ontology
GOI	Gene of interest
GSK3a/b	Glycogen synthase kinase 3
GTP	Guanosine triphosphate
h	Hour(s)
H_2O	Water
HGF	Hepatocyte growth factor
HKG	Housekeeping Gene
HNF	Hepatocyte nuclear factor
HoAc	Acetic acid
HPC	Hepatic progenitor cell
HRP	Horseradish peroxidase
HSC	Hepatic stellate cell
Hsp27	Heat shock protein 27
i.e.	id est (that is)
ICAM	Intercellular Adhesion Molecule
IF	Immunofluorescence
IHC	Immunohistochemistry
IkBα	Nuclear factor of kappa light polypeptide gene enhancer in B-cells inhibitor alpha
IKK	Kinase phosphorylating IkB
IL	Interleukin
IP3	Inositol trisphosphate
ITS	Insulin-Transferrin-Selenium media supplement
JAK	Janus Kinase
JNK	c-Jun N-terminal Kinase
K+	Potassium cation
KC	Kupffer cell
KCl	Potassium Chloride
KEGG	Kyoto Encyclopedia of Genes and Genomes
kg	Kilogram
KH2PO4	Potassium dihydrogen phosphate
L	Liter
Lcn2	Lipocalin-2
LETF	Liver-enriched transcription factors
LLL	Left lateral lobe
LML	Left median lobe
LPS	Lipopolysaccharide
LSEC	Liver sinusoidal endothelial cell
LSM	Laser Scanning Microscope
LXR	Liver X receptor
mA	Milli ampere
mAB	Monoclonal antibody
MAP2K, MEK, or MKK	MAPK kinase
MAP3K or MAPKKK	MAPK kinase kinase
MAPK	Mitogen-activated protein kinases

MAPK	Mitogen-activated protein kinases
MAPKKK	MAPK kinase kinase kinase
Mc	Monolayer confluent
Mdr	Multidrug-resistance protein
mg	Miligram
min	Minute(s)
ML	Median lobe
mL	Mililiter
mm	Milli meter
mRNA	messenger RNA
Mrp	Multidrug-resistance-associated protein
Ms	Monolayer subconfluent
Mt	Metallothionein
n	Number
N	Nucleus
Na+	Sodium cation
NaOH	Sodium hydroxide
NEMO	NF-kB essential modulator
NF-kB	Nuclear Factor-Kappa B
ng	Nano gram
NGAL	Neutrophil gelatinase-associated lipocalin
NGF	nerve growth factor
NO	nitric oxide
NPC	Non parenchymal cell
NR	Nuclear receptor
NTCP	Na+ /taurocholate co-transporting polypeptide
ø	Diameter
OATPs	organic anion-transporting polypeptide proteins
OATs	organic anion transporters
OCTs	organic cation transporters
p-	Phosphorylated/phospho-
p38	p38 mitogen-activated protein kinase
p44/42	see ERK
p70S6K	p70S6 kinase
pAB	Polyclonal antibody
PAGE	Polyacrylamide gel electrophoresis
PAMPs	Pathogen-associated molecular patterns
PBS	Phosphate buffered saline solution
PCNA	Proliferating cell nuclear antigen
PCR	Polymerase chain reaction
PFA	Paraformaldehyde
PHx	Partial hepatectomy
PI-3K	Phosphatidylinositol 3-kinase
PIP2	Phosphatidylinositol 4,5-bisphosphate
PIP-3	Phosphatidylinositol-3,4,5-trisphosphate
PKC	Protein kinase C
PLC	Phospholipase C
PMSF	Phenylmethylsulfonyl fluoride
PPARα	Peroxisome proliferator-activated receptor alpha
Pro	Proline
PRRs	Pattern-recognition receptors
PVDF	Polyvinylidene fluoride
PXR	Pregnane X receptor
qRT-PCR	Quantitative real time PCR
r	Correlation
RIPA	Radioimmunoprecipitation assay buffer
RML	Right median lobe

RNA	Ribonucleic acid
ROS	Reactive oxygen species
rpm	Revolutions per minute
RSK	Ribosomal S6 kinase
RT	Room temperature
RT-PCR	Reverse transcriptase PCR
RXR	Retinoid X receptor
s	Second
S	Collagen Sandwich culture
SAA	Serum amyloid A
SAP	Serum amyloid P
SAPK	Stress-activated protein kinases
SAPK	Stress-Activated Protein Kinase
SDS	Sodium dodecyl sulfate
Ser	Serine
SHP	Short heterodimeric partner
SP600125	JNK inhibitor
Sph	Spheroid
STAT	Signal Transducers and Activators of Transcription
t	Time
TBS-T	Tris Buffered Saline with Tween 20
TEMED	Tetramethylethylenediamine
TEY	Thr-Glu-Tyr
TF(s)	Transcription factor(s)
TGF-β	Transforming growth factor-β
TGY	Thr-Gly-Tyr
Thr	Threonine
Thy	Tyrosine
TLR	Toll-like receptor
TNF	Tumor necrosis factor
TPY	Thr-Pro-Tyr
Tris	Tris(hydroxymethyl)aminomethane
V	Volt
v/v	Volume per volume
WB	Western blotting
Wnts	Wnt pathway ligands
x	Fold
µg	Micro gram
µl	Micro liter
µm	Micro meter

1. INTRODUCTION

1.1 LIVER

The liver is the largest visceral organ of the body and plays a central role in metabolism. Over 500 metabolic functions have been described, including the uptake of nutrients absorbed from the digestive tract, and the metabolism of lipids, carbohydrates and proteins. A critical role of the liver is the production of bile, which is needed to support digestion. In addition, the liver synthetizes a large number of plasma proteins, including albumin and immune factors, such as acute-phase proteins. As the main detoxifying organ of the body, the liver inactivates toxins and xenobiotics by converting them from hydrophobic compounds into water-soluble products that can be more readily eliminated [2-5].

With two major sources of the blood, the liver has a blood supply network that is unique among other organs.Approximately 75% of the liver's blood supply comes from the portal vein that provides venous blood rich in nutrients from the digestive system. The hepatic artery provides the liver with oxygenated blood from the heart. In most mammalian species, the liver is multi-lobed, with each lobe composed of architectural, microcirculatory and functional units that are hexagonally–shaped, the so–called hepatic lobule (Figure 1). Portal triads consisting of a bile duct, a hepatic artery and a portal vein are located at the periphery of a lobule. Lobules consist of plates of liver cells – hepatocytes - radiating outward from the portal triads to meet the central vein. Hepatocytes, the parenchymal cell component of the liver, form tubular, apical spaces called bile canaliculi between adjacent cells along the hepatic plate. Hepatocytes secrete the bile into the bile canaliculi that run parallel to the sinusoids, but opposite in direction to the blood flow. The bile from the bile canaliculus drains into the bile ducts of the liver. The portal vein and hepatic artery empty together, thus mixing venous and oxygen-rich blood as it enters specialized capillaries, called the liver sinusoids. The sinusoids are porous vascular channels lined with fenestrated endothelial cells. As blood flows through the sinusoids, a rapid exchange of oxygen and nutrients occurs between the sinusiods and the adjacent liver cells. The sinusoids converge into the central vein, which then drains in the hepatic vein [1, 6, 7].

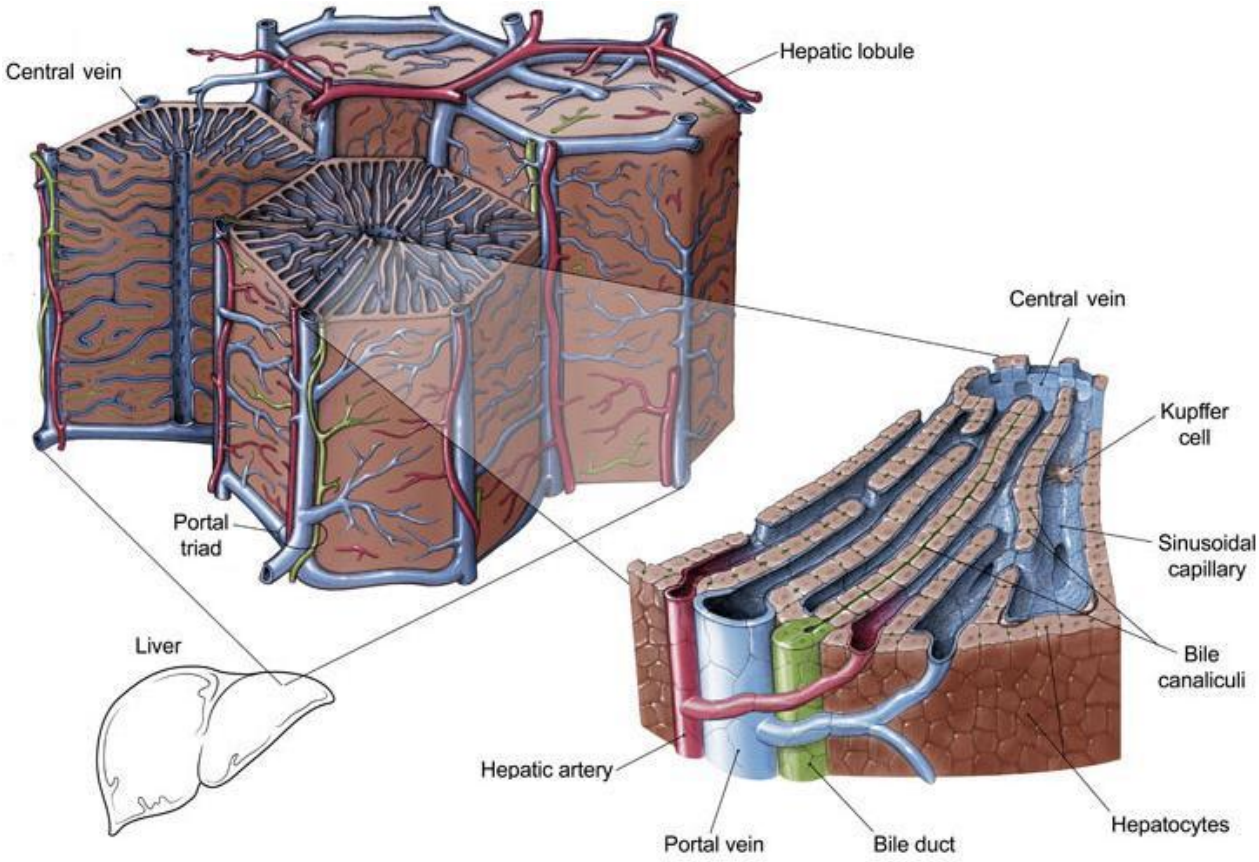

FIGURE 1: BASIC STRUCTURE OF A HEPATIC LOBULE
Three-dimensional architecture of the liver between a portal triad and the central vein. Figure adapted and modified from: http://illuminationstudios.com/archives/150/structure-of-a-hepatic-lobule

The directionality of the blood flow through the lobular units from the portal triad to the central vein creates various chemical gradients (oxygen and nutrients) and microenvironments [8]. In order to perform several metabolic functions simultaneously, the liver tissue exhibits a noticeable heterogeneity and functional plasticity, known as ‘‘metabolic zonation’’ [9]. The regional compartmentalization of metabolic capacities is characterized by the microcirculatory functional unit called the hepatic acinus and can be divided into three zones: a periportal zone 1; a transitional zone 2 and a pericentral zone 3 (Figure 2) [6, 10]. Such characteristic cyto-architecture of the liver supports diverse metabolic pathways within the different zones. The hepatocellular zonation is regulated by chemical gradients of oxygen, hormones, growth factors and metabolites, which are generated and maintained as a result of the specific characteristics of the extracellular matrix (ECM) and of the distribution of liver cells [8, 11]. Additionally, a biochemical gradient present in all three zones influences not only the metabolism but also the gene expression patterns of the liver tissue [12-14].

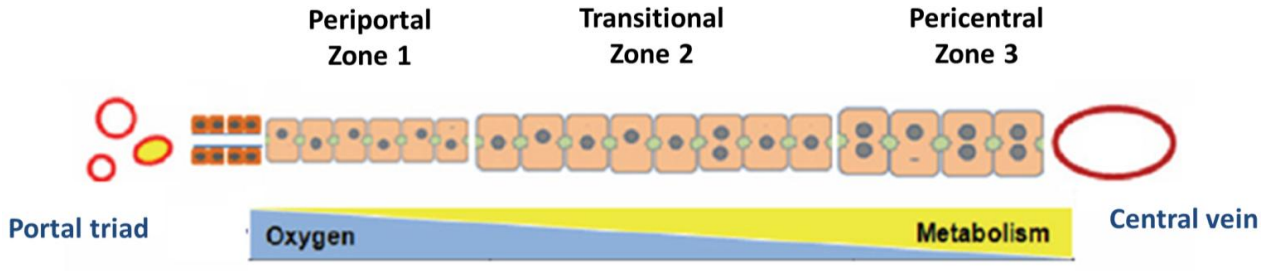

FIGURE 2: STRUCTURAL AND FUNCTIONAL ZONATION OF THE LIVER
Discrete zones of the liver between the portal vein and central vein illustrating the differences in cell size, phenotype and gradients in oxygen tension and metabolism. Figure adapted and modified from [15].

1.2 LIVER CELLS TYPES

The liver is comprised of several diverse cell types (Figure 3 and Figure 4). **Hepatocytes**, the liver parenchymal cells, account for 80% of liver mass. The other 20% comprises the non-parenchymal cells, including the **liver sinusoidal endothelial cells**, **Kupffer cells, hepatic stellate cells** (called also Ito or fat-storing cells), **cholangiocytes** (biliary epithelial cells), **hepatic progenitor cells** (bi-potential stem cells also known as oval cells), **lymphocytes** of various phenotypes (e.g. natural killer lymphocytes also called Pit cells), and **neutrophils.** All of the NPC are arranged in a matrix that facilitates their cooperative interaction [4, 16, 17].

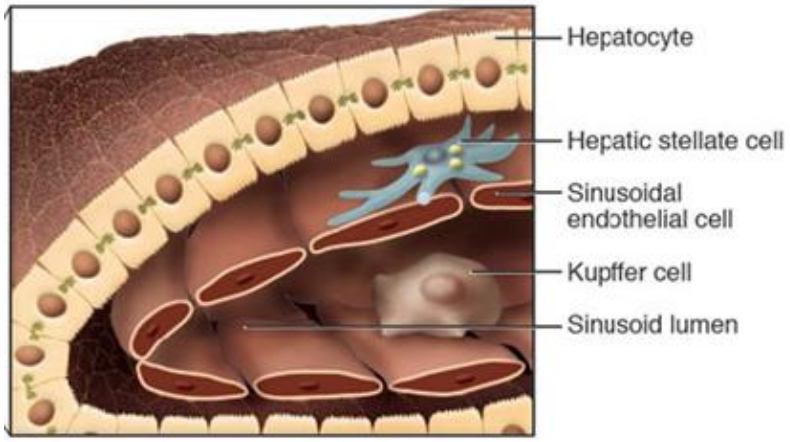

FIGURE 3: MAJOR CELL TYPES OF THE LIVER
The liver is comprised of several diverse cell types: hepatocytes, liver sinusoidal endothelial cells, Kupffer cells, hepatic stellate cells, cholangiocytes, hepatic progenitor cells, lymphocytes and neutrophils. Figure adapted and modified from [18].

The space of Disse is located between the hepatocytes and the sinusoids. It separates the hepatic epithelium from the sinusoidal endothelium. It is a thin reticular basement membrane, composed of a variety of extracellular matrix proteins such as fibronectin, laminin, proteoglycan, collagen IV, and collagen I. Hepatic architecture and sinusoidal organization are essential for proper and differentiated function of all resident liver cells [19-21].

The parenchymal cells or **hepatocytes** are highly specialized epithelial cells that line the sinusoids in the liver. They are cuboidal in shape (20–25 µm in diameter) with two distinct surfaces and possess one or more nuclei [1]. Hepatocytes perform most of the synthetic and metabolic functions of the liver. They are rich in various organelles: mitochondria (~1700 per cell on average), peroxisomes (~370 per cell), lysosomes (~250 per cell), Golgi complexes (~50 per cell), and aggregates of rough and smooth endoplasmic reticulum (~15% of cell volume) [22].

The **liver sinusoidal endothelial cells** (LSEC) line the walls of the hepatic sinusoids of the liver and contain numerous open pores in their membrane, called fenestra, which provide a large surface area for nutrient absorption of large macromolecules [1]. The **Kupffer cells** (KC) are the liver's specialized macrophages residing in the sinusoids and are essential for the effective phagocytosis of old erythrocytes, foreign particles and infecting organisms from the circulation. The Kupffer cells produce cytokines upon stimulation e.g. during tissue injury, stimulate the activation of the liver's acute phase reaction, and coordinate the responses of other liver cell types [1]. The **hepatic stellate cells** (HSC) are vitamin A-storing perivascular mesenchymal cells of the liver (previously called Ito cells, or fat-storing cells). Hepatic stellate cells synthesize, secrete, and degrade components of the peri-sinusoidal extracellular matrix. Through inflammatory processes during tissue injury, stellate cells become activated acquiring a myofibroblast-like phenotype, which allows them to become capable of both increasing collagen and DNA synthesis [5, 19, 23, 24]. **Lymphocytes** of various phenotypes are the liver-centered innate immune system to help resist infections. The **cholangiocytes** are epithelial cells that line the bile duct [1, 2, 7, 25]. **Hepatic progenitor cells** (short HPC also known as liver stem cells or oval cells) are bi-potential stem cells capable of differentiation towards both hepatocytes and cholangiocytes. The HPC reside within the most peripheral branches of the biliary tree, the so-called canals of Hering [26, 27].

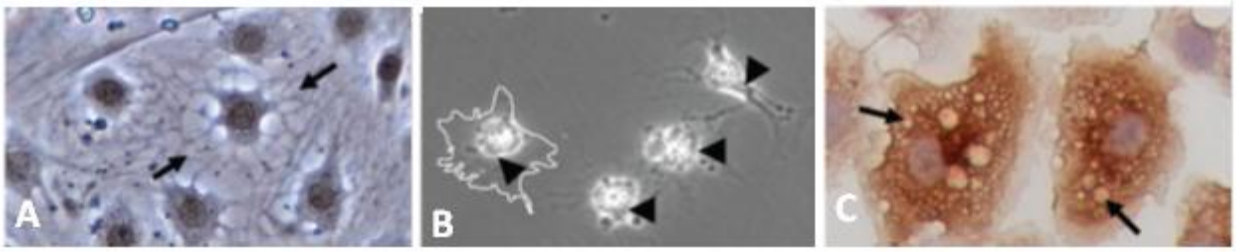

FIGURE 4: MORPHOLOGY OF NON-PARENCHYMAL CELL TYPES OF THE LIVER *IN VITRO*
(A) Liver Sinusoidal Epithelial Cells (LSEC) showing typical morphology *in vitro*. (B) Isolated quiescent HSC showing storage of vitamin A as bright "floating" vesicles within the cell body. Upon activation or injury the HSC undergo extensive morphological and biochemical changes, which include the synthesis, secretion and restructuring of ECM molecules. (C) Kupffer cells showing their dynamic morphology. Cells are loaded with vesicles containing cytokines and other secretory factors. Figure adapted and modified from [15].

1.3 LIVER EXTRACELLULAR MATRIX

The peculiar composition of the extracellular matrix (ECM) directs and maintains the architecture and differentiated phenotype of liver cells [20, 28]. The ECM is distributed in the Space of Disse and consists of collagen (types I–IV), laminins, fibronectin, glycosaminoglycans and proteoglycans, among many others [20, 28, 29] (Figure 5). Hepatocytes are in close contact with several extracellular matrix proteins. The ECM composition typically follows a pattern of gradients from the periportal zone 1 to pericentral zone 3 (Figure 2). The zonal composition of the ECM between the portal triad and the central vein is determined by multiple factors, e.g. the influence of other cell types, the gradient of oxygen and nutrients [27, 30].

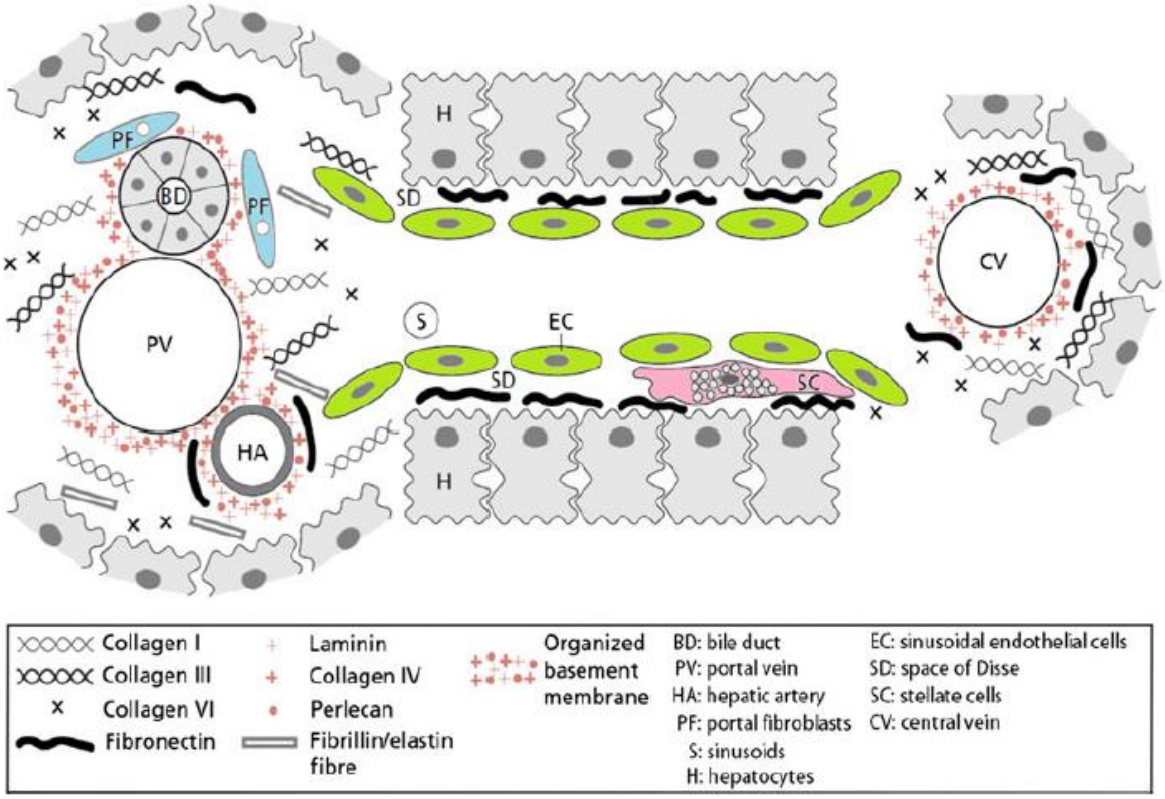

FIGURE 5: DISTRIBUTION OF THE EXTRACELLULAR MATRIX (ECM) IN THE LIVER
The composition of the different ECM zones between the portal triad and central vein is partially determined by factors in the microenvironment, such as other cell types, oxygen, nutrients, and endogenous/endogenous substrates. Figure adapted and modified from [10].

1.4 HEPATOCYTES AND THEIR METABOLIC FUNCTION

The unique vascular organization of the liver exposes hepatocytes to a lobular gradient of oxygen, nutrients, toxins and other biologically active molecules. To ensure the liver's exocrine, endocrine and blood filtering functions, the hepatocytes as highly specialized epithelial cells are characterized by a distinct polarity [1].

The hepatocytes' polarity represents a unique and complex cyto-architecture compared with the polarity of most epithelial cells [31] (Figure 6). Typically, an epithelial cell exhibits one apical and one basolateral side on opposing surfaces of an epithelial sheet. In contrast, hepatocytes possess two basolateral (sinusoidal) domains that interface with the space of Disse on opposite sides of the cell plates, and an apical (canalicular) domain between adjacent hepatocytes [10]. The basolateral sides of hepatocytes are in contact with the blood, where the uptake of recycled bile salts and secretion of various components into the circulation occur. The neighboring hepatocytes secrete the bile into a belt-like structure formed at the apical side, called bile canaliculi (BC). These tubular compartments of ~0.5–1.0 µm in diameter constitute a continuous network throughout the cell plates of the liver lobule. Both the apical and the basolateral sides are separated by tight junctions and desmosomes that seal off the border of bile canaliculi at apical sides. The networks of BC from a liver lobule terminate at the portal triad and merge via the canals of Hering with the bile ducts, finally leading into the common bile duct and the gall bladder [10, 15, 32].

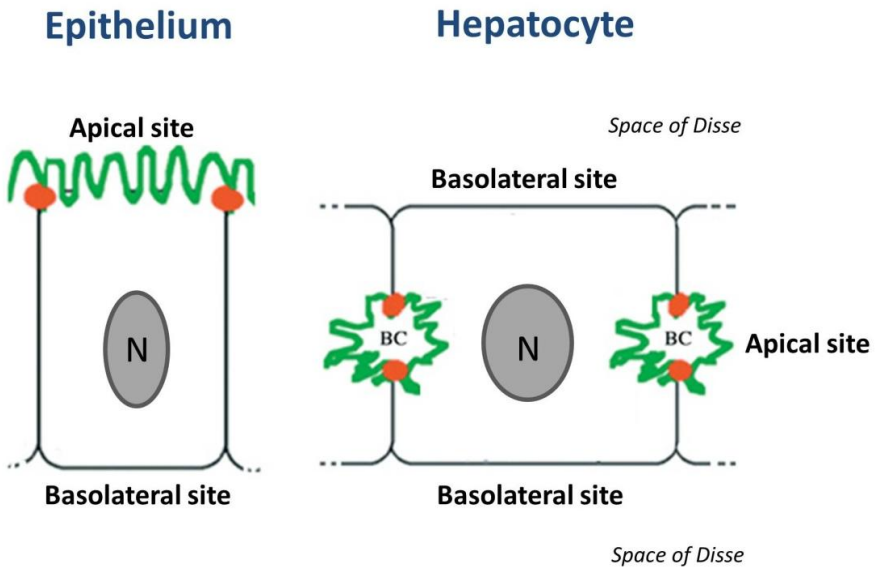

FIGURE 6: THE STRUCTURE OF EPITHELIAL AND HEPATOCYTE CELL POLARITY
Epithelial cells exhibit one apical and one basolateral side on opposing surfaces of an epithelial sheet. In contrast, hepatocytes possess two basolateral domains that interface with the space of Disse on opposite sides of cell plates. The apical side (surface marked in green) in hepatocytes is separated from the basolateral pole by tight junctions (orange marks). BC (bile canaliculi), N (nucleus). Figure adapted and modified from [32].

The apical and basolateral surface membranes of hepatocytes are polarized by special membrane protein distribution, including receptors, pumps, transport channels, and carrier proteins [33] (Figure 7). The directional transport of the bile acids from the blood through hepatocytes into the bile canaliculi is a multistep process [1]. Mainly, NTCP (Na+ /taurocholate co-transporting polypeptide) and the family of organic anion-transporting polypeptide proteins (OATPs) together with the organic anion transporter (OATs) and the organic cation transporter (OCTs) families mediate the uptake of the bile acids from the portal circulation. The uptake is driven as a result of electrical and ionic gradients generated by the Na+/K+ ATPase and diffusion of K+ ions through potassium channels [34]. The bile, which plays an essential role in the digestion of lipids from the diet, is a complex aqueous secretion composed of bile salts, organic anions, phospholipids, cholesterol and bilirubin [35]. In the classic pathway, the bile acids can be synthesized *de novo* from cholesterol that is converted to 7α-hydroxycholesterol via the microsomal cytochrome P450 enzyme, cholesterol 7α-hydroxylase (CYP7A1), belonging to the P450 superfamily of mono-oxidases metabolizing organic compounds of endo- and exogenous origin [36]. The secretion of *de novo* synthetized bile acids into bile canaliculi is mediated by several apical ATP-binding cassette (ABC) transport proteins, primarily via Bsep (bile-salt-export pump), but also by Mrp2 (multidrug-resistance-associated protein 2), Mdr1 and -3 (multidrug-resistance protein 1 and 2). Bsep is the main transporter ensuring bile secretion [37, 38]. Cholestatic conditions activate compensatory mechanism of basolateral efflux of bile salts and organic anions from hepatocytes into blood by Mrp3 and Mrp4 [39, 40].

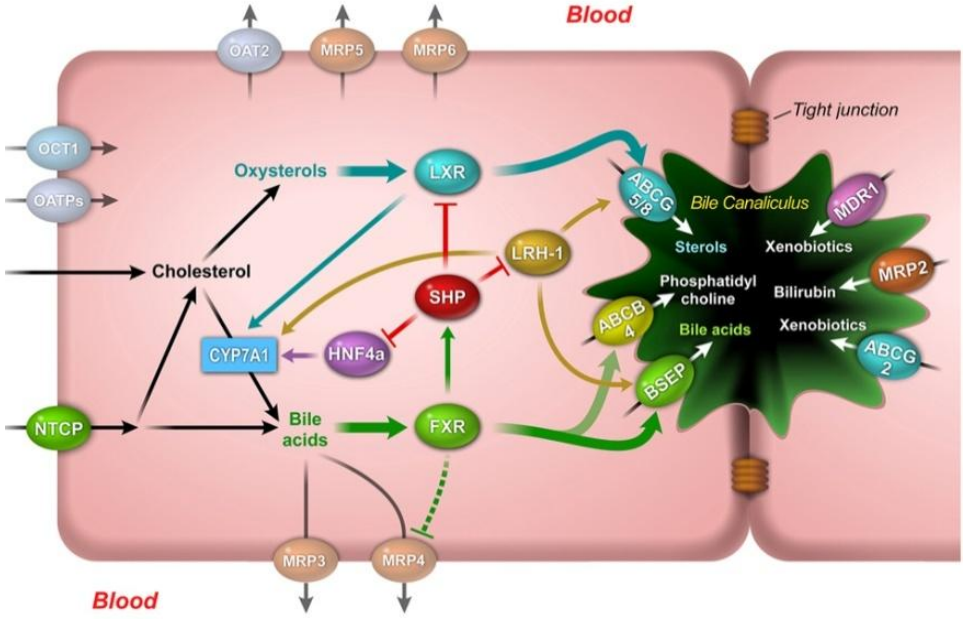

FIGURE 7: SCHEMATIC BILE ACID METABOLISM AND ELIMINATION IN THE HEPATOCYTE

Uptake of bile acids from the portal circulation is mediated mainly by NTCP and OATP family. Additionally, cholesterol is converted into bile acids by CYP7A1 and eliminated into the bile canaliculi by Bsep and other canalicular transporters, such as Mrp2 which mediates excretion of bilirubin, ABCB4, which exports phosphatidyl-choline, and the multidrug transporters Mdr1 together with ABCG2 which mediate excretion of a wide variety of xenobiotics. During cholestasis bile acids can also be excreted back into the circulation via Mrp3 and 4. Figure adapted from [41].

The liver metabolizes various endogenous and exogenous substances by a series of complex, chemical reactions called biotransformation. The biotransformation process can lead to detoxification, and excretion, or to bioactivation of the chemical compound [42], which is achieved in three metabolic phases: phases I and II, and transport phase III. The phase I reactions alter the basic structure of a compound to a more polar metabolite by means of oxidation, reduction or hydrolysis. The main enzymes responsible for metabolism of phase I are members of the cytochrome P450 (CYPs) superfamily. Cytochrome P450 enzymes, located in the smooth endoplasmic reticulum, function as mono-oxygenases that insert one atom of oxygen into the substrate molecule [43]. Products of phase I metabolism that are sufficiently water soluble are eliminated by biliary or renal excretion or they may form substrates for phase II enzymes. Phase II metabolism involves the conjugation of a water-soluble chemical moiety to a phase I metabolite by transferases [44, 45]. The products of phase II reactions are generally detoxifying. However, some conjugates can cause adverse effects [46]. Phase III involves bile secretion through active membrane transporters (Figure 7) such as ABC transporter proteins and families of OATs, OCTs and OATPs [47, 48].

1.5 *IN VITRO* CULTURE SYSTEMS & IMPROVEMENTS

The liver plays a major role in metabolism and clearance of digested compounds, but is however susceptible to toxicity that may arise from the biotransformation of the compounds [1]. Exogenous compounds such as medicinal drugs may affect the liver in various ways. Compounds causing liver injury are generally termed hepatotoxicants. More than 900 drugs are known to cause liver injury [49]. Moreover, drug-induced liver injury (DILI) is responsible for 50 % of all acute liver failures [50]. DILI is not only an important cause of morbidity and mortality but also is the most common reason for withdrawing newly tested drugs [51] giving liver a unique and central role in toxicological studies.

The purpose of modern toxicology is to investigate and evaluate toxic effects of chemicals and drugs. The standard approach to fully understand potential hepatotoxic effects involves the use of complex and costly *in vivo* models based on animal testing [52]. This approach contradicts the simultaneous effort of reducing the number of animals used in experiments for ethical and cost reasons based on the principle of the three ”Rs” [53]. The 3 ”Rs” refers to the improvement of ethical standards by reducing the number of tests and animal used (use of *in vitro, ex vivo* and *in silico* approaches), the refinement of existing procedures to reduce animal tests or replace them entirely. Due to concerns about the animal welfare and concerns about the predictive accuracy of rodent *in vivo* testing for human adverse health effects, a large number of *in vitro* systems were developed as an alternative to *in vivo* models and are currently applied in not only toxicological, but also in pharmacological studies together with basic and applied research. The use of *in vitro* systems has many advantages including reduced numbers of animal and costs, shortening the time needed for analysis as well as conduction of analyses under well-defined conditions [54]. Well-established *in vitro* systems include the isolated perfused liver, precision-cut liver slices, 3D bioreactors and organoids (spheroids), primary

hepatocyte culture from various species, co-cultures, suspension cultures, immortalized cell lines and sub-cellular fractions. However, each model has advantages and limitations (Figure 8). The currently available *in vitro* tests are not entirely adequate to replace animal testing. In order to fully elucidate the mechanisms of hepatotoxicity of substances and drugs, a combination of various *in vitro* models should be used for a thorough validation of a chemical.

Model system	Advantages	Disadvantages
Liver Slices	Fairly high throughput Retain liver structure; contain all cell types Functional bile canaliculi Good *in vitro*/*in vivo* correlation of xenobiotic metabolism Maintain zone-specific CYP activity; maintain toxicity mechanisms Stability of phase II enzymes, albumin production, gluconeogenesis for 20–96 hours	Cellular necrosis after 48–72 hours CYP levels quickly decrease (6–72 hours) Poor concordance with liver for intrinsic clearance rates and K_m values Diffusion-limited gradient of the exposure to a compound across the slice
Immortalized Hepatic Cell Lines	Throughput depends on application Unlimited amount of cells available Some cell lines retain expression of many liver-specific functions	Lacking most phenotypic and functional characteristics of the liver tissue
Primary Hepatocyte Suspensions	Fairly high throughput Better estimate of internal clearance than monolayer cultures Retain high level of enzyme functionality (close to *in vivo*)	Loss of cell–cell interactions Loss of cell–matrix interactions Limited viability allows short-term use only (<4 hours) Loss of cellular polarity No bile canaliculi
Primary Hepatocyte Cultures	Throughput depends on the application Cells can re-establish cell–cell interactions and polarity Cells retain some morphology and liver-specific functionality in short-term cultures (2–4 days) Induction/inhibition of the metabolizing enzymes can be studied	Inability to maintain *in vivo* liver-specific functionality for long-term culture Quick reduction in functionality and phenotype (24–48 hours) May not develop functional bile canaliculi
Primary Hepatocyte Cultures – Sandwich	Throughput depends on the application Restores *in vivo* polygonal morphology Better maintains liver-specific functionality Prevents loss of viability Functional bile canaliculi	Loss of liver-specific functionality, morphology and phenotype in long-term cultures Decline in metabolic enzyme activity in long-term culture

FIGURE 8: OVERVIEW OF LIVER *IN VITRO* SYSTEMS
Well-established *in vitro* systems include the isolated perfused liver, precision-cut liver slices, 3D bioreactors and organoids (spheroids), primary hepatocyte cultures from various species, co-cultures, suspension cultures, immortalized cell lines and sub-cellular fractions. However, each model possesses advantages and limitations, making available *in vitro* tests not entirely adequate to replace animal testing. Figure adapted and modified from [52].

Primary hepatocytes cultures from various species continue to be the most relevant *in vitro* tool to assess liver functions as well as transport, metabolism and toxicity of drugs [55, 56]. However, the limited life span and the rapid decrease in liver-specific functionality over culture time *in vitro* are common shortcomings for primary cultures [57]. The improvement of

primary cultures of hepatocytes regarding cell density, the composition of the culture medium or the use of different matrixes on which to seed hepatocytes are continuously developed to foster retention of hepatocyte function.

Traditional primary hepatocyte cultures involve the method of plating cells as a monolayer on surfaces coated with extracellular matrix proteins (e.g. collagens type I, III or IV, fibronectin and laminin) as substrata. In such culture system, primary hepatocytes rapidly undergo changes in cell morphology, polarity, gene expression, and liver-specific functions [58-61] in a process referred as de-differentiation.

Remarkably, primary hepatocytes cultured between two layers of gelled collagen-I or other extracellular matrix such as Matrigel™ (basement membrane preparation extracted from the Engelbreth-Holm-Swarm mouse sarcoma, a tumor rich in extracellular matrix) in so called 3D sandwich configuration, restore functional polarity, maintain differentiated morphology, liver-specific metabolic activity and longevity in culture [62-68]. Despite the significant improvements attributed to the sandwich culture method, expression of many liver-specific functions decreases over time in culture [69].

In order to provide a more physiological environment for cultured liver cells, co-culture conformation and other forms of organotypic microenvironments were further incorporated to preserve liver-specific morphology and functionality beyond those provided by standard cultures. The co-culture configuration supports the maintenance of normal hepatic structure and function [70, 71]. Similarly, primary hepatocytes cultured as spheroid aggregates forming sphere-shaped “spheroids” over several days [72, 73] exhibit improved cell survival and prolonged maintenance of differentiated functions [74, 75]. Additional examples of methods aiming at *in vitro* culture improvement include generation of transplantable liver grafts using de-cellularized liver matrix [76] and culture with improved oxygen supply [77]. Although some advancement has been achieved by all mentioned techniques, they were in most cases limited to a small number of readouts and usually did not rescue functions to the level of hepatocytes *in vivo*.

1.6 DE-DIFFERENTIATION IN CULTURE

The differentiation status of a cell can be evaluated by its genome wide gene expression pattern. Cultivation causes major alterations in gene expression of primary hepatocytes during the first 24 h of culture when compared to the liver *in vivo* [78]. The de-differentiation process that is triggered in cultures of primary hepatocytes leads to a rapid change in mRNA and protein levels of phase I and phase II biotransformation enzymes (e.g. CYPs 450 enzymes) together with the down-regulation in expression of bile acid transporters (e.g. Bsep and Mrp2) that taken together resembles the features of cholestasis [61, 79].

The extracellular environment has been shown to play a critical role in regulating both liver-specific function in culture and activation of liver transcription factors maintaining differentiation [58, 64, 80]. Such alterations can be partly explained by a drastic decrease in expression of hepatic master regulators, such as liver-enriched transcription factors (LETFs) [60, 81] or nuclear receptors [82, 83] (Figure 9).

The liver-enriched transcription factors (LETF) consist of six families of evolutionary conserved transcription factors: HNF-1, HNF-3, HNF-4, HNF-6, C/EBP, and D-binding protein (DBP) [84]. The C/EBP family of transcription factors is known to regulate not only hepatic functions but also the inflammatory response of the liver [85, 86]. The HNFs belong to the nuclear hormone receptor family and are required for cellular differentiation and metabolism [87]. HNF-1 has been shown to be one of the transactivators of liver-specific albumin transcription [88] and CYP7a1 [89]. HNF-4 regulates diverse metabolic pathways and developmental processes determining the hepatic phenotype [90, 91].

Nuclear receptors (NR) are a large family of ligand-dependent transcription factors that regulate many hepatic functions, including toxicologic processes and metabolic homeostasis [92]. The key nuclear receptors include farnesoid X receptor (FXR), short heterodimeric partner (SHP), pregnane X receptor (PXR), liver X receptor (LXR), peroxisome proliferator-activated receptor alpha (PPARa), and constitutive androstane receptor (CAR). These nuclear receptors are controlled by the action of small molecules such as steroid hormones, bile acids, fatty acids, thyroid hormones, certain vitamins and prostaglandins. Activated by small moelcules, nuclear receptors in the form ofa heterodimer with retinoid X receptor (RXR) [93], bind their DNA response elements located within a gene's promoter region and regulate gene expression of their targets, e.g. the superfamily of CYPs 450 enzymes [83]. Additionally, nuclear receptors cause adaptive changes of hepatic transporter expression at a transcriptional level in response to bile acids and proinflammatory cytokines [94]. For example, the transcriptional control of the Bsep and Mrp2 genes has been shown to be mediated by a group of nuclear hormone receptors including FXR, RAR, PXR, and CAR [95-97]. Overall, the transcriptional regulation of hepatic transporters comprises a complex interacting network of nuclear receptors and LEFT [37, 98].

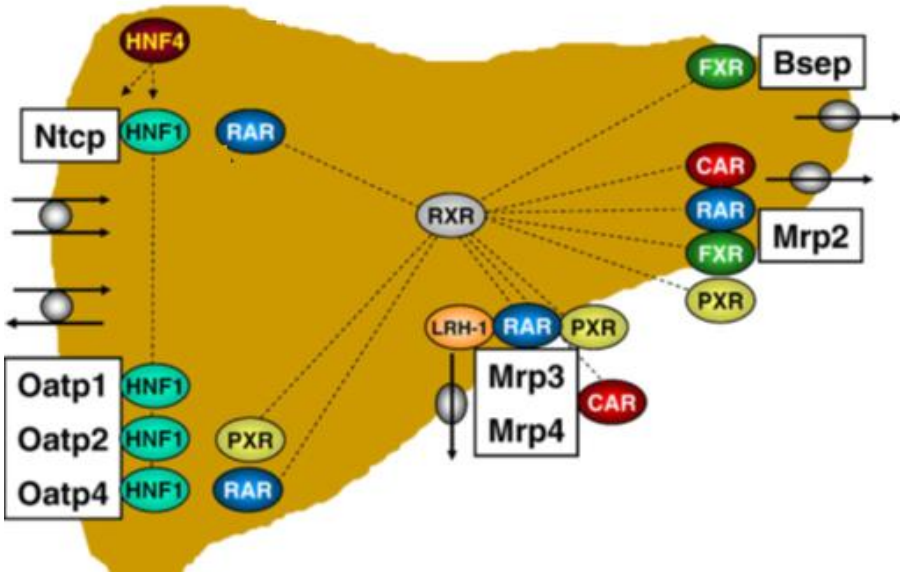

FIGURE 9: REGULATION OF TRANSCRIPTION OF TRANSPORTERS IN RAT LIVER
NR together with RXR as obligatory partner and LETF mediate the transcriptional regulation of hepatobiliary transporter systems. HNF1α, which is under positive feedback control of HNF4α is the common master regulator of basolateral Ntcp and Oatp1, 2 and 4. FXR positively regulates the canalicular bile acid transporters Bsep and Mrp2. The RARα: RXRα heterodimer again positively regulates Ntcp and also Mrp2. Adapted and modified from [94].

1.7 STRESS RESPONSE DURING ISOLATION AND CULTURE

During the isolation procedure, hepatocytes lose their normal microenvironment and cell-to-cell interactions thus undergoing ischemia-perfusion injury that together trigger responses in gene expression. A possible cause for the dramatic decrease in expression of LEFTs and nuclear receptors might come from the activation of various stress signaling pathways during the isolation procedure [99]. Indeed, it has been shown that isolation-induced stress initiates rapid activation of signaling cascades leading to proliferative and inflammatory responses that contributes to the de-differentiated cell phenotype [61, 100, 101].

Among the signaling pathways contributing to the altered gene expression of primary hepatocytes are the mitogen-activated protein kinases (MAPK) transduction pathways comprising the Extracellular Signal-Regulated Kinases (ERKs) 1 and 2 (ERK1/2); the Stress-Activated Protein Kinases/c-Jun amino-terminal kinases (SAPK/JNKs) 1, 2, and 3; the p38 isoforms α,β, γ, and δ , inflammatory pathways such as the Nuclear Factor-Kappa B (NF-kB); Janus Kinase/Signal Transducers and Activators of Transcription (JAK/STAT); the phosphatidylinositol 3-kinase (PI3K)/Akt and protein kinase C (PKC) signaling-pathway.

The MAPK signal transduction pathway is a highly conserved and widespread mechanism of eukaryotic cell regulation involved in various cellular functions such as cell proliferation, differentiation and migration (Figure 10). The MAPKs are serine/threonine kinases that mediate intracellular phosphorylation events in response to a wide variety of different

stimuli such as growth factors, hormones and environmental stresses acting through diverse receptor tyrosine kinase families [102, 103].

ERK1/2 is preferentially activated in response to growth factors, while the JNK and p38 are activated in response to stress stimuli: heat and osmotic shock, ionizing radiation, endotoxin encounter, and cytokine stimulation [104, 105]. However, ischemia and reperfusion activate JNK and p38 in various ways. Inactive JNK during ischemia gets activated during reperfusion, whereas the p38s are activated during ischemia and remain active during reperfusion [106, 107].

Recognition of extracellular stimuli activates a kinase cascade consisting of a MAPK kinase kinase (also known as MAP3K or MAPKKK) which phosphorylates and activates a MAPK kinase (also known as MAP2K, MEK, or MKK) which then phosphorylates and increases the activity of one or more MAPKs. This cascade is common to all MAPKs. Activated MAPKs further phosphorylate an array of targets including transcription factors, nuclear pore proteins, membrane transporters, cytoskeletal elements, and other protein kinases [103]. A dynamic balance between the ERK1&2/JNK/p38 pathways is vital to determining the fate of the cell (Figure 10) [108].

The JNK members (JNK 1, 2, and 3) are strongly activated by all the inflammatory cytokines of the TNF family such as tumor necrosis factor (TNF), interleukin (IL)-1, Fas ligand, receptor activator of NF-kB [109]. Activation of JNK requires dual phosphorylation on tyrosine and threonine residues within a conserved Thr-Pro-Tyr (TPY) motif catalyzed by MEK4 and MEK7, which are themselves phosphorylated and activated by several MAPKKKs, including MEKK1-4, MLK2 and -3, TAO1 and -2, TAK1, and ASK1 and -2. In turn, these are activated by GTP-binding proteins of the Rho family. Activated JNK phosphorylates c-Jun leading to an activation of the activator protein-1 (AP-1), as well as several other transcription factors, such as Elk-1, ATF-2, , NFAT, and STAT3 [103, 110]. It has been also suggested that the activation of JNK during the isolation procedure inhibits liver-specific gene transcription through inactivation of HNF-4α leading to a rapid loss of the cytochrome P450 enzymes [111].

The activation of the p38 members (α, β, δ, γ and p-38-2) has been observed in response to various physical and chemical stresses, such as oxidative stress, UV irradiation, hypoxia, ischemia, and cytokines, including IL-1 and TNF [112]. Activation of p38 requires dual phosphorylation on tyrosine and threonine residues within a conserved Thr-Gly-Tyr (TGY) dual phosphorylation motif catalyzed by MEK3 and MEK6 that are themselves phosphorylated and activated by a plethora of MAPKKKs, including TAK1 and ASK1. In turn, these are activated by GTP-binding proteins of the Rho family. Activated p38 phosphorylates several cellular targets, including transcription factors ATF1 and -2, MEF2, Elk-1, and NF- kB [103, 113].

The ERK members (ERK1 and ERK2) are strongly activated by mitogenic and growth factors. Activation of ERKs requires phosphorylation on tyrosine and threonine residues within a conserved Thr-Glu-Tyr (TEY) motif catalyzed by activated MEK1 and MEK2, which are

themselves phosphorylated and activated by Raf and Mos. In turn, these are activated by the induction of the small GTPase Ras. Activated ERK1/2 phosphorylates a vast array of substrates localized in all cellular compartments including signaling effectors, receptors, cytoskeletal proteins and nuclear transcriptional regulators transcription factors, such as Elk1 and c-Myc, and protein kinases, such as ribosomal S6 kinase (RSK) [114]. ERK1/2 signaling has been shown to be strongly activated during the isolation procedure [100, 115]. Moreover, primary hepatocytes in monolayer cultures acquire a de-differentiated and proliferative phenotype via activation of ERK1/2 signaling [78, 115]. ERK1/2 activation has been additionally shown to down-regulate the HNF-4α expression mediated by loss of C/EBPα and disruption of HNF-4α enhancer-promoter complex [116]. All these data suggests a pivotal role of ERK signaling in determining the fate of the cell.

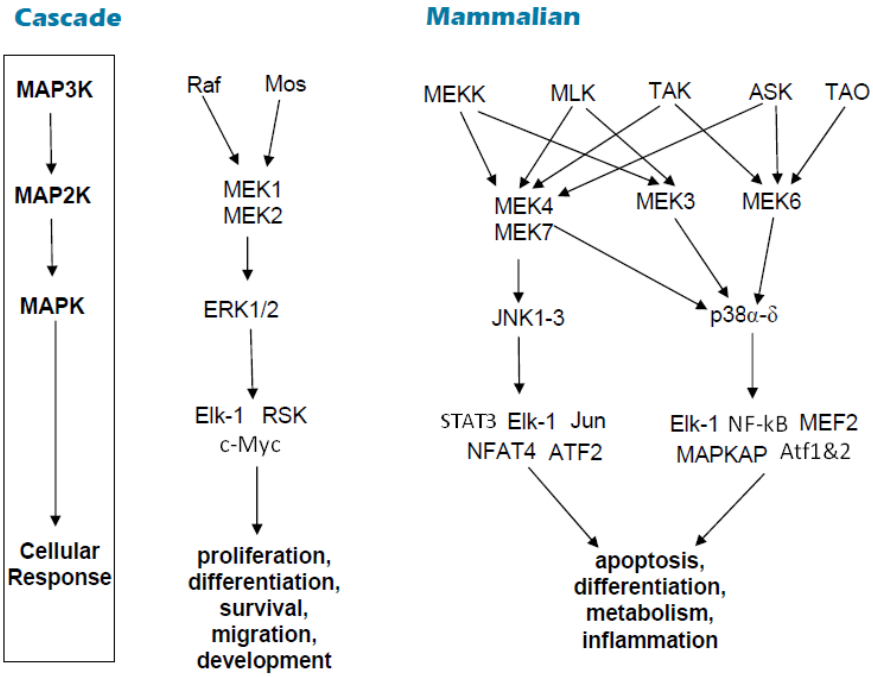

FIGURE 10: FLOW CHART REPRESENTING ACTIVATION AND CELLULAR RESPONSES OF MAPK MODULES (ERK, JNK AND P38)

Recognition of the extracellular stimuli activates a kinase cascade consisting of a MAPK kinase kinase (also known as MAP3K or MAPKKK) which phosphorylates and activates a MAPK kinase (also known as MAP2K, MEK, or MKK) which in turn phosphorylates and increases the activity of one or more MAPKs. In turn, activated MAPKs can further phosphorylate an array of targets including transcription factors, nuclear pore proteins, membrane transporters, cytoskeletal elements, and other protein kinases. A dynamic balance between the ERK1&2/JNK/p38 pathways is vital for determining the fate of the cell. Figure adapted and modified from: http://www.komabiotech.co.kr/pdf/mapk_signaling_review.pdf

NF-kB is a conserved transcription factor important for mediating the inflammatory response of the immune system. NF-kB regulates the expression of cytokines, growth factors and inhibitors of apoptosis. The five members of the NF-kB family are RelA (p65), RelB, c-Rel, p50/p105, and p52/p100 that are maintained in the cytoplasm as dimers bound to IkB family proteins [117]. In the canonical NF-kB pathway (Figure 11), the NF-kB dimer of p50/RelA

subunits is maintained in the cytoplasm by interacting with an independent IkBα molecule. Binding of the pro-inflammatory cytokine (e.g. TNF, IL-1 type pro-inflammatory cytokines, bacterial products such as lipopolysaccharides, reactive oxygen species and viral products) activates the IKK complex (containing the α and β catalytic subunits and two molecules of the regulatory scaffold protein called NF-kB essential modulator-NEMO). In turn, IKK phosphorylates IkBα at two serine residues, which leads to its subsequent ubiquitination and degradation by the proteasome. As a consequence, the NF-kB dimer is enabled to enter the nucleus to activate expression of many genes involved in inflammation [118]. NF-kB has also been shown to be activated within 20 min of the isolation procedure with collagenase indicating that NF-kB causes hepatocytes to undergo a pro-inflammatory response [100].

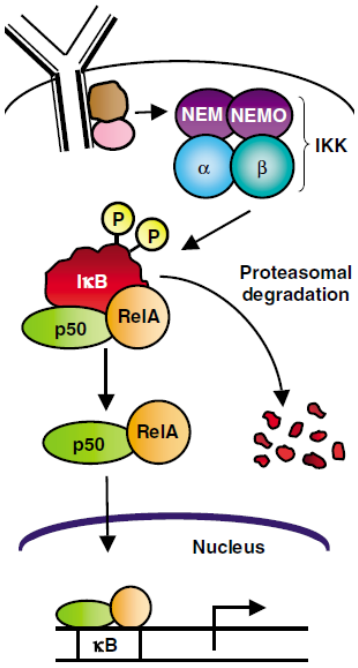

FIGURE 11: MECHANISM OF NFkB ACTIVATION
The NF-kB dimer of p50/RelA subunits is maintained in the cytoplasm by interacting with the IkBα molecule. Pro-inflammatory signals activate the IKK complex, that in turn phosphorylates IkBα leading to its subsequent ubiquitination and degradation by the proteasome. As a consequence, the NF-kB dimer enters the nucleus to activate expression of many genes involved in inflammation. Figure adapted and modified from [118].

The Janus kinase/signal transducers and activators of the transcription (JAK/STAT) pathway is the principal signaling mechanism for a plethora of cytokines (e.g. IL-6 type cytokines) and growth factors. Its activation stimulates cell proliferation, differentiation, cell migration and apoptosis and has an important role in the control of immune responses [119]. Binding of a cytokine to its surface receptor induces receptor dimerization (Figure 12), which in turn subsequently activates two JAK tyrosine kinases associated with the receptor allowing trans-phosphorylation of the cytoplasmic transcription factors STATs. Phosphorylated STATs dimerize and subsequently leave the receptor and translocate to the nucleus, where they bind specific regulatory sequences leading to the activation or repression of target genes providing a direct mechanism to translate an extracellular signal to a transcriptional response [120].

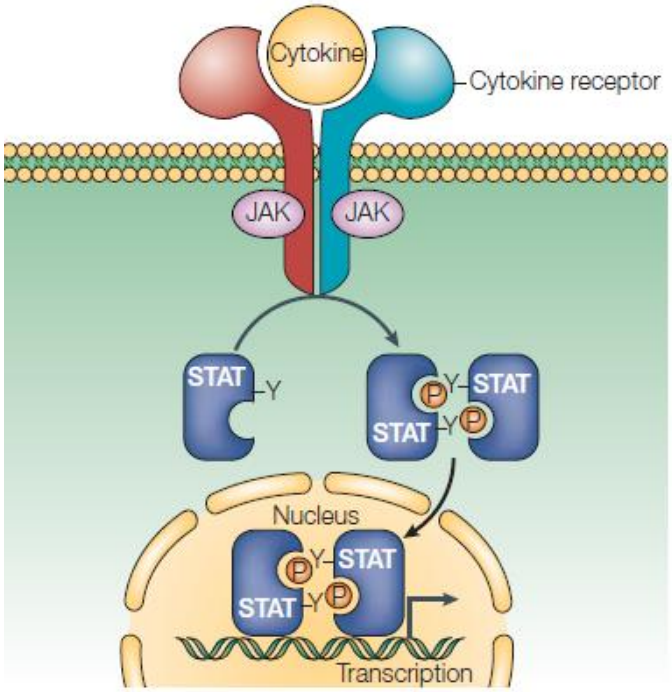

FIGURE 12: MECHANISM OF JAK/STAT ACTIVATION
Binding of a cytokine to its surface receptor induces receptor dimerization, which in turn subsequently activates two JAK tyrosine kinases associated with the receptor allowing trans-phosphorylation of the cytoplasmic transcription factors STATs. Phosphorylated STATs dimerize and subsequently leave the receptor and translocate to the nucleus, where they bind specific regulatory sequences to activate or repress transcription of target genes providing a direct mechanism to translate an extracellular signal into a transcriptional response. Figure adapted and modified from [121].

The phosphatidylinositol 3-kinase (PI3K)/Akt signaling cascade plays a central role in many physiological processes which include cell proliferation, differentiation, apoptosis, cytoskeletal rearrangements and metabolism [122, 123]. Activation of growth factor receptor protein tyrosine kinases results in auto-phosphorylation on tyrosine residues, which in turn recruits PI3K to the membrane. PI3K belongs to a conserved family of lipid kinases that generate the second messenger phosphatidylinositol-3,4,5-trisphosphate (PIP-3) at the inner side of the plasma membrane. The generated PIP-3 binds and activates different cellular proteins, by targeting them to membranes or modulating their enzyme activities. In this way, PIP-3 activates Akt that subsequently translocates to the nucleus to modulate activation of growth, survival and proliferation signaling [124].

The protein kinase C (PKC) family of multifunctional and phospholipid-dependent protein kinases is characterized by their ability to phosphorylate serine and threonine residues of receptors, enzymes, cytoskeletal proteins, and transcription factors. Activation of G protein-coupled receptors, tyrosine kinase receptors, or non-receptor tyrosine kinases by an array of extracellular signals induces phospholipase C (PLC) to hydrolyze the membrane lipid PIP2, producing IP3 and diacylglycerol (DAG). Subsequently, the IP3 diffuses to the ER inducing release of calcium stores from inside the ER into the cytoplasm. Together the interaction of

both DAG and calcium modulates PKC kinase activity allowing phosphorylation of many protein targets affecting cellular signal processing, cell proliferation, differentiation, survival and death [125, 126].

Importantly, these stress activated signaling pathways are also known to occur in different *in vivo* stress conditions, such as bacteria (i.e. lipopolysaccharide (LPS)-induced inflammation, sterile inflammation, and surgical resections. This suggests that metabolism may also be severely affected in those *in vivo* situations. Hence, it is important to gain a deeper understanding of the signaling processes occurring *in vivo* during stress responses.

1.8 LPS-INDUCED INFLAMMATION AND ACUTE PHASE RESPONSE

Liver inflammation results from hepatocyte damage caused by acute or chronic liver injury or by diseases. The immune system responds to pathogens with a complex set of defense mechanisms and is divided into two branches: innate (first line of the defense against a harmful stimulus and consisting of the innate immune cells such as monocytes, macrophages, mast cells, neutrophils and natural killer cells and dendritic cells) and the adaptive immunity (elimination of the harmful stimulus and the generation of immunological memory). The innate immune system recognizes microbial components (LPS, glycolipids, viral RNA and bacterial DNA among others), known as pathogen-associated molecular patterns (PAMPs) via pattern-recognition receptors (PRRs) such as Toll-like receptors. Recognition of the PAMPs activates immune cells leading to intracellular signaling cascades that elicit strong pro-inflammatory responses [127, 128].

The tissue injury or infection can cause an orchestrated inflammatory response of the liver, known as the acute phase response (APR). APR leads to an altered expression of a specific group of plasma proteins, collectively known as acute phase proteins, which attempts to restore liver homeostasis. Acute phase proteins consist of various plasma proteins synthesized in the liver, such as C-reactive protein (CRP), serum amyloid P (SAP), serum amyloid A (SAA), inhibitors of proteases, coagulation factors, transport proteins (lipocalin-2) [129, 130], and complement components [131].

LPS, a glycolipid located on the outer membrane of Gram-negative bacteria, is cleared from the circulation primarily by Kupffer cells, liver sinusoidal endothelial cells and hepatocytes [132]. Recognition of LPS occurs during bacterial encounter in the gastrointestinal track causing dimerization of Toll-like receptor 4 (TLR4) and myeloid differentiation factor 2 (MD-2) that results in an induction of innate immunity responses [133]. As a consequence, activated Kupffer cells release a variety of pro-inflammatory messengers such as TNF, IL-1β, and IL-6 [134, 135]. Binding of TNF and IL-1β to their respective receptors activates NF-kB that promotes transcription of acute-phase genes [136]. Many of the acute phase genes have DNA binding sites that are recognized by the family of liver specific transcription factors CCAAT/ Enhancer binding protein (C/EBP) [137]. IL-6, IL-1β, and TNF stimuli strongly induce two isoforms of C/EBP (C/EBPβ and –δ) and concurrently down-regulate C/EBPα [138]. C/EBPα activity is also

regulated by NF-kB, protein kinase C and MAPKs signaling [139]. Additionally, stimulation of macrophages with LPS activates other signaling pathways, such as ERK members (ERK1 and ERK2) [140], p38 [141] and both isoforms of JNK [104], indicating their importance in mediating LPS action in macrophages.

1.9 LIVER REGENERATION MODELS

1.9.1 CCl_4-INDUCED HEPATOTOXICITY

Carbon tetrachloride (CCl_4) belongs to the haloalkanes known to cause hepatic damage [142]. CCl_4-induced hepatotoxicity is the most widely studied model of liver injury. In this model, exposure to CCl_4 causes impairment of a number of cellular functions leading to acute and reversible necrosis of centri-lobular hepatocytes followed by liver regeneration. In the liver, CCl_4 requires metabolic activation by P450 enzymes of the endoplasmic reticulum, primarily by the isoform CYP2E1 (Figure 13). Biotransformation generates the highly reactive and hepatocyte-toxic trichloromethyl free radical (CCl_3*) which in turn interacts with various biologically important substances. Furthermore, the CCl_3* radical can be converted in the presence of oxygen to a more reactive trichloromethylperoxy radical, CCl_3OO*. As a result, lipid peroxidation and covalent binding of CCl_4- derived reactive metabolites affects cellular homeostasis causing severe oxidative stress and cell damage.

Additionally, secondary liver injury following CCl_4 administration can result from inflammatory processes mediated by activated Kupffer cells and stellate cells. Following CCl_4 exposure, Kupffer cells release a variety of pro-inflammatory messengers (TNF, nitric oxide, TGF-ß, and IL-1, IL-6, and IL-10) [142] and stellate cells display a typical acute-phase response [143]. The intraperitoneal injection of CCl_4 activates various molecular processes and signaling cascades such as ERK2 and causes down-regulation of liver- specific genes through suppression of LETFs, and induction of NF- kB signaling [144].

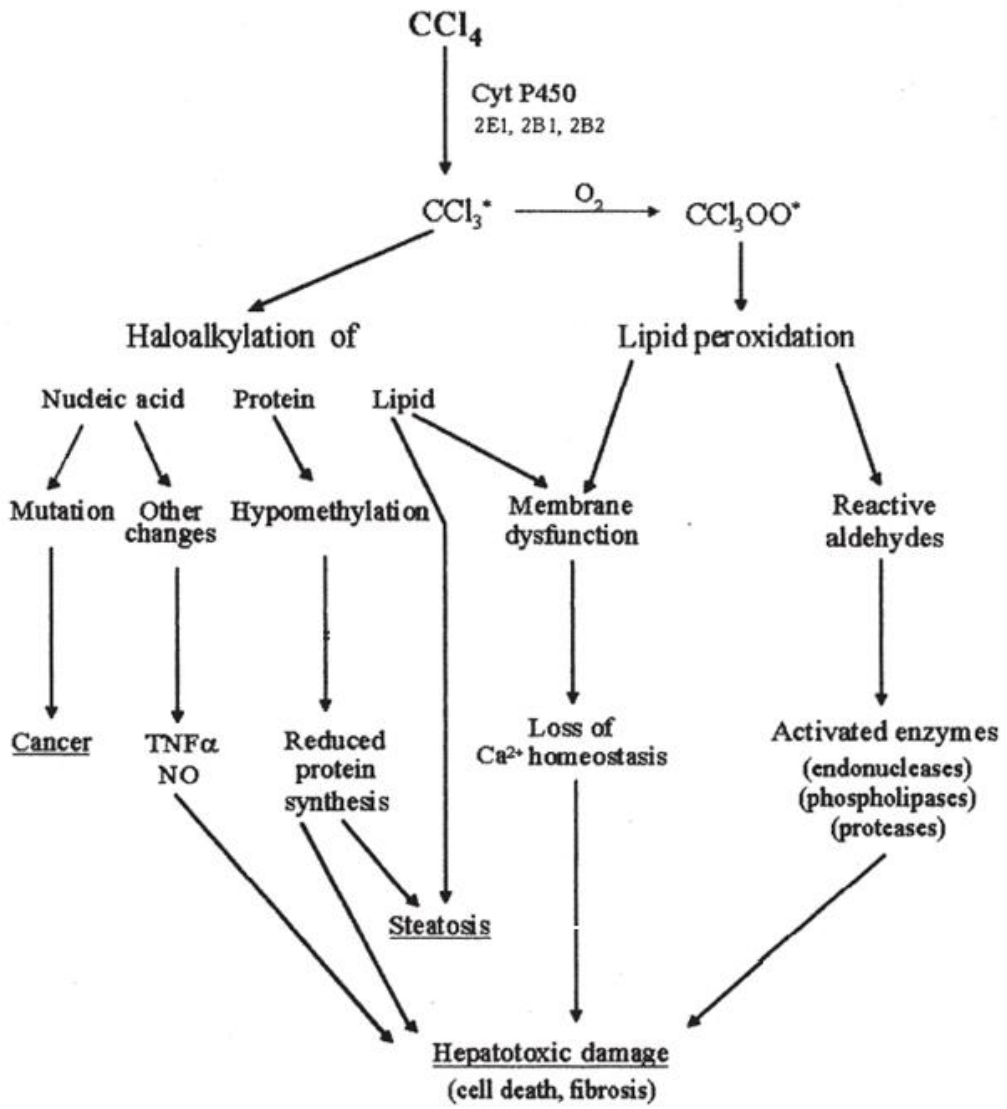

FIGURE 13: BIOTRANFORMATION OF CCL_4 LEADING THE LIVER DAMAGE

CCl_4 requires metabolic activation by P450 enzymes, primarily the isoform CYP2E1. Biotransformation generates the highly reactive and hepatocyte-toxic trichloromethyl free radical (CCl_3*) that can react with various biologically important substances. The CCl_3* radical can be converted in the presence of oxygen to a more reactive trichloromethylperoxy radical, CCl_3OO*. As a result, lipid peroxidation and covalent binding of CCl_4- derived reactive metabolites affects cellular homeostasis causing severe oxidative stress and cell damage. Figure adapted and modified from [142].

1.9.2 LIVER REGENERATION AFTER PARTIAL HEPATECTOMY (PHx)

Liver regeneration represents an orchestrated response induced by specific external stimuli and is associated with changes in gene expression, signaling cascades involving growth factors, cytokines, as well as matrix remodeling, and alteration of morphologic structures [145]. The most widely used model for the study of liver regeneration is a technique known as 2/3 partial hepatectomy (PHx) [146]. In this model, three of the five liver lobes (representing 2/3 of

the liver mass) are removed surgically, without damage to the residual two lobes. The remaining liver provides full support for body homeostasis during the entire regenerative process of about 7 days and enlarges until the original mass is restored. In the normal adult liver, the quiescent hepatocytes rarely proliferate [147]. However, following partial hepatectomy, all cellular populations of the resected liver rapidly re-enter the cell cycle. The first peak of DNA synthesis in murine hepatocytes occurs at about 36 hours followed by a smaller peak between 36 and 48 hours for the other cell types [4]. Moreover, PHx induces rapid induction of more than 100 genes not expressed in normal liver [4] substituting for preparative events for the entry of hepatocytes into the cell cycle. NFκB, STAT3 and AP1, are rapidly activated in remnant hepatocytes minutes after partial hepatectomy and may be a major part of the intracellular signaling cascade leading to DNA synthesis [147]. Similarly, intracellular-signalling pathways as MAPK and JNK are rapidly activated after PHx providing clues to the initiating signals [4]. Simultaneously with the induction of proliferation, hepatocytes maintain all essential metabolic functions needed for homeostasis. Functionality of hepatocytes during liver regeneration can be partly explained by the essentially unchanged levels of transcription factors such as hepatic nuclear factor 1, 3 and 4 [147]. Additionally, the C/EBPα isoform is down-regulated during liver regeneration, whereas expression of the C/EBPβ isoform increases [148, 149]. Although most of the signaling responses described above take place in hepatocytes, several ligands triggering these pathways are released by non-parenchymal cells, such as sinusoidal endothelial cells, Kupffer cells and stellate cells.

1.9.3 NPC AND THEIR ROLE DURING LIVER DAMAGE

Non-parenchymal cells (NPC) are responsible for producing a range of cytokines and chemokines that modulate not only liver function but also contribute to the response to acute hepatocyte injury (Figure 14) [150]. Various types of stress-induced stimuli can lead to the activation of non-parenchymal cells such as LSEC and Kupffer cells causing a release of diverse pro-inflammatory mediators, which recruits and activats other inflammatory cells including natural killer cells, natural killer T cells, T cells, dendritic cells and macrophages [150, 151].

Released cytokines control cellular homeostasis of other cell types by binding to highly specific cell-surface receptors triggering differentiation, proliferation, migration, adhesion or apoptosis processes. Cytokines consist of a variety of interleukins, growth factors, interferons and chemokines and are classified as pro- (e.g. IL- 1, IL-12, IL-18, TNF, and interferon-γ (IFN-γ)) or anti-inflammatory (e.g. IL-4, IL-10, IL-13, IFN-α, and transforming growth factor-β (TGF-β)) [152].

Activated Kupffer cells (KC) produce nitric oxide, reactive oxygen species and inflammatory cytokines to provoke liver inflammation upon liver injury. The released cytokines locally control the function of hepatocytes that bear a variety of cytokine receptors as well as other NPC under both normal and pathological conditions [153]. Activated KCs are capable of modulating cell death by inducing apoptosis of affected cell types. The interplay between

actions of pro-inflammatory (TNF, IL-1β and IL-6) and anti-inflammatory (IL-10) cytokines produced by KC is strictly regulated and modulates response to liver injury [3, 150].

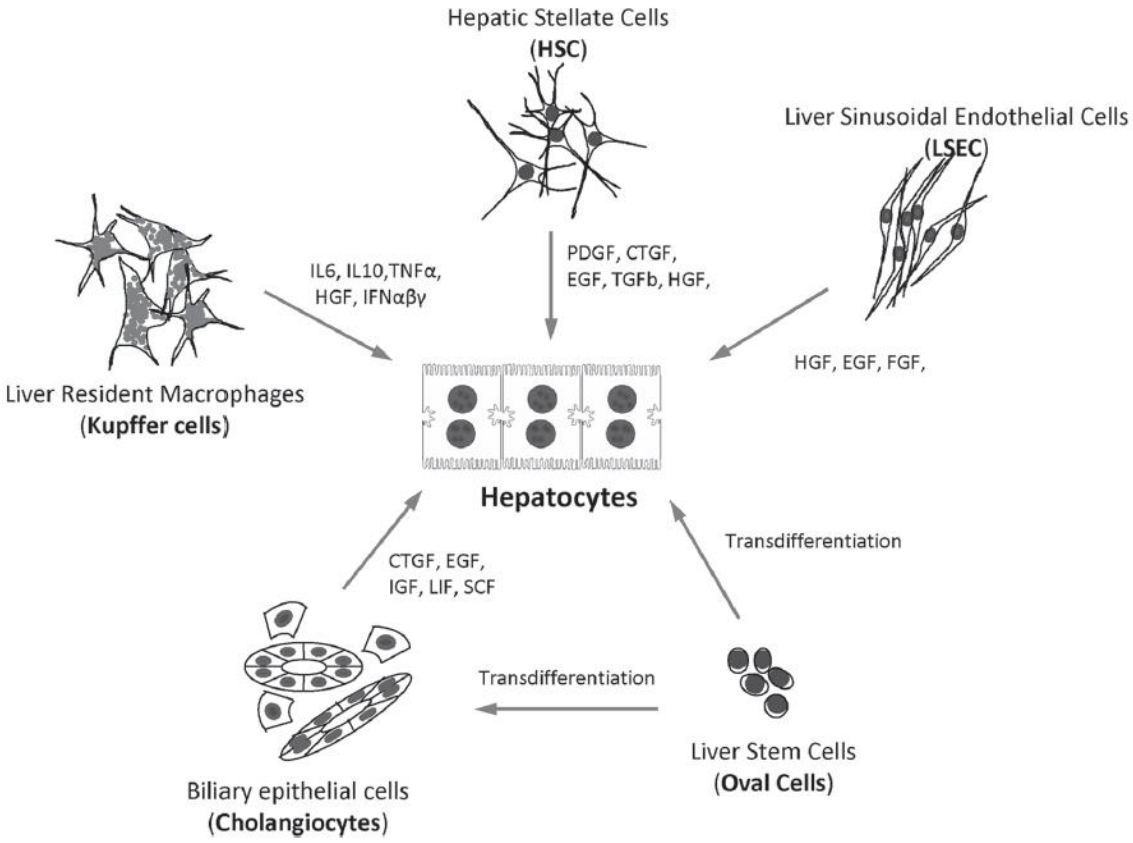

FIGURE 14: AUTOCRINE AND PARACRINE SIGNALS SECRETED BY NPC MODULATE HEPATOCYTE FUNCTIONS IN HEALTHY AND DISEASED LIVER TISSUE

The activation of non-parenchymal cells causes a release of diverse pro-inflammatory mediators. Figure adapted and modified from [15].

1.9.4 CHOLESTATIS IN MODELS OF LIVER INJURY

Cholestasis or impaired bile secretion frequently result from defects in transporter expression caused by inflammatory disorders [94, 154]. LPS-induced pro-inflammatory cytokines (TNF, IL-1β and IL-6) secreted by Kupffer cells [134] have been characterized as the key mediators regulating hepatic expression and activity of transporters (Figure 15) [97, 155, 156]. It has been shown that experimental administration of LPS, TNF, IL-1β or IL-6 reduces expression of several hepatic transporters at the basolateral or canalicular membrane [157-159]. Interestingly, the down-regulation of hepatic transporters during LPS-induced cholestasis can be viewed as part of the negative acute-phase response [98].

Hepatic transporters are regulated at both the transcriptional and post-transcriptional level [37]. The transcription factors such as families of LETF and nuclear receptors have a pivotal role in the transcriptional regulation of hepatic transporters (Figure 15) [37]. Moreover, LPS

treatment activates MAPK stress signaling pathways, including JNK [160] that leads to a decrease in expression of nuclear receptors [161, 162]. NR are known to regulate gene expression of hepatic transporters such as Bsep and Mrp2 [95, 97, 98]. Additionally, IL-1β induction after LPS-treatment *in vivo* seems to be the major regulator of rat Mrp2 expression [163]. In contrast to the down-regulation in rodent models, expression of hepatic transporters BSEP and MRP2 in humans have been shown to be regulated mainly by post-transcriptional mechanisms [164, 165].

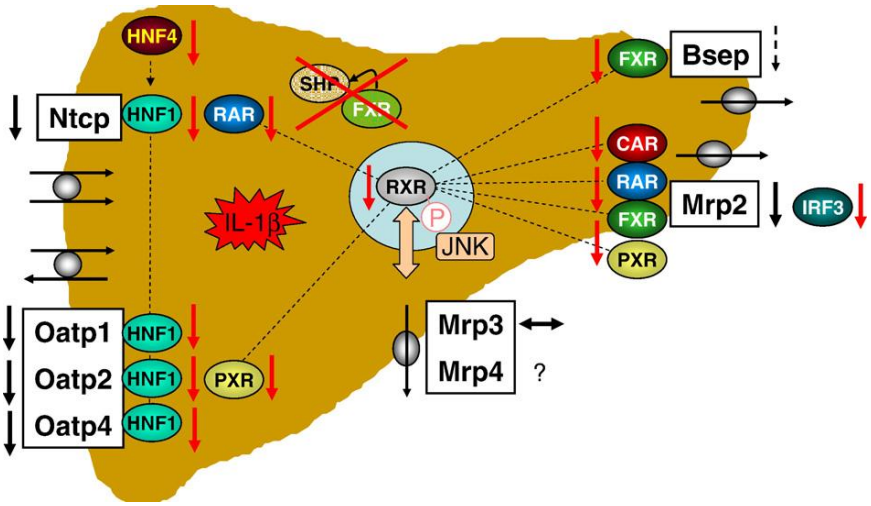

FIGURE 15: TRANSPORTER REGULATION IN INFLAMMATION-INDUCED CHOLESTASIS
LPS-mediated signals reduce the expression of several hepatic transporters at the basolateral or canalicular membrane. IL-1b is the major regulator of Ntcp and Mrp2 expression. The function of the RXRa component is thereby affected by RNA degradation and JNK-dependent phosphorylation. The transcriptional control of Bsep and Mrp2 is mediated by a decreased expression of nuclear hormone receptors including FXR, PXR, and CAR. Figure adapted and modified from [94].

Liver regeneration induces a coordinated down-regulation of basolateral transport systems while maintaining expression of canalicular transporters (Figure 16). In the model of partial hepatectomy, expression of basolateral transporters is reduced and the canalicular transporters Bsep and Mrp2 remain stably expressed at the protein level 24 h after surgery [166, 167]. Similar changes in both the canalicular and the basolateral transporter expression have been observed in CCl_4-induced liver damage [164, 168]. Such patterns of alteration can be partly explained by the massive induction of TNF occurring in both models of liver regeneration [168-170] since TNF has been shown to be the master regulatory cytokine for basolateral transporter gene expression during liver regeneration [164].

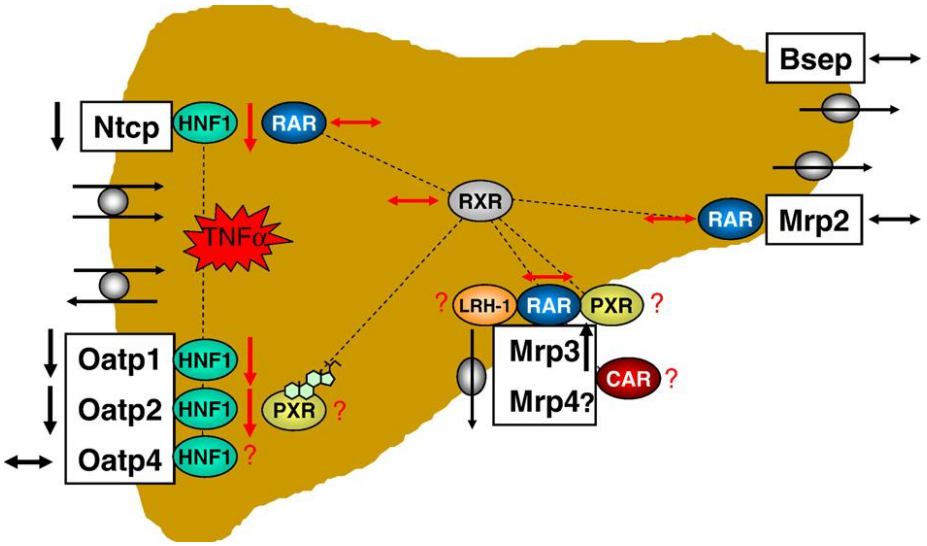

FIGURE 16: TRANSPORTER REGULATION DURING LIVER REGENERATION AND TOXIC LIVER INJURY
Models of liver regeneration induce a coordinated down-regulation of basolateral transport systems while maintaining expression of canalicular transporters. Tumor necrosis factor represents the master regulatory cytokine for the basolateral transporter gene expression during liver regeneration. Figure adapted and modified from [94].

Altogether, it is clear that common stress responses may occur in profoundly different conditions such as perfusion and culture (*in vitro*) and also *in vivo*. Therefore, it is crucial to fully understand these processes in order to establish proper *in vitro* systems.

1.10 AIM OF THIS WORK

The aim of this work was to gain insight into the molecular consequences of hepatocyte isolation and cultivation by comparing gene expression changes of hepatocytes cultivated in collagen sandwich cultures (S), confluent (M_C) as well as subconfluent (M_S) monolayer cultures with reference to their similarities and differences over time.

For this purpose, a time resolved global gene expression profiling of primary mouse hepatocytes was carried out using Affymetrix microarrays. A combination of gene array analyses, bioinformatics and knowledge-based interpretation of the identified deregulated genes was then used to identify mechanisms responsible for the observed transcriptional alterations. In the next step, the identified biological motifs associated with the deregulated genes were validated using qRT-PCR and Western blot. These analyses identified a strong upregulation of inflammation and proliferation as well as a downregulation of metabolism-associated genes in hepatocytes *in vitro*. The changes in the identified biological motifs were compared to those in stressed-hepatocytes after different types of hepatic injury, namely after treatment with CCl_4, lipopolysaccharide (LPS) or partial hepatectomy (PHx). Subsequently, I performed a series of experiments validating the contribution of other liver cell subpopulations, extracellular matrix and alternative culture configuration on the aforementioned transcriptional responses. Finally, I compared the transcriptional alterations observed in the mouse model with those in rat and human primary hepatocytes.

The specific aims of the present study are to:

- perform a time resolved global gene expression profiling of primary mouse hepatocytes by Affymetrix microarrays
- use a combination of gene array analyses, bioinformatics and knowledge-based interpretation of the identified deregulated genes in order to identify mechanisms regulated by the observed transcriptional alterations
- validate the identified biological motifs by qRT-PCR and western blot
- compare the observed transcriptional responses to livers *in vivo* after treatment with CCl_4, lipopolysaccharide (LPS) or partial hepatectomy (PHx)
- dissect signaling activities throughout the culture time by means of Luminex analysis
- study the effect of other liver cell subpopulations, extracellular matrix and spheroid configuration on the aforementioned transcriptional responses
- validate and compare the observed transcriptional responses of the mouse model with models of rat and human primary hepatocytes

2. MATERIALS AND METHODS

2.1 MATERIALS

2.1.1 CHEMICAL REAGENTS AND KITS

TABLE 1: CHEMICAL REAGENTS AND KITS

Chemical	Company	Catalog No
2-propanol	Carl Roth, Karlsruhe, Germany	AE73.1
Aminoacid solution (Costumer formulation)	PAN Biotech GmbH, Aidenbach, Germany	SO-33100
APS	Sigma-Aldrich Corp., St. Louis, MO, USA	3678-25g
Basement Membrane Matrix, Growth Factor Reduced (GFR), Phenol Red-free	BD Bioscience, San Jose, USA	356231
Bio-Plex Cell Lysis Kit	Bio-Rad Laboratories, Munich, Germany	171-304011
Bovine Albumin Fraction V (BSA)	Carl Roth, Karlsruhe, Germany	8076.4
BrdU	Sigma-Aldrich Corp., St. Louis, MO, USA	B5002
Bromphenol Blue	Merk, Darmstadt, Germany	108122
Buffer concentrate A	Carl Roth, Karlsruhe, Germany	L510.1
Buffer concentrate K	Carl Roth, Karlsruhe, Germany	L511.1
Collagenase from Clostridium hystolyticum	Sigma-Aldrich Corp., St. Louis, MO, USA	C2674
Complete feed for Rats&Mice - Maintenance	Ssniff Spezialdiaeten, Soest, Germany	V1534-000
DAPI	Invitrogen GmbH, Darmstadt, Germany	D3571
DEPC Treated Water	Invitrogen GmbH, Darmstadt, Germany	46-42224
di-Sodium Hydrogen Phosphat anhydrous (Na2HPO4)	Carl Roth, Karlsruhe, Germany	P030.2
DMSO	Sigma-Aldrich Corp., St. Louis, MO, USA	472301
DTT (DL-Dithiothreitol)	Sigma-Aldrich Corp., St. Louis, MO, USA	D9779
Easycoll Separating Solution 1.124g/mL	Biochrom AG, Berlin, Germany	L6143
EDTA	Carl Roth, Karlsruhe, Germany	8040.3
EGTA	Carl Roth, Karlsruhe, Germany	3054.2
Eosin Y disodium salt	Sigma-Aldrich Corp., St. Louis, MO, USA	E4382
Ethanol	Merk, Darmstadt, Germany	100983
Ethanol, 70%	Walter CMP, Kiel, Germany	WAL10506
FluorPreserve™ Reagent	Calbiochem, Darmstadt, Germany.	345787
Glycerin	Carl Roth, Karlsruhe, Germany	3783.2
Glycine	Carl Roth, Karlsruhe, Germany	HN07.3
GravityPLUS™ 3D Culture and Assay Platform	InSphero, Schlieren, Switzerland	CS-06-001
High Capacity cDNA Reverse Transcription Kit	Applied Biosystems, Karlsruhe, Germany	4368813
Hydrochloric Acid, 32%	Carl Roth, Karlsruhe, Germany	P074.4
Ketamin-ratiopharm® 50 mg O.K. Injection Solution	Ratio pharm, Ulm, Germany	N64477.04
Magic Mark XP Western Protein Standard	Invitrogen GmbH, Darmstadt, Germany	LC5602
Mayer´s Hemalum solution	Merk, Darmstadt, Germany	1.09249.0500
Methanol	Sigma-Aldrich Corp., St. Louis, MO, USA	322415

Microscopy Entellan	Merk, Darmstadt, Germany	1.07960.0500
Mouse Laminin	BD Bioscience, San Jose, USA	354232
Nonidet P-40 (NP-40)	Roche Diagnostics GmbH, Manheim,	11754599001
Phosphatase Inhibitor Cocktail II	Sigma-Aldrich Corp., St. Louis, MO, USA	P5726
Phosphatase Inhibitor Cocktail III	Sigma-Aldrich Corp., St. Louis, MO, USA	P0044
Pierce BCA Protein Assay Kit	Thermo Scientific, Braunschweig, Germany	23225
PMSF	Carl Roth, Karlsruhe, Germany	6367.2
Ponseau S	Carl Roth, Karlsruhe, Germany	5938.1
Potassium Chloride (KCl)	Carl Roth, Karlsruhe, Germany	6781 .1
Potassium dihydrogen phosphate (KH2PO4)	Carl Roth, Karlsruhe, Germany	3904.1
Precision Plus Protein standards	Bio-Rad Laboratories, Munich, Germany	161-0374
Protease Inhibitor Cocktail	Sigma-Aldrich Corp., St. Louis, MO, USA	P8340
Qiazol Lysis Reagent	Qiagen, Hilden, Germany	79306
Rompun 2%	Bayer Health Care, Leverkusen, Germany	
Roti Histofix 4%	Carl Roth, Karlsruhe, Germany	P087.5
Roti-Histol	Carl Roth, Karlsruhe, Germany	6640.1
Rotiphorese® Gel 30 (37,5:1)	Carl Roth, Karlsruhe, Germany	3029.1
SDS pellets	Carl Roth, Karlsruhe, Germany	CN30.1
Sera Plus (Special Processed FBS)	PAN Biotech GmbH, Aidenbach, Germany	3702-P103009
Sodium chloride	Carl Roth, Karlsruhe, Germany	3957.2
Sodium deoxycholate	Sigma-Aldrich Corp., St. Louis, MO, USA	D6750
Sodium hydroxide pellets	Merk, Darmstadt, Germany	1.06482
TaqMan® Universal Master Mix II, with UNG	Applied Biosystems, Karlsruhe, Germany	4440038
TEMED	Carl Roth, Karlsruhe, Germany	2367.1
Trichloroacetic Acid	Carl Roth, Karlsruhe, Germany	8789.2
Trichloromethane/Chloroform	Carl Roth, Karlsruhe, Germany	7331.2
TRIS	Carl Roth, Karlsruhe, Germany	4855.2
Tris-HCl	Sigma-Aldrich Corp., St. Louis, MO, USA	T3253
Triton X-100	Carl Roth, Karlsruhe, Germany	3051
Trizma base	Sigma-Aldrich Corp., St. Louis, MO, USA	33742
Trypan Blue	Sigma-Aldrich Corp., St. Louis, MO, USA	T6146
Tween 20	Sigma-Aldrich Corp., St. Louis, MO, USA	P7949
Western Lightning® Plus-ECL, Enhanced Chemiluminescence Substrate	Perkin-Elmer, Massachusetts, USA	NEL105001EA

2.1.2 CONSUMABLES

TABLE 2: CONSUMABLES

Consumable	Company	Catalog No
Biosphere Filtered Tip, 1000uL	Sarstedt, Numbrecht, Germany	70.762.211
Biosphere Filtered Tip, 100uL	Sarstedt, Numbrecht, Germany	70.760.212
Biosphere Filtered Tip, 200uL	Sarstedt, Numbrecht, Germany	70.760.211
Biosphere Filtered Tip, 20uL	Sarstedt, Numbrecht, Germany	70.1116.210
Blotting Paper Grade 703, 46x57cm	VWR international, Darmstadt, Germany	732-0591
Cell Scraper, 25cm	Sarstedt, Numbrecht, Germany	83.183
CHROMA SPIN™-100	Clontech, Mountain View, USA	636089
Cover glass, 18mm	Menzel, Braunschweig, Germany	CB00180RA1
Disposable semi-micro cuvette, 1.5mL	BRAND, Mannheim, Germany	7591 15

Embedding cassettes	Carl Roth, Karlsruhe, Germany	K113.1
FACSClean	BD Bioscience, San Jose, USA	340345
FACSFlow	BD Bioscience, San Jose, USA	342003
FACSRinse	BD Bioscience, San Jose, USA	340346
Falcon tube, 15mL	Sarstedt, Numbrecht, Germany	62.554.512
Falcon tube, 50mL	Sarstedt, Numbrecht, Germany	62.547.254
GeneChip 3' IVT Express kit	Affymetrix, Santa Clara, USA	901229-D
GeneChip Human Genome U133 Plus 2.0 Array	Affymetrix, Santa Clara, USA	520019
GeneChip Mouse Genome 430 2.0 Array	Affymetrix, Santa Clara, USA	900497
Gentle Skin Classic Laboratory Gloves	Meditrade, Kiefersfelden, Germany	1221R
GravityPLUS™ 3D Culture and Assay Platform	InSphero, Schlieren, Switzerland	CS-06-001
Hypodermic Needle, 26G	BD Bioscience, San Jose, USA	304300
Integra 300uL Tips	Viaflo, INTEGRA, Zizers, Switzerland	44343
Kimtech Science Delicate Task Wipes	Kimberly-Clark Professionals, Roswell, USA	7216
MicroAmp Optical 96-well Reaction Plate	Applied Biosystems, California, USA	N801-0560
Mouse Genome 430 2.0 Affymetrix genechips	Affymetrix, Santa Clara, USA	900497
Multiwell Flat-Bottom 12-Well Plate	BD Bioscience, San Jose, USA	353043
Parafilm Wrap	Cole-Parmer, Kehl/Rhein, Germany	PM-992
Pipette Tips, 1000uL	Sarstedt, Numbrecht, Germany	70.762
Pipette Tips, 200uL	Sarstedt, Numbrecht, Germany	70.760.002
Pipette Tips, 20uL	Sarstedt, Numbrecht, Germany	70.1116
Polyscreen PVDF Tranfer Membrane	Perkin-Elmer, Massachusetts, USA	NEF1002001PK
Polystyrene round-bottom tube with cell-strainer cap, 5mL	BD Bioscience, San Jose, USA	352235
RNase-free Microfuge Tubes 1.5 mL	Ambion, Thermo Fischer Scientific, Waltham, USA	AM12400
RNaseZap® RNase Decontamination Solution	Ambion, Thermo Fischer Scientific, Waltham, USA	AM9780/AM9782
SafeSeal 0.5mL microtube	Sarstedt, Numbrecht, Germany	72.699
SafeSeal 1.5mL micotube	Sarstedt, Numbrecht, Germany	72.706
SafeSeal 2.0mL microtube	Sarstedt, Numbrecht, Germany	72.695.500
Serological Pipette, 10mL	Sarstedt, Numbrecht, Germany	86.1254.001
Serological Pipette, 25mL	Sarstedt, Numbrecht, Germany	86.1685.001
Serological Pipette, 5mL	Sarstedt, Numbrecht, Germany	86.1253.001
SuperFrost Plus® microscopic slides	Thermo Scientific, Braunschweig, Germany	J1800AMNZ
Syringe, 1mL Luer	BD Bioscience, San Jose, USA	300013
Tissue Culture Plate Flat-Bottom 6-Well Plate	Sarstedt, Numbrecht, Germany	83.1839
Vacuum Filtration Unit, 0.22um, 250mL	Sarstedt, Numbrecht, Germany	83.1822.001
Wash and Stain (HWS) kit	Affymetrix, Santa Clara, USA	900720
WypeAll L30 wipes	Kimberly-Clark Professionals, Roswell, USA	7301

2.1.3 TECHNICAL EQUIPMENT

TABLE 3: EQUIPMENT

Equipment	Description, Company
Array scanner	Gene-Chip Scanner-3000-7G, Affymetrix
Array scanner software	GeneChip Operating Software GCOS, Affymetrix
Array washing station	GeneChip Fluidics Station 450, Affymetrix
Autoclave	5075 ELV, Tuttenauer
Balance	EW, Kern
Bio-Plex system	Bio-Rad
Bright Field Microscope	Eclipse TS 100
Bunsen Burner	IBS Fireboy Plus, Integra Bioscences
Centrifuge	Megafuge 1.0R, Thermo Scientific
Centrifuge	Centrifuge 5415 R, Eppendorf
Centrifuge with cooling function	5424R, Eppendorf
Centrifuge with cooling function	Biofuge Fresco, Heraeus
Channel pipette	8 Channel Vision Pipette Viaflo, INTEGRA
Flow Cytometer	FACSCalibur, BD Bioscence
Freezer, -20 degrees	Comfort NoFrost, Liebherr
Freezer, -80 degrees	HeraFreeze, Heraeus
Hybridization Oven	Gene-Chip Hybridization Oven 645, Affymetrix
Ice Flaker	AF 100, Scotsman
Image acquisition system	Fusion Fx7, Vilber Lourmat
Incubators	Co2 Incubator C150 R Hinge 230, Binder
Laminar Flow Hood	Electronics FAZ 2, Waldner
Low Voltage Power Supply	Standard Power Pack P25, Biometra
Magnetic stirrer	IKAMAG RCT, IKA
Microcentrifuge	Mini Spin Plus, Eppendorf
Minicentrifuge	FVL-2400N Combi-Spin, Biosan
Minishaker	MS 2, IKA
pH meter	CG 842, Schott
Pipetteboy	Integra
Pipettes	Research and Reference, Eppendorf
Precision balance	EW 150-3M, Kern
Real Time PCR System	7500 Real-Time PCR System, Applied Biosystems
RNA quality analyser	Agilent 2100 Bioanalyzer
Safety Cabinet	HERA-Safe, Heraeus
Shaker	KS 260 basic, IKA
Shaker	Orbital Shaker S03, Stuart Scientific
Shaker	Rocking Platform, VWR
Sonicator	Bandelin, SONOPLUS
Spectrometer	NanoDrop 2000, Thermo Scientific
Thermocycler	TGRADIENT, Biometra
Thermoshaker	HTM 130, HLC
Thermoshaker	PHMT Grant-bio, Keison
Transfer chamber	Fastblot B44, Biometra

UV/Vis Spectrometer	V-530, Jasco
Vacuum pump	Diaphragm Vacuum Pump, Vacuumbrand
Vortex	Vortex-Genie 2, Bender&Hobein
Water purification system	Maxima Ultra-Pure Water, ELGA
Waterbath	GFL 1083, Gesellschaft für Labortechnik
Western blot Chamber	Bio-Rad Mini PROTEAN Tetra System
Cell culture microscope:	
Bright Field Microscope	Primo Vert, Zeiss
Microscope CCD-Camera	AxioCam ICm 1
Software	ZEN, Zeiss
Epi-fluorescence microscope:	
Fluorescence Microscope	Olympus BX 41
Microscope CCD-Camera	Olympus ColorView
Video system	Olympus U-CMAD3; Olympus U-TV1x-2
Mercury Lamp	Lamp Olympus U-RFL-T
Software	Olympus Cell^F
Confocal Laser Scanning Microscope:	
Microscope	Olympus BX61 microscope
LSM Scanning Unit	Olympus Fluoview FV1000
Mercury Lamp	Lamp Olympus U-RFL-T
Laser Combiner	Olympus FV10-MCPSU
Software	Olympus Fluoview Ver. 4.0b

2.1.4 PERFUSION BUFFERS

TABLE 4: PERFUSION BUFFERS

Buffer	Chemical	Amount
Collagenase buffer	Amino acid solution	30 ml
	$CaCl_2$ solution (19 g/l CaCl2* 2 H2O)	10 ml
	Collagenase Type 1	100 mg
	Glucose solution (9 g/l)	155 ml
	Glutamine (7 g/ml)	2.5 ml
	HEPES (60 g/l) (pH 8.5)	25 ml
	KH buffer	25 ml
EGTA buffer	Amino acid solution	60 ml
	EGTA solution (47.5 g/l)	1.6 ml
	Glucose solution (9 g/l)	248 ml
	Glutamine (7 g/l)	4 ml
	KH buffer	30 ml
	HEPES (60 g/l) (pH 8.5)	30 ml
KH buffer	Potassium chloride (KCl)	1.75 g
	Potassium dihydrogene phosphate	1.6 g
	Sodium chloride 60 g/L	60 g
	filled to 1l with H_2O	
	set pH to 7.4	
Suspension buffer	Albumin Fraction V	400 mg
	Amino acid solution	30 ml
	$CaCl_2$ solution (19 g/l CaCl2* 2 H2O)	1.6ml
	Glucose solution (9 g/l)	124 ml
	Glutamine (7 g/ml)	2 ml
	HEPES (60 g/l) (pH 7.6)	20 ml
	KH buffer	20 ml
	$MgSO_4$ solution (24,6 g/L MgSO4 * 7H2O)	0.8 ml

2.1.5 CELL CULTURE

2.1.5.1 CELL CULTURE MEDIUM

TABLE 5: CELL CULTURE MEDIUM

Additives for cell culture medium	Final Concentration	For 500mL Medium	Company	Catalog No
William's Medium E	-	-	PAN Biotech GmbH, Aidenbach, Germany	P04-29510
Dexamethasone	100 nM	20 µl from 2.5 mM stock in EtOH	Sigma-Aldrich Corp., St. Louis, MO, USA	D4902-25MG
Gentamycin	10 µg/ml	500uL	PAN Biotech GmbH, Aidenbach, Germany	P06-13001
Insulin (ITS) 100x	2 ng/ml	5uL	Sigma-Aldrich Corp., St. Louis, MO, USA	I3146
Penicillin/Streptomycin	100 U/ml Pen; 100 U/ml Strep	5mL	PAN Biotech GmbH, Aidenbach, Germany	P06-07100
Stable L- Glutamine	2 mM	5mL	PAN Biotech GmbH, Aidenbach, Germany	P04-82100
Sera Plus (Special Processed FBS)	10% (Full Media only)	50 mL	PAN Biotech GmbH, Aidenbach, Germany	3702-P103009

2.1.5.2 CELL CULTURE CHEMICALS

TABLE 6: CELL CULTURE CHEMICALS

Other Chemicals	Company	Catalog No
Acetic acid glacial	Carl Roth, Karlsruhe, Germany	3738.5
Basement Membrane Matrix, Growth Factor Reduced (GFR), Phenol Red-free	BD Bioscience, San Jose, USA	356231
Collagen Sandwich - Collagen lyophilize (rat-tail), 10mg	Roche Diagnostics GmbH, Manheim,	11171179001
Collagen Monolayer - Collagen lyophilize (rat-tail), 10mg	Roche Diagnostics GmbH, Manheim,	11171179001
Dexamethasone	Sigma-Aldrich Corp., St. Louis, MO, USA	D4902-25MG
DMEM low glucose 1.0 g/L 10x	BioConcept, Allschwil, Switzerland	1-25K03-I
DMSO	Sigma-Aldrich Corp., St. Louis, MO, USA	472301
Easycoll Separating Solution 1.124g/mL	Biochrom AG, Berlin, Germany	L6143
Gentamycin	PAN Biotech GmbH, Aidenbach, Germany	P06-13001
Insulin (ITS) 100x	Sigma-Aldrich Corp., St. Louis, MO, USA	I3146
Mouse Laminin	BD Bioscience, San Jose, USA	354232
Penicillin/Streptomycin	PAN Biotech GmbH, Aidenbach, Germany	P06-07100
Sera Plus (Special Processed FBS)	PAN Biotech GmbH, Aidenbach, Germany	3702-P103009
Sodium hydroxide pellets	Merk, Darmstadt, Germany	1.06482

Stable L- Glutamine	PAN Biotech GmbH, Aidenbach, Germany	P04-82100
William's Medium E	PAN Biotech GmbH, Aidenbach, Germany	P04-29510

TABLE 7: SMALL CHEMICAL INHIBITORS

Pathway	Chemical	Company	Catalog No	Concentration used
JNK	SP600125	Sigma-Aldrich Corp., St. Louis, MO, USA	S5567-10MG	10uM, 25uM, 50uM
ERK	U0126 monoethanolate	Sigma-Aldrich Corp., St. Louis, MO, USA	U120-1MG	10uM, 25uM, 50uM
JAK	Jak inhibitor I	Calbiochem, Darmstadt, Germany.	420097	5nM, 10nM, 25nM
NF-kB	JSH_23	Santa Cruz Biotechnology, Inc., California, USA	sc-222061	5uM, 10uM, 25uM
p38	SB 203580	Sigma-Aldrich Corp., St. Louis, MO, USA	S8307-1MG	10uM, 25uM, 50uM
PI-3K	LY-294	Sigma-Aldrich Corp., St. Louis, MO, USA	L9908	5uM, 10uM, 25uM
PKC	GF109203X	Enzo Life Sciences, Lörrach, Germany	ALX-270-049	5nM, 10nM, 25nM

2.1.6 TAQMAN ASSAYS

TABLE 8: TAQMAN ASSAYS (APPLIED BIOSYSTEMS, CALIFORNIA, USA)

Target gene	Assay Catalog No		
	Mouse	Rat	Human
Bsep	Mm00445168_m1	Rn00669268_m1	Hs00184824_m1
CAR	Mm_01283978_m1	-	-
Ccl2	Mm00441242_m1		
CebpD	Mm00786711_s1	-	-
Cyp7a1	Mm00484152_m1	Rn00564065_m1	Hs00167982_m1
FXR	Mm1240553_m1	-	-
GAPDH	4352932E	Rn01749022_m1	4352934E
HNF4	Mm00433964_m1	Rn00573309_m1	-
Ier3	Mm00519290_g1		
Klf6	Mm00516184_m1	-	-
Lcn2	Mm01324470_m1	Rn01439062_g1	Hs01008571_m1
Mrp2	Mm00496899_m1	Rn00563231_m1	Hs00166123_m1
Mt2	Mm00809556_s1	Rn99999155_g1	Hs02379661_g1
PXR	Mm01344139_m1	-	-
RXR	Mm01332431_m1	-	-
SAA3	Mm00441203_m1	-	Hs01380779_m1
Sp1	Mm00489039_m1	-	-

2.1.7 PROTEIN LYSATES BUFFERS

TABLE 9: RIPA BUFFER FOR WESTERN BLOT

RIPA buffer	
50 mM Tris-Cl (pH 7,5)	
150 mM NaCl	
1% Nonidet P-40 (NP-40)	
0,5% sodium deoxycholate	
0,1% SDS	
Added prior to use:	
Protease inhibitor	1:100
Phosphatase inhibitor 2	1:100
Phosphatase inhibitor 3	1:100

TABLE 10: LYSIS BUFFER FOR THE LUMINEX ANALYSIS

Bio-Plex Cell Lysis Kit	Per sample
Bio-Plex Lysis Buffer	500 µL
Bio-Plex Factor 1	1:250
Bio-Plex Factor 2	1:500
Added prior to use:	
PMSF (50mM in DMSO)	1:250

2.1.8 BUFFERS FOR SDS ELECTROPHORESIS AND WESTERN BLOT

TABLE 11: BUFFERS FOR SDS ELECTROPHORESIS AND WESTERN BLOT

Buffer	Chemical and amount
Anode buffer	Buffer concentrate A (Roth) 80 ml Methanol 160 ml Dest. Water 560 ml
Cathode buffer	Buffer concentrate K (Roth) 40 ml Methanol 80 ml Dest. Water 280 ml
Loading buffer (5 x)	Bromphenol blue 5 mg DTT 1 M 2.5 ml Glycerol 5 ml SDS 0.5 g Tris-HCl 1 M 2.25 mL
PBS (10x)	KCl 10g KH2PO4 10g NaCl 400g Na2HPO4 46g set pH to 7.4 filled up to 5 L with distilled water
Ponseau S	1 g Ponseau S in 500 ml of 3 % Trichloroacetic acid set pH to 7.4
Running buffer (10x)	Glycine 144.0 g SDS 10.0 g Tris base 30.3 g
TGP Separation buffer (3M Tris-HCl)	Tris 36.34 g in 100 ml water set pH to 8.8
SGP Stacking buffer (0.47M Tris-HCl)	Tris 5.69 g in 100 ml water set pH to 6.7
Stripping buffer	Glycine 15 g SDS 1 g Tween 20 10 ml set pH to 2.2 filled up to 1 L with distilled water
TBS (10x)	NaCl 265g TRIS 60g filled up to 5 L with distilled water set pH to 7.4
TBS-T	10x TBS 250 ml Tween-20 2.5 ml Dest. Water 250 ml filled up to 2.5 L with distilled water
5 % BSA solution	5 g Bovine Albumin Fraction V (BSA) in 100 ml TBS-T
10 % SDS	0.5 g SDS in 5 ml water
10 % APS	0.5 g APS in 5 ml water

2.1.9 ANTIBODIES

2.1.9.1 LIST OF PRIMARY ANTIBODIES

TABLE 12: PRIMARY ANTIBODIES

Antigen	Origin	Company	Catalog No	Dilution
BrdU	Rat	AbD Serotec, Raleigh, USA	MCA2060	1:25 (IF)
DPP4/CD26	Goat	R&D, Minneapolis, USA	AF954	1:300 (IF)
GAPDH	Rabbit	Cell Signaling New England Biolabs GmbH, Frankfurt am Main, Germany	2118	1:1000 (WB)
HNF-4α	Goat	Santa Cruz Biotechnology, Inc., California, USA	sc-6556	1:200 (WB) 1:50 (IF)
ICAM1	Rabbit	ProteinTech Group, Chicago, USA	10020-1-AP	1:200 (IF)
Klf6	Rabbit	Santa Cruz Biotechnology, Inc., California, USA	sc-7158	1:100 (IF)
Lipocalin-2/NGAL	Goat	R&D, Minneapolis, USA	AF1857	1:500 (WB)
p44/42 (ERK1/2)	Rabbit	Cell Signaling New England Biolabs GmbH, Frankfurt am Main, Germany	9102	1:1000 (WB)
PCNA	Mouse	Cell Signaling New England Biolabs GmbH, Frankfurt am Main, Germany	2586	1:2000 (WB)
pERK1/2, Alexa Fluor 647 Conjugate	Rabbit	Cell Signaling New England Biolabs GmbH, Frankfurt am Main, Germany	4284	1:50 (IF)
Phalloidin, Rhodamine conjugate	-	Biotium, Hayward, USA	00027	1:100 (IF)
p-p44/42 (p-ERK1/2)	Rabbit	Cell Signaling New England Biolabs GmbH, Frankfurt am Main, Germany	9101	1:1000 (WB)
p-SAPK/JNK	Rabbit	Cell Signaling New England Biolabs GmbH, Frankfurt am Main, Germany	4668	1:1000 (WB)
SAPK/JNK	Rabbit	Cell Signaling New England Biolabs GmbH, Frankfurt am Main, Germany	9252	1:1000 (WB)
Sp1	Rabbit	Abcam, Cambridge, UK	ab13370	1:300 (IF)

2.1.9.2 LIST OF SECONDARY ANTIBODIES

TABLE 13: SECONDARY ANTIBODIES

Antigen	Origin	Company	Catalog No	Dilution
Alexa Fluor-555 Anti-Rabbit IgG	Goat	Invitrogen GmbH, Darmstadt, Germany	A-21428	1:500 (IF)
Alexa Fluor-555 Anti-Goat IgG	Donkey	Invitrogen GmbH, Darmstadt, Germany	A-21431	1:500 (IF)
Alexa Fluor-647 Anti-Goat IgG	Rabbit	Invitrogen GmbH, Darmstadt, Germany	A-21446	1:500 (IF)
Anti-Goat IgG, HRP-linked	Rabbit	Santa Cruz Biotechnology, Inc., California, USA	sc-2768	1:5000 (WB)
Anti-Mouse IgG, HRP-linked	Horse	Cell Signaling New England Biolabs GmbH, Frankfurt am Main, Germany	7076	1:1000 (WB)
Anti-Rabbit IgG, HRP-linked	Goat	Cell Signaling New England Biolabs GmbH, Frankfurt am Main, Germany	7074	1:1000 (WB)

2.2 METHODS

2.2.1 PRIMARY HEPATOCYTE ISOLATION FROM MOUSE, RAT AND HUMAN LIVERS

Primary mouse and rat hepatocytes were obtained from male C57BL6/N mice (8-12 week old) or male Wistar rats (220-300 g body weight), respectively using a two-step perfusion technique [171]. The animals were housed according to the animal welfare regulation and all of the handling procedures were approved by the animal experimental committees. Prior to the isolation of hepatocytes, animals were weighed and anesthetized using an intraperitoneal injection containing a mixture of sedative 2% Rompun (20 mg/kg) and anesthetic Ketamin (120 mg/kg) with a 26G cannula in a 1ml syringe. After ensuring that the animals were fully narcotized, that is all reflexes were suppressed, they were placed on an operatic stand under a heating lamp and the abdominal cavity was opened for cannulation. Exposed inferior vena cava were cannulated with a 24G cannula connected to a peristaltic pump with a rate flow of 15 ml/min through the portal vein. Successful cannulation of the liver could be observed by an instant and even color change of the liver tissue from red-brown to beige. Afterwards, the vena cava was incised to ensure proper outflow of the buffers. All buffers used during perfusion are described in Table 4. The liver was perfused through the inferior vena cava, first with the EGTA buffer warmed up to 37 °C for ca. 15 min at a rate flow of 15 mL/min to remove the blood volume and Ca^{2+} dependent adhesion factors. The perfusion was then continued with the collagenase buffer warmed up to 37 °C for ca. 15 min at a rate flow of 15 mL/min to digest collagen in the extracellular matrix. Depending on the collagenase enzymatic activity, this step lasted between 5-15 min. Following collagen digestion, the liver was excised from the animal and transferred onto a Petri dish filled with suspension buffer. The following steps were performed in a sterile hood. The liver capsule was opened carefully with forceps and dissociated by gentle shaking. The resulting single-cell suspension was filtered through a 100 µm sieve into a glass beaker. The suspension was then transferred to a 50 ml Falcon tube and centrifuged (5min at 50g at 4 °C). As hepatocytes are larger and heavier than other non-parenchymal cell types, they pellet quickly at the bottom of the tube. After centrifugation, the supernatant containing mainly NPC and cell debris was either discarded or used in co-culture experiments (for further NPC-enriched fraction purification, see chapter 2.2.2.6). Subsequently, the remaining hepatocyte pellet was further purified by washing twice with the suspension buffer and re-centrifuged. Finally, the hepatocyte-enriched pellet was re-suspended in 10 ml suspension buffer and placed on ice until counting, plating, and/or Percoll purification. Viability of hepatocytes was determined by trypan blue vital stain. Briefly, an aliquot of cell suspension was diluted 1:5 with the suspension buffer and further mixed with 0.4% trypan blue solution at a ratio of 1:1. This mixture was loaded onto a Neubauer chamber hemocytometer. Stained cells, representing dead cells, together with the unstained living cells were counted in each of the four corner squares. The average number of viable cells was multiplied by 1×10^5 (accounted for diluting factor and volume of a big square) to obtain the cell number per milliliter of cell suspension. On average 90-95% of the cells were viable with a total amount of cells ranging $5\text{-}7 * 10^6$/mL.

Primary human hepatocytes from three donors were obtained from liver sections of patients undergoing surgical liver resection. Informed consent was obtained from each patient as previously described [171, 172]. The percentage of viable cells was determined by trypan blue exclusion; the minimal viability was 65%.

2.2.1.1.1 PURIFICATION WITH PERCOLL CENTRIFUGATION

For some experiments, freshly isolated hepatocytes were further purified from the remaining non-parenchymal cells, and cell debris removed by one, two or three additional Percoll centrifugations steps. For this purpose, Easycoll® (Biochrome, 1.124 g/mL) was diluted with sterile PBS to a final density of 1.063 g/mL. Next, 7.5 mL from the hepatocyte-enriched cell suspension was gently added on top of the diluted Easycoll® solution and centrifuged for 5 min at 28G at 25°C. The resulting cell pellet was washed carefully with 25 mL of sterile PBS and centrifuged for 5 min at 50G at 4°C. The cell pellet was then resuspended in 7.5 mL of suspension medium. From this purified cell suspension, 2.5 ml were collected and labeled '1X Percoll'. Cell viability in this fraction was determined by trypan blue exclusion. Two aliquots of 1 million cells each were collected for quantification of hepatocytes and non-parenchymal cells by flow cytometry and hematoxilin & eosin (H&E) staining, respectively (procedures for flow cytometry and H&E staining are described below). The remaining cells were used for cultivation in collagen sandwich. This procedure was repeated twice with the remaining 5 mL cell suspension, herein referred to as '2X- or 3X Percoll'.

2.2.1.1.2 FLUORESCENT ACTIVATED CELL SORTING (FACS) ANALYSIS

The purity of each hepatocyte preparation before and after the purification steps with Easycoll was determined by fluorescence activated cell sorting (FACS) using a BD FACS-Calibur flow cytometer, and the data processed using the CellQuest Pro software. A representative scatter plot analysis (Figure 45) shows a large and granular hepatocyte population (designated here as R1) together with a clearly distinguishable smaller and less granular non-parenchymal cell population (designated as R2).

2.2.1.1.3 PERFUSION WITH SMALL CHEMICAL INHIBITORS

In some experiments, the small chemical inhibitor SP600125 was added to the perfusions buffers (EGTA and collagenase buffers) at a final concentration of 50 µM, using DMSO as the vehicle. In these experiments, addition of the JNK inhibitor, SP600125 was applied as follows (Figure 17):

(i) SP600125 was added to the perfusion buffers (EGTA + Collagenase) but not to the cell culture medium,
(ii) SP600125 was added to the culture medium directly upon plating but not to the perfusion buffer,
(iii) SP600125 was added to both perfusion buffers and culture medium.

The DMSO was added at 0.5% as a solvent control either to the perfusion solutions or to the cell culture medium, as indicated in Figure 17. Primary mouse hepatocytes were cultivated with or without the inhibitor for up to 24 hours in sandwich cultures and the gene expression profile of selected markers was analyzed via quantitative RT-PCR.

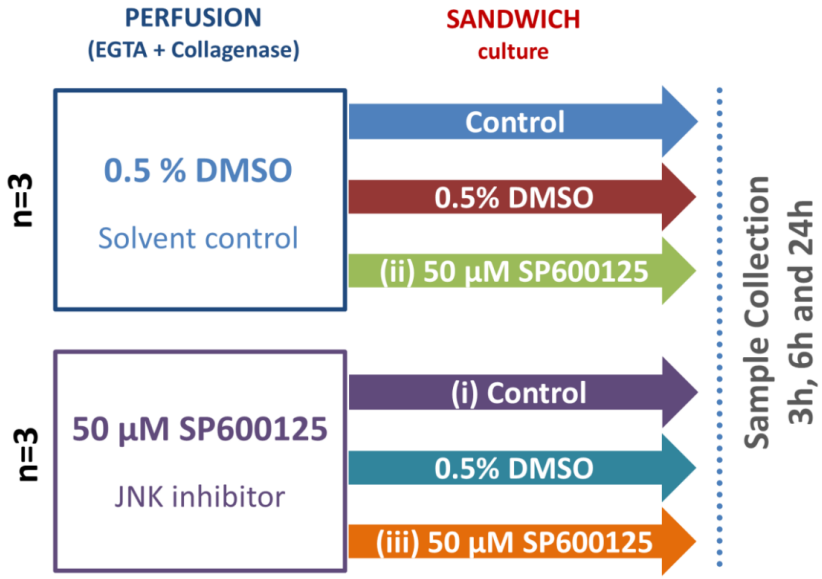

FIGURE 17: EXPERIMENTAL SET-UP FOR PERFUSION WITH JNK INHIBITOR

2.2.2 *IN VITRO* CULTURE OF HEPATOCYTES

Primary hepatocytes were cultured on different extracellular matrix compositions, in a hanging drop conformation or in a co-culture with non-parenchymal cells (NPC). During all experiments, cells were maintained at 37 °C and 5% CO_2.

2.2.2.1 COLLAGEN MONOLAYER: CONFLUENT AND SUB-CONFLUENT

To obtain a rat collagen-I stock of 250 µg/mL, 10mg of rat-tail collagen-I was dissolved in 40 mL of 0.2 % acetic acid resulting in a solution of 250 µg/mL. This stock solution was used to pre-coat tissue culture plates used for collagen monolayer cultures and allowed to dry overnight under the tissue culture bench. Shortly before plating, all pre-coated plates were washed twice with PBS. For conventional culture configurations (monolayer confluent-M_C or monolayer subconfluent-M_S), hepatocytes were plated onto dishes according to the densities specified in TABLE 14. The appropriate cell number were seeded in Williams E medium (Table 5) with 10% Sera Plus during the first 3h of attachment. Afterwards, unattached cells were removed by washing three times with medium, and the final volume of fresh Williams E medium was added. For longer culture periods, fresh medium was changed daily.

TABLE 14: COLLAGEN MONOLAYER CULTURE SPECIFICATIONS FOR DIFFERENT PLATE FORMATS

Plate format	Confluent Condition (M_C) Amount of cells [x 10^6]	Sub-confluent Condition (M_S) Amount of cells [x 10^6]	Medium [mL/well]
Petri dish (ø6cm)	2	0.3	3
6-well plate	1	0.125	2
12-well plate	0.6	0.075	1
24-well plate	0.3	0.0375	0.5

2.2.2.2 COLLAGEN SANDWICH

To obtain a rat collagen-I stock of 1 mg/mL, 10mg of rat-tail collagen-I was dissolved in 9 mL of 0.2 % acetic acid resulting in a solution of1.1 mg/mL. For polymerization of collagen gel, a solution of 1.1 mg/mL collagen was mixed with 10x DMEM at a ratio of 9:1, resulting in a yellow colored (pH indicator) solution of 1 mg/mL. The solution was then neutralized on ice with 1 M NaOH until a visible change of color from yellow to fuchsia was observed. Finally, an appropriate amount of collagen solution was evenly distributed in wells and allowed to polymerize for 45 min at 37°C. Subsequently, primary hepatocytes were plated onto dishes coated with the first collagen gel layer at a density that was dependent on the plate format as described in Table 15. The appropriate amount of cells were seeded in William's E medium (Table 5) with 10% Sera Plus during the first 3h of attachment. Afterwards, unattached cells were removed by washing three times with culture medium and a second layer of collagen gel was added and allowed to polymerize for 40 min at 37 °C. Fresh William's E medium was added. For longer culture periods, fresh medium was changed daily.

TABLE 15: COLLAGEN SANDWICH CULTURE SPECIFICATIONS FOR DIFFERENT PLATE FORMATS

Plate format	1st and 2nd collagen gel layer volume (µl/well)	Amount of cells (x10^6)	Medium (mL/well)
ø6cm Petri dish	700	2	3
6-well plate	350	1	2
12-well plate	200-300	0.3-0.4	1
24-well plate	100-200	0.1-0.2	0.5

2.2.2.2.1 CULTURE WITH SMALL CHEMICAL INHIBITORS

Where applicable, small chemical inhibitors (Table 7) were added to the cell culture medium, either during plating and/or after attachment of the primary mouse hepatocytes to the collagen sandwich (CS) for up to 24h. As a vehicle control, DMSO was added at 0.5%. For all concentrations used (Table 7), additional DMSO was added to the culture medium so that every condition contained the same amount of vehicle representing the maximal concentration used. RNA samples were collected at 3 h, 6 h and 24 h timepoints.

2.2.2.3 MATRIGEL

Primary hepatocytes were plated onto Matrigel™-coated 12-well dishes following the "Thin Gel Method" following manufacturer's instructions. Plates were coated evenly with Matrigel at a density of 50 µg/cm^2 and incubated for 30min at 37°C. Afterwards, cells were seeded at a density of 100,000 cells/cm^2 in Williams E medium (Table 5) with 10% Sera Plus during the first 3h of attachment. Any unattached cells were then removed by washing three times with medium, and the final volume of fresh Williams E medium was added. RNA samples were collected after 24h in culture with 500 µL of Qiazol.

2.2.2.4 LAMININ

Primary hepatocytes were plated in laminin-coated 12-well dishes following the manufacturer's instructions. Laminin was diluted with Williams E medium at 10 µg/cm^2. All wells were coated evenly and incubated for 1 h at room temperature. Afterwards, any remaining material was aspirated and cells were seeded at a density of 100,000 cells/cm^2 in William's E medium (Table 5) with 10% Sera Plus during the first 3h of attachment. Any unattached cells were removed by washing three times with medium and a final volume of fresh Williams E medium was added. RNA samples were collected after 24 h in culture with 500 µL of Qiazol.

2.2.2.5 HEPATOCYTE SPHEROIDS

Mouse hepatocyte spheroids were prepared using the hanging drop method in 96 well GravityPLUS plates. Hepatocyte-enriched cell suspension was diluted to a density of 2000 cells/40 µL of William's E medium with additives (Table 5) and 20% Sera Plus. This cell suspension was resuspended as a 40 µl drop into each well and cultivated according to the manufacturer's instructions (InSphero®, Schlieren, Switzerland) until day 5. Medium was exchanged on day 4 by gently aspirating 20 µl from each drop making sure that the spheroid remained untouched in the well. Subsequently, 20 µl of fresh medium was added to each well and this procedure was repeated once more resulting using a ratio 1:3 of old to fresh media.

2.2.2.6 CO-CULTURE WITH NON-PARENCHYMAL CELLS (NPC)

For co-culture experiments, freshly isolated hepatocytes were plated with a combined non-parenchymal cell fraction in a ratio of 2 to 1. The supernatant obtained after the first centrifugation step of the liver cell suspension (5 min, 50G at 4°C) was collected into a 50 ml tube and centrifuged at 400G, 4°C for 10 min. The cell pellet was resuspended in 2 ml of suspension buffer, and the cells were counted using a Neubauer chamber. This cell population contains a mixture largely composed of liver sinusoidal endothelial cells, and fewer hepatic stellate cells and Kupffer cells [173].

Co-cultures experiments were performed as follows:

A) **Collagen monolayer confluent (M_C)** – freshly isolated hepatocytes were plated onto collagen coated plates in William's E medium with additives (Table 5) with 10% Sera Plus

at a density of 75,000 cells/cm^2, allowed to attach for 3h, and washed twice with William's E medium. Non-parenchymal cells were then added to the attached hepatocytes in William's E medium with additives (Table 5) with 10% Sera Plus at a density of 37,500 cells/cm^2, allowed to attach for 3h, washed twice with William's E medium, upon which a final volume of fresh culture medium was added and cells were placed into the incubator.

B) **Collagen sandwich (S) –** freshly isolated hepatocytes were firstly plated onto a collagen gel in William's E medium with additives (Table 5) with 10% Sera Plus at a density of 75,000 cells/cm^2, allowed to attach for 3 h, and washed twice with William's E medium. Non-parenchymal cells were then added to the attached hepatocytes in William's E medium with additives (Table 5) together with 10% Sera Plus at a density of 37,500 cells/cm^2. Cells were allowed to attach for 3 h, washed twice with William's E medium, upon which a second layer of collagen gel was added to achieve a collagen sandwich as described for the hepatocyte cultures. After 40min of polymerization of the second gel layer, culture medium was added and cells were placed in the incubator.

2.2.3 *IN VIVO* MODELS OF LIVER DAMAGE, INFLAMMATION AND REGENERATION

All experiments were performed using male C57BL6/N mice (8-12 weeks old, Charles Rivers, Sulzfeld, Germany). The mice were fed ad libitum with Ssniff R/M-H, 10 mm standard diet. All experiments were approved by the local ethic committee. Experiments were performed as follows:

A) **CCl_4–induced acute liver damage model (CCl_4)** – mice received a single injection of CCl_4 (1.6 g/kg body weight) dissolved in 0.5 ml olive oil as previously described [174]. As controls, mice received a single injection of olive oil. The solutions were freshly prepared before the injection and mixed by vortexing. The volume injected was 4 ml/kg per mice. Liver tissue samples for protein extracts and RNA isolation were collected from: (i) 5 independent biological replicates at each of the CCl_4–treated timepoint (2h, 8h, day 1, day 2, day 4,day 6, day 8 and day 16), (ii) 5 independent solvent control mice injected with olive oil at each timepoint (day 1 and 3), and (iii) 5 independent untreated, control mice. Additionally, protein extracts and samples for RNA isolation were collected from hepatocyte-enriched fraction obtained from 3 independent freshly-perfused, mice livers after CCl_4–treatment at each timepoint (days 1 and 3).

B) **Lipopolysaccharide–induced inflammation model (LPS)** – mice received a single intraperitoneal injection of LPS (750 ng/kg) dissolved in sterile PBS. Liver tissue samples for protein extracts and RNA isolation were collected from: (i) 5 independent biological replicates at 24 hours after single injection, and (ii) 3 independent untreated, control mice. Additionally, protein extracts and samples for RNA isolation were collected from hepatocyte-enriched fraction obtained from 3 independent freshly-perfused mice livers 24 hours after a single injection with LPS and the corresponding three independent freshly perfused untreated, control mice.

C) **70% Partial hepatectomy liver regeneration model (PHx)** – experiments were performed by our collaborators at the Department of General, Visceral and Vascular Surgery, University Hospital Jena, Germany [171]. All surgical interventions were performed under inhalation of 2% isoflurane mixed with an oxygen flow of 0.3 L/min (isoflurane vaporizer, Sigma Delta, UK) in an S1 operation room. A precise vessel-oriented, parenchyma-preserving surgical technique was used for 70% partial hepatectomy using a modification of the technique described by Madrahimov for rats [175]. The procedure started with a laparotomy via a transverse abdominal incision. The whole liver was well exposed by elevating the xiphoid process. Skin and muscle were fixed by retractors, and the small bowel was moved out to the left side of the abdomen and covered with saline soaked gauze. The liver was freed from the falciform ligament and the triangular ligamentum. The liver lobes were positioned so that the hilum of the left lateral lobe (LLL) and median lobe (ML) were clearly visible. All subsequent steps were performed using a stereo microscope with 10x magnification. A ligature (6-0 silk) was applied loosely to the pedicle of LLL. The ligature was tightened, keeping a distance of about 3 mm from the cava while the LLL remained in its anatomical position and the lobe resected. Next, a cholecystectomy was performed after double ligating the cystic duct and cystic artery using a 7-0 prolene suture. For resection of the median lobe, a virtual line was drawn between the left side of the cava and the gallbladder. The clamp was placed roughly perpendicular to the surface of the left median lobe (LML), about 3mm lateral to this line and the left median lobe was removed. Proximal to the clamp, a piercing suture was positioned according to the vascular anatomy in order to ligate the left median hepatic vein and the clamp was removed. The right median lobe (RML) was also similarly clamped. After resection, two piercing sutures were placed to ligate the right and median hepatic veins as well as the arterial and portal supply. Finally, the abdomen was irrigated with warm saline solution and closed with a two layer running suture (6-0 prolene). At the end of the anesthesia, animals were allowed to recover on a heating pad. Temgesic (0.05 mg/kg) was applied subcutaneously after operation and at an interval of 12 hours over the next 3 days. Body weight and activity were monitored daily using a scoring system [176]. Briefly, mice with normal activity, physiological position, no jaundice, and no signs of bleeding were regarded as healthy (+++); animals showing a weaker activity, hunched back position and/or signs of jaundice or bleeding were regarded as weak (++); and animals with no spontaneous activity and lying position and signs of jaundice or bleeding were regarded as severely ill (+). Liver tissue samples for protein extracts and RNA isolation were collected from three independent biological replicates at each of the timepoints (1h, 6h, 12h, day 1, day 2, day 3, day 4, one week, two weeks, four weeks and three months). Sections of about 0.5 cm^2 were snap frozen in liquid nitrogen and stored at -80°C for subsequent isolation of proteins or RNA.

For liver tissues samples, mice were anesthetized at the indicated timepoints and the liver was resected, washed in ice cold PBS and sectioned for further analysis. Sections of about 0.5

cm^2 were snap frozen in liquid nitrogen and stored at -80°C for subsequent isolation of RNA and proteins (described in chapter 2.2.4.1 and 2.2.7.1 respectively).

For freshly isolated hepatocyte-enriched fraction, one million cells in suspension medium were used for subsequent isolation of RNA and proteins (described in chapter 2.2.4.1 and 2.2.7.1 respectively).

2.2.4 RNA ISOLATION AND cDNA SYNTHESIS

2.2.4.1 RNA ISOLATION FROM PRIMARY HEPATOCYTES AND LIVER TISSUE

The RNA was isolated from cultured hepatocytes and from mouse liver tissue using the Phenol/Chloroform method and QIAzol Lysis Reagent according to the Qiagen manufacturer's description:

A) **Freshly isolated hepatocytes**: 1 million cells in suspension medium were centrifuged at 3,000 rpm, at 4°C for 5 min. The supernatant was quickly removed and the cell pellet was lysed in 1 ml of QIAzol by 10 repetitive aspirations in a micropipette.
B) **Primary hepatocytes from *in vitro* cultures:** culture medium was removed and the cells were lysed with 1mL QIAzol with a cell scraper and subsequently micropipetted into a pre-cooled, sterile 1.5ml tube that was kept on ice. For liver tissue, snap frozen sections were lysed in a 1.5 ml tube with 1 ml QIAzol using a plastic pestle and subsequent sonication on ice.
C) **Spheroids:** all micro-tissues were collected from three independent plates by gently passing the hanging drops into a sterile Petri dish. The spheroids were concentrated by swirling the dishes, collected with a micropipette and transferred to a 1.5 ml tube. After sedimenting for 10 minutes on ice, the medium was removed and the microtissues were lysed in 500 µl QIAzol.
D) **Snap frozen liver tissue:** sections of about 0.5 cm^2 liver tissue were lysed in 1 ml QIAzol and homogenized with a plastic pistol while kept on ice.

All samples homogenized in QIAzol reagent were subsequently sonicated for 30s on ice. For every 1 mL QIAzol, 0.2 ml chloroform was added and the samples maxed vigorously for 15 s. Samples were kept at room temperature for 2–3 min for thorough phase separation and later centrifuged at 12,000 G for 15 min at 4°C. After centrifugation, the samples separate into 3 phases: an upper, colorless, aqueous phase containing RNA; a white interphase; and a lower, red, organic phase. The upper, aqueous phase was transferred into a new tube containing 0.5 ml isopropanol (per 1 mlQIAzol) and mixed thoroughly. All tubes were incubated at room temperature for 10 min and centrifuged at 12,000 xg for 10 min at 4°C. The supernatant was discarded and the RNA pellet was resuspended in 1 mL of 100% ethanol and centrifuged at 7,500 xg for 5 min at 4°C. The supernatant was discarded and the RNA pellet was resuspended in 1mL of 75% ethanol and centrifuged at 7,500 x g for 5 min at 4°C. Finally, supernatant was removed and RNA pellet was air-dried for 30 min and re-dissolved in an appropriate volume of

RNase-free water (10-30 µL). RNA concentration and integrity were determined spectrophotometrically using a Nanodrop 2000. The extracted RNA was stored at -80°C until further analysis.

2.2.4.2 Reverse Transcription Polymerase Chain Reaction (RT-PCR)

For the complementary DNA synthesis, 2 µg of RNA were transcribed using TGRADIENT thermocycler with the High Capacity cDNA reverse transcription kit. The reaction mixture for cDNA synthesis is specified in Table 16. The PCR conditions were programmed for 25°C for 10 min, 37°C for 120 min, followed by 85°C for 5min for all PCR reactions. The resulting cDNA were diluted with DEPC-treated water to a final concentration of 10 ng/ µl and stored at -20°C.

TABLE 16: COMPOSITION OF THE REACTION MIXTURE FOR cDNA SYNTHESIS

Master mix	
10x RT-Buffer	2µl
25x dNTP	0.8µl
Random primer	2µl
Reverse transcriptase	1µl
H_2O	4.2µl
Total volume 1	**10µl**
RNA	2µg
H_2O up to	10µl
Total volume 2	**10µl**
Final total volume	**20µl**

2.2.5 QUANTATIVE REAL TIME PCR (qRT-PCR)

The quantitative real-time RT-PCR (qRT-PCR) was performed using Taq-Man-PCR technology with a 7500 Real-Time PCR System using TaqMan® Universal Master Mix II, with UNG. All reagents were purchased from Applied Biosystems. All TaqMan primer probes used are listed in Table 8. Samples were run in duplicates. 25ng of transcribed cDNA was mixed with 17.5 µl of qRT-PCR reaction mixture (Table 17). The conditions for all qRT-PCR reactions are specified in Table 18. For all PCR analyses, a no-template negative control was included. PCR products were analyzed with the 7500 Real-Time PCR System software.

TABLE 17: COMPOSITION OF THE REACTION MIXTURE FOR qRT-PCR

Kit	**µl for 1 sample**
TaqMan Master Mix	10 µl
DEPC H_2O	6.5 µl
TaqMan primer probe	1 µl

TABLE 18: THERMOCYCLER PROGRAM FOR qRT-PCR REACTION

Stage	Temperature [°C]	Time	Repetitions
1	50	2 min	1
2	95	10 min	1
3	94	15s	40
	60	30s	
	72	35s	
4	95	15s	1
	60	20s	
	95	15s	
	60	15s	

The relative mRNA content was normalized to glyceraldehyde-3-phosphate dehydrogenase (GAPDH) mRNA expression in each sample. For mouse and rat studies, the expression levels in freshly isolated hepatocytes and hepatocytes in culture were normalized to the levels of healthy liver tissue. For human studies, the expression levels of cultivated hepatocytes were normalized to freshly isolated hepatocytes. For calculations of relative gene expression, the $2^{-\Delta\Delta Ct}$ method was used [177] as described in Table 19. The results shown correspond to means of three independent cell batches or tissues preparations unless otherwise described.

TABLE 19: CALCULATIONS STEPS FOR ANALYZING qRT-PCR RESULTS

Calculation step	Formula
1.	ΔCt1 = Ct Gene of interest (GOI) – Ct Housekeeper gene (HKG)
2.	ΔCt2 = Ct GOI of control samples – Ct HKG of control samples
3.	ΔΔCt = ΔCt1 – ΔCt2
4.	Calculation of $2^{-\Delta\Delta Ct}$

2.2.6 AFFYMETRIX GENE ARRAY ANALYSIS

The RNA samples from the cultivation systems and all three *in vivo* models were further analyzed in time resolved global gene expression profiling [78]. RNA concentration and integrity of all samples were determined spectrophotometrically using a Nanodrop 2000 and a Bioanalyzer respectively. For global gene expression profiling in murine and human hepatocytes, Affymetrix Mouse GenChip® Genome 430 2.0 arrays and GeneChip® Human Genome U133 Plus 2.0 array were used, respectively. All labeling reagents and instrumentation regarding microarrays were acquired from Affymetrix.

A total of 100ng RNA were transcribed into cDNA by oligo dT primers, and reverse transcribed to biotinylated cRNA with the GeneChip 3' IVT Express Kit. After 16 hours of *in vitro* transcription, the amplified RNA was purified using magnetic beads and 15 µg of amplified RNA was fragmented with the fragmentation buffer using Affymetrix's protocol. In the next step, 12.5 µg of labeled and fragmented cRNA was hybridized to Mouse Genome 430 2.0 Affymetrix

GeneChips along with a hybridization cocktail and placed in a hybridization oven rotating at 60 RPM at 45 ºC for 16 h. Microarrays were washed using an Affymetrix fluidics station 450 and stained initially with streptavidin-phycoerytherin. For each sample, the signal was further enhanced by incubation with biotinylated goat anti-streptavidin followed by a second incubation with streptavidin-phycoerytherin, and a second round of intensities were measured. Microarrays were scanned with an Affymetrix Gene-Chip Scanner-3000-7G controlled by GCOS software. Mouse Genome 430 2.0 Affymetrix GeneChips contain over 45,000 probe sets from over 34,000 well-characterized mouse genes. Human Genome U133 Plus 2.0 Affymetrix GeneChips contain 54,000 probe sets including more than 38,500 well-characterized genes. GeneChips microarray study followed MIAME guidelines issued by the Microarray Gene Expression Data group.

2.2.6.1 MICROARRAY PROCESSING AND STATISTICAL ANALYSIS

Biostatistical analysis was performed by our collaborators at the Leibniz Institute for Natural Product Research and Infection Biology Hans-Knöll-Institute (HKI) in Jena, Germany. Affymetrix gene expression data were pre-processed using 'affyPLM' packages [178] from the Bioconductor Software [179]. The pre-processed dataset was analyzed for differential gene expression using linear models with least squares regression and empirical Bayes moderated t-statistics of the LIMMA (Linear Models for Microarray Data) package [180] of Bioconductor software [179] for the statistical programming language R [181]. The obtained p-values were adjusted for multiple comparisons using the Benjamini Hochberg false discovery rate correction (FDR) [182]. Data obtained from fresh hepatocytes were used as reference. The custom chip definition file from Brainarray [183] based on Unigene ID's was used to annotate the microarrays. A dual selection criteria (p-value < 0.05 and an absolute fold change > 2) was chosen as significance level to detect differentially expressed genes (DEGs). Processing and visualization (Principal Component Analysis) of data were performed using MATLAB tools (The MathWorks Inc., Natick, MA).

2.2.6.2 FUZZY CLUSTERING OF GENE EXPRESSION PROFILES

The time-profiles of the differentially expressed genes in cultivated mouse hepatocytes were scaled between their respective absolute temporal extreme values to focus on subsequent cluster analysis on the qualitative behavior of the expression profiles. The time series were clustered using fuzzy c-means [184] (fuzzy exponent = 1.5; maximum number of iteration = 200; minimum cost function improvement = 10-10). The optimum number N of cluster was estimated by repeated calculation (number of iterations = 100) of the fuzzy cluster index 'Separation Index'.

2.2.6.3 GENE ONTOLOGY (GO), WIKI AND KEGG PATHWAY ANALYSES

Genes which show change ratios greater (or less) than 2-fold in the triplicate arrays at any one of the timepoints have been considered as up or down-regulated and subjected to gene ontology (GO) and pathway analyses. Differentially regulated genes were categorized using the manually curated Gene Ontology of the Biobase Knowledge Library (BKL) of the ExPlain™ webservice (BioBase GmbH, Wolfenbüttel, Germany).

2.2.6.4 PROMOTOR ANALYSIS

To identify transcription factors (TFs) whose binding sites are enriched in a given set of promoters, the algorithm PRIMA (PRomoter Integration in Microarray Analysis; [185]) of the Expander Software 6.1 (EXPression ANalyzer and DisplayER; [186]) was used. Genes that show a fold change greater than 2-fold (p-value cut off is 0.05) were used for analysis. All genes from the mouse (Ensembl release 42) were used as the background set; the threshold of the p-value was set to 0.01 and the region was scanned from -3000 to +200. The results are shown as a snapshot in Figure 34.

2.2.6.5 SPEARMAN'S RANK CORRELATION ANALYSIS

To calculate the strength of the relationship between cultivation (M_C, M_S, S) and the *in vivo* models CCl_4, PHx and LPS, we used Spearman's rank correlation. The changes in gene expression at different timepoints in cultivation (M_C, M_S, S) versus changes in CCl_4, PHx and LPS were used for the calculation of the correlation coefficients.

2.2.6.6 METAGENE ANALYSIS

The 'inflammation' and 'metabolism' metagenes were obtained as follows: (i) The overlap between deregulated genes (2-fold, p≥0.05, FDR adjusted) of all culture systems (M_C, M_S, S) and all *in vivo* models (CCl_4, PHx, LPS) at day 1 was determined. This resulted in 74 genes; (ii) of these 74 genes, 19 and 28 belonged to the 'inflammation' and 28 'metabolism' clusters, respectively, as defined in Table 22 and Table 23. The 19 inflammation- and 28 metabolism-associated genes were used to calculate the 'inflammation' and 'metabolism' metagenes, respectively; and (iii) for this purpose, the expression level of each gene was normalized in the following way: the mean value (of the normalized gene expression values) of the 19 inflammation-associated genes was defined as the ´inflammation` metagene. The same technique was applied to the metabolism-associated genes. This calculation was performed in each independent biological replicates (n=3 for cultivation and freshly isolated hepatocytes; n=5 for CCl_4, PHx and LPS). For the *in vitro* samples, (M_C, M_S, S) the metabolism and inflammation metagenes were calculated using deregulated genes after 1 day in culture. Similarly, *in vivo* samples (CCl_4, PHx and LPS) were analyzed one day after administration of CCl_4, LPS or after performing PHx. The timepoint of 1 day was chosen because this represents the earliest timepoint where a strong correlation (r>0.6) between all genes deregulated *in vivo* and *in vitro* was obtained (Figure 41). In contrast, for proliferation-associated genes the correlation between *in vitro* and *in vivo* did not occur before two days after cultivation or *in vivo*

intervention (CCl_4, PHx) (Figure 43). This was not unexpected because it is well known that proliferation of hepatocytes in mice only occurs approximately 2 days after administration of CCl4 or PHx (Hoehme 2010). Therefore, all calculations for the proliferation metagene shown were calculated using the expression values of commonly deregulated genes (Table 24) on day 2 in culture, and in the *in vivo* models CCl_4 and PHx.

2.2.7 WESTERN BLOT ANALYSIS

2.2.7.1 PROTEIN COLLECTION AND QUANTIFICATION

Protein extracts were performed as follows:

A) **Freshly isolated hepatocytes**: 1 million cells in suspension medium were centrifuged at 3,000 rpm, 4°C for 5 min. The supernatant was discarded and pelleted cells were lysed with 1 mL of ice-cold RIPA buffer (Table 9) by thorough mixing (3-5 times) with a pipette and kept on ice.
B) **Primary hepatocytes from *in vitro* cultures:** culture medium was gently removed and cells were lysed with 300 µl of ice-cold RIPA buffer. Cells were scraped and collected in 1.5 ml tubes kept on ice.
C) **Snap frozen liver tissue:** sections of about 0.5 cm^2 of liver tissue were lysed with 1 mL of ice-cold RIPA buffer and homogenized with a plastic pistol while kept on ice.

Afterwards, all collected samples were sonicated for 30s while kept on ice. The homogenates were further incubated on ice for 30 min, and centrifuged for 10 min at 13.000 rpm at 4°C. The clear supernatant containing solubilized proteins was collected in pre-chilled 1.5 ml tube and stored at -20 °C until further analysis. The pellet containing most of the collagen and insoluble proteins was discarded. The protein concentration in the collected supernatants was determined using a bicinchoninic acid (BCA) protein assay. Protein concentration was calculated for the average value of three counts and related to the protein standard curve.

2.2.7.2 SDS/PAGE ELECTROPHORESIS

30 to 50 µg of protein extract adjusted to 30 µl volume with sterile water were heat denaturated under reducing conditions for 5 min at 95 °C with 6 µl Laemli buffer (5x). Afterwards, the samples were shortly centrifuged at 13.000 rpm. For electrophoresis, 10% SDS-PAGE gels with a 1.5 mm x 10 wells or 1.5 mm x 15 wells were used. Components of a 10% SDS-PAGE gel are listed in the Table 20. To correctly estimate the molecular weight of separated proteins expressed in samples, two different protein standard markers (4 µl of both Precision plus protein standard and MagicMark TM XP Western Protein Standard) were additionally loaded on the 10% SDS-PAGE gel (inserted with a 1.5 mm x 10 wells or 1.5 mm x 15 wells comb) in the first two lanes. The remaining samples were then loaded into the following lanes of the

gel and casted in the Bio-Rad Mini PROTEAN Tetra System filled with 1X running buffer. The electrophoresis was carried out using a Biometra Standard Power Pack P25 for about 3 hours at a constant voltage of 25 mA/gel.

TABLE 20: COMPONENTS OF A 10% SDS GEL

Separation gel (10%)		**Stacking gel**	
	1 Gel		**1 Gel**
H_2O	3.2 ml	**H_2O**	2.4 ml
Acrylamide	2.64 ml	**Acrylamide**	0.5 ml
Separation buffer	2 ml	**Stacking buffer**	0.4 ml
10% SDS	80 µl	**10% SDS**	32.5 µl
TEMED	3.2 µl	**TEMED**	2.5 µl
10% APS	80 µl	**10% APS**	50 µl

2.2.7.3 WESTERN TRANSFER

Protein transfer was performed using a semi-dry Fastblot B44 blotting system with a 5x8 cm size gel-membrane sandwich containing from the bottom: 12pieces of Whatman blotting paper equilibrated in the anode buffer, PVDF transfer membrane activated in methanol, SDS-PAGE gel with resolved proteins and 4 pieces of Whatman blotting paper equilibrated in the cathode buffer. Blotting was performed with Biometra Standard Power Pack P25 for 40 min at a constant current of 250 mA/gel-membrane sandwich. The membranes were then washed in distilled water and stained with Ponseau S in Triclorite acid for 1 minute to visualize successful transfer of proteins. Finally, Ponseaus S stain was removed by thorough washing of membranes with TBS-T for 5 min.

2.2.7.4 IMMUNODETECTION OF PROTEINS

For detection of proteins, the blotting membranes were later blocked for 1h with 5% BSA in TBS-T buffer (pH 7.2) at room temperature, followed by overnight incubations at 4°C with primary antibodies enlisted in Table 12 diluted in 5% BSA-TBS-T. Afterwards, the membranes were washed three times in TBS-T buffer at room temperature for 10 min each, followed by an incubation step with horseradish peroxidase-labeled secondary antibodies (Table 13)), which were incubated in 5% BSA-TBS-T for 1 h at room temperature. Subsequently, the membranes were washed three times in TBS-T, 10 min each, at room temperature. Bands were detected by chemiluminescence using the Western Lightning ECL substrate in a Fusion-FX7 imager equipped with a CCD camera. Membranes were then washed in TBS-T for 5 minutes and probed antibodies were stripped of the membranes by 45 min incubation with the stripping buffer followed by a washing step of 5 minutes in TBS-T. Complete removal of all antibodies was ensured by additional control imaging of the membranes.

2.2.8 MULTIPLEX ANALYSIS OF SIGNAL TRANSDUCTION (LUMINEX SCREENING)

Luminex screening was performed by our collaborators at the Systems Biology of Molecular Networks Department at the Institute of Pathology of the Charité Medical University in Berlin, Germany. Protein extracts were collected using the Bio-Plex Cell Lysis Kit following the manufacturer's instructions:

A) **Freshly isolated hepatocytes**: 1 million cells in suspension medium were centrifuged at 3,000 rpm, 4°C for 5 min. Supernatant was discarded and pelleted cells where lysed with 500 µL of lysis buffer with additives (Table 10) by thorough mixing (3-5 times) with a pipette and kept on ice.
B) **Primary hepatocytes from *in vitro* cultures:** culture medium was gently removed and cells were washed 3 times with ice-cold Bio-Plex Cell Wash Buffer. Afterward cells were lysed with 500 µL of lysis buffer with additives, collected with a cell scraper and re-pipetted into pre-chilled 1.5mL tubes.
C) **Snap frozen liver tissue:** sections of about 0.5 cm^2 liver were lysed with 500 µL of lysis buffer with additives and homogenized with a plastic pistol while kept on ice.

Afterwards, all collected samples were sonicated for 30 s while kept on ice. The homogenates were further incubated on ice for 30 min, and centrifuged for 10 min at 13.000 rpm at 4 °C. The clear supernatant containing solubilized proteins was collected in pre-chilled 1.5 ml tube and stored at -20 °C until further analysis. The pellet containing insoluble proteins was discarded. The protein concentration in the collected supernatants was determined using a bicinchoninic acid (BCA) protein assay. Protein concentration was calculated for the average value of three counts and related to the protein standard curve. Afterwards, an aliquot from each sample was normalized to a concentration of 1 µg/µl in 100 µl with the lysis buffer with additives. Phospho-protein levels were analyzed using the Bio-Plex system with total protein amount of 25 µg per sample and Multi-Plex-Assay consisting of antibodies against p-Akt (Ser473), p-c-jun (Ser63), p-ERK2(Thy185/Thr187), p-GSK3α/β (Ser9/Ser21), p-Hsp27 (Ser78), p-JNK (Thy193/Thr185), p-MEK1 (Ser217/Ser221), p-NFκB (Ser536), p-p38 (Thr180/Thy182), p-p70S6K (Thr421/Ser424) and pSTAT3 (Ser727). The assay was performed according to the manufacturer's instructions with minor modifications (beads and detection antibodies were diluted 4-fold). All antibodies were purchased from Cell Signaling (Cell Signaling, New England Biolabs GmbH, Frankfurt am Main, Germany).

2.2.9 HEMATOXYLIN-EOSIN STAINING OF HEPATOCYTES

Primary mouse hepatocytes from standard or Percoll purified preparations were allowed to attach to collagen coated glass slides for 3 h, washed two times with sterile PBS, and fixed with 4%paraformaldehyde in PBS, 15 min at room temperature. Afterwards, cells were

permeabilized with 0.5% triton X-100 in PBS (15 min, room temperature) and washed three times in PBS (5 min, room temperature). The slides were briefly soaked in distilled water, stained with Hematoxylin (7.5 g/l) for 1 min at room temperature, and washed in distilled water for 15 min. The slides were shortly soaked in 1% HCl in 70% ethanol, stained with Eosin (1%) for 1 min, and washed in distilled water for 10 min. Afterwards, the samples were dehydrated by sequential incubation using increasing concentrations of ethanol (50%, 70%,90% and 100%, 2 min in each solution). Finally, the slides were incubated in Roti-Histol for 2-3 min, mounted onto glass slides with Entellan and air-dried overnight. Hepatocytes and non-parenchymal cells were identified with bright field microscopy, and 10 randomly selected fields were counted (20X magnification).

2.2.10 IMMUNOFLUORESCENCE

Primary mouse hepatocytes were plated onto collagen-coated glass slides and allowed to attach for 30 min (representing freshly isolated hepatocytes) or cultivated for a period of 1, 3, 5 or 7 days in M_C, M_S or S configurations in 12 well culture plates as previously described. After the indicated timepoints, the medium was removed, the cells were immediately fixed with 4% paraformaldehyde in PBS for 15 min at 37°C. Afterwards, the cells were permeabilized using 0.5% Triton X-100 in PBS for 15 min at room temperature, and washed three times with PBS, 5 min each. From here on, all incubations were performed in a humidified chamber. Unspecific binding sites were blocked by incubating with a blocking solution containing 3% BSA / 0.1% Tween 20 in PBS for 1 h at room temperature. Afterwards, the blocking solution was removed, and the cells were incubated overnight at 4 °C with the following antibodies in 0.3% BSA / 0.1% Tween®20 in PBS: anti-HNF4α, anti DPPIV. Subsequently, the antibody solutions were removed and samples were washed three times for 10 min with PBS at room temperature. Afterwards, the samples were incubated for 1 h at room temperature with the following secondary antibodies labeled with Alexa 555 or Alexa 647 (for detection of HNF4α or DPPIV, respectively) dissolved in 0.3% BSA / 0.1% Tween20 in PBS. For staining the stress fibers (F-actin) and nuclei, cells were incubated with a mixture of rhodamine-labeled phalloidin at 2 U/mL and DAPI at 0.5 ng/µL in PBS for 20 min at room temperature, respectively. Afterwards, slides were washed three times with PBS for 10 min each, and mounted onto SuperFrost Plus microscopic slides using FluorPreserve™ Reagent, allowed to air dry for 30 min at room temperature, and fixed with nail polish. Afterwards, slides were kept at 4°C until imaging.

For HNF4α staining, the samples were analyzed using an Olympus BX41 epifluorescence microscope, and images were acquired using the Cell^F software. For DPPIV and rhodamine labeled phalloidin stainings, the images were acquired on a Olympus FV-1000. Detailed description of microscopes is provided in Table 3. The excitation and emission wavelengths were used as specified by the manufacturer. The colors assigned to DPPIV, rhodamine-labeled phalloidin and DAPI were green, red and blue, respectively.

3. RESULTS

3.1 RAPID TRANSCRIPTIONAL RESPONSES ARE INDUCED IN PRIMARY MOUSE HEPATOCYTES UPON ISOLATION AND CULTIVATION

3.1.1 INFLUENCE OF THE EXTRACELLULAR MATRIX CONFIGURATION ON THE MORPHOLOGY OF CULTIVATED MOUSE HEPATOCYTES

To gain insight into the molecular effects of hepatocyte isolation and cultivation, time resolved global gene expression profiling using Affymetrix microarrays was carried out in: (i) collagen sandwich cultures (S), (ii) confluent (M_C) as well as subconfluent (M_S) monolayer cultures. For this purpose, primary mouse hepatocytes were cultivated in biological triplicates under the indicated conditions for up to one week and samples intended for whole genome expression profiling were collected at 1, 2, 3, 5 and 7 days after plating.

Primary hepatocytes *in vitro* acquire a profoundly distinguishable morphology depending on the extracellular matrix used as the culture substratum. In the presented study, all three culture systems show well-reported morphological features (Figure 18, A). Hepatocytes in M_S culture acquire a fibroblast-like morphology that becomes more prominent at late timepoints. M_C cultures maintain a cuboidal morphology during the first day in culture. However EMT features [115, 187] are also observed from day 7 in culture.

hepatocytes present the most stable morphology resembling the *in vivo* phenotype. They appear more differentiated, as evidenced by the *in vivo*-like cuboidal shape and distinct bile canaliculi network formation, even after longer periods in culture.

Confocal microscopy reveals structural details of cultivated hepatocytes (Figure 18, B). In M_S culture, actin (stained in red) forms stress fibers such as microspikes associated with lamellipodia and filopodia [188] indicating typical features of epithelial to mesenchymal transition (EMT). The bile canaliculi marker DPPIV (stained in green) is observed as diffusely distributed all over the membrane, consistent with a loss of normal hepatocyte polarity in this culture configuration. In M_C, hepatocytes preserve some degree of polarity, indicated by the preferential localization of DPPIV at cell-cell contacts. Nevertheless, microspikes of actin clearly occur at cell borders. In sandwich-cultured hepatocytes, actin fibers accumulate around the bile canaliculi and also discretely at cell borders. However, they do not form microspikes. Moreover, DPPIV staining is strongly visible at bile canaliculi, showing a high degree of colocalization with f-actin, which is revealed by the yellow color (merged of red actin and green DPPIV). In conclusion, primary hepatocytes showed the expected morphology over the entire cultivation period, including bile canaliculi formation by sandwich cultures and epithelial-to-mesenchymal transition (EMT) in M_C and even more pronounced in M_S [115].

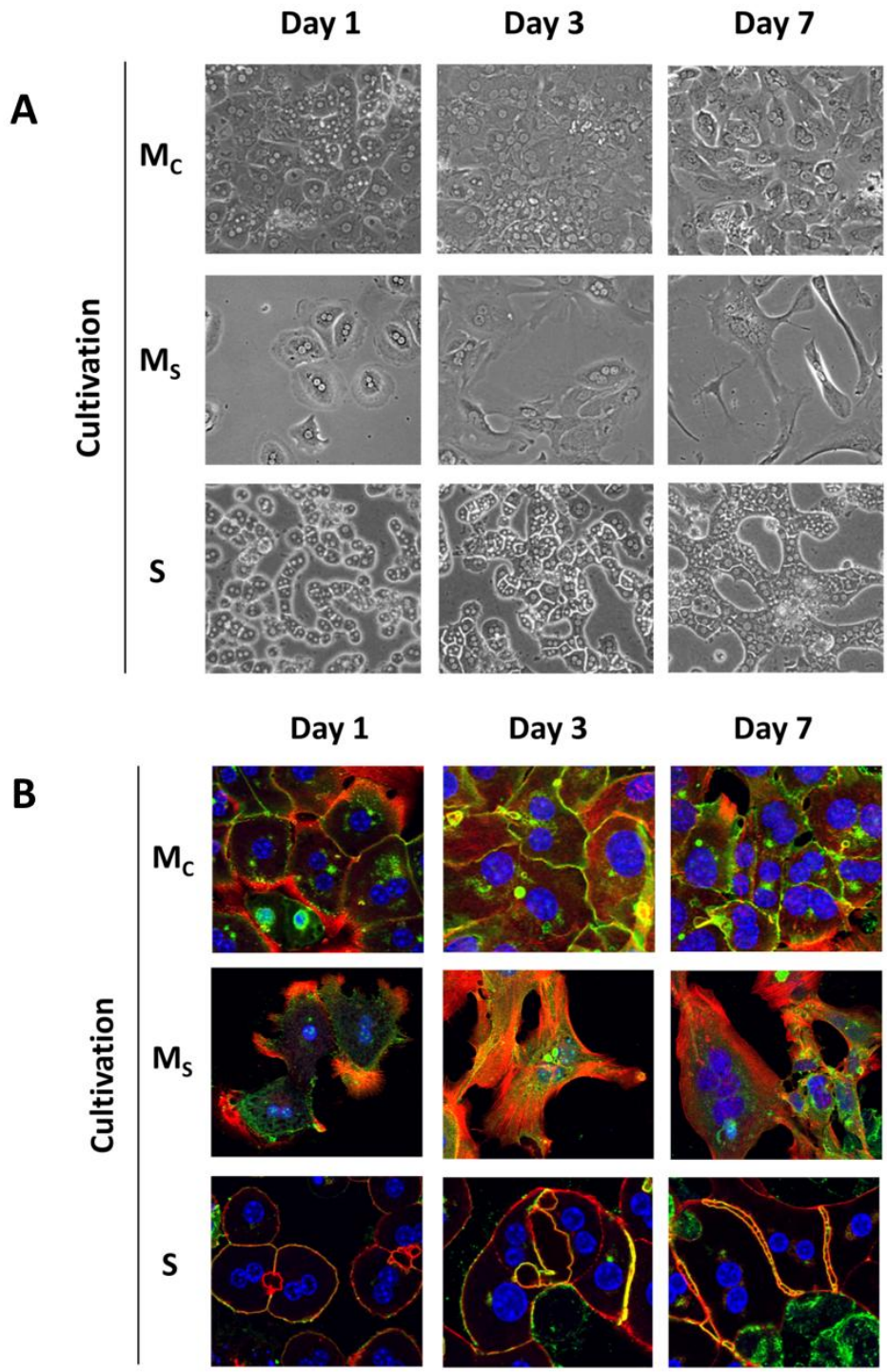

FIGURE 18: DIFFERENT EXTRACELLULAR MATRIX CAUSES MORPHOLOGICAL CHANGES IN PRIMARY MOUSE HEPATOCYTES *IN VITRO*

A) Light microscopy shows typical morphology of primary hepatocytes in three culture systems: monolayer confluent (M_C), monolayer subconfluent (M_S) and Sandwich (S) cultures, for the indicated periods of time. Magnification of 20X. B) Confocal microscopy reveals structural details in cultivated primary hepatocytes. F-actin in red, DPPIV in green and nuclei in blue. Magnification of 40X.

3.1.2 GENE ARRAY ANALYSIS REVEALS PROFOUND ALTERATIONS IN CULTURE

After performing the gene array analysis in primary mouse hepatocytes, the obtained dataset was submitted to further gene bioinformatics analysis. One of the tools used to interpret the gene array data is a principal component analysis (PCA). The PCA reduces the dimensionality of the multivariate data set, making it possible to easily compare similarities and differences between samples and to determine whether samples can be grouped [189].

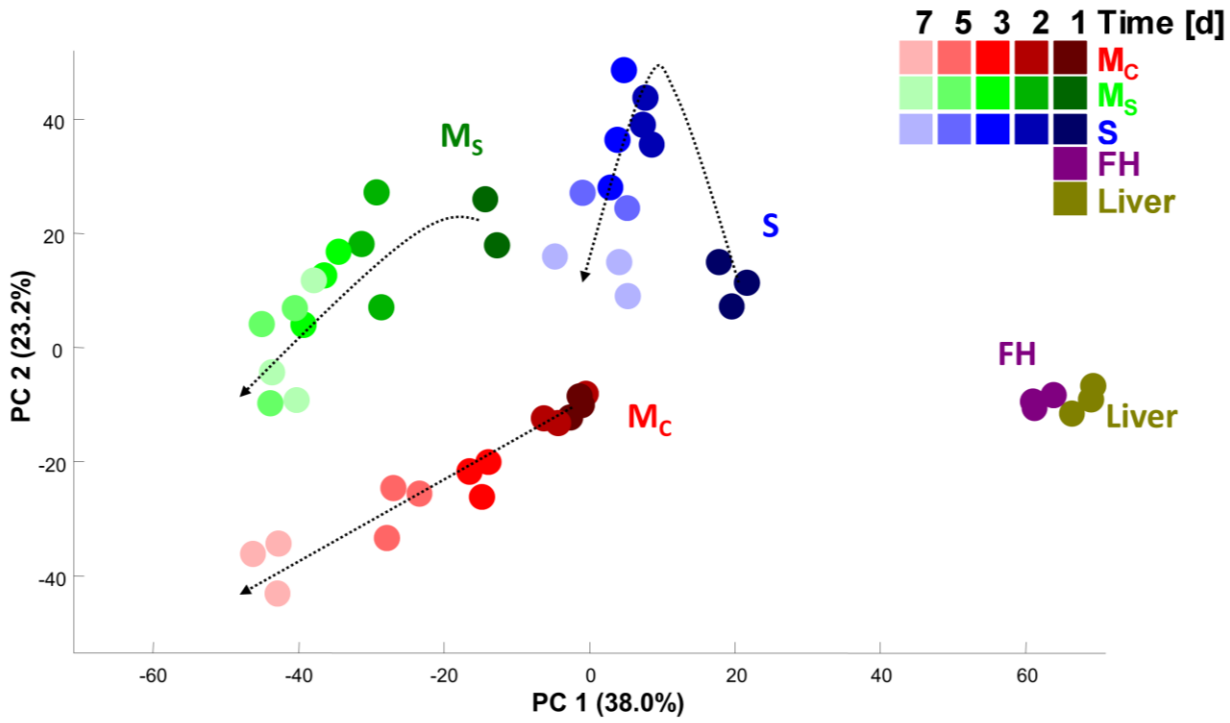

FIGURE 19: GENE ARRAY ANALYSIS REVEALS PROFOUND ALTERATIONS IN CULTURE
Alterations of gene expression, illustrated as principal component analysis, of cultivated hepatocytes (M_C, M_S and S), freshly isolated hepatocytes (FH) and liver tissue (Liver).

The PCA of the gene array data (Figure 19) represents directional changes in gene expression of primary mouse hepatocytes compared to a reference state of fresh liver tissue and freshly isolated hepatocytes (FH). This analysis reveals that the two-monolayer systems progressively deviate from fresh liver tissue and freshly isolated hepatocytes. Compared to all cultivation systems, only small differences were seen between liver tissue and FH. A different track of M_C and M_S culture illustrate that the state of confluency influences the extent of changes in gene expression.

In conclusion, the global gene expression profiling revealed profound alterations in all primary hepatocyte cultivation systems that result in a strong deviation from the *in vivo*-like state.

3.1.3 PRIMARY HEPATOCYTES *IN VITRO* SHOW RAPID EXPRESSIONAL CHANGES THAT OVERLAP BETWEEN ALL SYSTEMS

To determine the extent of expressional changes occurring in culture over time, the number of differentially expressed genes using two-fold change as a cut-off value was analyzed. The total number of differentially expressed genes (DEGs) (Figure 20) was lowest in sandwich cultures (n = 3296, ≥ 2-fold) compared to M_C and M_S (n = 4002 for M_C and n = 4287 for M_S; ≥2-fold).

	M_S	M_C	S
DEGs up and down (fold-2)	4287	4002	3296

FIGURE 20: AMONG CULTIVATION SYSTEMS, MONOLAYER SUBCONFLUENT (M_S) EXHIBITS THE HIGHEST EXPRESSIONAL CHANGES
Total number of differentially expressed genes (DEGs) in three culture systems: monolayer confluent (M_C), monolayer subconfluent (M_S) and sandwich (S) cultures.

The PCA analysis suggested that a massive alteration in gene expression occurs already at day 1 in culture. To determine the extent of the additional deregulated genes in culture, a more detailed analysis of DEGs on a day-by-day basis was employed. Figure 21 represents the number of DEGs in all culture systems, which are added to those deregulated at each preceding timepoint. It shows that in all culture systems the majority of alteration in the gene expression occurs during the first 24h. In line with the total number of DEGs, M_S represent a culture system with the highest dynamic of changes. In fact, 2257 genes were deregulated by day 1 in M_C with only 455 and 184 further added genes by day 2 and day 3, respectively. Sandwich cultures also show a dynamic expression pattern with 1551 genes of at least two-fold up or down by day 1. It should be mentioned that a high fraction of these genes is over ten-fold deregulated. These results suggest that the most important transcriptional alterations are determined early on in culture, i.e. during the first 24h after isolation.

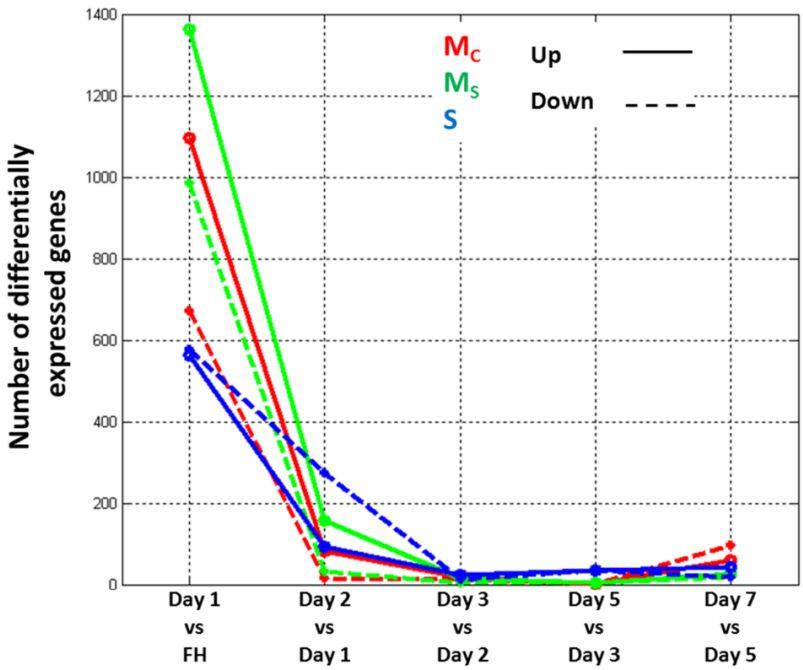

FIGURE 21: MOST OF THE GENE EXPRESSION CHANGES OCCUR WITHIN THE FIRST 24 HOURS OF CULTURE
Day-by-day analysis of differentially deregulated genes (DEGs) in three culture systems: monolayer confluent (M_C), monolayer subconfluent (M_S) and sandwich (S) culture for the indicated timepoints. The graph represents the number of up- or down-regulated genes which are added to those deregulated at each preceding timepoint.

The similar pattern of coordinates in the PCA space for all culture systems suggested that common expression profiles might be induced in all systems. Indeed, Venn diagrams reveal a high degree of overlap between genes up- or down-regulated (≥ 2-fold) in culture systems on Day 1 (Figure 22). Considering the differentiated morphology of sandwich cultures in contrast to the EMT-like morphology of monolayers, one may have expected a larger difference.

In conclusion, cultivation induces strong expressional changes that occur mostly within the first 24 hours. Nevertheless, the analysis of the differentially expressed genes proves that sandwich cultures offer clear advantages over monolayers maintaining a more stable profile of expressional changes.

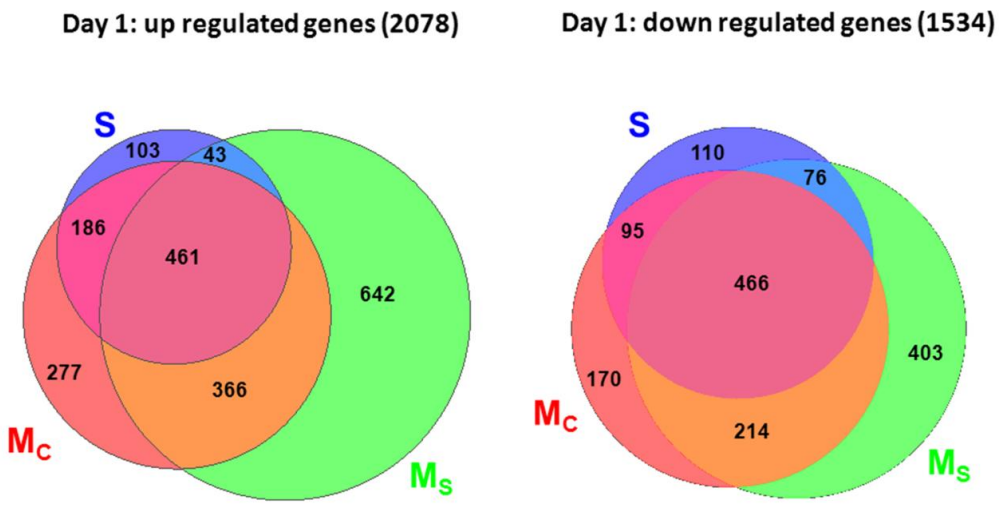

FIGURE 22: CULTIVATION CAUSES CHANGES OF AN OVERLAPING SET OF GENES AT DAY 1 IN ALL CULTURE SYSTEMS

Venn diagram of differentially expressed genes (DEGs, ≥ 2-fold) on day 1 in three culture systems: monolayer confluent (M_C), monolayer subconfluent (M_S) and sandwich (S) cultures. The number of genes in each overlapping segment indicates genes commonly deregulated.

3.1.4 ALL CULTURE SYSTEMS EXPRESS SIMILAR PATTERNS OF TOP UP- AND DOWN-REGULATED GENES

In the next step, the strongest (i.e. top) up- and down-regulated genes were analyzed. An overview of selected most up- and down-regulated genes in sandwich culture is shown in Table 21 together with references indicating their functions. The strongest up-regulated gene in sandwich culture is lipocalin-2 (Lcn2) with a 247-fold expression already at day 1. The strongest down-regulated gene in sandwich culture at day 1 with a more than 26-fold down-regulation is Cyp8b1, a member of the cytochrome P450 family.

TABLE 21: OVERVIEW OF SELECTED MOST UP- AND DOWN-REGULATED GENES IN SANDWICH CULTURE ON DAY 1

	Among most up-regulated genes:		**Sandwich (Day 1)**	
N°	**Symbol**	**Description**	**Fold**	**p-value**
1	**Lcn2**	Lipocalin 2 [130, 190, 191]	**247.1**	**7.33E-34**
2	**Mt4**	Metallothionein 4 [192]	**117.75**	**1.90E-21**
3	**Mt2**	Metallothionein 2 [192, 193]	**87.84**	**1.15E-33**
4	**Ier3**	Immediate early response 3 [194]	**34.67**	**2.10E-20**
5	**Saa3**	Serum amyloid A 3 [195, 196]	**32.16**	**1.46E-13**
6	**Mt1**	Metallothionein 1 [192]	**29.14**	**1.45E-26**
7	**Cebpd**	CCAAT/enhancer binding protein (C/EBP), delta [137]	**25.06**	**1.72E-17**
8	**Cpe**	Carboxypeptidase E [197]	**20.23**	**5.82E-14**
9	**Tnfrsf12a**	Tumor necrosis factor receptor superfamily, member 12a [198]	**18.05**	**1.34E-28**
10	**Klf6**	Kruppel-like factor 6 [199, 200]	**14.74**	**2.98E-19**

TABLE 21: CONTINUED

11	**Anxa2**	Annexin A2 [201]	**12.6**	**6.97E-24**
12	**Sprr1a**	Small proline-rich protein 1A [202, 203]	**8.59**	**7.09E-15**
13	**Psat1**	Phosphoserine aminotransferase 1	**4.42**	**5.53E-10**
14	**Ctgf**	Connective tissue growth factor [204]	**4**	**7.52E-10**
15	**S100a6**	S100 calcium binding protein A6 (calcyclin)	**2.2**	**5.55E-05**

	Among most down-regulated genes:		**Sandwich (Day 1)**	
N°	**Symbol**	**Description**	**Fold**	**p-value**
1	**Cyp8b1**	Cytochrome P450, family 8, subfamily b, polypeptide 1	**-26.78**	**2.18E-24**
2	**Sucnr1**	Succinate receptor 1	**-20.49**	**4.01E-23**
3	**Car3**	Carbonic anhydrase 3	**-14.88**	**7.54E-19**
4	**Slc17a3**	Solute carrier family 17 (sodium phosphate), member 3	**-8.79**	**9.16E-18**
5	**Abcb11 (Bsep)**	ATP-binding cassette, sub-family B (MDR/TAP), member 11 [37]	**-7.77**	**6.60E-14**
6	**Abat**	4-aminobutyrate aminotransferase	**-7.75**	**2.63E-13**
7	**Colec10**	Collectin sub-family member 10	**-7.75**	**1.73E-19**
8	**Hacl1**	2-hydroxyacyl-CoA lyase 1	**-7.13**	**1.53E-23**
9	**Apol7a**	Apolipoprotein L 7a	**-7.02**	**9.59E-11**
10	**Camk1d**	Calcium/calmodulin-dependent protein kinase ID	**-6.74**	**1.03E-18**
11	**Acsm5**	Acyl-CoA synthetase medium-chain family member 5	**-6.18**	**2.29E-13**
12	**Abca8a**	ATP-binding cassette, sub-family A (ABC1), member 8a	**-5.82**	**1.33E-10**
13	**Cyp7a1**	Cytochrome P450, family 7, subfamily a, polypeptide 1 [36]	**-5.42**	**1.33E-13**
14	**Abcc2 (Mrp2)**	ATP-binding cassette, sub-family C (CFTR/MRP), member 2 [37]	**-3.69**	**1.38E-12**
15	**Slco1a1**	Solute carrier organic anion transporter family, member 1a1	**-2.34**	**1.03E-08**

The results of the microarray analyses were confirmed by qRT-PCR (Figure 23) for a selected panel of genes (Table 21, red colored for chosen up-regulated and green colored for chosen down-regulated). All cultivation systems - sandwich (S), confluent (M_C) and subconfluent (M_S) - expressed similar pattern of up-regulation for Lcn2, Mt2 and Saa3 and down-regulation of Bsep, Mrp2 and Cyp7a1.

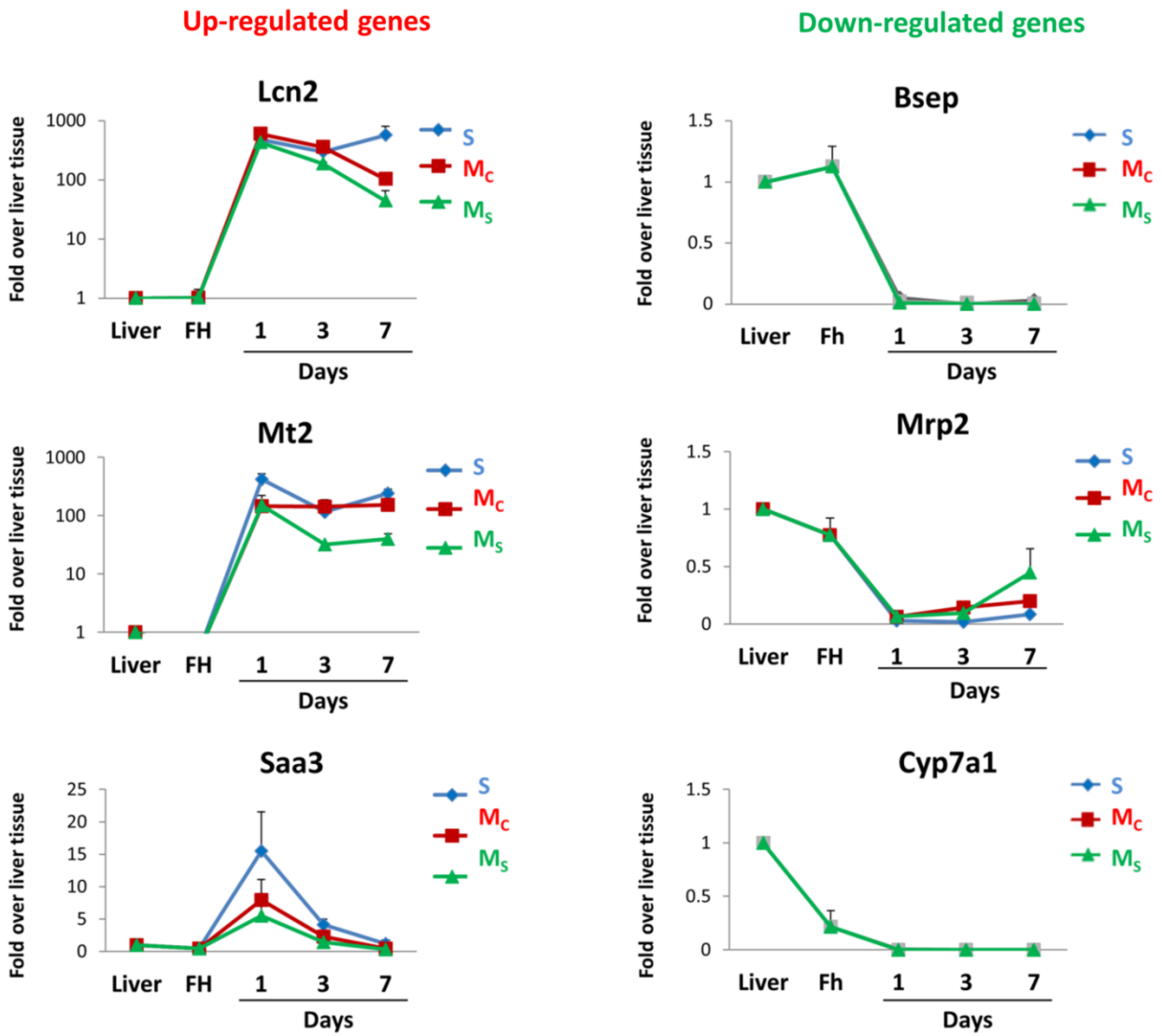

FIGURE 23: TOP UP- AND DOWN-REGULATED GENES ARE SIMILARLY DEREGULATED IN ALL CULTIVATION SYSTEMS
Quantitative RT-PCR analysis of inflammation- (Lcn2, Mt2 and Saa3) or metabolism-associated genes (Bsep, Mrp2 and Cyp7a1) in healthy liver tissue (Liver), freshly isolated hepatocytes (FH), hepatocytes in sandwich (S) culture, confluent (M_C) culture and subconfluent (M_S) culture for the indicated time. GAPDH was used as an endogenous control. Data are expressed as fold change relative to healthy liver tissue. Values represent mean ± SD (*n=3*).

Furthermore, the strong expression of lipocalin-2 was also detected at the protein level (Figure 24).

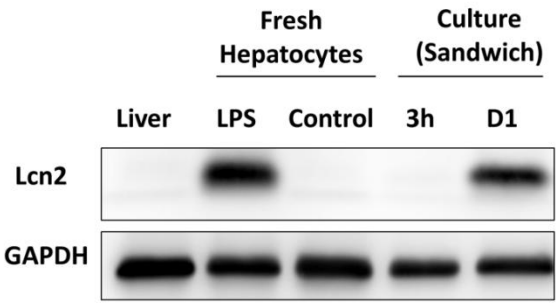

FIGURE 24: LCN2 PROTEIN IS UP-REGULATED IN SANDWICH CULTURE
Immunoblot analysis using antibody against Lcn2 in healthy liver tissue (Liver), freshly isolated hepatocytes and hepatocytes in sandwich (S) culture for the indicated time. GAPDH was used as an endogenous control. Protein extract from healthy liver tissue and freshly isolated hepatocytes were used as negative controls, while freshly isolated hepatocytes from mice treated for 24h with LPS (750 ng/kg, intraperitoneally) were used as positive controls. Representative images for 3 independent experiments are shown. Lcn2 expression is clearly observed in sandwich-cultured hepatocytes on day 1.

3.1.5 EXPRESSION OF TOP UP- OR DOWN-REGULATED GENES OCCURS EARLY IN CULTURE

As shown previously in Figure 21, the microarray data analysis reveals rapid gene expression changes within the first 24 hours in culture. Therefore, the aim of the next experiment was to determine the kinetics of the expression changes of the most up- and down-regulated genes in primary mouse hepatocytes cultivated in a collagen sandwich during the first hours after plating.

The induction of the most up-regulated genes and decrease in expression of the most down-regulated genes occur already in freshly isolated hepatocytes or at latest 3h after plating (Figure 25). These results confirm the interpretation of the gene array analysis, which suggested that the strongest transcriptional alterations already occur during the first hours of cultivation.

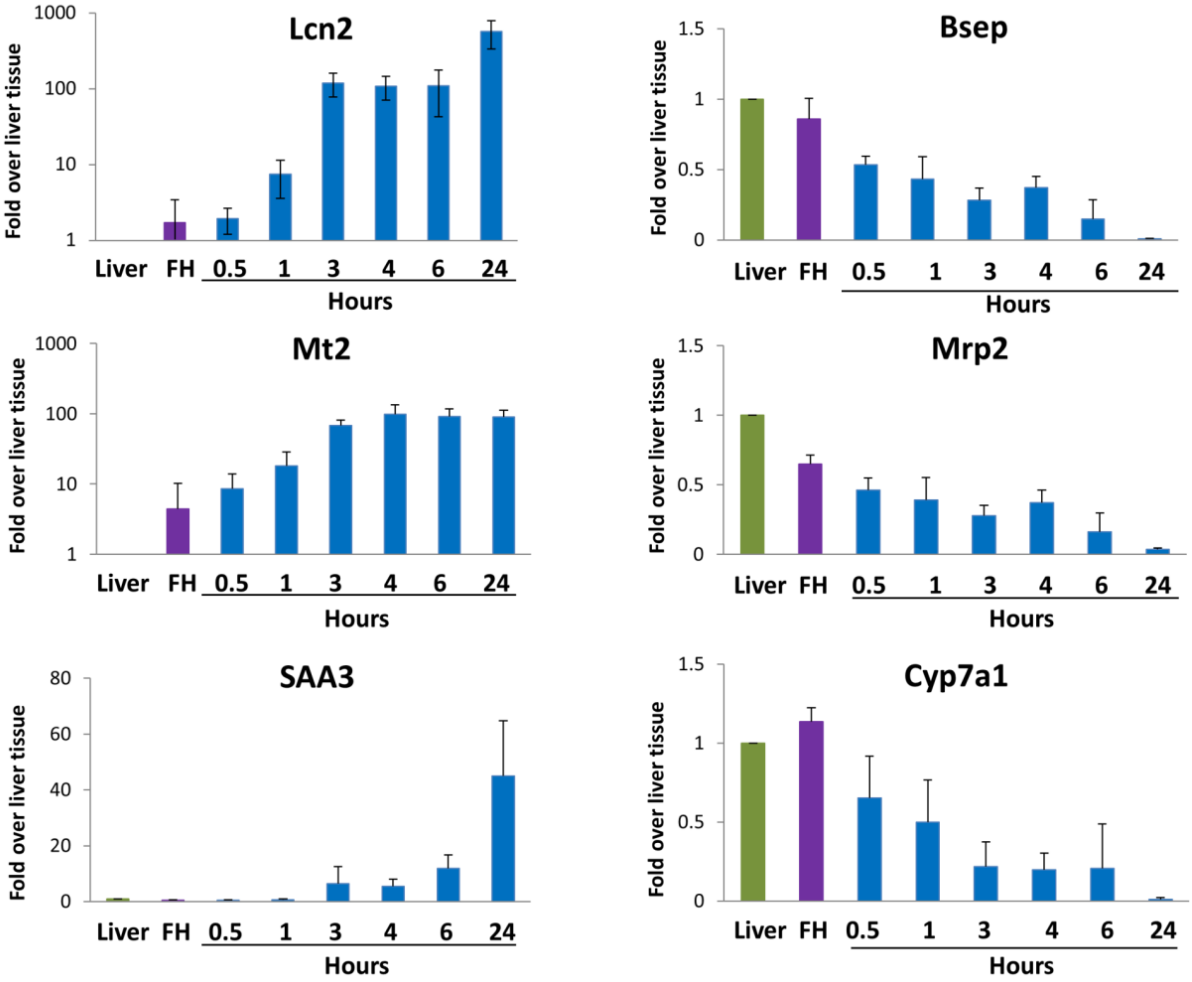

FIGURE 25: INDUCTION OF UP- AND DOWN-REGULATED GENES OCCURS ALREADY IN FRESHLY ISOLATED HEPATOCYTES OR AT THE LATEST AT 3 HOURS AFTER PLATING

Quantitative RT-PCR analysis of inflammation-associated genes (Lcn2, Mt2 and Saa3) and metabolism-associated genes (Bsep, Mrp2 and Cyp7a1) in healthy liver tissue (Liver), freshly isolated hepatocytes (FH) and hepatocytes in sandwich (S) for the indicated time. GAPDH was used as an endogenous control. Data are expressed as fold change relative to healthy liver tissue. Values represent mean ± SD (*n=3*).

3.2 FUZZY C-MEANS CLUSTERING ANALYSIS IDENTIFIES FIVE MAIN GENE EXPRESSION CLUSTERS

A clustering analysis allows pattern recognition in a large set of data. Therefore, the differentially expressed genes were analyzed based on the time-dependent Fuzzy C-Means clustering [184]. This technique identified five main clusters of which 2A and 2B as well as 3A and 3B were closely related (Figure 26).

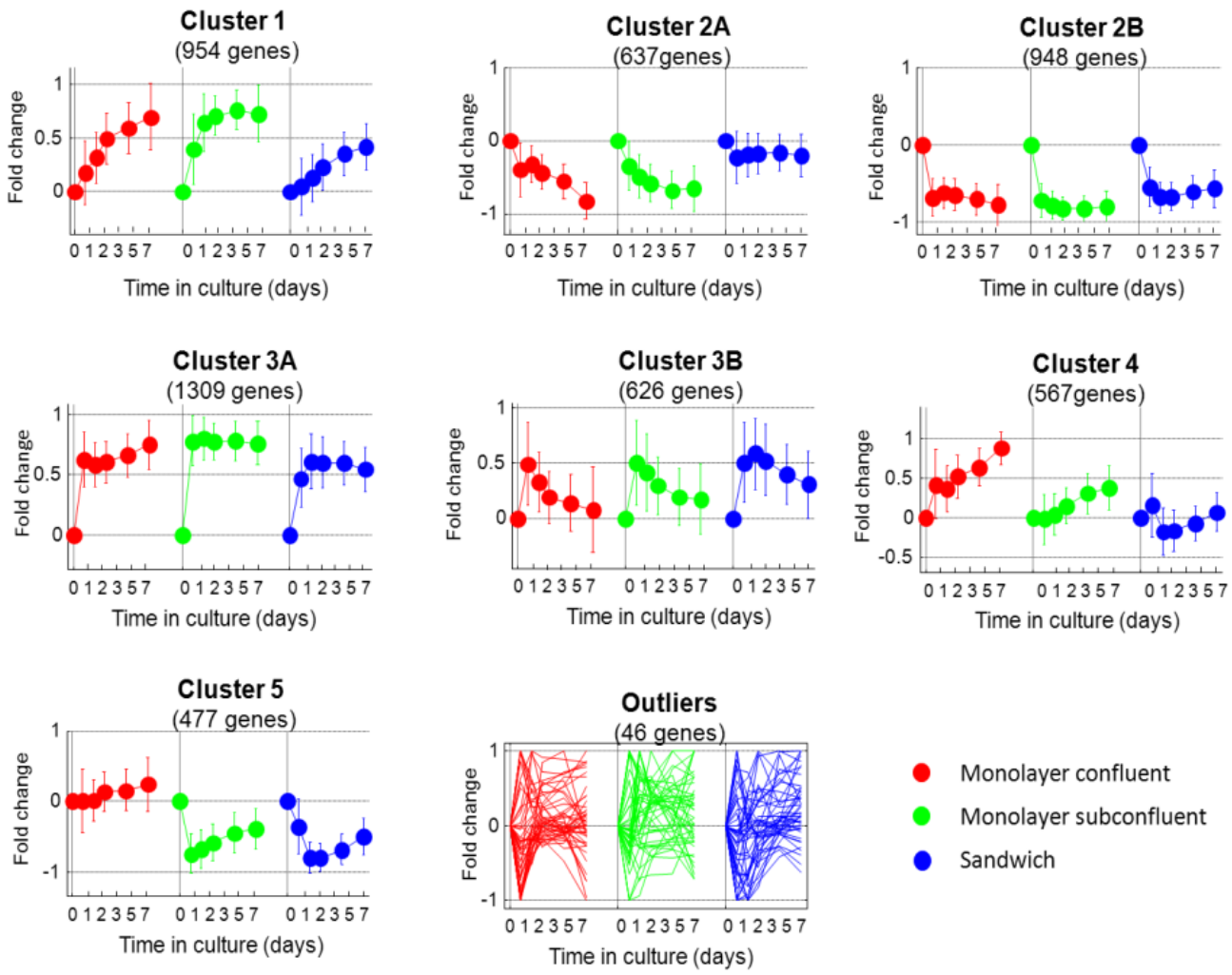

FIGURE 26: FUZZY C-MEANS CLUSTERING ANALYSIS IDENTIFIES FIVE MAIN GENE EXPRESSION CLUSTERS
The differentially expressed genes were subjected to a Fuzzy C-Means clustering analysis. Five main clusters were identified of which 2A and 2B as well as 3A and 3B were closely related.

The separation of DEGs in distinct clusters allowed for a more precise bioinformatics analysis of the biological motifs. Kyoto Encyclopedia of Genes and Genomes (KEGG at http://www.genome.ad.jp/kegg/) represents a reference knowledge database that integrates current knowledge on molecular interaction and can help to identify biological motifs in gene array data [205]. For this purpose, each gene cluster was assessed for over representation of KEGG motifs (Figure 27). This analysis resulted in the identification of clearly enriched motifs for 'proliferation' in Cluster 1; whereas, a strong overrepresentation of 'metabolism' was detected in Clusters 2A and B (Figure 27). This observation is consistent with the well-established loss of function induced during cultivation of primary hepatocytes [69]. Clusters 3A and 3B did not contain a specific GO or KEGG motif. However, a knowledge-based curation of these clusters strongly suggested that they represent a 'inflammation' motif (Figure 27 continued). The validation of the aforementioned motifs is demonstrated in the following sections.

	pValue < 1e-5		Cluster-1		Cluster-2A		Cluster-2B	
Kegg-ID	Description	Size	Count	p-value	Count	p-value	Count	p-value
01100	Metabolic pathways	959	47	9.95E-01	**112**	**1.08E-14**	**141**	**6.88E-18**
04610	Complement and coagulation cascades	61	3	7.81E-01	**26**	**1.14E-16**	**13**	**5.80E-04**
04146	Peroxisome	72	1	9.93E-01	**12**	**1.09E-03**	**28**	**7.33E-14**
00280	Valine, leucine and isoleucine degradation	42	2	7.79E-01	**9**	**7.17E-04**	**21**	**2.69E-13**
00100	Steroid biosynthesis	15			**11**	**3.54E-11**	1	7.00E-01
00640	Propanoate metabolism	29			5	2.79E-02	**15**	**4.16E-10**
00380	Tryptophan metabolism	38	2	7.29E-01	**7**	**6.82E-03**	**17**	**5.06E-10**
00071	Fatty acid metabolism	39	1	9.32E-01	**9**	**4.00E-04**	**17**	**8.35E-10**
00982	Drug metabolism - cytochrome P450	51	3	6.68E-01	**16**	**2.14E-08**	**11**	**1.37E-03**
03320	PPAR signaling pathway	64	2	9.33E-01	**13**	**8.70E-05**	**19**	**1.47E-07**
03040	Spliceosome	98	12	2.76E-02	1	9.98E-01		
00260	Glycine, serine and threonine metabolism	28	1	8.55E-01	**10**	**2.74E-06**	**12**	**3.50E-07**
00330	Arginine and proline metabolism	46	3	5.98E-01	6	5.65E-02	**15**	**8.15E-07**
00910	Nitrogen metabolism	22	1	7.80E-01	1	7.47E-01	**10**	**1.79E-06**
00980	Metabolism of xenobiotics by cytochrome P450	46	2	8.20E-01	**13**	**1.80E-06**	**9**	**7.31E-03**
00250	Alanine, aspartate and glutamate metabolism	28	2	5.64E-01	3	2.38E-01	**11**	**3.10E-06**
00830	Retinol metabolism	39			**10**	**7.31E-05**	**13**	**3.40E-06**
03030	DNA replication	34	**11**	**6.61E-06**	1	8.81E-01		
04510	Focal adhesion	181	**23**	**1.73E-03**	3	9.99E-01	4	1.00E+00
00340	Histidine metabolism	25	1	8.21E-01	2	4.52E-01	**10**	**7.32E-06**
04530	Tight junction	120	12	9.92E-02	3	9.80E-01		
00410	beta-Alanine metabolism	21			3	1.30E-01	**9**	**1.09E-05**
05100	Bacterial invasion of epithelial	64	**11**	**2.86E-03**				
04110	Cell cycle	115	**21**	**1.56E-05**	1	9.99E-01	3	9.95E-01
00120	Primary bile acid biosynthesis	13	1	5.91E-01	3	3.98E-02	**7**	**1.72E-05**
03020	RNA polymerase	24						
00983	Drug metabolism - other enzymes	35	2	6.86E-01	**7**	**4.24E-03**	**11**	**3.68E-05**
00650	Butanoate metabolism	24	1	8.09E-01	5	1.28E-02	**9**	**3.93E-05**
04115	p53 signaling pathway	63	**14**	**4.57E-05**			2	9.61E-01
00500	Starch and sucrose metabolism	31	3	3.40E-01	**9**	**5.84E-05**	6	2.82E-02
00620	Pyruvate metabolism	33	2	6.54E-01	5	4.59E-02	**10**	**1.19E-04**
02010	ABC transporters	41	4	2.88E-01	3	4.55E-01	**11**	**1.83E-04**
03010	Ribosome	20	1	7.48E-01	1	7.13E-01		
01040	Biosynthesis of unsaturated fatty acids	19	1	7.30E-01	**6**	**6.41E-04**	**7**	**3.36E-04**
04114	Oocyte meiosis	101	12	3.40E-02			3	9.87E-01
00770	Pantothenate and CoA	14			2	2.06E-01	**6**	**3.50E-04**

FIGURE 27: ANALYSIS OF KEGG PATHWAY OVERREPRESENTATION IN TIME-DEPENDENT GENE CLUSTERS

The figure shows a snapshot of the results obtained for overrepresentation of KEGG pathway. The strongest overrepresentations of KEGG pathways were observed in the clusters containing down-regulated genes (cluster 2A and B), which showed a high enrichment of metabolic pathways. In cluster 1, a high enrichment of KEGG pathways associated with proliferation was observed. Gray colored boxes indicate p-values<10^{-5}.

	pValue < 1e-5		Cluster-3A		Cluster-3B		Cluster-4		Cluster-5		Outlier	
Kegg-ID	Description	Size	Count	p-value	Count	p-value	Count	p-value	Count	p-value	Count	p-value
01100	Metabolic pathways	959	73	9.87E-01	**59**	**2.76E-03**	13	9.98E-01	15	9.70E-01	3	7.17E-01
04610	Complement and coagulation cascades	61	2	9.83E-01	3	5.10E-01			1	7.59E-01		
04146	Peroxisome	72	2	9.93E-01	1	9.62E-01			1	8.14E-01		
00280	Valine, leucine and isoleucine degradation	42							2	2.50E-01		
00100	Steroid biosynthesis	15										
00640	Propanoate metabolism	29					1	5.17E-01	1	4.90E-01		
00380	Tryptophan metabolism	38							1	5.87E-01	1	1.31E-01
00071	Fatty acid metabolism	39							2	2.24E-01		
00982	Drug metabolism - cytochrome P450	51	2	9.60E-01	6	2.37E-02						
03320	PPAR signaling pathway	64	1	9.98E-01	1	9.46E-01	1	8.01E-01	2	4.34E-01		
03040	Spliceosome	98	**27**	**1.49E-07**	3	8.16E-01	**9**	**6.22E-04**	4	1.86E-01	1	3.05E-01
00260	Glycine, serine and threonine metabolism	28	3	4.97E-01					1	4.78E-01		
00330	Arginine and proline metabolism	46	1	9.90E-01	4	1.44E-01	1	6.86E-01	2	2.84E-01		
00910	Nitrogen metabolism	22	1	8.86E-01					1	4.00E-01		
00980	Metabolism of xenobiotics by cytochrome P450	46	2	9.39E-01	6	1.48E-02					1	1.56E-01
00250	Alanine, aspartate and glutamate metabolism	28	4	2.66E-01	1	7.19E-01			1	4.78E-01		
00830	Retinol metabolism	39	2	8.93E-01	2	5.20E-01	1	6.25E-01	1	5.96E-01	1	1.34E-01
03030	DNA replication	34	3	6.32E-01	**7**	**5.74E-04**						
04510	Focal adhesion	181	22	1.22E-01	2	9.98E-01	**16**	**7.00E-06**	4	6.01E-01	1	4.93E-01
00340	Histidine metabolism	25	1	9.16E-01					1	4.41E-01		
04530	Tight junction	120	**27**	**1.09E-05**	5	6.19E-01	2	8.04E-01	3	5.23E-01		
00410	beta-Alanine metabolism	21			1	6.14E-01			1	3.86E-01		
05100	Bacterial invasion of epithelial	64	**18**	**1.36E-05**	2	7.83E-01	3	2.10E-01	2	4.34E-01		
04110	Cell cycle	115	17	3.84E-02	10	2.97E-02	7	2.29E-02	4	2.69E-01	1	3.48E-01
00120	Primary bile acid biosynthesis	13			1	4.45E-01						
03020	RNA polymerase	24	**10**	**2.80E-05**	3	8.71E-02						
00983	Drug metabolism - other enzymes	35	2	8.54E-01	4	6.65E-02			1	5.57E-01		
00650	Butanoate metabolism	24										
04115	p53 signaling pathway	63	6	5.49E-01	**10**	**3.71E-04**	3	2.04E-01	1	7.70E-01		
00500	Starch and sucrose metabolism	31	2	8.03E-01	5	1.07E-02						
00620	Pyruvate metabolism	33	1	9.62E-01	1	7.76E-01	1	5.64E-01	2	1.74E-01		
02010	ABC transporters	41			1	8.45E-01	1	6.44E-01	1	6.15E-01		
03010	Ribosome	20	**8**	**2.57E-04**			1	3.95E-01	2	7.55E-02		
01040	Biosynthesis of unsaturated fatty acids	19					1	3.79E-01				
04114	Oocyte meiosis	101	**21**	**3.40E-04**	7	1.58E-01	1	9.23E-01	3	4.09E-01		

FIGURE 27: CONTINUED

ANALYSIS OF KEGG PATHWAY OVERREPRESENTATION IN TIME-DEPENDENT GENE CLUSTERS

The figure shows a snapshot of the results obtained for overrepresentation of KEGG pathway. Clusters 3A and 3B did not contain a specific GO or KEGG motif. However, a knowledge-based curation of these clusters strongly suggested that they represent a ´inflammation` motif asthese clusters contain all of the top up-regulated genes in cultivation shown in Table 21. Gray colored boxes indicate p-values<10^{-5}.

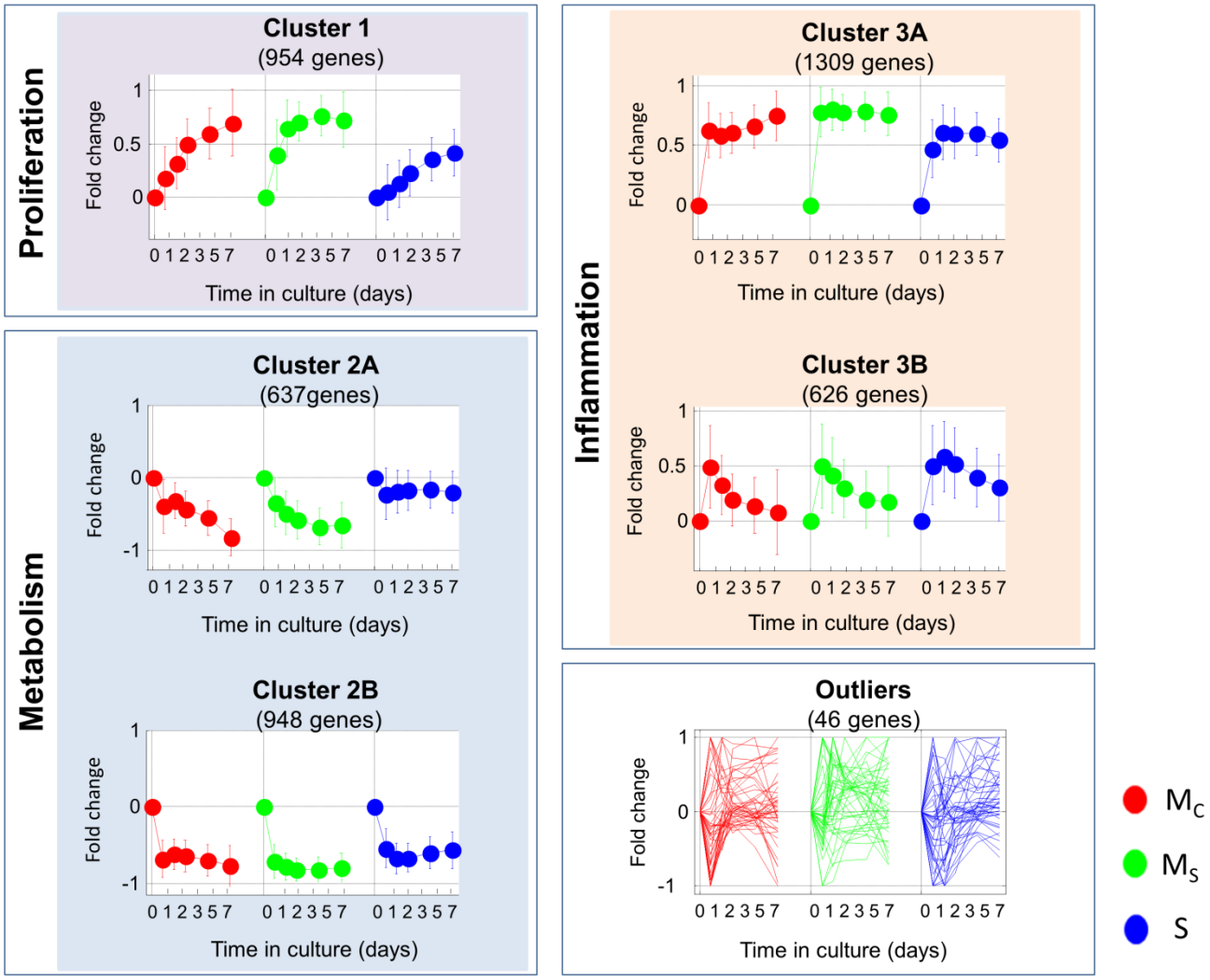

FIGURE 28: PROLIFERATION, METABOLISM AND INFLAMMATION AMONG BIOLOGICAL MOTIFS ASSIGNED TO IDENTIFIED CLUSTERS

The graphs represent the mean scaled value of all genes contained in each cluster, at each timepoint, for each cultivation system. The assignment of gene clusters to 'proliferation' and 'metabolism' motifs was based on enrichment analysis of GO and KEGG terms, while the 'inflammation' motif was determined experimentally by comparison to well-known liver inflammation models *in vivo*.

3.2.1 CULTIVATION INDUCES DOWN-REGULATION OF METABOLISM-ASSOCIATED GENES

Identified as closely related, clusters 2A and 2B (Figure 28) exhibit an expression pattern of a persistent down-regulation among all three cultivation systems. Only cluster 2A-associated genes are maintained in sandwich culture (S). In contrast, cluster 2B represents metabolic genes that are not maintained by the collagen sandwich, but rather decrease similarly as in the monolayer culture (Figure 28, Cluster 2B). Among those, many of the top down-regulated genes

such as Bsep, Mrp2 and Cyp7a1 are assigned to cluster 2B (Table 21). The data analysis using KEGG pathways identified an enrichment of metabolism-associated genes in both clusters 2A and 2B (Figure 27). KEGG and GO analysis identify cytochrome P450, sterol and cholesterol metabolism, as well as coagulation and complement factors among the 'sandwich culture maintained' genes in cluster 2A.

Moreover, Transcription Factor Binding Sites analysis (TFBS with PRIMA algorithm [185]) of the promoter regions of associated genes identified Hepatocyte Nuclear Factors (HNF-4α and -1α) among the overrepresented transcription factors in clusters 2A and B (a snapshot shown in Figure 29). Consistently, the expression of HNF4α and HNF1α was markedly down-regulated during the first hours in culture (Figure 30**,** A). Likewise, HNF4α nuclear expression was clearly reduced in cultivated cells compared to freshly isolated hepatocytes (Fresh Heps) (Figure 30, B).

pValue < 1e-5	Cluster-1		Cluster-2A		Cluster-2B		Cluster-3A		Cluster-3B		Cluster-4		Cluster-5		Outlier	
TF	Count	p-value	Count	p-value	Count	p-value	Count	p-value	Count	p-value	Count	p-value	Count	p-value	Count	p-value
M00196[Sp1]	575	1.28E-07			484	8.00E-03	867	4.16E-23	403	3.29E-11	290	8.00E-03	227	8.00E-03	30	3.50E-02
M00025[Elk-1]	214	3.40E-02					412	4.29E-21	138	6.00E-02	129	1.00E-03	101	2.20E-02		
M00803[E2F]	433	2.54E-10					644	2.83E-20	267	5.03E-04	235	2.42E-08	183	5.50E-08	26	1.79E-05
M00695[ETF]	299	2.40E-07					473	1.10E-19			183	2.07E-13	149	1.42E-10		
M00976[AHRHIF]							431	3.90E-15	181	1.13E-04	139	1.00E-03	106	3.60E-02		
M00652[Nrf-1]	298	6.25E-04					483	4.37E-14	190	9.00E-03	160	8.13E-04	142	2.14E-06		
M00341[GABP]	257	5.60E-02					439	1.26E-12	182	3.00E-03	134	2.30E-02				
M00189[AP-2]	321	2.71E-05					471	3.89E-11	197	4.00E-02	167	1.20E-04	134	1.00E-03		
M00716[ZF5]	328	6.94E-08					471	7.48E-10	202	5.00E-03	177	3.99E-07	139	1.31E-04	17	6.00E-02
M00797[HIF-1]	296	2.40E-02					471	9.64E-10	209	7.00E-03	169	1.60E-02	124	3.70E-02		
M00451[NKX3A]											181	1.55E-09	136	5.01E-05		
M00938[E2F-1]	273	1.94E-07					384	3.67E-09	173	1.00E-03	125	2.30E-02	107	1.10E-02	16	3.30E-02
M00778[AhR]	190	1.10E-02					303	2.51E-08	147	2.15E-06	98	6.60E-02	85	6.00E-03		
M00800[AP-2]	324	1.13E-07					465	2.67E-08	198	2.60E-02	172	1.84E-04			18	2.70E-02
M00987[FOXP1]					490	3.60E-02			361	2.90E-02	315	4.12E-08	238	1.00E-03		
M00138[Oct-1]											223	1.56E-05	200	1.28E-07		
M00148[SRY]					538	3.60E-02	832	5.80E-02			313	5.00E-03	284	1.67E-07		
M00224[STAT1]			82	7.20E-02			202	2.30E-07			67	5.40E-02				
M00017[ATF]	250	3.82E-05					355	3.61E-07	152	4.00E-02	146	8.32E-06	101	3.30E-02		
M00081[Evi-1]											174	2.00E-03	157	7.40E-07		
M00471[TBP]											147	8.00E-03	135	1.60E-06		
M00489[Nkx6-2]											161	4.00E-03	146	3.85E-06		
M00465[POU6F1]											145	5.22E-06	92	4.90E-02		
M00322[c-Myc:Max]	256	1.50E-02					384	5.70E-06	182	9.56E-04	140	1.00E-03	104	6.70E-02		
M00940[E2F-1]	103	3.00E-03					149	2.77E-04	69	3.00E-03	57	1.00E-02	59	6.32E-06		
M01113[CACD]	242	3.90E-02					383	8.99E-06	179	1.00E-03					20	2.00E-03
M00807[EGR]	395	5.12E-04	251	7.90E-02			563	1.03E-05	262	3.00E-03	203	3.30E-02			21	2.50E-02
M00915[AP-2]	310	1.35E-05					434	3.68E-05	207	9.47E-04	149	3.60E-02	119	6.10E-02		
M00423[FOXJ2]											147	6.60E-05	123	1.93E-05		
M00744[POU1F1]											176	5.96E-05	155	2.02E-05		
M00026[RSRFC4]					224	7.70E-02					154	2.11E-05	114	6.00E-03		
M01033[HNF4]	603	1.20E-02	423	2.21E-05					393	8.00E-03					34	6.50E-02
M00099[S8]													122	2.23E-05		
M01075[PLZF]											136	2.50E-02	128	2.53E-05		
M01072[HIC1]	343	2.74E-05					474	3.71E-05	219	8.00E-03	174	7.00E-03	137	1.50E-02		
M00478[Cdc5]													101	2.78E-05		

FIGURE 29: ANALYSIS OF TRANSCRIPTION FACTOR BINDING SITE (TFBS) ENRICHMENT IN TIME-DEPENDENT GENE CLUSTERS

The figure shows a snapshot of the results obtained for overrepresentation of TFBS. The TFBS with the strongest overrepresentation were Sp1, E2F, ETF, all of which were highly enriched in up-regulated gene clusters. Conversely, HNF4α was the most overrepresented TFBS in down-regulated gene clusters. Gray colored boxes indicated p-value<10^{-5}.

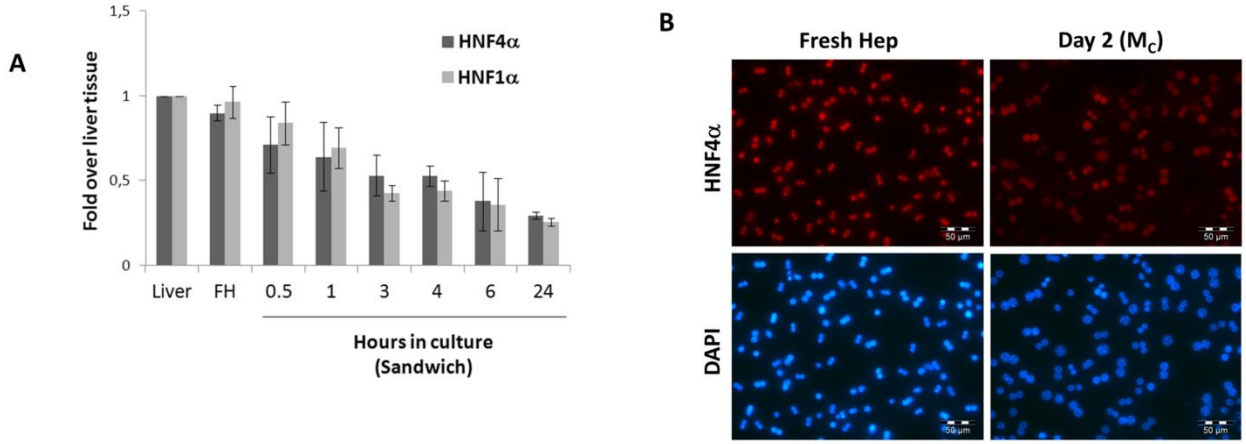

FIGURE 30: DECREASE IN EXPRESSION OF TRANSCRIPTION FACTORS (HNF-4α and -1α) REGULATING METABOLISM-ASSOCIATED GENES IN CULTURE

A) Quantitative RT-PCR analysis of HNF4α and HNF1α in healthy liver tissue (Liver), freshly isolated hepatocytes (FH), hepatocytes in sandwich culture for the indicated time. GAPDH was used as an endogenous control. Data are expressed as fold change relative to healthy liver tissue. Values represent mean ± SD (*n=3*). **B)** Fluorescence microscopy analysis of HNF4α expression (red) in freshly isolated hepatocytes (Fresh Hep) and in hepatocytes in monolayer culture (M_C) two days after plating. Nuclei are stained blue (DAPI). Scale bars represent 50µm.

Moreover, the expression of nuclear receptors known to regulate many hepatic functions was rapidly decreased in culture (Figure 31). Interestingly, nuclear receptors were not listed among the down-regulated genes coming out of the gene array data and therefore represented a false negative result. This should emphasize the need of manual curation when dealing with gene array data and validation of mRNA expression levels via qRT-PCR or on a protein level via Western blotting.

In conclusion, a combination of time-resolved gene clustering and bioinformatics analysis (GO and KEGG motifs), together with TFBS enrichment provided important insights into the biological processes and revealed that cultivation induces down-regulation of metabolism-associated.

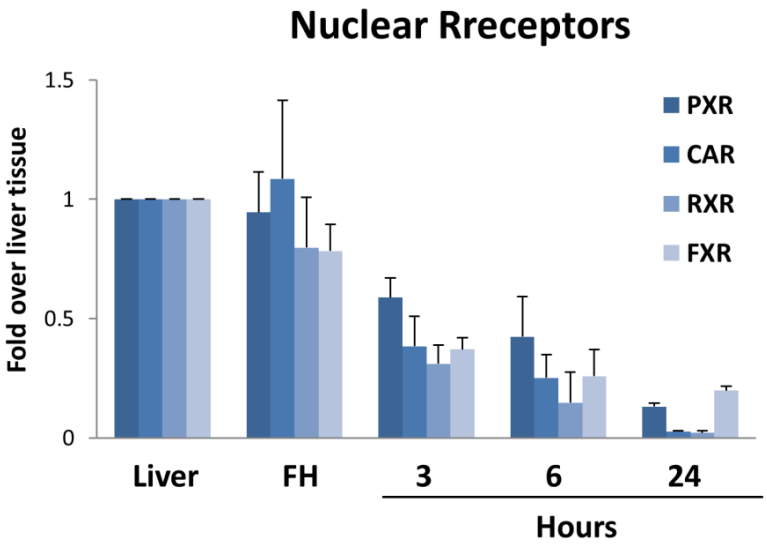

FIGURE 31: DECREASE IN EXPRESSION OF NUCLEAR RECEPTORS REGULATING METABOLISM-ASSOCIATED GENES IN CULTURE

Quantitative RT-PCR analysis of nuclear receptors: pregnane X receptor (PXR), constitutive androstane receptor (CAR), retinoid X receptor (RXR), farnesoid X receptor (FXR) in healthy liver tissue (Liver), freshly isolated hepatocytes (FH), hepatocytes in sandwich culture for the indicated time. GAPDH was used as an endogenous control. Data are expressed as fold change relative to healthy liver tissue. Values represent mean ± SD (n=3).

3.2.2 MONOLAYER CULTURES INDUCE PROLIFERATION INDEPENDENT OF ADDITIONAL GROWTH FACTORS

Cluster 1 (Figure 28) contained genes whose expression was quickly and strongly induced in monolayer cultures, particularly in Ms. This is in contrast to S cultures where genes are upregulated only at later timepoints. KEGG analysis identified a strong overrepresentation of 'DNA replication pathway' motif (Figure 27). The intensity of the proliferation cluster correlates with the proliferation activity of hepatocytes in the three culture systems as evidenced by PCNA expression (Figure 32). The strongest time dependent increase in the proliferation cluster was observed in M_S compared to M_C and S.

In conclusion, Fuzzy C-Means clustering reveals that cultivation induces a time-dependent increase in proliferation rate.

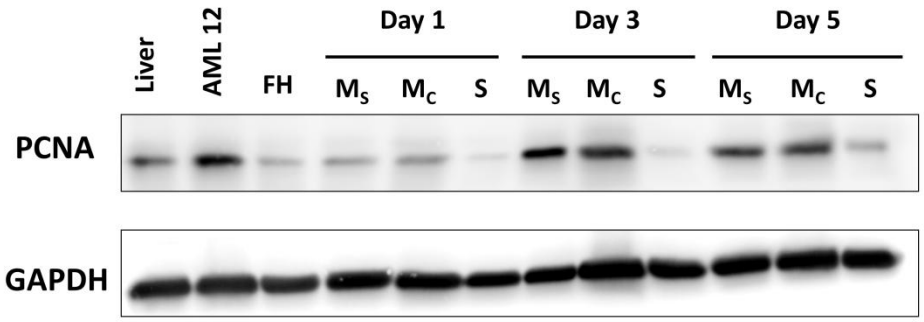

FIGURE 32: M_S CULTURE SHOWS A TIME-DEPENDENT INCREASE IN THE PROLIFERATION MARKER PCNA
Immunoblot analysis using antibody against proliferating cell nuclear antigen (PCNA) in healthy liver tissue (Liver), AML12 cells stimulated with interferon γ, freshly isolated hepatocytes (FH), hepatocytes in sandwich (S) culture, confluent (M_C) culture and subconfluent (M_S) culture for the indicated time. GAPDH was used as an endogenous control. Protein extracts from healthy liver tissue and freshly isolated hepatocytes were used as negative controls, while AML12 cells stimulated with interferon γ (AML12) were used as positive control. Representative images for 3 independent experiments are shown. The strongest time dependent increase of PCNA was observed in M_S.

3.2.3 CULTIVATION INDUCES AN INFLAMMATORY RESPONSE

The closely related, clusters 3A and 3B (Figure 28) exhibit a strong increase in expression among all three cultivation systems, with cluster 3A showing a permanent and cluster 3B a transient up-regulation. Clusters 3A and 3B contain all of the top up-regulated genes in cultivation as shown in Table 21. Most of those genes belong to the permanently up-regulated cluster 3A (thirteen out of fifteen including Lcn2 and Mt2), with only two (Mt1 and Saa3) belonging to the transiently up-regulated cluster 3B. Among the top up-regulated genes in cultivation, thirteen out of fifteen have been shown to play a role in inflammation processes (Table 21**,** brackets indicate references for the top up-regulated genes). Therefore, this group of genes clearly represents an inflammation cluster. Importantly, a downregulation of Cebp/α and a concomitant upregulation of Cebp/β and Cebp/δ was observed in cultivated hepatocytes (Figure 33). This pattern has been previously shown to occur *in vivo* during inflammation [138], supporting the interpretation of an inflammatory response being triggered in cultivated hepatocytes.

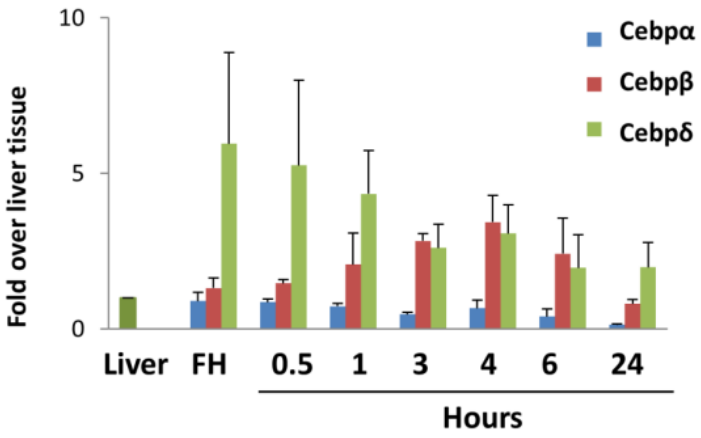

FIGURE 33: CULTIVATION INDUCES AN INFLAMMATORY RESPONSE
Quantitative RT-PCR of CCAAT/Enhancer Binding Protein α, -β and -δ (Cebpα, -β and -δ) in healthy liver tissue (Liver), freshly isolated hepatocytes (FH), hepatocytes in sandwich culture for the indicated time. GAPDH was used as an endogenous control. Data are expressed as fold change relative to healthy liver tissue. Values represent mean ± SD (*n=3*). Sandwich culture induces downregulation of Cebpα and a concomitant upregulation of Cebpβ and Cebpδ.

The transcription Factor Binding Sites analysis (using PRIMA algorithm) of the promoter regions of inflammation gene clusters identified Sp1, Elk1 and ETF among the overrepresented transcription factors in the inflammation Cluster 3A but not in 3B. The highest ranked TF for up-regulated genes in cultivation is Sp1. Although Sp1 is not up-regulated transcriptionally, immunostaining shows that its expression increases in hepatocyte nuclei in culture (Figure 34, A). Klf6, belonging to the same family of transcription factors, turned out to be one of the strongest transcriptionally up-regulated transcription factors (Figure 34, B and C) with an enhanced nuclear localization *in vitro* (Figure 34, D). Klf6 has been reported to cooperate with Sp1 in the regulation of gene induction [206]. Hence, it is likely that the Sp1 overrepresentation reflects a synergistic effect due to Klf6 upregulation.

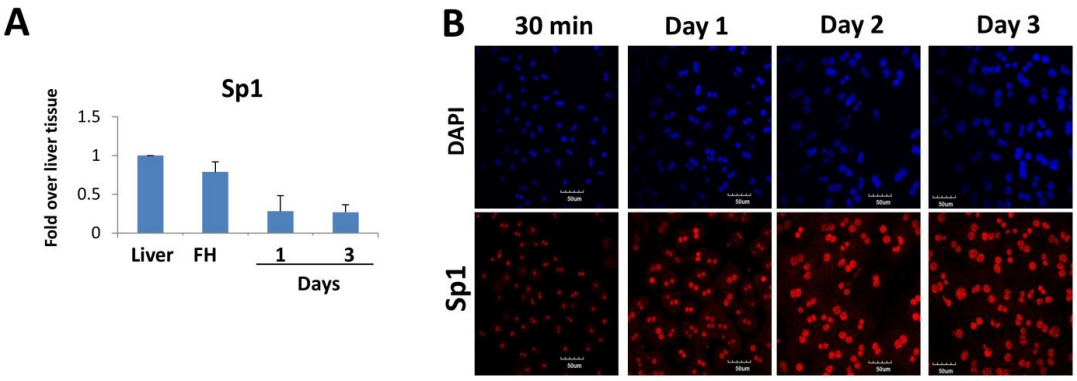

FIGURE 34: TFBS ANALYSIS IDENTIFIES SP1 AMONG OVERREPRESENTED TRANSCRIPTION FACTORS *IN VITRO*
A) Quantitative RT-PCR analysis of Sp1 in healthy liver tissue (Liver), freshly isolated hepatocytes (FH), hepatocytes in sandwich culture at day 1 and 3 of culture. GAPDH was used as an endogenous control. Data are expressed as fold change relative to healthy liver tissue. Values represent mean ± SD (*n=3*). **B)** Fluorescence microscopy analysis of Sp1 expression (red) in freshly isolated hepatocytes (Fresh Hep) and in hepatocytes in monolayer culture (M_C) for the indicated timepoints. Nuclei are stained blue (DAPI). Scale bars represent 50µm.

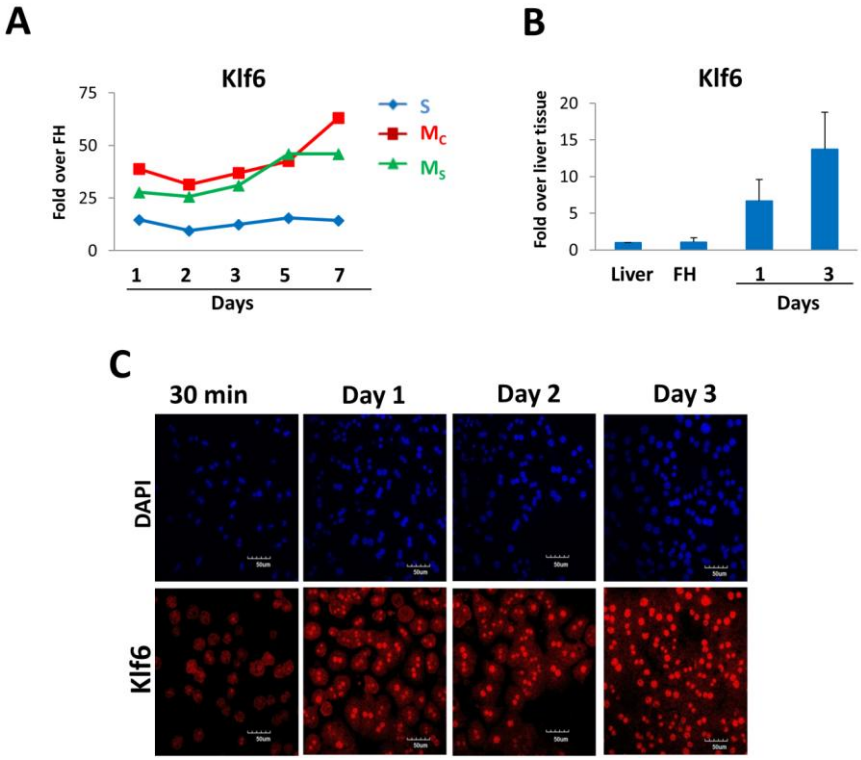

FIGURE 35: EXPRESSION OF Klf6 TRANSCRIPTION FACTOR IS INDUCED IN CULTURE
A) Gene array data on Klf6 expression in all three cultivation systems: sandwich (S) culture, confluent (M_C) culture and subconfluent (M_S) culture for the indicated time in comparison to freshly isolated hepatocytes. **B)** Quantitative RT-PCR analysis of Klf6 in healthy liver tissue (Liver), freshly isolated hepatocytes (FH), hepatocytes in sandwich culture at day 1 and 3 of culture. GAPDH was used as an endogenous control. Data are expressed as fold change relative to healthy liver tissue. Values represent mean ± SD (*n=3*). **C)** Fluorescence microscopy analysis of Klf6 expression (red) in freshly isolated hepatocytes (Fresh Hep) and in hepatocytes in monolayer culture (M_C) for the indicated timepoints. Nuclei are stained blue (DAPI). Scale bars represent 50µm.

Additionally, a number of genes belonging to cluster 3A increase their expression during cultivation, for example, the expression of Ctgf, Ier3 and Ccl2 progresively increases reaching their maximum at later timepoints (Figure 36).

In conclusion, cultivation induces inflammatory response, with genes showing permanent or transient up-regulation *in vitro*.

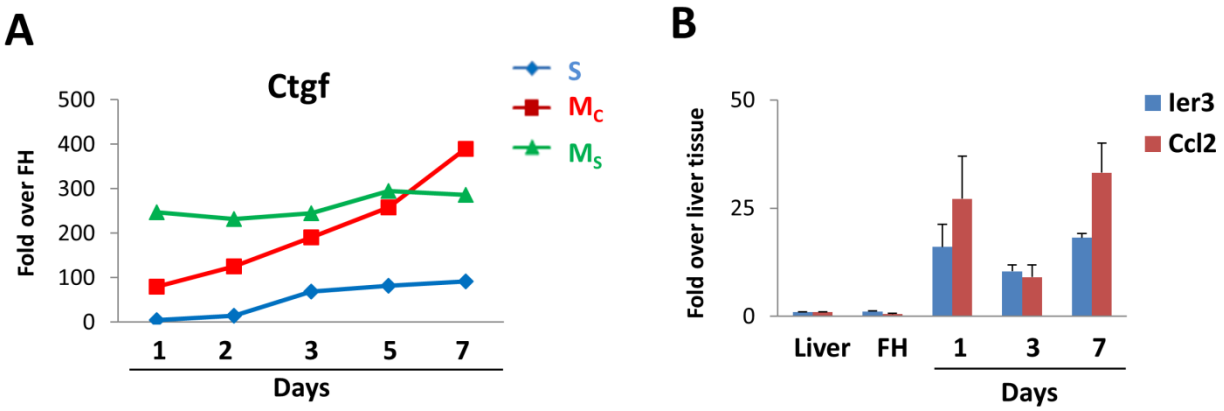

FIGURE 36: OTHER INFLAMMATORY MARKERS ARE PROGRESSIVELY INDUCED IN CULTURE REACHING THEIR MAXIMUM EXPRESSION AT LATER TIMEPOINTS

A) Gene array data on Ctgf expression in all three cultivation systems: sandwich (S) culture, confluent (M_C) culture and subconfluent (M_S) culture for the indicated time in comparison to freshly isolated hepatocytes. **C)** Quantitative RT-PCR analysis of Ier3 and Ccl2 in healthy liver tissue (Liver), freshly isolated hepatocytes (FH), hepatocytes in sandwich culture at day 1 and 3 of culture. GAPDH was used as an endogenous control. Data are expressed as fold change relative to healthy liver tissue. Values represent mean ± SD (*n=3*).

3.3 HEPATOCYTE CULTIVATION INDUCES AN *IN VIVO*-LIKE INFLAMMATION RESPONSE

The strongest up-regulated gene in sandwich culture, lipocalin-2 (Lcn2), is a pentraxin which is known as a key factor in LPS-induced inflammation [130], suggesting that its upregulation reflects a stereotypical inflammatory response of hepatocytes as observed *in vivo*. To test this hypothesis, the transcriptional response *in vitro* was compared to that of the well-established *in vivo* sterile inflammation models: CCl_4, partial hepatectomy (PHx), and LPS-induced inflammation (described in chapter 2.2.3).

Time resolved global gene expression profiling revealed that Lcn2 was among the most up-regulated genes in all three *in vivo* models of liver damage (Figure 37). Importantly, Lcn2 upregulation is mostly a consequence of altered expression in hepatocytes, and not the other liver cell types. This observation is confirmed by comparing expression changes obtained from freshly isolated hepatocytes purified from CCl_4- or LPS-exposed livers (Figure 37, CCl_4 FH D1 vs. Control FH D1 and LPS FH D1 vs. Control FH D1) to untreated livers.

Lcn2 expression		
Treatment vs. Control condition	**Fold**	**p-value**
PHx D1 vs. Control liver	**443.23**	5.88E-10
CCl_4 liver D1 vs. Control liver	**43.28**	2.50E-07
CCl_4 FH D1 vs. Control FH D1	**21.3**	1.77E-03
LPS FH D1 vs. Control liver	**124.08**	5.60E-05
LPS FH D1 vs. Control FH D1	**121.37**	8.59E-05

FIGURE 37: LCN2 IS UP-REGULATED IN ALL *IN VIVO* MODELS OF LIVER DAMAGE
Time resolved global gene expression profiling was performed for different types of liver damage. Lcn2 expression was analysed after partial hepatectomy (PHx) or after single injection with CCl_4 or LPS on day 1. Liver or freshly isolated hepatocytes (FH) collected from treated animals were compared with representative controls. Gene array analysis reveals Lcn2 up-regulation in all *in vivo* models.

Comparison of differentially expressed genes (DEG) between all three *in vitro* and three *in vivo* models revealed a large overlap in their expression profiles (Figure 38). Cultivation systems (Cult) exhibit a higher magnitude of expressional response than *in vivo* models of liver damage (Figure 38, A). The CCl_4 model shows the highest overlap with cultivation systems when comparing the total number of deregulated genes (Figure 38, B). In addition, genes altered *in vivo* after one day treatment with CCl_4, LPS or PHx show a relatively large (<60%) overlap with the *in vitro* deregulated genes on day 1 (Figure 38, B).

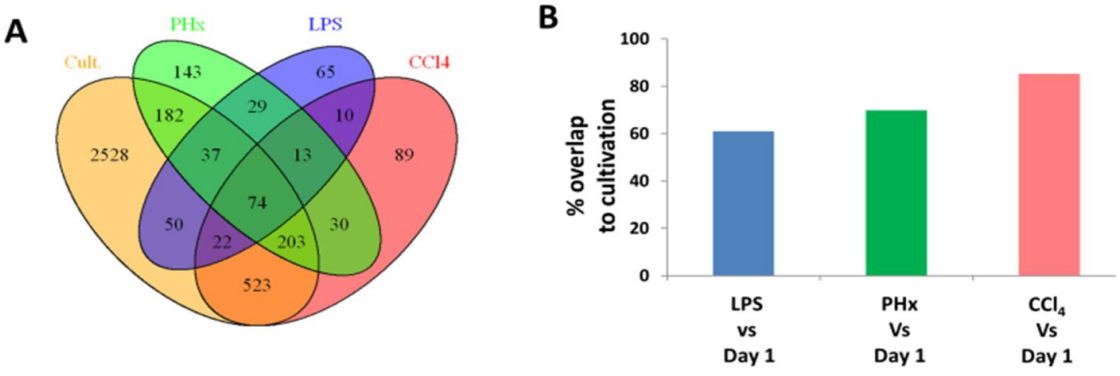

FIGURE 38: *IN VITRO* AND *IN VIVO* MODELS EXHIBIT STRONG OVERLAP OF DIFFERENTIALLY EXPRESSED GENES (DEG)
A) Venn diagrams indicating the overlap between DEGs on all cultivation (Cult) systems (M_C, M_S and S), and day 1 after partial hepatectomy (PHx), CCl_4 or LPS administration. **B)** Percentage of DEGs on day 1 from each *in vivo* model (LPS, PHx and CCl_4) which overlap with DEGs in cultivation on day 1.

Addition of CCl_4-induced liver damage to the principal component analysis (PCA) of the cultivation gene array data (Figure 19) clearly shows that CCl_4-induced liver damage represents a model of liver regeneration (Figure 39). As seen in Figure 39, gene expression alternations in

the CCl_4 model led to liver tissue repair as indicated by the dotted black arrow representing a return to the gene expression of the reference state of fresh liver tissue and freshly isolated hepatocytes (FH). Primary hepatocytes were also compared to non-parenchymal liver cells (day 2 in culture), which cluster far away from the other clusters (Figure 39, orange dots).

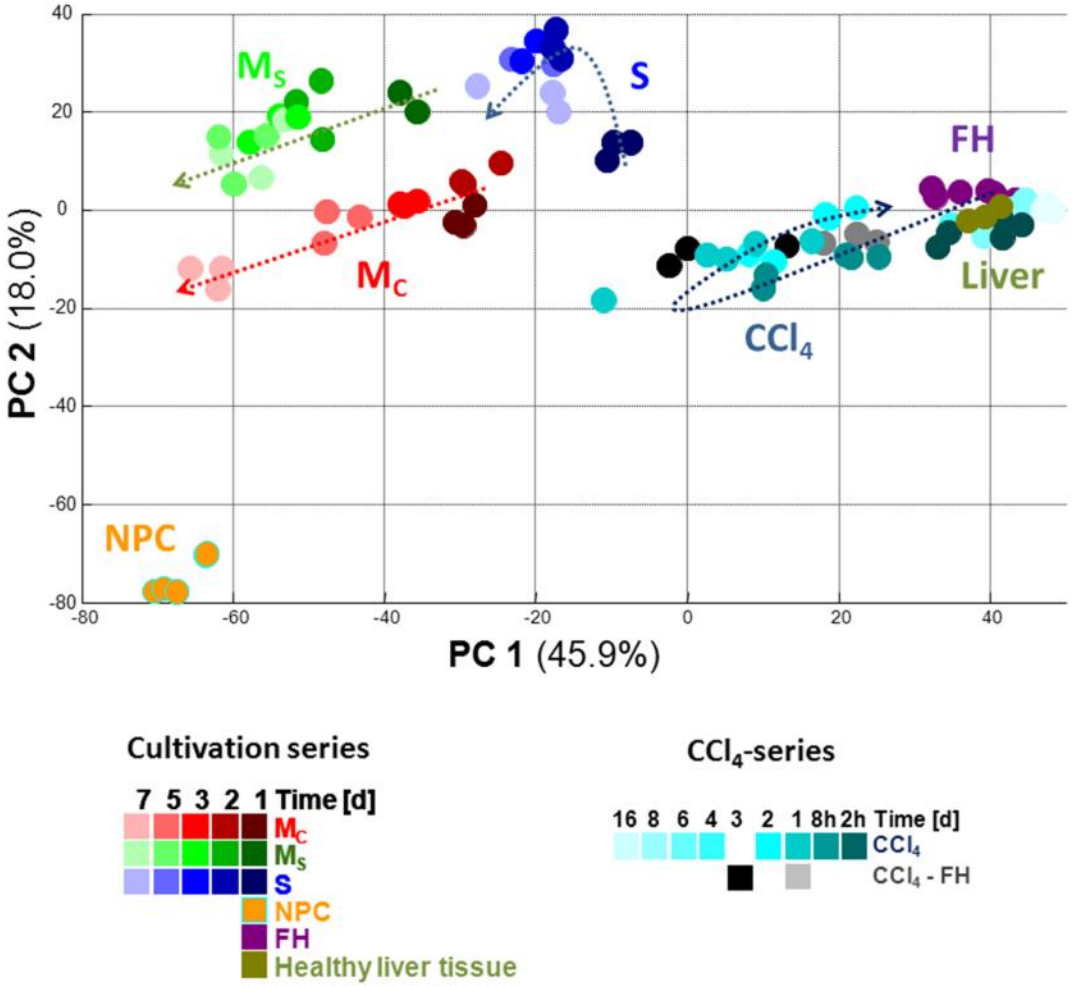

FIGURE 39: GENE ARRAY ANALYSIS REVEALS STRONG SIMILARITIES BETWEEN CULTIVATION AND *IN VIVO* LIVER DAMAGE MODELS

Alterations of gene expression, illustrated as principal component analysis, of cultivated hepatocytes (M_C, M_S and S), non-parenchymal cells (NPC), and liver tissue after damage induced by a single injection of CCl_4. Black and gray circles correspond to freshly isolated hepatocytes after 1 and 3 days, respectively, of CCl_4 administration *in vivo*. NPC correspond to a mix ed population of all non-parenchymal cells, 2 days in culture.

In cultivation, the most significant expression changes occur within the first 24 hours. Therefore, in the next step a ranking analysis was performed to compare differentially expressed genes between Sandwich culture on day 1 and the CCl_4 *in vivo* model on day 1 (Figure 40). Besides Lcn2, a ranking analysis demonstrates the same set of top up-regulated genes in sandwich culture as in the CCl_4 *in vivo* model. Most of the top ten up-regulated genes are known to play a key role in inflammation or cellular stress (Table 21, brackets indicate references for the top up-regulated genes).

In conclusion, a comparison of the different cultivation methods with all three *in vivo* models of liver damage show great similarities with respect to their inflammatory response profiles, with Lcn2 among the most up-regulated genes.

		Sandwich (day1)			CCl_4 (day 1)			Sum	
	Symbol	fold	adj. p-val	rank	fold	adj. p-val	rank	fold	rank
1	Lcn2	247.1	7.33E-34	1	43.2	2.50E-07	1	290.3	2
2	Mt2	87.8	1.15E-33	2	16.6	3.62E-07	6	104.4	8
3	Ier3	34.7	2.10E-20	6	10.0	1.27E-09	10	44.7	16
4	Cpe	20.2	5.82E-14	13	17.1	8.99E-06	4	37.4	17
5	Mt1	29.1	1.45E-26	10	8.7	4.75E-08	15	37.8	25
6	Anxa2	12.6	6.97E-24	21	17.0	5.99E-20	5	29.6	26
7	Tubb6	12.0	3.21E-19	22	9.4	2.04E-12	13	21.4	35
8	Tnfrsf12a	18.0	1.34E-28	16	7.5	2.44E-13	20	25.5	36
9	Ifrd1	9.7	1.11E-12	28	12.9	6.03E-13	8	22.7	36
10	Srxn1	10.9	9.86E-18	25	9.6	3.45E-13	12	20.6	37
11	Sprr1a	8.6	7.09E-15	35	18.7	1.19E-10	3	27.3	38
12	Slpi	34.6	1.29E-18	7	4.5	8.47E-06	34	39.1	41
13	Saa3	32.2	1.46E-13	8	4.6	1.13E-03	33	36.8	41
14	Klf6	14.7	2.98E-19	20	5.9	1.05E-08	26	20.7	46
15	Cd14	9.0	9.64E-13	33	8.0	6.38E-11	18	17.0	51

FIGURE 40: SANDWICH CULTURE AND CCl_4 TREATMENT *IN VIVO* INDUCE STRONG UP-REGULATION OF THE SAME INFLAMMATORY GENES

Ranking analysis of the top 15 up-regulated genes in sandwich culture (day 1) versus CCl_4 (day 1). All 15 genes rank top among the 50 strongest up-regulated regulated genes. Lcn2 ranks as the top up-regulated gene in both conditions. All top ten of up-regulated genes are known to play a key role in inflammation or cellular stress (Table 21, brackets indicate references for the top up-regulated genes).

3.3.1 *IN VITRO/IN VIVO* SIMILARITIES

To analyze the *in vitro/in vivo* similarities in a more detailed and unbiased manner, a Spearman correlation analysis was performed. Genes altered *in vitro* during the first 24h were correlated with genes altered *in vivo* in response to CCl_4 considering intervals from 2h to 16 days (Figure 41). The similarity between *in vitro* and *in vivo* models is presented as Spearman's rank correlation coefficient (Figure 41). The result demonstrates remarkable time dependent differences, with maximal correlations between 8 and 48 h (marked in red and highest on day 1); this is in direct contrast to the no relevant correlations at later timepoints.

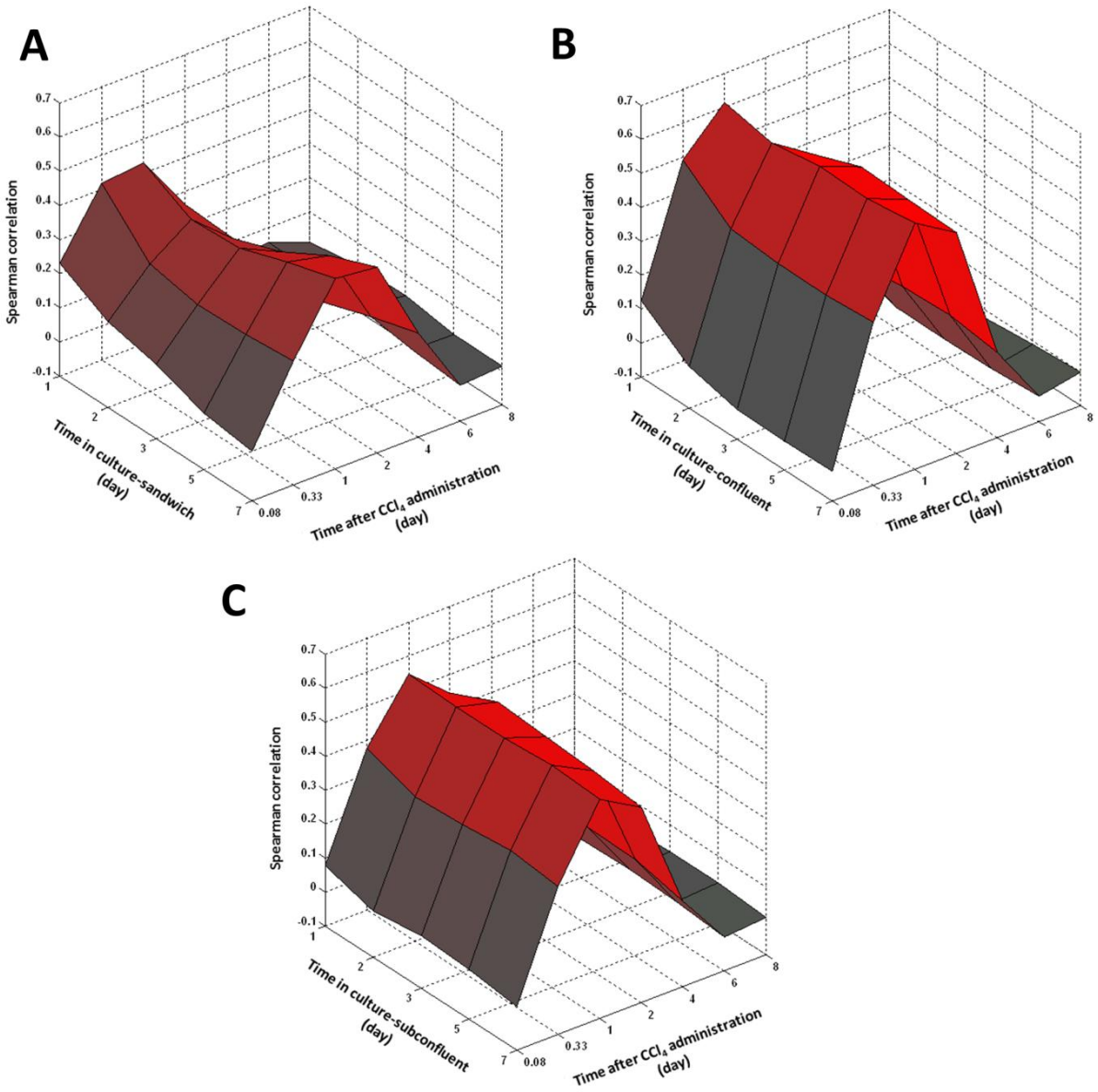

FIGURE 41: PRIMARY MOUSE HEPATOCYTES IN CULTURE EXHIBIT MAXIMAL SIMILARITIES IN EXPRESSION CHANGES WITH LIVER TISSUE 1 DAY AFTER CCL_4 ADMINISTRATION

Spearman's rank correlation coefficient of deregulated genes (≥ 2-fold) between cultivation in sandwich culture (panel A), M_C (panel B) or M_S (panel C) versus CCl_4 treated liver tissue in a time-resolved manner. Maximal correlations are observed between all timepoints in culture versus liver tissue 1 day after CCl_4 administration.

A similar correlation analysis was applied to both the LPS and PHx models. Genes altered *in vitro* at the indicated timepoints were correlated with genes altered *in vivo* in response to PHx considering intervals from 2 h to 2 weeks or after 24 hours after a single injection with LPS. Similar correlation patterns as seen for the CCl_4 model were observed for both the PHx and LPS data (Figure 42).

It should be considered that *in vivo* altered genes are mainly due to the altered expression in hepatocytes, and by the infiltration of leukocytes, since similar expressiona changes were obtained from freshly isolated hepatocytes that were purified from CCl_4-exposed livers (Figure 39**,** black and gray dots).

In conclusion, these results demonstrate that cultivation and different types of liver damage can trigger similar expression changes in hepatocytes.

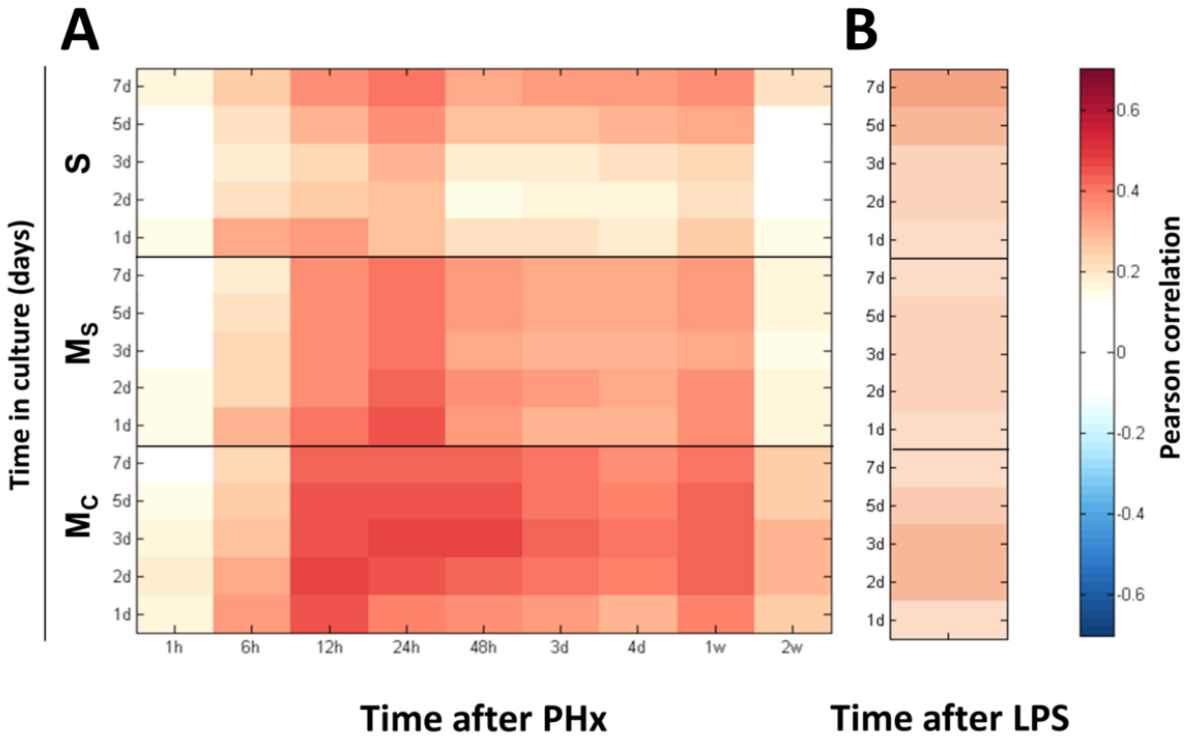

FIGURE 42: PRIMARY MOUSE HEPATOCYTES IN CULTURE SHOW A CORRELATION IN EXPRESSION CHANGES WITH LPS-TREATED LIVER, AND EVEN STRONGER SIMILARITIES WITH PHX LIVERS, WITH MAXIMAL CORRELATION AT 12-48 HOURS AFTER PHX

Spearman rank correlation analysis between differentially expressed genes in cultivated hepatocytes and liver tissue after partial hepatectomy (PHx) **(A)** or intraperitoneal injection of LPS **(B)**. The legend of the heatmap indicates the strength of correlation between cultivation (M_C, M_S or S) versus each timepoint after PHx or 24h after LPS injection *in vivo*. Maximal correlations are observed between all timepoints in culture versus liver tissue between 12 and 48h after PHx.

In the next step, a correlation analysis was applied for “proliferation”-associated genes that are listed in Cluster 1. Genes altered *in vitro* were correlated with genes altered *in vivo* in response to PHx or after a single injection with CCl_4 in a time-resolved manner (Figure 43). Comparable to the general expression changes presented in the previous paragraph, primary hepatocytes *in vitro* show a similar induction in proliferation as shown for a timeframe from 2-4 days after PHx and CCl_4-treatment.

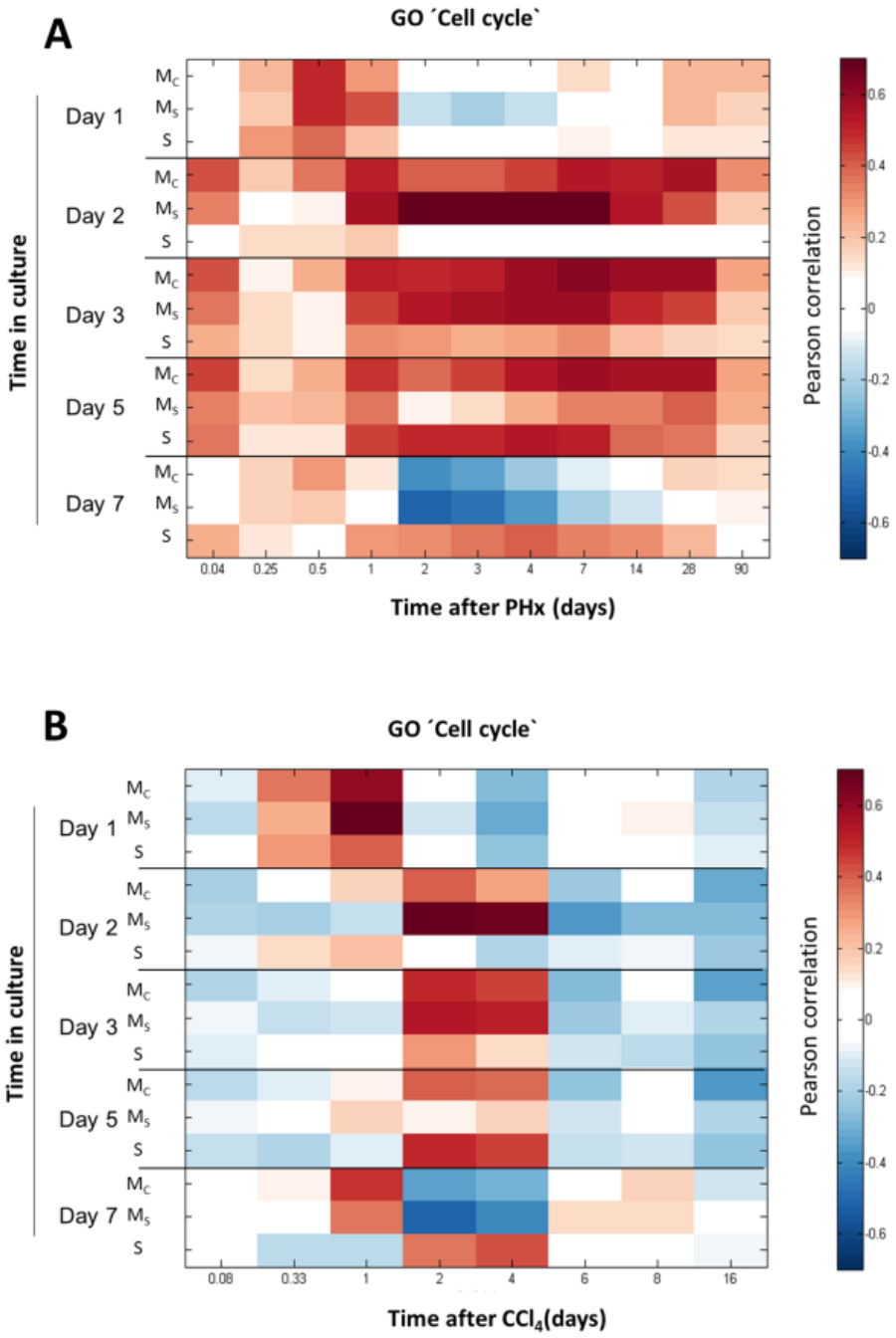

FIGURE 43: PRIMARY MOUSE HEPATOCYTES IN CULTURE SHOW A SIMILAR INDUCTION OF PROLIFERATION AS LIVER TISSUE *IN VIVO* 2-4 DAYS AFTER PHX AND CCl_4-TREATMENT

Spearman rank correlation analysis of GO 'Cell Cycle' genes assigned to Cluster 1, between cultivated hepatocytes and liver tissue after partial hepatectomy (PHx) **(panel A)** or CCl_4 administration **(panel B)**. The legend of the heatmap indicates the strength of correlation between cultivation (M_C, M_S or S) versus each timepoint after PHx or CCl_4 *in vivo*.

3.3.2 METAGENE ANALYSIS PRECISELY IDENTIFIES THE SIMILARITIES IN PROLIFERATION, INFLAMMATION AND METABOLISM CLUSTERS BETWEEN *IN VIVO* AND *IN VITRO* MODELS

To further characterize the clusters of highly correlated genes between the *in vitro* and *in vivo* models, so-called ´metagenes` can be calculated (for detailed explanation see Chapter 2.2.6.6) and their scores compared. A metagene considers genes of a cluster normalized in a way that each individual gene contributes equally. The score of a metagene corresponds to the mean scaled value of all genes in each metagene. This analysis resulted in three metagenes representing the biological motifs proliferation, metabolism, and inflammation (Figure 44). The genes composing the 'metabolism' and 'inflammation' metagenes were determined by selecting genes from each Fuzzy cluster (Table 22 and Table 23 in APPENDIX) which were also commonly deregulated in all *in vivo* models on day 1. For the 'proliferation' metagene, the genes selected correspond to those identified on the GO ´Cell Cycle` cluster (Table 24 in APPENDIX) which are also deregulated in the *in vivo* models involving liver regeneration. This approach was used to compare scores of ´proliferation`, ´inflammation` and ´metabolism` metagenes in each condition (Figure 26) in reference to healthy liver tissue (Healthy liver) and freshly isolated hepatocytes (Fresh hep) (Figure 44).

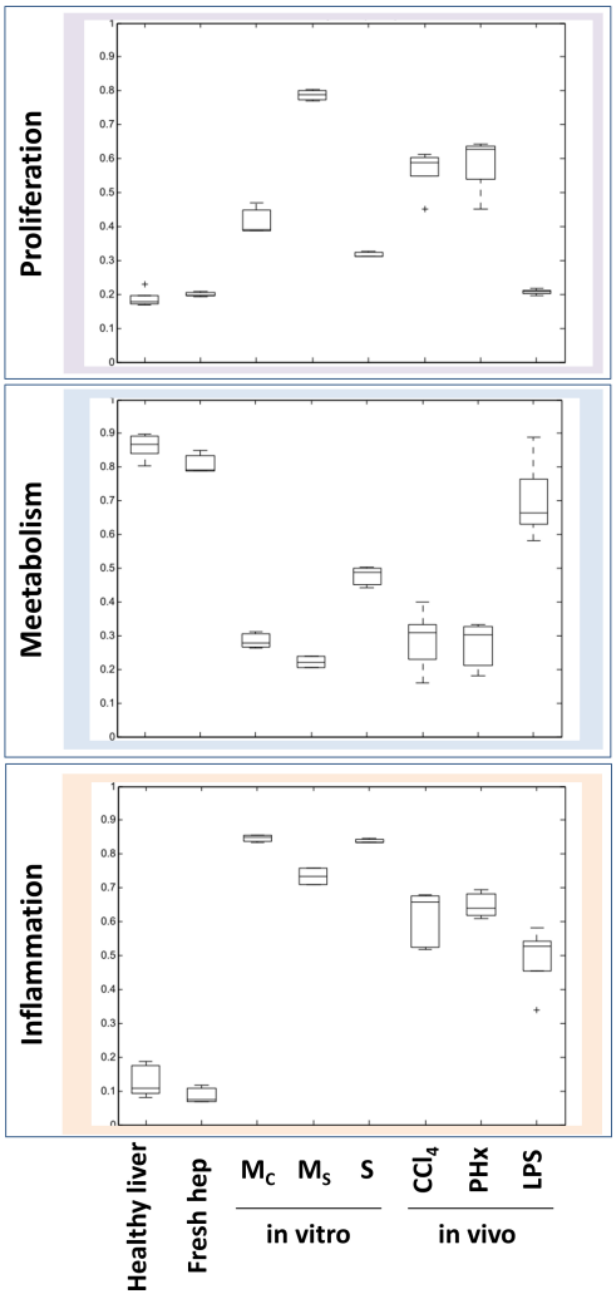

FIGURE 44: *IN VITRO* AND *IN VIVO* MODELS ARE CHARACTERIZED BY AN INCREASE IN PROLIFERATION AND INFLAMMATORY RESPONSE AND A DECREASE IN METABOLISM CLUSTERS
Comparison of metagene scores for ´proliferation`, ´metabolism` and ´inflammation` between cultivation (M_C, M_S and S) and the *in vivo* models CCl_4, PHx and LPS.

The results illustrate an increase in the proliferation metagenes, not only in all *in vitro* conditions, with a particularly strong increase in M_S, but also in CCl_4 and PHx, the two *in vivo* models that involve liver regeneration. Likewise, an increase in inflammation and a decrease in metabolism metagenes were observed for all studied interventions.

The results also suggest that sandwich culture show certain advantages over other culture systems. Sandwich culture exhibits similar inflammatory response as that triggered in other cultivation systems, but exhibited a more *in vivo*-like profile as its "proliferation" score was shown to be lowest among all cultivation systems and its "metabolism" cluster shows great recovery towards healthy liver tissue and freshly isolated hepatocytes (Fresh hep).

In conclusion, these results illustrate that seemingly different stress conditions such as hepatocyte isolation and culture, as well as CCl_4, LPS or PHx liver damage, induce similar cellular responses in hepatocytes.

3.4 MINOR ROLE OF NPC IMPURITIES AND EXTRACELLULAR MATRIX (ECM)

3.4.1 CHARACTERIZATION OF THE NON-PARENCHYMAL CELLS (NPC) FRACTION

As shown in the previous chapter, primary mouse hepatocytes demonstrate a strong inflammatory response in culture that is similar to that of a stressed-inflamed liver *in vivo*. A possible explanation for this could be the influence of impurities from the Non Parenchymal Cells (NPC). Stellate cells, Kupffer cells or sinusoidal endothelial cells might be activated in culture to secrete cytokines and cause the inflammatory transcription response in the neighboring hepatocytes.

In order to assess the influence of other liver cell types, the NPC fraction remaining in hepatocytes after the isolation procedure was thoroughly characterized using Fluorescence-Activated Cell Sorting analysis (FACS) (Figure 45, upper of panel A) and manual counting of H&E stained cell suspensions (Figure 45, B). Hepatocytes are larger than NPCs (as evidenced by measuring the Forwards Scatter – FSC-H), and due to the high content of various organelles such as endoplasmic reticulum, they are characterize by their higher granularity [22] as shown with the measure of Side Scatter – SSC-H). The H&E-stained hepatocytes are easily distinguished as the large cells with the intensely stained red cytoplasm (Figure 45, B indicated with arrows); whereas, non-parenchymal cells show pale blue nuclei with a faintly stained cytoplasm (Figure 45, B indicated with arrowheads). Both cell populations were counted manually after H&E staining with a resulting score of 86.84% for hepatocytes (Figure 46, panel B, row "-") and 13.16% for NPCs. In the second method, population distribution was analyzed by their size (FSC-H) and granularity (SSC-H) by FACS in a high throughput manner (Figure 45, panel A, upper). FACS analysis identifies the hepatocytes-enriched fraction as large and granular (87.55% of the whole population); whereas, non-parenchymal cells are defined as the small and non-granular population (9.36% of the whole population).

In conclusion, both techniques indicate a relatively high fraction of approximately 10-13% NPC impurities in the hepatocyte-enriched fraction obtained after the isolation procedure.

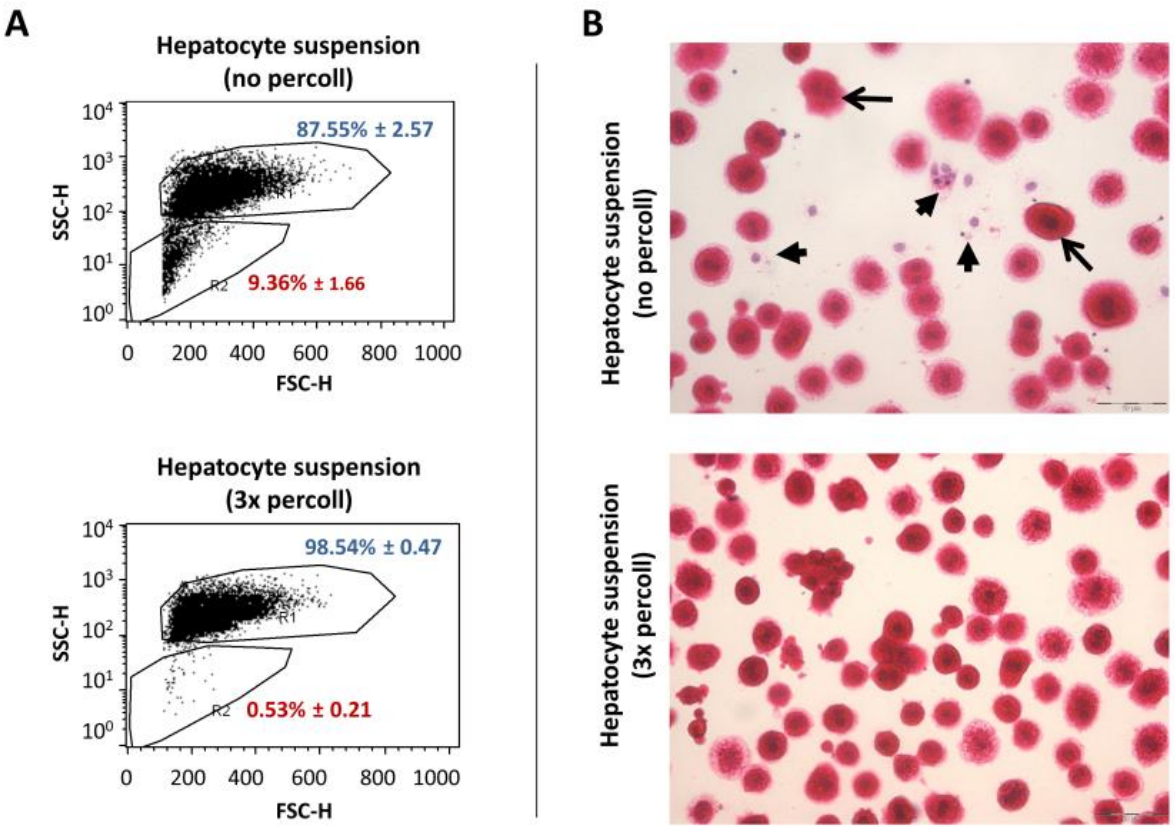

FIGURE 45: THE HEPATOCYTE-ENRICHED FRACTION CONTAINS APPROXIMATELY 10-13% OF NPC IMPURITIES
Characterization of the NPC population in the hepatocyte-enriched fraction after isolation**. A)** FACS analysis of hepatocytes and non-parenchymal cells in suspension. Blue indicates the hepatocyte population, identified as large and granular, whereas red indicates non-parenchymal cells which are defined as the small and non-granular population. The non-parenchymal cell population is almost completely removed by three Percoll purification steps (A lower, 3x Percoll). Values represent mean ± SD (*n=3*). SSC-H stands for granularity scale and FSC-H stands for size scale. **B)** Bright field microscopy of hematoxilin & eosin stained hepatocyte suspensions, without or with three Percoll purification steps. Hepatocytes are easily distinguished as large cells with intense red cytoplasm (arrows) whereas non-parenchymal cells appear with pale blue nuclei and faint cytoplasm (arrowheads). The non-parenchymal cell population is almost completely removed by three Percoll purification steps (B lower, 3x Percoll).

To investigate the role of NPC impurities on the hepatocyte gene expression profile, an additional purification step with Percoll was established to obtain a hepatocyte-enriched fraction. This fraction was then purified by an additional one (1x), two (2x) or three (3x) centrifugation steps in addition to the Percoll solution. After each purification procedure, both cell populations were analyzed by FACS and H&E staining (Figure 46). The results demonstrated that the fraction of NPC could be eliminated by the additional Percoll centrifugation steps (Figure 46). Despite the small residual fraction of approximately 1% NPC that could not be removed by further purifications, the difference when compared to the unpurified cells (13%

NPCs), indicates that this highly purified hepatocyte preparation offers appropriate conditions to study a possible influence of the NPC fraction.

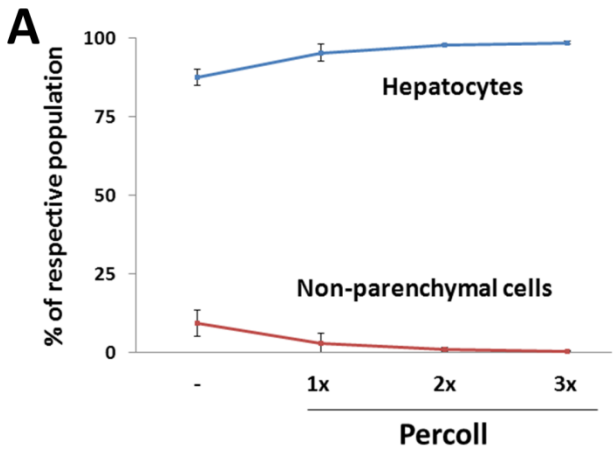

B

	Percoll			
	-	1x	2x	3x
Hepatocytes %	86.84 (± 1.29)	96.30 (± 3.05)	98.14 (± 0.81)	99.21 (± 0.43)
NPC %	13.16 (± 1.29)	3.70 (± 3.05)	1.86 (± 0.81)	0.79 (± 0.43)

FIGURE 46: ADDITIONAL CENTRIFUGATION STEPS OF THE HEPATOCYTE-ENRICHED FRACTION ON TOP OF PERCOLL SOLUTION ALMOST COMPLETELY REMOVES THE NPC IMPURITIES
Quantification of hepatocytes and non-parenchymal cells by (A) FACS or (B) microscopy in conventional or Percoll-purified freshly isolated cell suspensions. Both techniques indicated almost complete removal of NPC impurities.

3.4.1 INFLUENCE OF NON PARENCHYMAL CELLS (NPC)

To assess the influence of NPC impurities on hepatocytes gene expression profile, hepatocyte-enriched fraction of distinct purities were analyzed for the expression of the following selected markers: Lcn2 and Mt2 representing inflammation cluster 3A; Saa3 representing inflammation cluster 3B; and Bsep, Mrp2 and Cyp7a1 representing metabolism-associated cluster 2B (Figure 47).

NPCs had no influence on most of the analyzed metabolism cluster genes. Similarly, the inflammation cluster 3A genes Lcn2 and Mt2 showed no major NPC dependency. For Lcn2, a slightly decreased expression was observed after Percoll purification but the difference was not significant when considering the huge difference between percentage scores of freshly isolated hepatocytes and either purified or unpurified cell populations. A different result was obtained for the inflammation cluster 3B gene Saa3. In this case, Percoll purification caused a relevant decrease in expression.

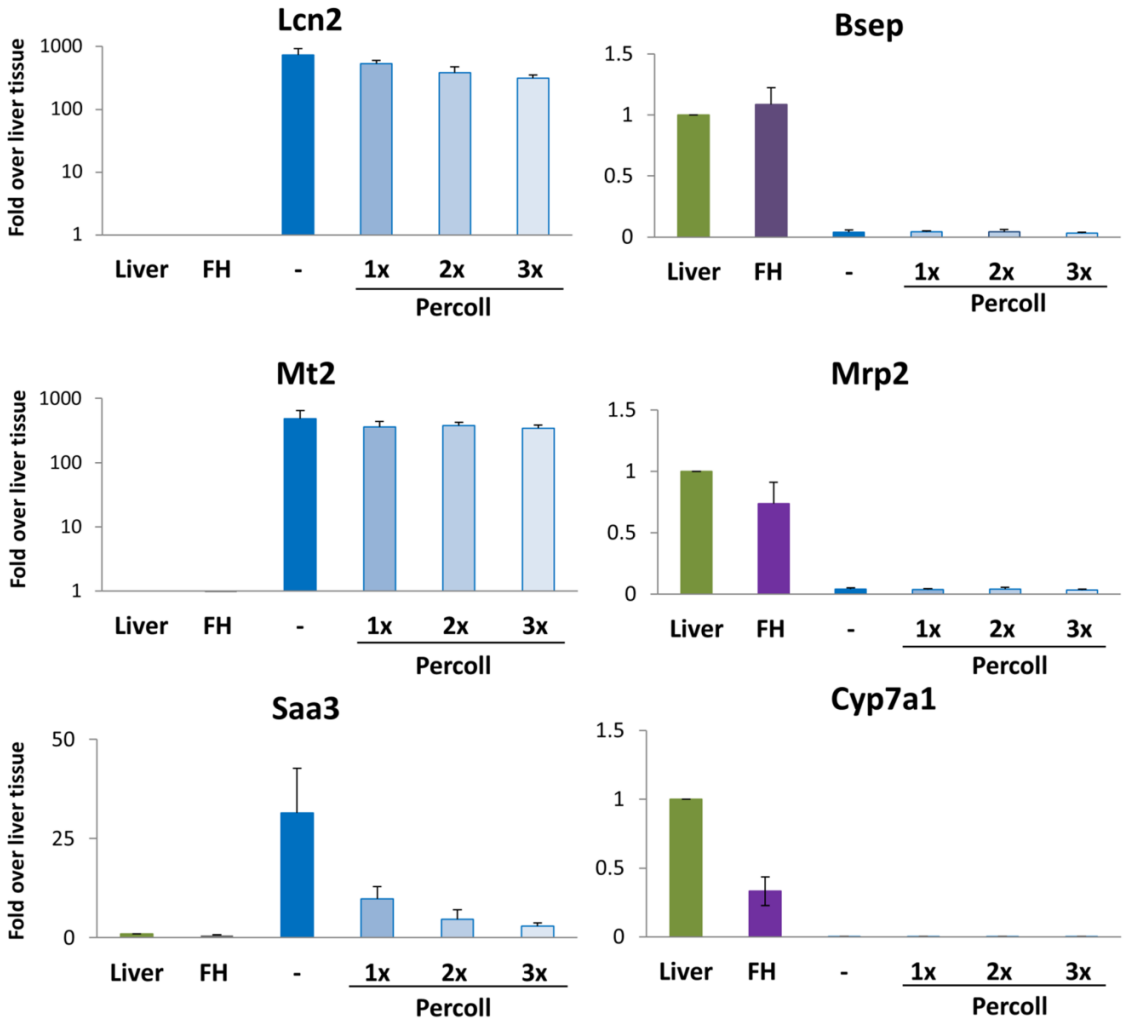

FIGURE 47: ADDITIONAL PURIFICATION STEPS DO NOT RESCUE THE METABOLISM CLUSTER AND DO NOT DIMINISH THE INFLAMMATORY RESPONSE *IN VITRO*

Quantitative RT-PCR analysis of inflammation- (Lcn2, Mt2 and Saa3) or metabolism-associated genes (Bsep, Mrp2 and Cyp7a1) in healthy liver tissue (Liver), freshly isolated hepatocytes (FH) and hepatocytes in sandwich culture at day 1, either from conventional or Percoll-purified cell suspensions. GAPDH was used as an endogenous control. Data are expressed as fold change relative to healthy liver tissue. Values represent mean ± SD (*n=3*).

In order to fully understand the contribution of NPC on hepatocytes' gene expression profile in culture, a population of NPC was added to Percoll purified hepatocytes in a ratio of 1:2 and plated on sandwich or monolayer confluent culture for the indicated timepoints (described in chapter 2.2.2.6). The aforementioned principles were confirmed, whereby NPC slightly enhanced Saa3 expression but had no major influence on Lcn2, Mt2, Bsep, Mrp2 or Cyp7a1 (Figure 48).

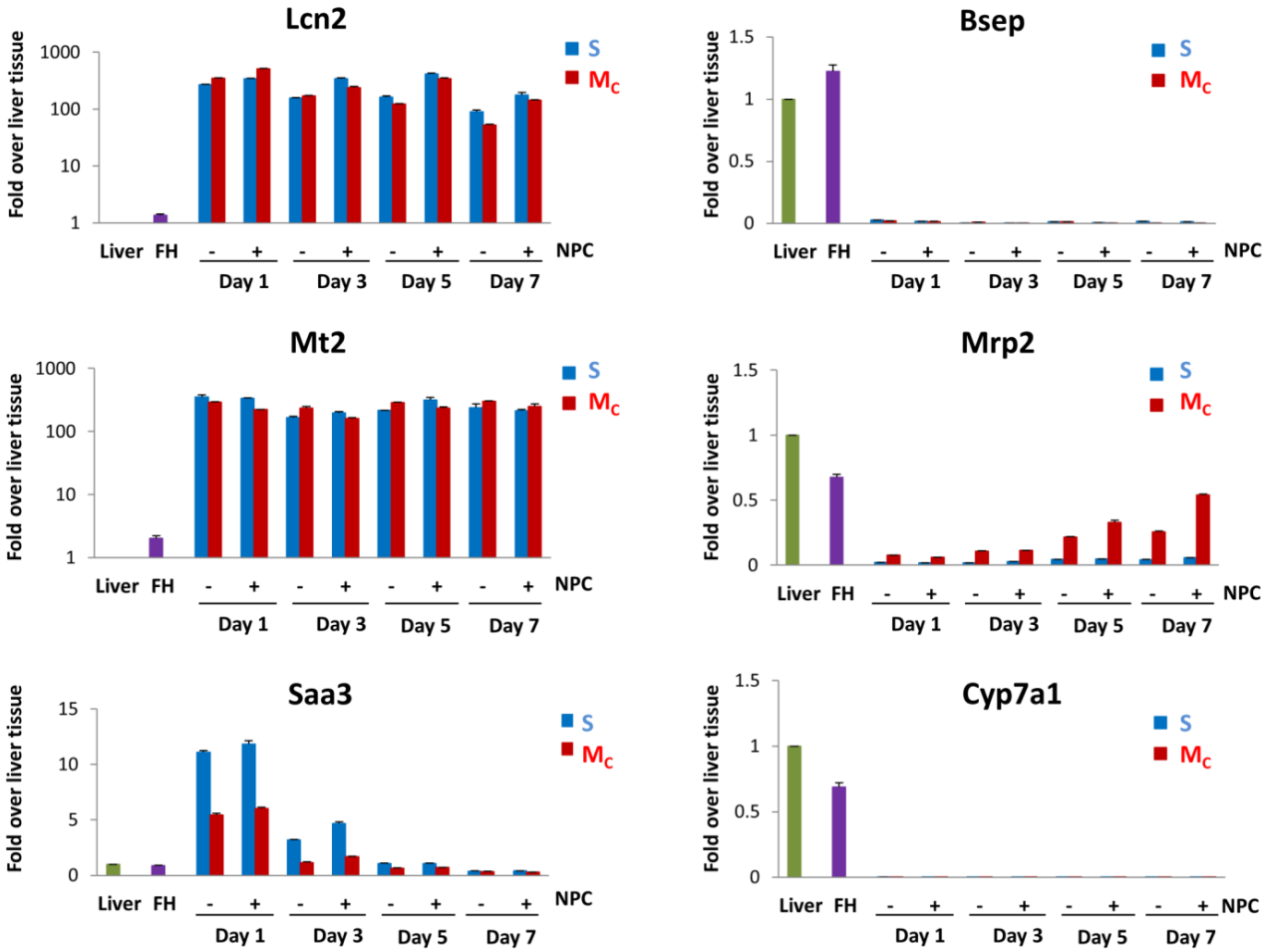

FIGURE 48: THE EFFECT OF CO-CULTURE ON INFLAMMATORY AND METABOLISM CLUSTERS
Quantitative RT-PCR analysis of inflammation- (Lcn2, Mt2 and Saa3) or metabolism-associated genes (Bsep, Mrp2 and Cyp7a1) in healthy liver tissue (Liver), freshly isolated hepatocytes (FH) and hepatocytes in sandwich (S), monolayer confluent (M_C) culture, alone or in combination with non-parenchymal cells at a ratio of 2:1 for the indicated time. GAPDH was used as an endogenous control. Data are expressed as fold change relative to healthy liver tissue. Values represent mean ± SD (*n=3*).

In conclusion, non parenchymal cells do not influence hepatocytes' expression profile in culture with respect to the identified gene clusters. However, NPC seem to support the upregulation of Saa3. This suggests that genes in Cluster 3B may be dependent upon NPC.

3.4.2 INFLUENCE OF THE EXTRACELLULAR MATRIX

3.4.2.1 NO MAJOR INFLUENCE OF DIFFERENT TYPES OF ECM ON CULTIVATION-INDUCED GENE EXPRESSION PROFILES

Another possible cause for the change in the hepatocyte cellular response may be due to the cell attachment onto a collagen matrix. Therefore, the aim of the next experiment was to validate the influence of the extracellular matrix. Hepatocytes were cultivated on different

extracellular matrixes for the indicated timepoints and the gene expression profiles of selected markers (Lcn2 and Mt2 representing inflammation cluster 3A; Saa3 representing inflammation cluster 3B; Bsep, Mrp2 and Cyp7a1 representing metabolism-associated cluster 2B were analyzed (Figure 49).

A comparison of collagen sandwich and monolayer confluent culture to other types of commercially available matrices, such as Matrigel™ and laminin demonstrated similar alterations of metabolism and inflammation gene clusters as observed for the collagen matrixes. The results show that the systemic alteration in gene expression occurs independently of the specific type of extracellular matrix.

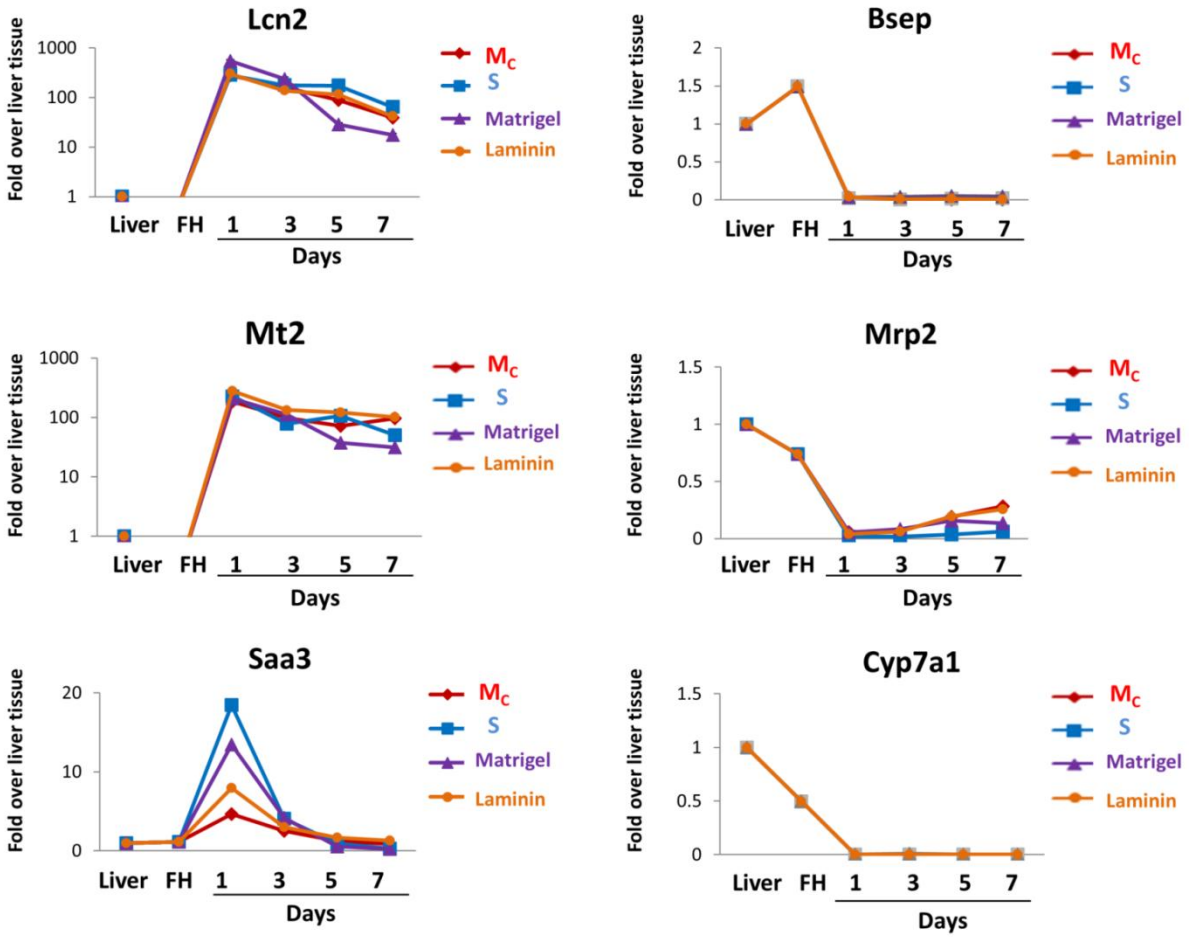

FIGURE 49: SYSTEMIC ALTERATIONS IN GENE EXPRESSION OCCURS INDEPENDENT FROM THE SPECIFIC TYPE OF EXTRACELLULAR MATRIX

Quantitative RT-PCR analysis of inflammation- (Lcn2, Mt2 and Saa3) or metabolism-associated genes (Bsep, Mrp2 and Cyp7a1) in healthy liver tissue (Liver), freshly isolated hepatocytes (FH) and hepatocytes in sandwich (S), monolayer confluent (M_C) culture, or cultured in matrigel or laminin for the indicated time. GAPDH was used as an endogenous control. Data are expressed as fold change relative to healthy liver tissue. Values represent mean ± SD (*n=3*).

3.4.2.1 SPHEROIDS

In sandwich cultures, hepatocytes are kept between two layers of collagen type-I, which is isolated from rat-tail and does not represent the natural matrix of hepatocytes in the liver. A method for aggregating spheroids, on the other hand, offers conditions where cells can produce their own matrix [72]. The aim of the next experiment was to validate the effect of the natural extracellular matrix. Primary mouse hepatocytes were used to generate spheroids for the the indicated timepoints (described in chapter 2.2.2.5) and the gene expression profile for the previously described, selected markers was analyzed (Figure 51).

In both cultivation systems (sandwich and spheroids), hepatocytes established a polar phenotype as shown with DPPIV staining of the bile canaliculi (Figure 18 and Figure 50).

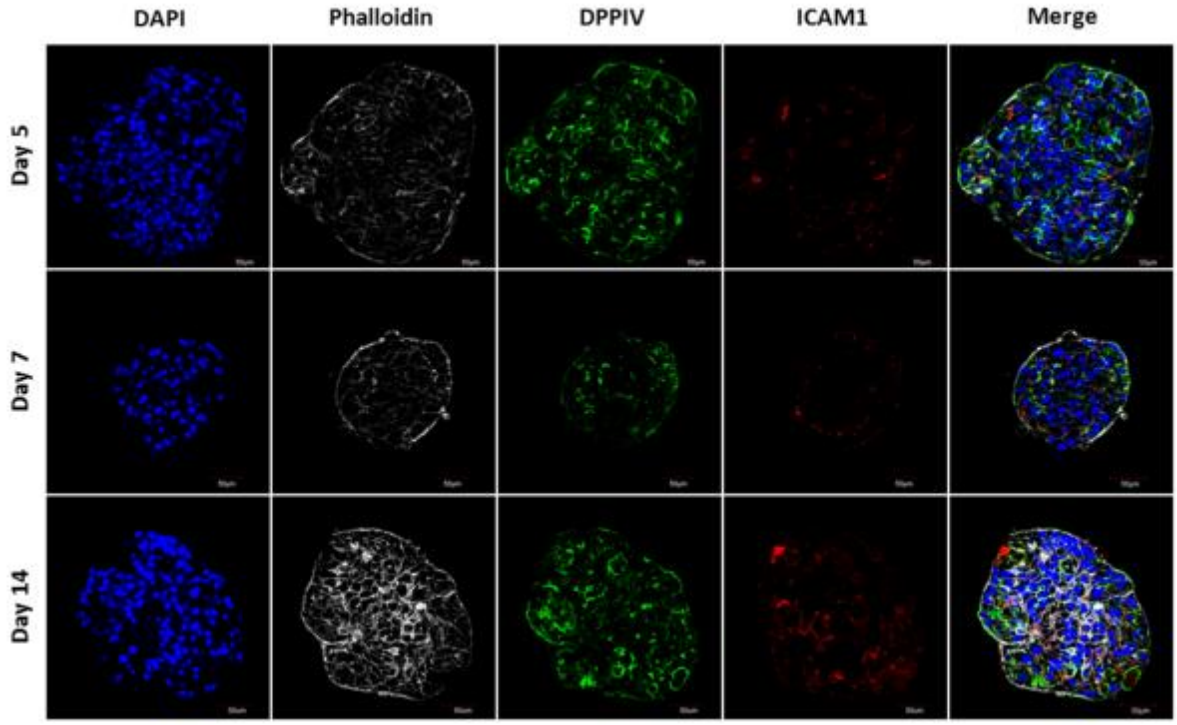

FIGURE 50: PRIMARY MOUSE HEPATOCYTES ESTABLISH A POLAR PHENOTYPE IN SPHEROIDS CULTURE
Morphology of primary mouse hepatocytes in spheroids. Confocal microscopy of primary mouse hepatocytes in spheroids reveals structural details: nuclei marked with DAPI (blue), F-actin marked with phalloidin (gray), bile canalicular enzyme dipeptidyl peptidase IV (DPPIV in green) and Intercellular Adhesion Molecule 1 (ICAM1 in red). Magnification of 40X. Hepatocyte polarity is clearly observed in all timepoints, as revealed by bile canalicular-like structures similar to those formed in sandwich culture (Figure 18).

Analysis of gene clusters markers show that the same principles are valid in both culture systems, whereby genes of the metabolism and inflammation clusters are down and up-regulated, respectively (Figure 51). However, the degree of downregulation of some metabolism cluster genes (e.g. Mrp1 and Cyp7a1) is ameliorated in the spheroids compared to

sandwich, which may represent an advantage of the latter system. Consistently, expression of HNF4α, whose binding site is overrepresented in the metabolism cluster genes, was better maintained in spheroids than in sandwich culture. However Cebpδ, a transcription factor responsible for expression of inflammation genes (Poli 1998), is higher in spheroids, illustrating that this culture type does not ameliorate the inflammation response.

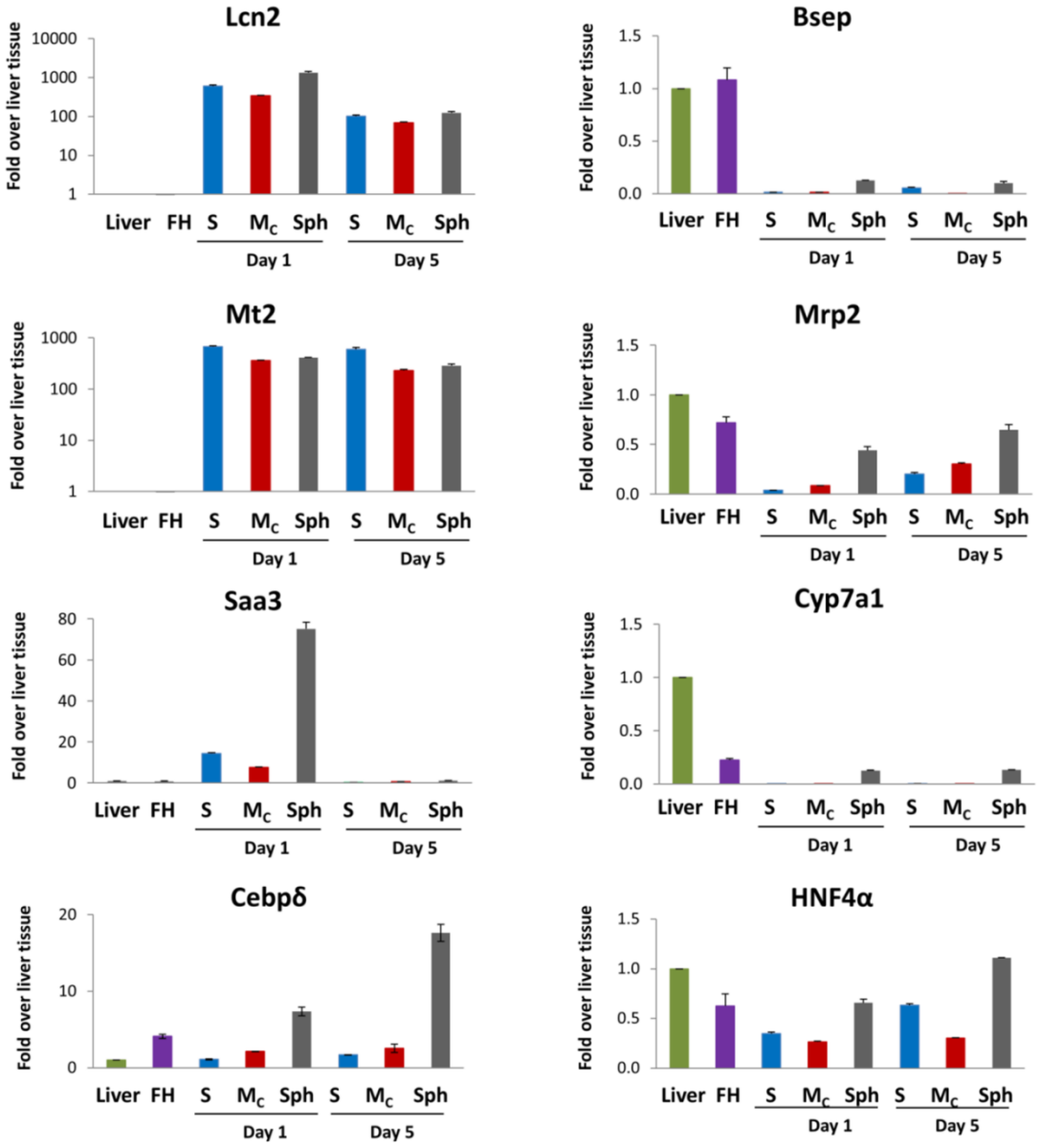

FIGURE 51: COMPARISON OF THE SPHEROIDS SYSTEM AND SANDWICH CULTURE

Quantitative RT-PCR analysis of inflammation- (Lcn2, Mt2, Saa3 and Cebpδ) or metabolism-associated genes (Bsep, Mrp2, Cyp7a1 and HNF4α) in healthy liver tissue (Liver), freshly isolated hepatocytes (FH) and hepatocytes in sandwich (S), monolayer confluent (M_C) culture, or spheroids (Sph) for the indicated time. GAPDH was used as an endogenous control. Data are expressed as fold change relative to healthy liver tissue. Values represent mean ± SD (*n=3*).

In conclusion, the presented results show that the systemic alterations in gene expression are independent from the specific type of extracellular matrix. Additionally, the spheroid culture may represent a certain advantages over monolayer or sandwich cultures in regards to some gene clusters.

3.5 JNK SIGNALING DRIVES INFLAMMATION

3.5.1 STRESS SIGNALING PATHWAYS ARE QUICKLY ACTIVATED DURING ISOLATION OF HEPATOCYTES

After describing the stereotypic gene expression response of isolated hepatocytes in detail, the next step was to investigate how signaling proteins were altered during the isolation procedure and cultivation. For this reason, a time resolved Luminex Bead-Based Multiplex Assay was performed. Primary mouse hepatocytes were cultivated on monolayer confluent and sandwich (S) culture for the indicated timepoints and protein lysates were analyzed with the use of specific antibodies (described in chapter 2.2.8).

Luminex analysis reveals a strong alteration of p-ERK, p-JNK, p-MEK1 and p-p38 signaling in freshly isolated hepatocytes (Figure 52). In culture, most activities decreased once more, but usually not back to the levels found in healthy liver tissue.

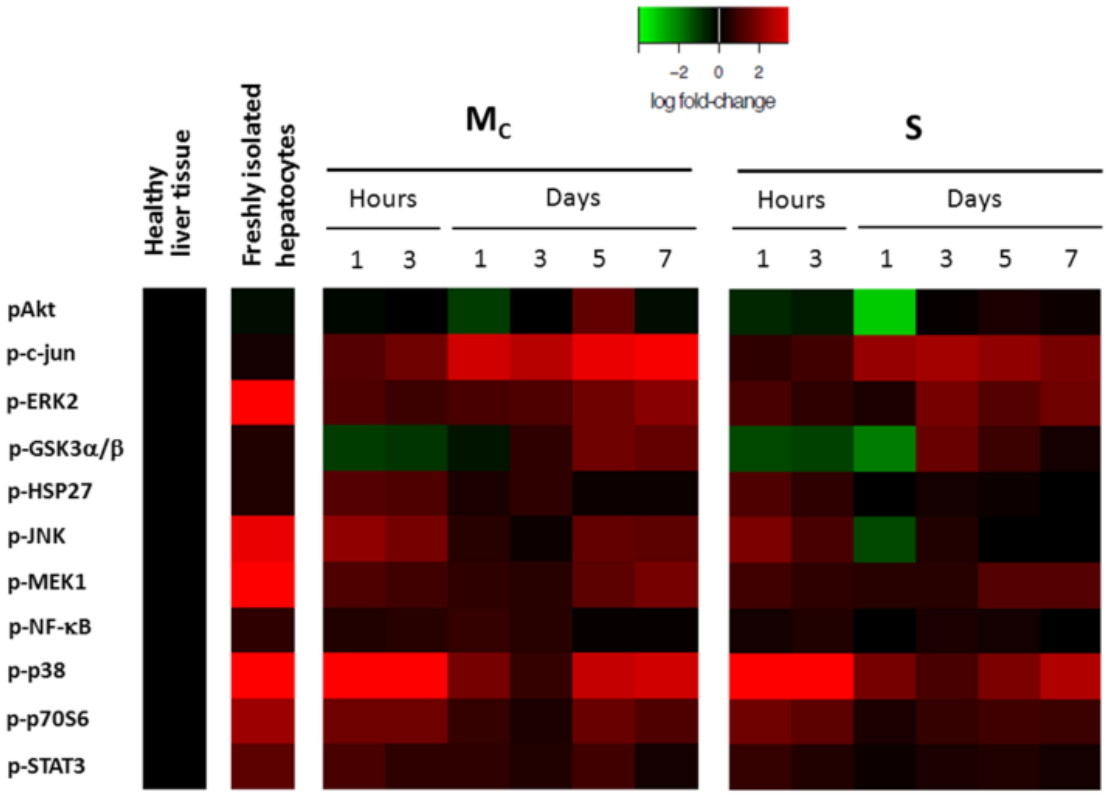

FIGURE 52: STRESS SIGNALING PATHWAYS ARE QUICKLY ACTIVATED DURING ISOLATION OF HEPATOCYTES
Luminex analysis of signal transduction pathway-associated proteins, comparing healthy liver tissue, freshly isolated hepatocytes, and hepatocytes in monolayer confluent (M_C) or sandwich (S) culture for the indicated time. The heatmap represents fold change compared to healthy liver tissue, from three independent biological replicates.

Additionally, a strong increase in ERK and JNK activation in freshly isolated hepatocytes was validated by Western blot (Figure 53).

In conclusion, stress-signaling pathways are activated quickly during isolation of hepatocytes suggesting that interventions to block or prevent the activation of these stress pathways should be applied at early stages directly upon isolation or cultivation.

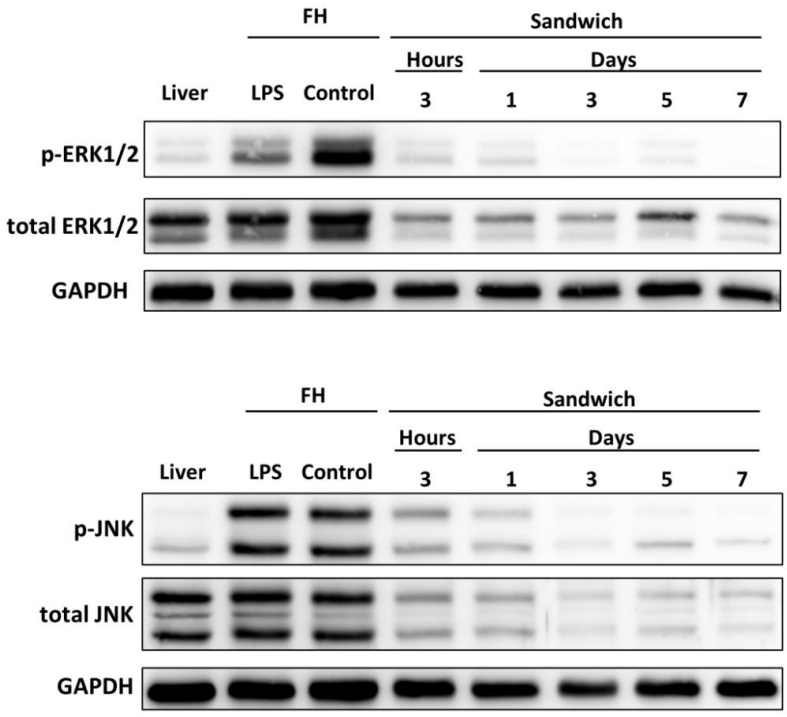

FIGURE 53: ERK1/2 AND JNK SIGNALING ARE ACTIVATED DURING PERFUSION
Validation of Luminex screening. Immunoblot analysis of ERK1/2 and JNK signaling activation in healthy liver tissue (Liver), freshly isolated hepatocytes (FH), hepatocytes in sandwich (S) culture for the indicated time. GAPDH was used as an endogenous control. Protein extract from healthy liver tissue and freshly isolated hepatocytes were used as negative controls, while freshly isolated hepatocytes from mice treated for 24h with LPS (750 ng/kg, intraperitoneally) were used as positive control. Representative images from 3 independent experiments are shown.

3.5.2 A SCREENING USING CHEMICAL INHIBITORS REVEALS THE CONTRIBUTION OF SPECIFIC SIGNAL TRANSDUCTION PATHWAYS IN CULTIVATION-INDUCED GENE EXPRESSION

The rapid activation of stress signaling pathways during isolation is a potential explanation for the transcriptional response described above for the primary hepatocytes in culture. Therefore, the aim of next experiments was to ameliorate gene expressional changes using small chemical inhibitors of the specific signaling pathways. For this purpose, primary mouse hepatocytes were cultivated in the presence of a battery of inhibitors (Table 7) for 24 hours in sandwich culture and the gene expression profile of the previously described, selected markers was analyzed (Figure 54 and Figure 55). These compounds were added to the hepatocytes in suspension directly prior to plating (in culture medium) and re-added with fresh serum-free medium after 3 hours of attachment, to ensure that the pathways remain inhibited during the critical 24 hour period where most transcriptional alterations occur. DMSO was used as the solvent control at concentration of 0.5%.

Of all the inhibitors tested, the most profound effect was observed for the JNK inhibitor SP600125, particularly for genes representing the inflammation response, such as Lcn2 (representative of Cluster 3A), and Saa3 (representative of Cluster 3B) (Figure 54). After 24 hours, a consistent concentration-dependent decrease of inflammation genes was observed, indicating that the JNK pathway is critical for the inflammation response. Other inhibitors also repressed the induction of Saa3, showing that the transiently-induced inflammation gene cluster (Cluster 3B) may be controlled by pathways other than JNK.

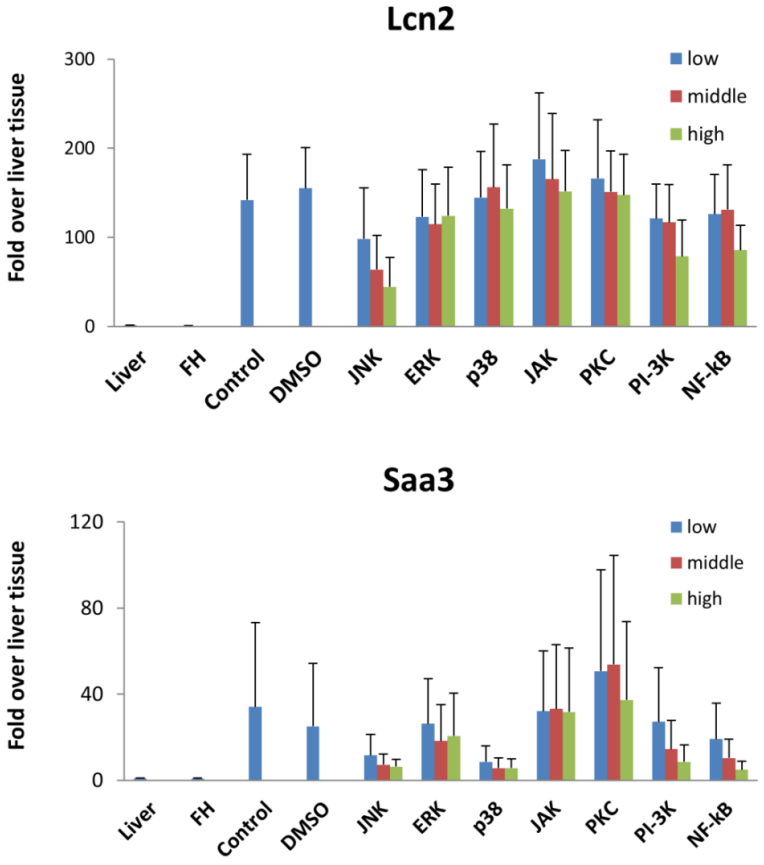

FIGURE 54: THE JNK PATHWAY IS CRITICAL FOR THE INFLAMMATION RESPONSE

Quantitative RT-PCR analysis of inflammation-associated genes (Lcn2 and Saa3) in healthy liver tissue (Liver), freshly isolated hepatocytes (FH) and hepatocytes in sandwich culture (S) on day 1 in the presence of inhibitors at different concentrations (low, middle and high) for the indicated pathways. DMSO was used as the solvent control at a concentration of 0.5%. GAPDH was used as an endogenous control. The inhibitors and concentrations used are described in Table 7. Data are expressed as fold change relative to healthy liver tissue. Values represent mean ± SD (*n=3*).

In contrast, none of the tested inhibitors was able to rescue the profound repression of metabolism-associated genes (Figure 55), indicating that yet undiscovered pathways control this response.

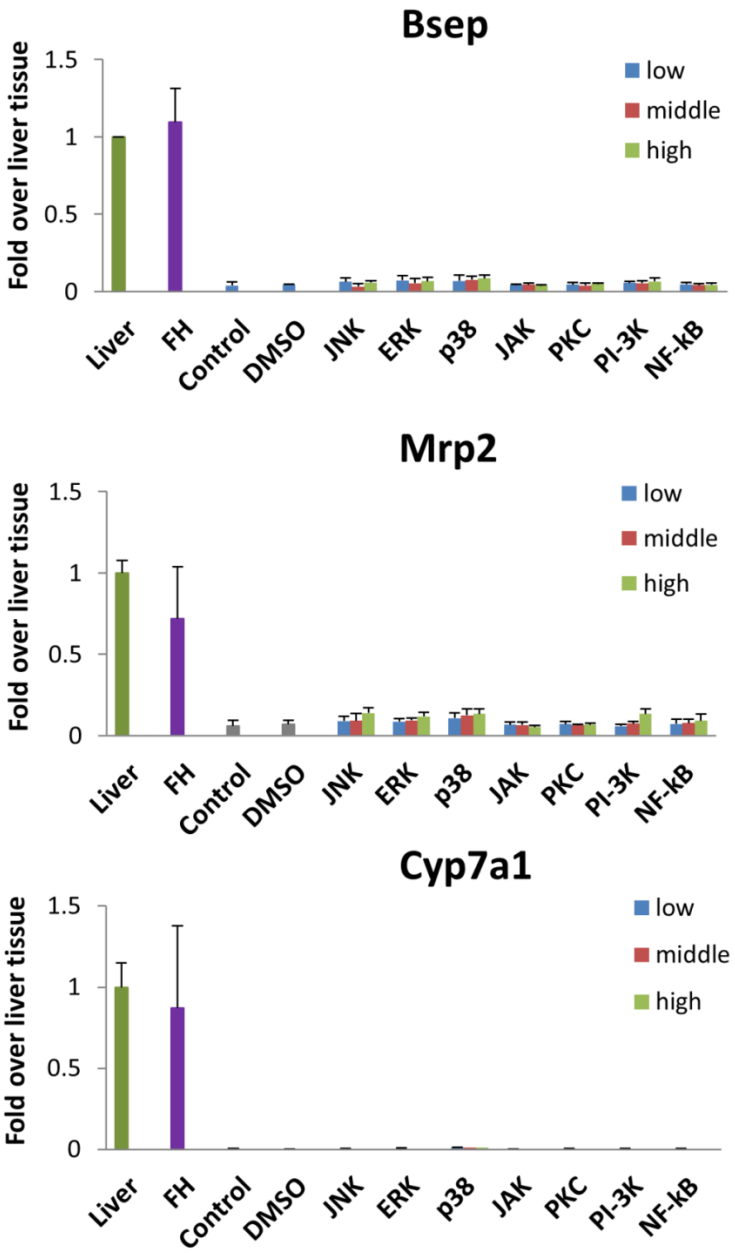

FIGURE 55: SO FAR UNDISCOVERED PATHWAYS CONTROL THE METABOLISM GENE CLUSTER

Quantitative RT-PCR analysis of metabolism-associated genes (Bsep, Mrp2 and Cyp7a1) in healthy liver tissue (Liver), freshly isolated hepatocytes (FH) and hepatocytes in sandwich culture (S) on day 1 in the presence of inhibitors at different concentrations (low, middle and high) for the indicated pathways. DMSO was used as the solvent control at a concentration of 0.5%. GAPDH was used as an endogenous control. The inhibitors and concentrations used are described in Table 7. Data are expressed as fold change relative to healthy liver tissue. Values represent mean ± SD (*n=3*).

3.5.3 ACTIVATION OF JNK SIGNALING OCCURS ALREADY DURING PERFUSION WITH EGTA BUFFER

The results presented in the previous chapter highlighted the potential importance of the JNK signaling pathway, in particular its early activation, on the changes observed in the inflammation and metabolism clusters in freshly isolated hepatocytes. Therefore, the aim of the next experiments was to determine the step during the isolation process that was responsible for the observed JNK activation. For this purpose, mouse livers at different stages of the perfusion process were analyzed, namely (i) after 5 minutes of EGTA buffer, (ii) 5 minutes, plus 15 minutes collagenase buffer perfusion, and (iii) 20 minutes of EGTA buffer perfusion (Figure 56).

The result shows that EGTA buffer perfusion alone is sufficient to induce JNK activation (and ERK1/2, which was used as a positive control). Activation occurs between 5 and 20 minutes of EGTA perfusion. Combined EGTA plus collagenase perfusion causes a similar activation.

In conclusion, activation of JNK signaling occurs between 5 and 20 minutes of perfusion with EGTA buffer, suggesting that interventions with inhibitors should already start early, ideally during perfusion.

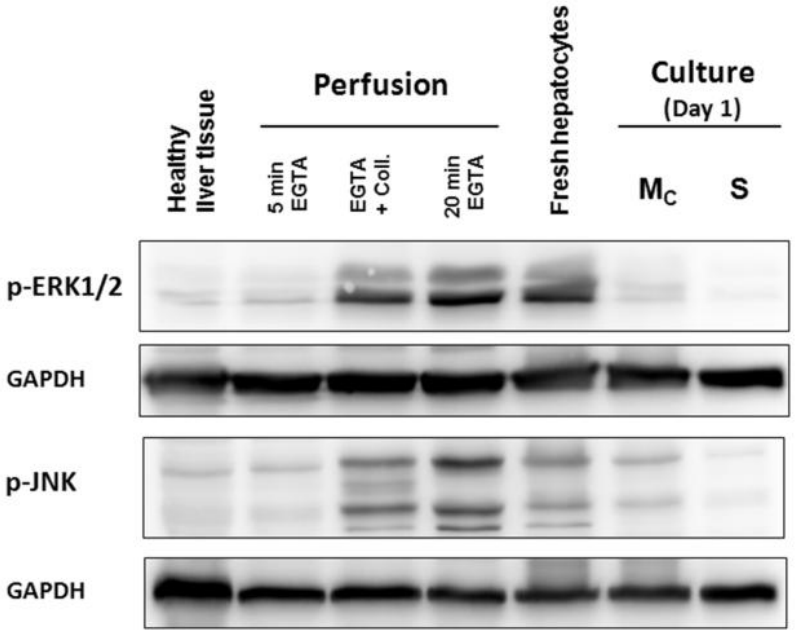

FIGURE 56: EGTA BUFFER PERFUSION ALONE IS SUFFICIENT TO INDUCE JNK ACTIVATION
Immunoblot analysis of JNK signaling and ERK1/2 signaling (positive control) activation in healthy liver tissue (Liver), livers after 5 minutes of EGTA buffer perfusion (5 min EGTA), 5 minutes EGTA buffer plus 15 minutes collagenase buffer perfusion (EGTA + Coll.), or 20 minutes of EGTA buffer perfusion, freshly isolated hepatocytes (FH), hepatocytes in monolayer confluent (M_C) or sandwich (S) culture on day 1. GAPDH was used as an endogenous control. Representative images for 3 independent experiments are shown.

3.5.4 JNK INHIBITOR REDUCES THE CULTIVATION-INDUCED INFLAMMATORY RESPONSE

JNK signaling was identified as the signaling pathway that is activated early during the isolation procedure influencing induction of inflammatory response in primary mouse hepatocytes *in vitro*.

In the next step, the significance of JNK and its role in modulating the gene expression response of primary mouse hepatocytes was addressed by performing early interventions during perfusion with the JNK inhibitor-SP600125. For this reason, addition of JNK inhibitor SP600125 was applied as follows (Figure 17): (i) SP600125 was added to the perfusion buffers (EGTA + Collagenase) but not to the cell culture medium, (ii) not to the perfusion buffer but to the culture medium directly upon plating, and (iii) to both perfusion buffers and culture medium. DMSO was added at 0.5% as a solvent control either to the perfusion solutions or to the cell culture medium, as indicated in the insert box. Primary mouse hepatocytes were cultivated with or without the inhibitor for up to 24 hours in sandwich culture and the gene expression profile of previously described, selected markers was analyzed (Figure 57 and Figure 58).

SP600125, when added alone to the perfusion buffers, clearly reduced Lcn2 levels in hepatocytes of all three independent biological replicates (Figure 57). However, Lcn2 expression increased during the cultivation period once the inhibitor was removed. When SP600125 was added only to the culture medium, a decrease in Lcn2 was also seen but this effect lasted longer compared to the ´buffers only` experiment. Consistent with these observations, the presence of SP600125 in the perfusion buffers as well as in the culture medium caused the strongest and most permanent decrease in Lcn2 expression.

In contrast, the JNK inhibitor did not influence the expression of the metabolism cluster biomarkers Bsep and Mrp2 in hepatocytes in all three independent biological replicates (Figure 58).

In conclusion, these results indicate that early activation of JNK during perfusion modulates the induction of an inflammatory response of primary mouse hepatocytes *in vitro*.

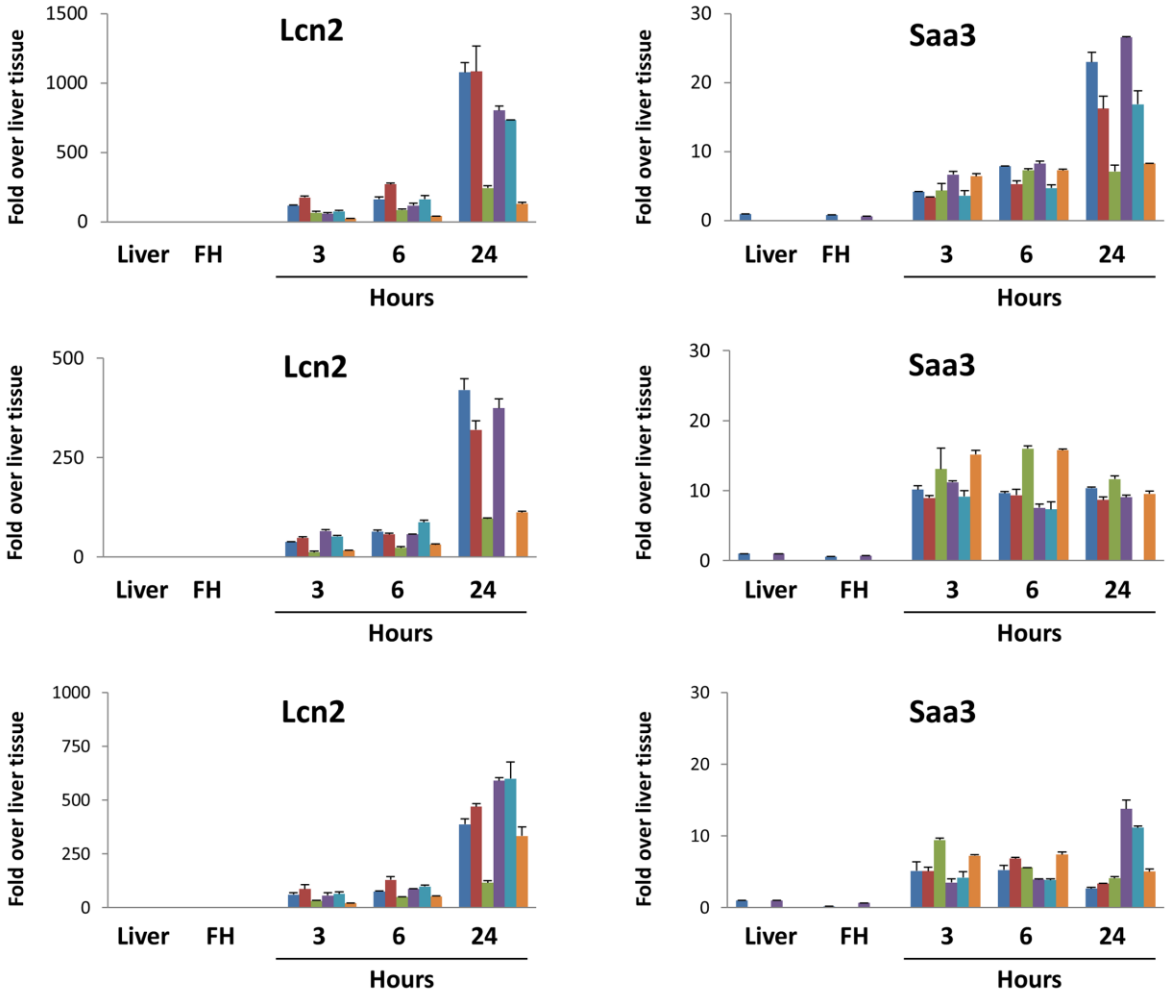

FIGURE 57: INTERVENTION WITH THE JNK INHIBITOR REDUCES THE INFLAMMATORY RESPONSE

Quantitative RT-PCR analysis of inflammation-associated genes (Lcn2 and Mt2) in healthy liver tissue (Liver), freshly isolated hepatocytes (FH), hepatocytes in sandwich (S) culture for the indicated time, in the presence or absence of the JNK inhibitor (SP600125) at 50 µM, using DMSO as a vehicle. The addition of the JNK inhibitor SP600125 was applied as follows (Figure 17): (i) SP600125 was added to the perfusion buffers (EGTA + Collagenase) but not to the cell culture medium, (ii) not to the perfusion buffer but to the culture medium directly upon plating and (iii) to both perfusion buffers and culture medium and maintained throughout the cultivation time until 24h. DMSO was added at 0.5% as a solvent control either to the perfusion solutions or to the cell culture medium, as indicated in the insert box. GAPDH was used as an endogenous control. Data are expressed as fold change relative to healthy liver tissue. Each graph represents an independent biological replicate. Values represent mean ± SD (*n=3*).

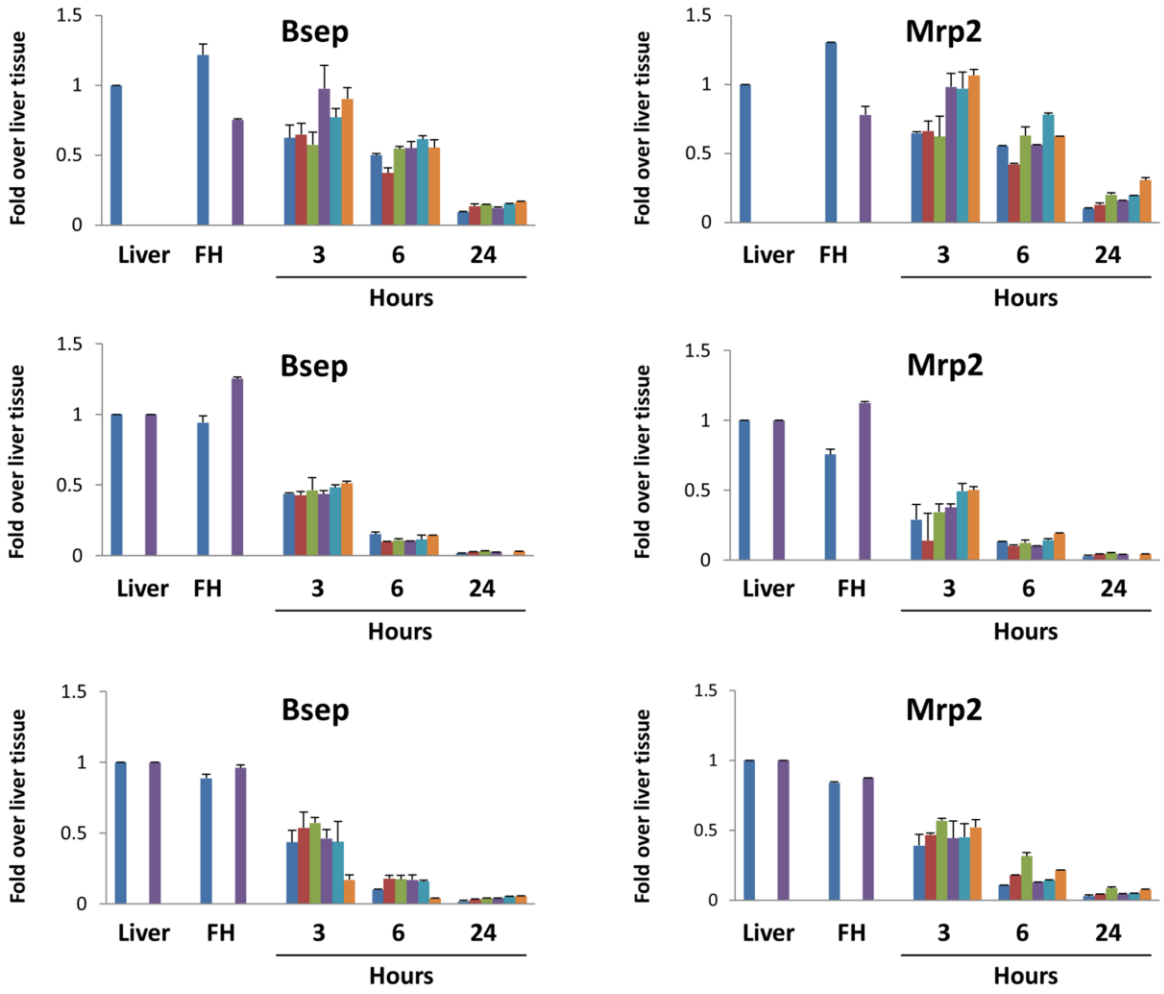

FIGURE 58: INTERVENTION WITH THE JNK INHIBITOR DOES NOT RESCUE METABOLISM DOWN-REGULATION

Quantitative RT-PCR analysis of metabolism-associated genes (Bsep and Mrp2) in healthy liver tissue (Liver), freshly isolated hepatocytes (FH), hepatocytes in sandwich (S) culture for the indicated time, in the presence or absence of the JNK inhibitor SP600125 at 50 µM, using DMSO as a vehicle. The addition of the JNK inhibitor SP600125 was applied as follows (Figure 17): (i) SP600125 was added to the perfusion buffers (EGTA + Collagenase) but not to the cell culture medium, (ii) not to the perfusion buffer but to the culture medium directly upon plating and (iii) to both perfusion buffers and culture medium and maintained throughout the cultivation time until 24h. DMSO was added at 0.5% as a solvent control either to the perfusion solutions or to the cell culture medium, as indicated in the insert box. GAPDH was used as an endogenous control. Data are expressed as fold change relative to healthy liver tissue. Each graph represents an independent biological replicate. Values represent mean ± SD (*n=3*).

3.6 COMPARISON TO RAT AND HUMAN PRIMARY HEPATOCYTES

3.6.1 CULTIVATION-INDUCED INFLAMMATORY RESPONSE AND METABOLISM DECREASE ARE SIMILAR IN HEPATOCYTES OF MICE AND RATS

Although primary mouse hepatocytes represent a fundamental tool for biomedical research, it is important to extrapolate mouse *in vitro* data to other species such as rat and human. Therefore, the aim of the next study was to validate the effect of cultivation conditions on primary rat hepatocytes' gene expression regarding inflammation and metabolism gene clusters. For this purpose, primary rat hepatocytes were cultivated in monolayer Confluent(M_C) and sandwich (S) culture for the indicated timepoints and the gene expression profile of selected markers was analyzed.

Similarl to the mouse hepatocytes (Figure 18, A), primary rat hepatocytes *in vitro* (Figure 59) acquire a profoundly distinguishable morphology depending on the extracellular matrix used as culture substratum. Similar to mouse hepatocytes, M_C culture maintain a cuboidal morphology during the first day in culture; however, after longer cultivation periods EMT-features are visible. In contrast, sandwich-cultured hepatocytes presents the most stable morphology resembling an epithelial-like phenotype. Sandwich cultures appear more differentiated, as seen by their *in vivo*-like cuboidal shape and distinct bile canaliculi network even after longer periods in culture.

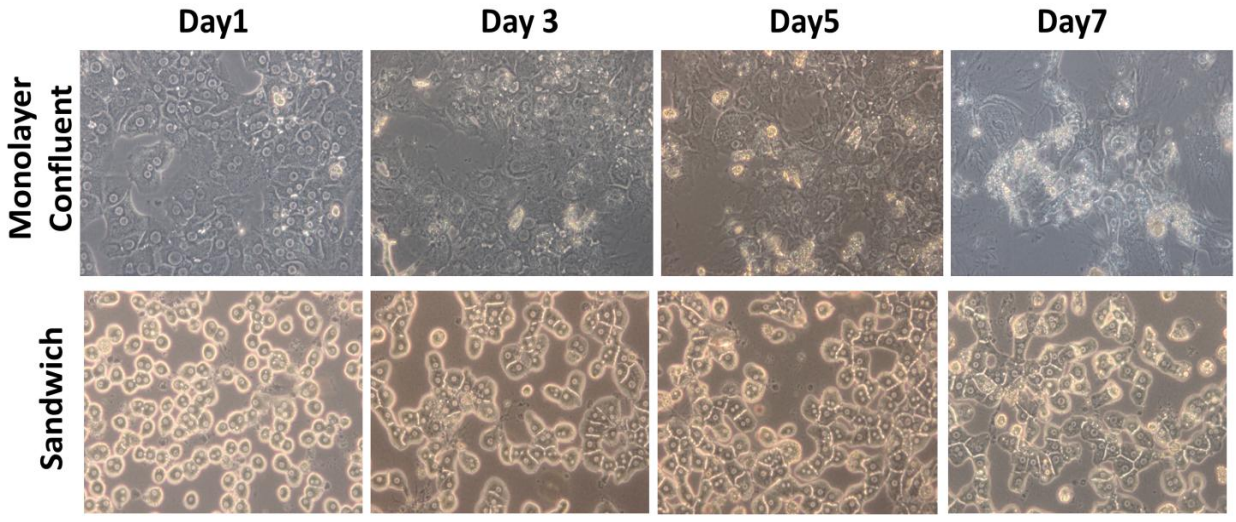

FIGURE 59: EXTRACELLULAR MATRIX CAUSES MORPHOLOGICAL CHANGES IN PRIMARY RAT HEPATOCYTES *IN VITRO*
Light microscopy of primary rat hepatocytes in two culture systems: monolayer confluent and sandwich culture for the indicated periods of time. Magnification of 20X.

qRT-PCR analysis of selected genes indicate that the same principles observed in the mouse model were identified in primary rat hepatocytes, namely induction of inflammation and repression of metabolism-associated genes (Figure 60). These results confirm the occurrence of

the aforementioned principles of inflammation induction and metabolism decrease in primary rat *in vitro* culture, and support a similar stress response of mouse and rat primary hepatocytes that includes features of inflammation and a decline in expression of metabolism-associated genes.

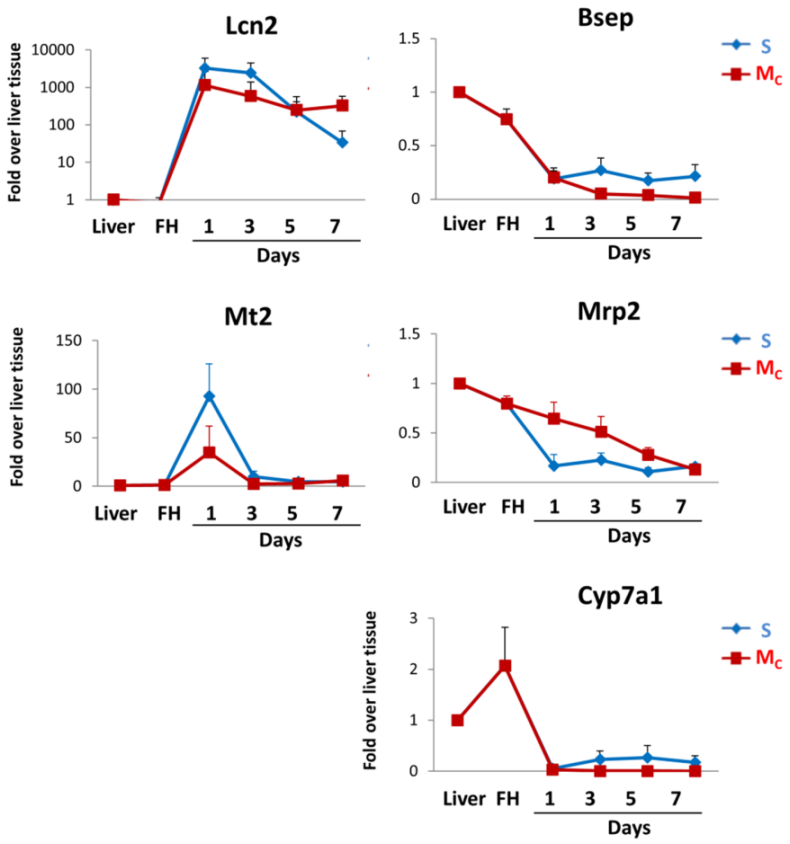

FIGURE 60: SIMILAR TO THE MOUSE MODEL, PRIMARY RAT HEPATOCYTES EXHIBIT INDUCTION OF INFLAMMATION AND LOSS OF METABOLISM *IN VITRO*

Quantitative RT-PCR analysis of inflammation- (Lcn2 and Mt2) or metabolism-associated genes (Bsep, Mrp2 and Cyp7a1) in healthy liver tissue (Liver), freshly isolated hepatocytes (FH), hepatocytes in sandwich (S) culture or monolayer confluent (M_C) culture for the indicated times. GAPDH was used as an endogenous control. Data are expressed as fold change relative to healthy liver tissue. Values represent mean ± SD (*n=3*).

3.6.2 HUMAN PRIMARY HEPATOCYTES ARE MORE STABLE THAN RODENT HEPATOCYTES

It has been shown that the isolation procedure causes strong expressional changes in primary rodent hepatocytes during cultivation that affects functionality of these *in vitro* systems that are used in both basic and applied research. However, it is not known whether the same processes are triggered during isolation and culture of primary human hepatocytes. Therefore, the aim of the next study was to gain detailed insight into the molecular mechanisms orchestrating gene expression of human hepatocytes in culture. For this purpose,

time-resolved global gene expression profiling using Affymetrix microarrays was carried out in primary human hepatocytes cultivated in sandwich (S) and monolayer confluent (M_C) culture for up to one week.

Similar to the mouse hepatocytes (Figure 18, A) and rat hepatocytes *in vitro* (Figure 59), primary human hepatocytes (Figure 61) acquire a distinguishable morphology depending on the extracellular matrix used as the culture substratum. M_C cultures maintain a relatively cuboidal but flattened morphology. On the other hand, sandwich-cultured hepatocytes appear more differentiated, as evidenced by their *in vivo*-like cuboidal shape and distinct bile canaliculi network, even after longer periods in culture.

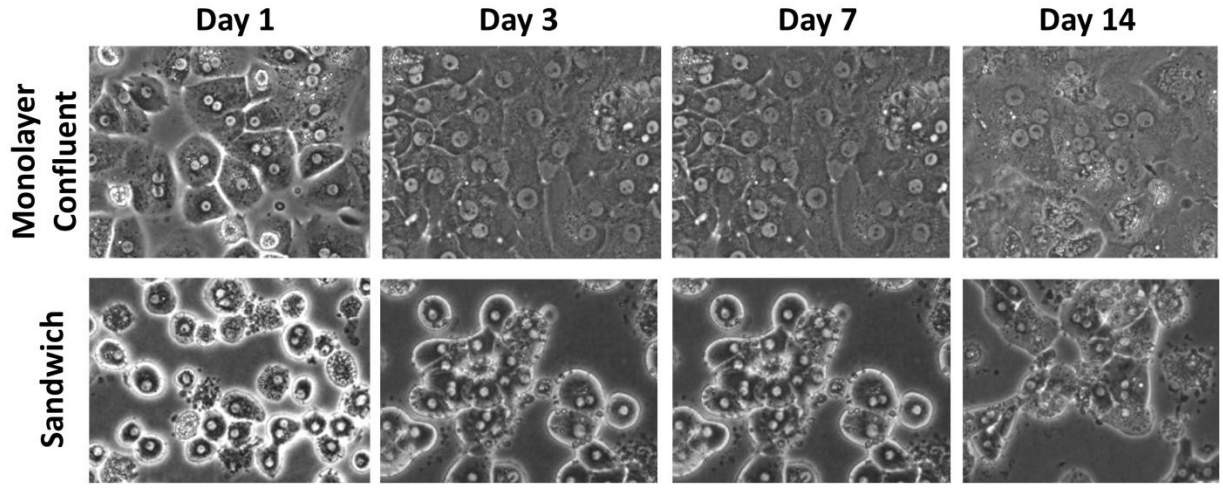

FIGURE 61: DIFFERENT EXTRACELLULAR MATRIX CAUSES MORPHOLOGICAL CHANGES IN PRIMARY HUMAN HEPATOCYTES *IN VITRO*
Light microscopy reveals the morphology of primary human hepatocytes in two culture systems: monolayer confluent and sandwich culture for the the indicated culture periods. Magnification of 20X.

Principal component analysis (PCA) of the gene array data (Figure 62) represents directional changes in gene expression of cultivated primary human hepatocytes compared to a reference state of freshly isolated hepatocytes (Fresh Hep, FH). PCA analysis reveals that the sandwich and monolayer confluent systems progressively deviate, with a slight shift of change, from freshly isolated hepatocytes. The observed direction of time-dependent changes shows a similar trend to the data obtained with mouse hepatocytes (Figure 19).

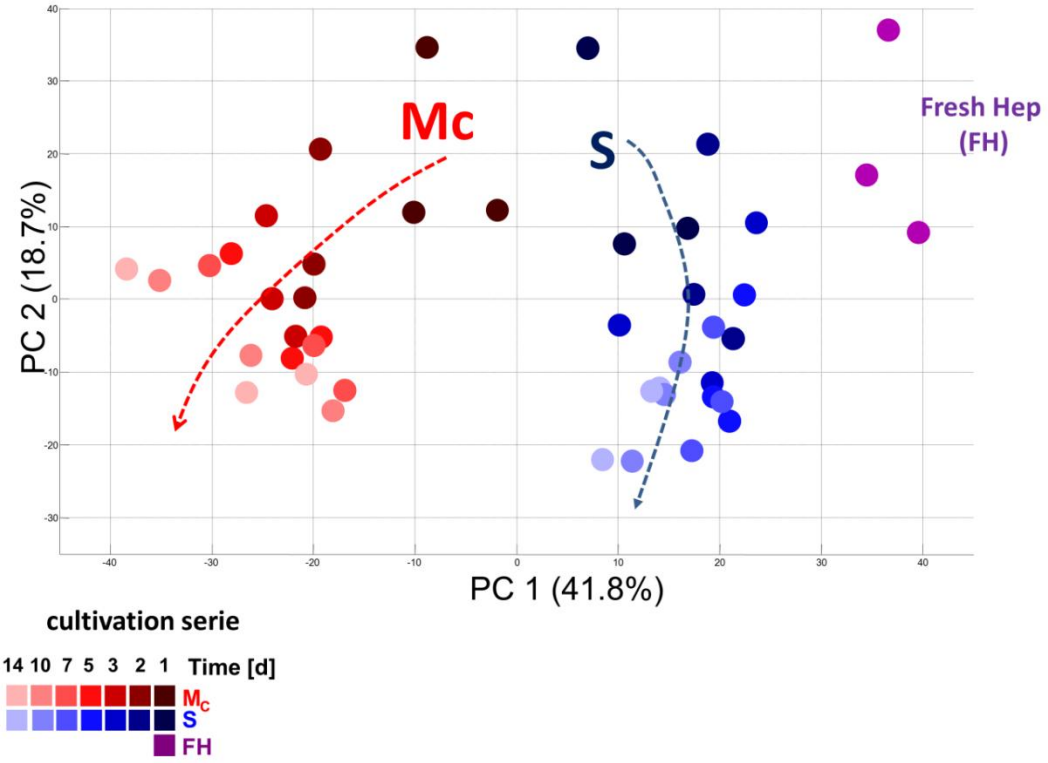

FIGURE 62: GENE ARRAY ANALYSIS REVEALS PROFOUND TIME-DEPENDENT ALTERATIONS OF CULTIVATED PRIMARY HUMAN HEPATOCYTES

Alterations of gene expression of cultivated primary human hepatocytes in monolayer confluent (M_C) and sandwich (S) cultures illustrated as principal component plot (PCA).

Therefore, the aim of the next study was to validate the effect of cultivation conditions on primary human hepatocytes' gene expression regarding the inflammation and metabolism gene clusters. For this purpose, primary human hepatocytes were cultivated in monolayer confluent (M_C) and sandwich (S) culture for the indicated timepoints and gene expression profiles of selected markers were analyzed (Figure 63).

The principles of inflammatory response and decline in metabolism were also observed in human hepatocytes (Figure 63). However, humans differ in three aspects. First, the maximal expression levels of inflammation-associated genes Lcn2 and Mt2 were lower in humans than in mice (Figure 23) and rats (Figure 60). Second, induction of inflammation genes was transient in human, but permanent in rodents. Third, sandwich cultures of human hepatocytes allowed a partial recovery of some metabolism-associated genes such as Bsep and Cyp7a1, which was not the case for mice or rats.

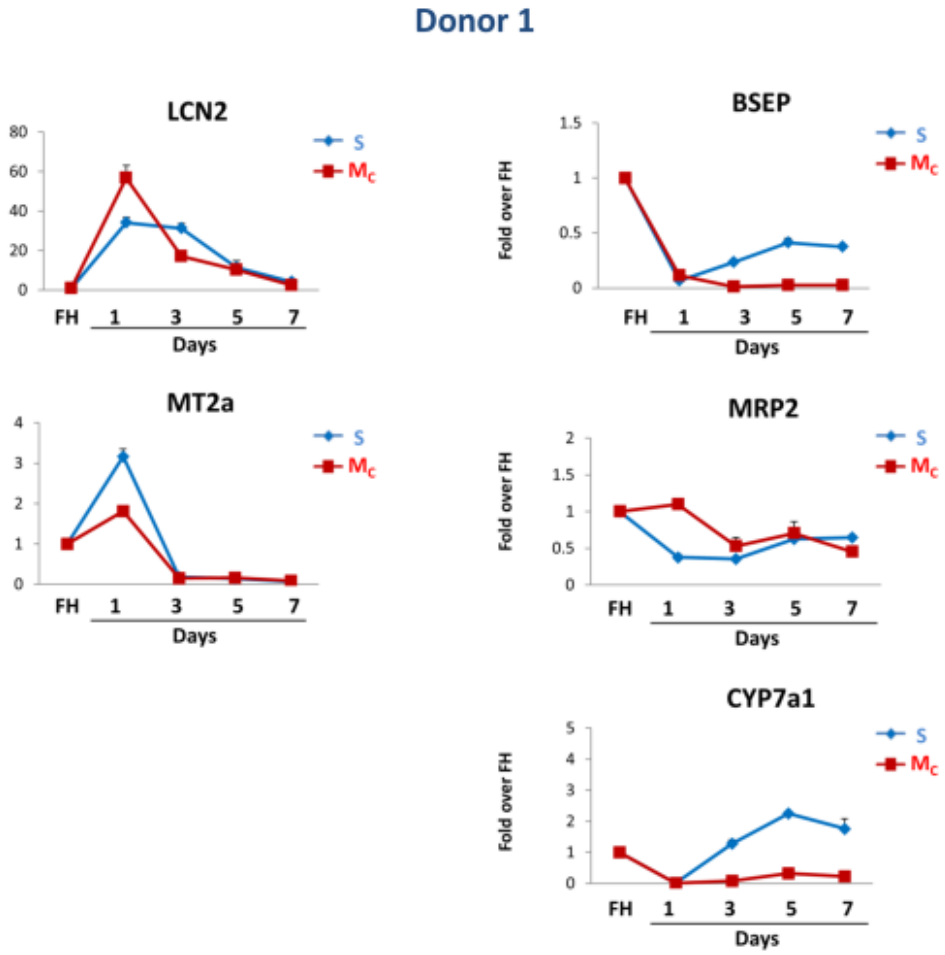

FIGURE 63: HUMAN PRIMARY HEPATOCYTES ARE MORE STABLE THAN RODENT HEPATOCYTES

Quantitative RT-PCR analysis of inflammation- (Lcn2, Mt2 and Saa3) or metabolism-associated genes (Bsep, Mrp2 and Cyp7a1) in freshly isolated hepatocytes (FH), hepatocytes in sandwich (S) culture or monolayer confluent (M_C) culture for the indicated time. GAPDH was used as an endogenous control. Each graph represents an independent biological replicate. Data are expressed as fold change relative to in freshly isolated hepatocytes. Values represent mean ± SD (*n=3*).

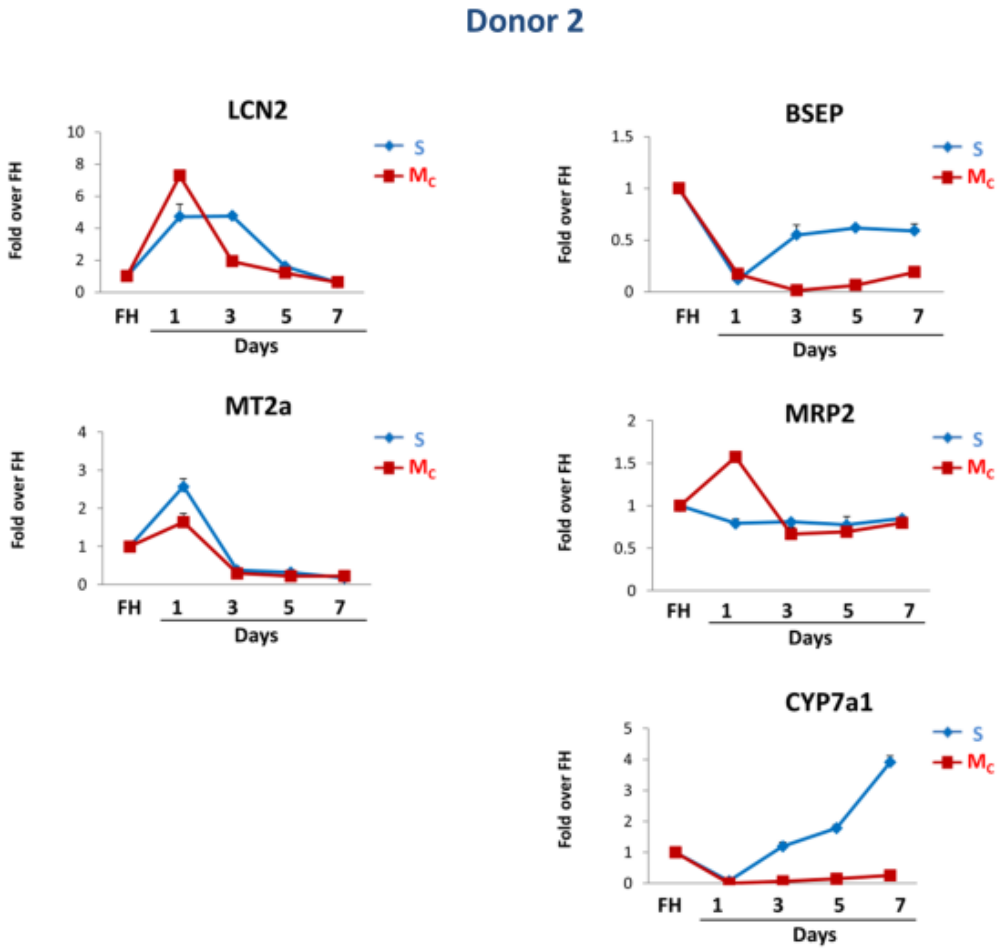

FIGURE 63: CONTINUED
HUMAN PRIMARY HEPATOCYTES ARE MORE STABLE THAN RODENT HEPATOCYTES

Quantitative RT-PCR analysis of inflammation- (Lcn2, Mt2 and Saa3) or metabolism-associated genes (Bsep, Mrp2 and Cyp7a1) in freshly isolated hepatocytes (FH), hepatocytes in sandwich (S) culture or monolayer confluent (M_C) culture for the indicated time. GAPDH was used as an endogenous control. Each graph represents an independent biological replicate. Data are expressed as fold change relative to in freshly isolated hepatocytes. Values represent mean ± SD (*n=3*).

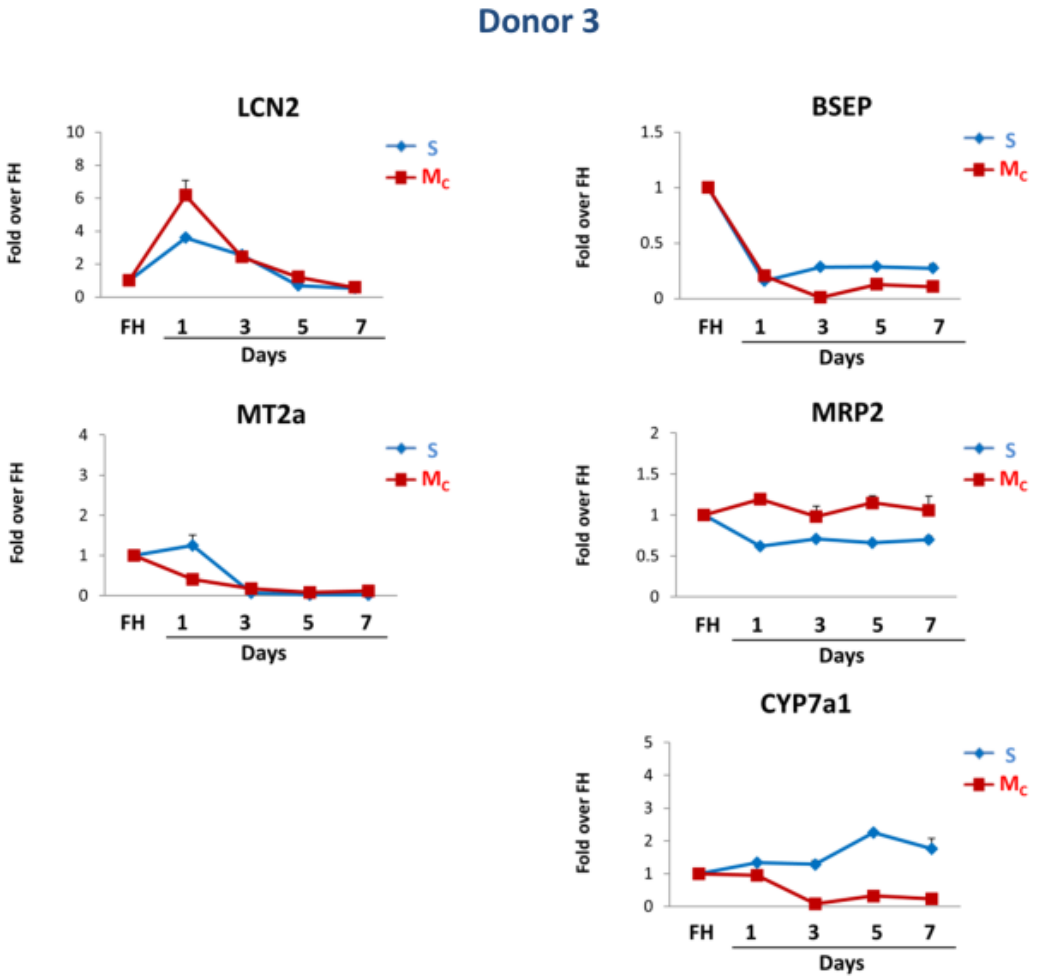

FIGURE 63: CONTINUED
HUMAN PRIMARY HEPATOCYTES ARE MORE STABLE THAN RODENT HEPATOCYTES
Quantitative RT-PCR analysis of inflammation- (Lcn2, Mt2 and Saa3) or metabolism-associated genes (Bsep, Mrp2 and Cyp7a1) in freshly isolated hepatocytes (FH), hepatocytes in sandwich (S) culture or monolayer confluent (M_C) culture for the indicated time. GAPDH was used as an endogenous control. Each graph represents an independent biological replicate. Data are expressed as fold change relative to in freshly isolated hepatocytes. Values represent mean ± SD (*n=3*).

In conclusion, global gene expression profiling exposed similarities in gene expression alterations between cultivated rodent and human hepatocytes.

4. DISCUSSION

4.1 GENE ARRAY ANALYSIS REVEALS PROFOUND ALTERATIONS IN CULTURE

Hepatocyte *in vitro* systems represent a well-accepted tool in many fields of research. Despite their widespread use, research with primary hepatocytes remains challenging [171, 207]. Complex cellular networks regulate regeneration, detoxification and differentiation of hepatocytes. Disrupting hepatocytes from their normal microenvironment, as during toxic compound insult or hepatectomy, causes major alterations in cell physiology [4]. Relevant for the field of *in vitro* studies, isolation and cultivation of hepatocytes induces massive transcriptional responses [78]. To date, great efforts have been spent to control or attenuate the alteration of hepatocytes *in vitro*. However, expression levels or activities comparable to the liver *in vivo* have rarely been achieved, and the precise mechanisms controlling de-differentiation are still poorly understood. Therefore, to obtain a comprehensive overview of the expression alterations caused by various culture conditions and after radically different interventions, a time-resolved gene array analysis of mouse hepatocytes in sandwich and monolayer cultures was carried out, and compared to livers *in vivo* after treatment with CCl_4, lipopolysaccharide (LPS), or partial hepatectomy (PHx). Global gene expression profiling exposed profound alterations within the first 24 hours that orchestrate cellular response of primary mouse hepatocytes *in vitro*. All cultivation systems - sandwich (S), confluent (M_C) and subconfluent (M_S) - expressed similar patterns of up-regulation of Lcn2, Mt2 and Saa3 and down-regulation of Bsep, Mrp2 and Cyp7a1 (Table 21). These features were not dependent on the culture configuration, including confluent or sub-confluent conditions, 2 or 3D matrix and type of extracellular matrix, including self-generated ECM in spheroids. Most importantly, this study identified a stereotypic gene expression response, which occurs similarly after different types of stress - isolation by collagenase perfusion, intoxication with CCl_4 or LPS as well as PHx - namely an upregulation of inflammation and proliferation as well as a downregulation of metabolism-associated genes.

The degree of overlap of these expression responses was remarkable considering the different nature of the stimuli. For example, more than 80% of up- or down-regulated genes after CCl_4 exposure were also altered in culture after hepatocyte isolation, PHx and LPS treatment (Figure 38). Gene cluster analysis of deregulated genes revealed the molecular architecture of this stereotypic expression response consisting of an inflammation, metabolism and proliferation motif (Figure 28). The alterations of the metagenes follow a characteristic time schedule: (*i*) i*n vitro*, most alterations occur within 24h and remain deregulated (Figure 21), (*ii*) *in vivo,* alterations are also maximal after approx. 24h (CCl_4 and PHx) but later return to control levels (Figure 41 and Figure 42). This explains why the *in vitro/in vivo* correlation of the gene expression alterations is maximal after 24h.

In order to obtain some insight into the mechanisms controlling the aforementioned transcriptional responses, Luminex analysis was performed to dissect the signaling activities throughout the culture time (Figure 52). JNK and ERK2 were identified as the strongest and earliest phosphorylated signaling proteins, with responses already observed during the isolation procedure (Figure 53). Stress signaling pathways have been previously demonstrated to play pivotal roles in de-differentiation processes of primary hepatocytes, thus contributing to the described alterations [61, 100].

4.2 MONOLAYER CULTURES INDUCE PROLIFERATION INDEPENDENT OF ADDITIONAL GROWTH FACTORS

Of all presented transcriptional alterations, activation of proliferative response is, perhaps, the best understood. It has been recently described that the activation of MAPK/ERK1/2 and Akt signaling of primary mouse hepatocytes in monolayers causes a "proliferation primed state" with more than 1000 genes strongly up or down-regulated [78]. This "proliferation primed state" leads to a phenotype of enhanced basal BrdU incorporation, epithelial-to-mesenchymal transition (EMT)-like de-differentiation, and resistance to apoptosis [115, 208]. However, this phenotype could be ameliorated by a 3D collagen sandwich culture, where a differentiated polarized phenotype and sensitivity to TGFβ-induced apoptosis was achieved [115]. ERK2 signaling was already observed during the isolation procedure (Figure 53). However, this activation is absent or much weaker in the sandwich culture, and only monolayer systems exhibit renewed activation of ERK1/2 signaling at 48h representing a link to the induction of proliferation and EMT-features observed in confluent and subconfluent configurations (compare results from [78, 115] and Figure 53). The results presented in my thesis also demonstrate that the subconfluent cultures exhibited the highest expression of the proliferation metagene; sandwich cultures were lowest; and confluent monolayer cultures and the *in vivo* samples ranked intermediate. In addition, from the presented results, the sandwich culture system offers clear advantages over monolayers by maintaining a more stable profile of expressional changes and preserving more of the *in vivo*-like features.

4.3 HEPATOCYTE CULTIVATION INDUCES AN *IN VIVO*-LIKE INFLAMMATION RESPONSE

To date, studies characterizing liver cultivation systems, focusing especially on monolayer configurations, point out the relevance of EMT as a feature of hepatocyte de-differentiation *in vitro* [78, 115]. However, a particularly important aspect revealed during my thesis is the strong activation of inflammation, which has not yet been described for cultivated hepatocytes. Most of the top up-regulated genes in culture are well-known inflammation-associated factors (Inserts with References in Table 21) [130, 137, 192, 194, 195]. The top marker of the inflammatory cluster - Lcn2 - was the most up-regulated gene in all five systems.

Likewise, a time-dependent and strong increase in expression of Lcn2 during culturing has been previously reported for rat primary hepatocytes [209]. A strong inflammatory response was also evidenced by the at least 5-fold induction of inflammatory factors in all models, such as Mt2 and Saa3 among the top ten up-regulated genes. Additionally, upregulation of the inflammation-associated transcription factor C/EBPδ and downregulation of C/EBPα shortly after isolation and during culture support previously published results [60]. A possible explanation for these alterations is the stress signaling triggered during the isolation procedure of hepatocytes. NPC are known as major regulators of liver function. Pro-inflammatory cytokines produced by NPC initiate an acute phase response and affect liver functions [25]. During ongoing liver injury, damage-associated molecular patterns molecules (DAMPs) cause an increased production of inflammatory cytokines and reactive oxygen species (ROS) by NPC [210]. This results in activation of the C/EBP family of transcription factors and subsequent induction of an acute phase response [137]. According to this hypothesis, the isolation procedure sensed as an ongoing tissue injury could cause activation of non-parenchymal cell population and trigger the release of ROS and/or cytokines that in turn activate stress signaling in hepatocytes. In addition, treatment *in vivo* with LPS and pro-inflammatory cytokines (including IL-6, IL-1 and TNF) induces expression of C/EBPδ and concurrently down-regulates C/EBPα [137, 138, 211, 212]. Similar patterns of downregulation of C/EBPα have also been reported during liver regeneration [148, 149]. This would suggest that the observed stress response and subsequent wave of inflammation occurs very early on, starting during the isolation procedure, indicating a potential time frame for intervention. However, the results presented in my thesis do not allow a precise identification of a mechanism, which induces the inflammatory response during isolation and in culture. Further experiments using knockout mice (signaling or liver cell type specific), depletion of certain NPC population (irradiation of infiltrating monocytes or depletion of KC by administration of clodronade liposomes) or specific antibodies to deplete their respective cytokines could address this question in more detail.

A central result in this study was that the isolation and cultivation of hepatocytes lead to an *in vivo*-like inflammation profile. In order to quantify the inflammation response, I used a normalized mean value of all genes from the inflammation cluster (´inflammation metagene`). Comparison of cultivation with all three *in vivo* models of liver damage show great similarities in their inflammatory response profiles, with Lcn2 among the most up-regulated, with the strongest response in the three culture systems followed by CCl_4, PHx and LPS (Figure 37). Lcn2 has been shown to be highly up-regulated during several pathologic conditions [130, 191] and is known to be involved in the regulation of cell proliferation [213], the immune response [214], inflammatory reactions [215], and cytokine-dependent renal regeneration [216]. In both primary hepatocytes and HepG2 cell line, induction of Lcn2 occurs in response to IL-1β via NF-κB signaling [209], suggesting that Lcn2 expression correlates with liver damage and the resulting inflammatory responses in a cytokine-dependent manner. Lcn2 is also strongly induced during liver injury such as partial hepatectomy [217] and after CCl_4 intoxication [190]. Furthermore, Lcn2 has been shown to exert protective effects during acute liver injury after

CCl_4 intoxication [190]. In conclusion, Lcn2 positively correlates to inflammation and has been suggested as a reliable indicator of liver damage. In line with this knowledge, the liver seems to respond to injury and stress with a general feature of inflammation. This has also been shown in my study, where seemingly different stress conditions such as hepatocyte isolation and culture, as well as CCl_4, LPS or PHx liver damage, induce similar cellular responses in hepatocytes such as inflammation. It sheds a new light on the consistency of the hepatocyte response, which exerts a similar gene expression pattern despite the model of liver injury. In contrast to the behavior of hepatocytes *in vitro*, culture-induced activation of hepatic stellate cells (HSC) showed a low correlation to the *in vivo*-activated HSC after bile duct ligation or CCl_4 treatment [218]. This discrepancy emphasizes that the almost identical gene expression patterns of both *in vivo* fibrotic models should be considered the gold standard for the study of HSC activation. However, the high correlation between the cultivated hepatocytes and the *in vivo* models of liver injury shown in my study leads to the conclusion that the hepatocyte *in vitro* systems commonly used in pharmacology, hepatology and toxicology [171] represent an inflamed and not a healthy liver.

4.4 OVERREPRESENTED TRANSCRIPTION FACTORS FOR THE UP-REGULATED GENE CLUSTERS

Having identified the molecular architecture of transcriptional responses, I next identified overrepresented transcription factors regulating the aforementioned alterations using a bio-statistical approach by means of transcription factor binding site (TFBS) analysis. The inflammation and proliferation gene clusters were shown to be enriched for Sp1, Elk1, E2F, ETF, similarly as already reported [78]. Moreover, TFBS analysis suggests that most up-regulated genes contain GC-rich promoters. The highest ranked TF for up-regulated genes - Sp1 - belongs to the mammalian family of ‘Krüppel-like’ transcription factors. It represents a ubiquitous TF maintaining the basal transcription of ‘house-keeping’ genes that lack a TATA-box but instead binds to GC-rich sequences (GGGGCGGGG) [219, 220]. Surprisingly, Sp1 is not transcriptionally up-regulated in hepatocytes *in vitro*, but immunostaining shows that its expression increases in hepatocyte nuclei in culture. It has been shown that Sp1 co-operates with other ‘Krüppel-like’ transcription factor, such as Klf6 to regulate gene expression [206]. Klf6 has been shown to play a role in tissue injury as indicated by its rapid induction among the immediate-early genes in *in vivo* activated HSC [199, 200]. Indeed, Klf6 turned out to be one of the strongest transcriptionally up-regulated TF with an enhanced nuclear localization in hepatocytes *in vitro*. This result suggests that Klf6 may be one of the driving TFs for other partner binding CG-rich promoters to activate upregulation of target genes involved in tissue repair. Additionally, Klf6 increases in the CCl_4 model of liver damage, proposing a possible role in the upregulation of inflammation genes *in vivo*. Furthermore, phosphorylation of Sp1 by ERK1/2 is required for

mediating EGF-induced Apo lipoprotein A-I gene transcription in the HepG2 cell line [221]. Therefore, it is tempting to speculate that ERK1/2 signaling activation during the isolation procedure leads to the activation of Klf6-Sp1 co-operation resulting in an induction of genes involved in both inflammation and proliferation processes. Further studies using targeted knock-down via siRNA technology or knock-out mice could explain the contribution of these transcription factors in more detail.

Manually curated analysis of deregulated genes and TFBS lead to the identification of other TF that could be responsible for the observed transcriptional alterations. Most of stress-signaling pathways are activated rapidly during isolation. In culture, most activities decreased once more, but usually not back to the levels found in healthy liver tissue. However, induction of phosphorylated c-jun has been shown to appear later in culture (Figure 52). c-Jun is a transcription factor that is a member of a dimeric complex known as AP-1. It is implicated in various, often opposing cellular responses [222]. In hepatocytes, c-Jun is a positive regulator of cell proliferation, as the lack of c-Jun impairs liver regeneration [223]. The AP-1 (activator protein-1) family consists of several groups of proteins: JUN, FOS, activating transcription factor (ATF) and MAF, making it possible to form many different combinations of homo- and heterodimers [224]. The mitogen-activated protein kinase (MAPK) signaling pathways are principal regulators of AP-1 activity [225]. Therefore, it is likely that induction of MAPK signaling during the isolation procedure could result in a subsequent activation of c-jun and its target genes. This hypothesis is additionally supported by the TFBS analysis, which showed an enrichment of ATF family among transcription factors controlling the up-regulated gene clusters. Moreover, preliminary data obtained from a proteomic analysis of cytosolic and nuclear extracts of monolayer confluent cultures on day one suggested a significant enrichment of MAF transcription factor - MafF and MafK - in the nucleus of hepatocytes *in vitro*. Therefore, it is likely that the family of proteins forming AP-1 complexes represent the main group of transcription factors activated in culture and regulating the up-regulated gene clusters. However, the results presented in my thesis do not allow a precise identification of the transcription factors regulating these clusters. Further studies using targeted knock-down *via* siRNA technology or knock-out mice for suggested transcription factors or analysis with chromatin immune-precipitation could address this question in more detail.

4.5 POSSIBLE FACTORS INFLUENCING GENE EXPRESSION PROFILE OF HEPATOCYTES IN CULTURE

Although the massive activation of stress pathways early upon isolation can explain the transcriptional alterations observed during the first hours in culture, it is intriguing that these expression alterations do not return to basal levels, even after several days in culture when the aforementioned stress pathways are long terminated. A possible explanation is that the initial

events lead to the induction of growth factors, cytokines or signaling adaptors that generate a feed-forward loop of gene expression. Among these candidate effectors is Connective tissue growth factor (Ctgf), chemokine Ccl2, and Immediate early response 3 (Ier3). They represent inflammatory markers, whose transcriptional expression progressively increases in culture (Figure 36). Ctgf is a secreted protein and a downstream mediator of the pro-fibrogenic effects of TGF-β signaling [226]. It is strongly up-regulated in fibrotic tissue and during wound healing [204]. CTGF plays a crucial role in invasive processes of human breast cancer by integrin-dependent activation of the ERK1/2 pathway [227]. Moreover, CTGF has been shown to induce IL-6 expression via αvβ5 integrin receptor, JNK/p38 and AP-1/NF-κB signaling pathways in human synovial fibroblasts [228]. All together, the results suggest that Ctgf may further influence gene expression of hepatocytes by activating various signaling pathways. Ccl2 is another cytokine that is induced during late timepoints in culture. This chemokine activates a myriad of signaling cascades including Akt, ERK and p38 via its cognate receptor Ccr2, a G-coupled protein, resulting in enhanced migration and infiltration of monocytes/macrophages [229, 230]. Another candidate is the Immediate-early response 3 (Ier3) gene associated with cycle progression and proliferation [194] that becomes induced in response to a variety of stimuli, including growth factors, cytokines, and cellular stress, e.g. NF-κB in response to TNF [231]. Additionally, upon ERK1/2-mediated phosphorylation, Ier3 prolongs ERK1/2 activation contributing to the phosphorylation of ERK substrates [232]. A probable explanation for these permanent alterations in culture is the possibility that cell fate can be determined long before it is apparent in cellular behavior [233]. The increasing amount of studies show that the dynamics of early signaling cause long-term cellular responses. For example, the duration of ERK activation is critical for cell signaling decisions in PC12 cells [234]. In these cells, sustained stimulation of ERK signaling with nerve growth factor (NGF) leads to neurite outgrowth, whereas transient ERK activation following epidermal growth factor (EGF) stimulation results in proliferation. Therefore, Ctgf, Ier3 and Ccl2 could represent a set of genes affected transcriptionally by early signaling events, e.g. during isolation. Furthermore, these late-induced genes may exert a positive feed-forward loop in cultivated hepatocytes that promotes an inflammatory response after the initial burst of stress signaling has waned. However, it remains to be determined how these factors are precisely regulated during cultivation and their precise contribution to the aforementioned alterations.

The liver microenvironment is complex and exposes hepatocytes to a plethora of cellular interactions and signals, whereas *in vitro* culture systems represent an artificial environment and do not contain many of the interactions present *in vivo*. Therefore, disruption of the normal liver architecture during the isolation procedure and the adaptation to the *in vitro* environment may be responsible for many of the aforementioned transcriptional alterations *in vitro.* For example, Wnt/β-catenin signaling is a key pathway controlling liver metabolism. β-catenin - mediated gene transcription is activated after binding of secreted

ligands (Wnts) [235] and has been shown to have a major role in determining the final patterning of the adult liver [236]. Therefore, it is likely that hepatocytes *in vitro* are lacking certain ligands, such as Wnts that when present *in vivo* guard transcriptional control over liver zonation. Consequently, shortage of important factors during cultivation could represent another possible link to the repressed metabolic functions and ongoing transcriptional alterations *in vitro*.

4.6 MINOR ROLE OF NPC IMPURITIES ON THE EXPRESSION OF TARGET GENES DURING CULTIVATION

The strong inflammatory response observed in culture could result from the influence of Non Parenchymal Cells (NPC) residuals in culture. NPC are known to secrete cytokines and cause the inflammatory transcriptional response in the neighboring hepatocytes *in vivo* [150]. My analysis revealed that the hepatocyte-enriched fraction obtained after the isolation procedure contains a relatively high fraction of approximately 10-13% of NPC impurities. Nevertheless, further removal of these impurities by additional Percol centrifugation steps (end content of approximately 1% NPC) had only a minor effect on most of the marker genes. However, Saa3 turned out to be the only marker affected by this approach indicating that although the inflammation gene clusters are similarly affected in all *in vitro* models, the specific genes may be regulated by different mechanisms. The opposite approach of adding NPC to normal sandwich and monolayer confluent culture confirmed the aforementioned principles, whereby NPC slightly enhanced Saa3 expression but had no major influence on other markers: Lcn2, Mt2 as well as Bsep, Mrp2 and Cyp7a1. Such divergence could be explained by the responsiveness of acute phase proteins (Saa3 and Lcn2 for example) to different cytokines controlling their expression. TNF, IL-1 β and IL-6 represent major triggers for the synthesis of acute phase proteins in the liver [237]. Saa3 represents type I of acute phase proteins that become induced by IL-1-like cytokines such as IL-1α, -β and TNF. In contrast, the IL-6 family of cytokines induces acute phase proteins type II. However, the effect of IL-6 can further synergize with IL-1-like cytokines leading to the induction of type I markers but not the other way round [238]. In line with this, responsiveness of Saa3 only to the IL-1 family of cytokines could explain its dependence on NPC residuals. Activated macrophages are known to produce TNF, IL-1 β and IL-6 [3] and, therefore macrophages may be the effector cell type that up-regulates Saa3 *in vitro*. However, further studies using Küpffer cell depletion or cytokine-antagonizing antibodies prior to isolation and culture may reveal the precise regulatory mechanisms responsible for these alterations.

4.7 JNK SIGNALING DRIVES INFLAMMATION

The activation timing of signaling pathways suggests that interventions with kinase inhibitors during perfusion and plating may abrogate inflammation and rescue metabolism. Therefore, in order to determine how certain signaling pathways contribute to the aforementioned transcriptional changes, I performed a series of experiments with different small molecule inhibitors to repress signaling pathways. Of all the inhibitors tested, only the JNK inhibitor - SP600125 – had an effect *in vitro* and clearly reduced the inflammatory response by suppressing the upregulation of both Lcn2 and Saa3 in both inflammation clusters (Figure 54), indicating that the JNK pathway is critical for the inflammation response. Additionally, the transiently-induced inflammation gene cluster represented by Saa3 was also influenced by the presence of p38 and NF-κB inhibitors suggesting that this cluster may be controlled by pathways other than JNK. This suggests that the upregulation of Lcn2 and Saa3 depends on various cytokines. Yet, both markers are induced in response to IL-1β indicating their association with type I acute phase proteins [209, 238]. Moreover, Saa3 expression is affected by various signaling pathways and it is the only inflammatory marker affected by the content of non-parenchymal cells. Taken together, this suggests that although inflammation gene clusters are similarly affected in all *in vitro* models, the specific marker genes are controlled by different mechanisms. To further assess the importance of the JNK signaling pathway, I added JNK inhibitors early on during the liver perfusion procedure. However, only addition of the JNK inhibitor into the perfusion buffers as well as to the cell culture medium clearly reduced the inflammatory response by suppressing the upregulation of inflammation clusters (Figure 57). However, none of the tested inhibitors were able to rescue the profound repression of metabolism-associated genes (Figure 55 and Figure 58). These results demonstrate that early activation of JNK during perfusion is responsible for the inflammatory response of primary mouse hepatocytes *in vitro*. Furthermore, the molecular structure of this stereotypical stress response provides possibilities of intervention by small molecule inhibitors. Nevertheless, the lack of response of genes from the metabolism cluster shows that the underlying signaling network is complex and still far from being fully understood.

4.8 CULTIVATION INDUCES DOWN-REGULATION OF THE METABOLISM-ASSOCIATED GENES

In contrast to the inflammation response, downregulation of the metabolism-associated genes in culture has been previously described [69, 239]. Transcriptional control of Bsep, and Mrp2 is known to be regulated by a group of nuclear receptors (NRs), including FXR, RAR, PXR, and CAR [95-98]. Similarly, the superfamily of cytochrome P450 is a key gene target of the nuclear receptors [83]. Therefore, strong downregulation of Bsep, Mrp2 and Cyp7a1 in all cultivation systems (Table 21) most likely results from the observed decrease of nuclear

receptors (Figure 31). This seems very plausible since binding of nuclear receptor agonists (e.g. bile acids) or antagonists can directly alter gene expression [37, 98], suggesting that stimuli triggering such changes occur early during the isolation procedure. Bile acid feedback is known to regulate CYP7A1 transcription through the nuclear receptor farnesoid X receptor (FXR) [240] and hepatocyte nuclear factor-4 (HNF-4) [241]. On the other hand, activation of JNK can lead to a decreased expression of nuclear receptors [161, 162]. Therefore, repression of Cyp7a1 could be partially explained as a response to the activation of MAPK kinases during the isolation procedure. This hypothesis is supported by studies where expression of Cyp7a1 was shown to be strongly down-regulated by bile acid- activated JNK in primary rat hepatocytes [242] and by HGF-induced activation of MAPK kinases, ERK1/2 and JNK, in primary human hepatocytes [243]. Another link to stress signaling has been confirmed by the treatment of HepG2 cells with bile acids that led to the inhibition of the transactivation potential of HNF4α via activation of MAPK signaling, thus leading to the repression of CYP7A1 transcription [244]. As ERK and JNK kinases become activated early during isolation, it is tempting to speculate that there is a causal link to the expression of NRs, HNF4α and Cyp7a1. However, addition of a JNK inhibitor during perfusion and culture did not ameliorate downregulation of these metabolism-associated genes. This indicates that perhaps the simultaneous activation of ERK signaling may be sufficient to trigger such downregulation and it remains to be determined how the underlying signaling networks are regulating these complex responses.

Comparison of the ´metabolism metagene` reveals a comparable strong downregulation of metabolism-associated genes in both *in vitro* and in *in vivo* models of CCl_4, LPS and PHx. This suggests that a decrease in expression of metabolism-associated genes may represent a general feature of liver stress responses. Liver regeneration induces a coordinated downregulation of metabolism-associated genes to prevent cellular damage [245]. However, the protein expression of Bsep and Mrp2 remains stable 24 h after the procedure in the model of partial hepatectomy [166, 167] and similarly unchanged in the model of CCl_4-induced liver damage [164, 168]. The much slower decrease at the protein level is due to the relatively long half-life of these factors. Downregulation of hepatic transporters is mediated *in vivo* and *in vitro* by pro-inflammatory cytokines (TNF, IL-1β and IL-6) [97, 155-159]. In line with the strong effect of cytokines on inflammation- and metabolism-associated genes, it is tempting to speculate that tissue injury sensed during the isolation procedure leads to a release of cytokines from NPC. This release in turn influences gene expression of hepatocytes triggering in parallel the inflammatory response and the decrease in metabolic functions. However, further experiments are needed to fully dissect the role of the isolation procedure on cytokine release and signaling activation that may explain the described alterations.

TFBS analysis suggested HNF4α and -1α as the most overrepresented TFs regulating the metabolism gene cluster. Immunostaining and qRT-PCR revealed a decrease in expression and

loss of nuclear HNF4α, respectively, within a few hours after isolation. Since HNF4α is fundamental for the expression of liver-specific metabolism-associated genes, loss of metabolism may be mediated via a loss of this transcription factor [87]. Additionally, expression of HNF4α is mostly regulated by the nuclear receptor family of transcription factors [37, 98]. These factors were shown to be rapidly and persistently repressed shortly after isolation and during culture. It remains unclear how disruption of the normal liver architecture during the isolation procedure and culture microenvironment modulate HNF4α expression. Nevertheless, it seems likely that the isolation procedure plays a critical role. This hypothesis is supported by an *in vitro* study where ERK2 activation causes downregulation of HNF4α expression in human hepatoma cells at the transcriptional level via mechanisms that involve loss of C/EBPα [116]. Stress signaling pathways have been previously demonstrated to play pivotal roles in the de-differentiation processes of primary hepatocytes [61, 100] suggesting that ERK1/2 activation during isolation down-regulates expression of HNF4α in isolated hepatocytes. However, the results presented in my thesis do not allow a precise identification of mechanism regulating the downregulation of HNF4α and consequently metabolism-associated genes. Therefore, further studies using HNF4α over-expression *in vitro* or deactivation of the ERK1/2 signaling by use of small molecule inhibitors during isolation could address this question in detail.

4.9 SYSTEMIC ALTERATIONS IN GENE EXPRESSION ARE INDEPENDENT FROM THE SPECIFIC TYPE OF EXTRACELLULAR MATRIX

Currently, there is much expectation surrounding the development of organotypic hepatocyte *in vitro* systems [171]. Spheroids or micro-tissues are considered particularly attractive because they produce their own extracellular matrix [72]. Mouse spheroids allowed a better maintenance of some metabolism-associated genes compared to sandwich culture, which may represent an advantage of the latter system [75]. However, in my thesis I demonstrate that a spheroid culture system did not avoid the stereotypical gene expression response. In contrast, even a stronger upregulation of the inflammation cluster gene Saa3 and C/EBPδ was observed. Different types of commercially available matrixes including Matrigel™ and Laminin, as an approach to create a more *in vivo*-like environment and to achieve a better comparison to the spheroid system, did not ameliorate the overall gene expression response. All together, these results show that systemic alterations in gene expression of primary hepatocytes occur independently from the specific type of extracellular matrix *in vitro*.

4.10 COMPARISON TO RAT AND HUMAN PRIMARY HEPATOCYTES

A remarkable feature of the described stereotypical expression response is that its basic features were conserved across species including human. This is noteworthy considering several publications that challenged the usefulness of animal data to study human inflammatory diseases and to predict human safety [246, 247]. Nevertheless, my study

demonstrates that both human and rodent hepatocytes respond to the isolation procedure with a conserved stress response that includes features of inflammation and a decline in expression of metabolism-associated genes. However, there is a major quantitative difference and some alterations in human hepatocytes are only transient. This illustrates the need for a similar comprehensive human study comprising isolated hepatocytes and liver tissue, both healthy and inflamed, *ex vivo*.

4.11 CONCLUSIONS AND FUTURE PERSPECTIVES

Elucidation of the molecular anatomy of gene expression patterns in stressed hepatocytes presented in my thesis has several implications. First, the broadly applied hepatocyte *in vitro* systems do not represent a model system for the healthy liver but rather a critically inflamed state. In this context, it was a surprise that the stress-induced response of inflammation and metabolism in sandwich cultures and spheroids could not be avoided, despite the polarized and well-differentiated morphology of hepatocytes observed in those systems. Second, unveiling the molecular anatomy of gene expression also demonstrates that cultivated hepatocytes may be used to study pathological situations. For example, expressional patterns of primary mouse hepatocytes in sandwich cultures resemble those observed in stressed-inflamed liver tissue such as after hepatectomy or in response to CCl_4 or LPS.

In conclusion, the identification of remarkable similarities of inflamed livers *in vivo* and cultivated hepatocytes opens new paths for mechanistic studies on liver inflammation and a more accurate use of hepatocyte *in vitro* systems.

5. APPENDIX

TABLE 22: GENES INCLUDED INTO THE METAGENE ANALYSIS FOR THE PROCESS OF INFLAMMATION

Inflammation metagene

UniGene-ID	Symbol	Description
Mm.4533	Apoa4	4903. Apolipoprotein A-IV
Mm.3460	Cd14	527. CD14 antigen
Mm.195663	Cdkn1a	103. Cyclin-dependent kinase inhibitor 1A (P21)
Mm.347407	Cebpd	2447. CCAAT/enhancer binding protein (C/EBP), delta
Mm.290991	Cpne8	5684. Copine VIII
Mm.149403	Cyb561	14819. Cytochrome b-561
Mm.387108	Ero1l	5828. ERO1-like (S. cerevisiae)
Mm.582	Fabp4	1866. Fatty acid binding protein 4, adipocyte
Mm.25613	Ier3	14610. Immediate early response 3
Mm.9537	Lcn2	1356. Lipocalin 2
Mm.192991	Mt1	235. Metallothionein 1
Mm.147226	Mt2	687. Metallothionein 2
Mm.14173	Orm2	17944. Orosomucoid 2
Mm.326167	Pkm2	1518. Pyruvate kinase, muscle
Mm.14277	Saa3	6241. Serum amyloid A 3
Mm.28405	Sgk1	827. Serum/glucocorticoid regulated kinase 1
Mm.371583	Slpi	8132. Secretory leukocyte peptidase inhibitor
Mm.338790	Srgn	7359. Serglycin
Mm.330731	Tgm2	672. Transglutaminase 2, C polypeptide

TABLE 23: GENES INCLUDED INTO THE METAGENE ANALYSIS FOR THE PROCESS OF METABOLISM

Metabolism metagene

UniGene-ID	Symbol	Description
Mm.290727	2810007J24Rik	24930. RIKEN cDNA 2810007J24 gene
Mm.355174	9130409I23Rik	11043. RIKEN cDNA 9130409I23 gene
Mm.344148	Abca8a	5877. ATP-binding cassette, sub-family A (ABC1), member 8a
Mm.81793	Acacb	409. Acetyl-Coenzyme A carboxylase beta
Mm.255026	Acss2	1948. Acyl-CoA synthetase short-chain family member 2
Mm.29125	Agxt2l1	7039. Alanine-glyoxylate aminotransferase 2-like 1
Mm.423137	Arrdc3	11201. Arrestin domain containing 3
Mm.300	Car3	5696. Carbonic anhydrase 3
Mm.29110	Ces1f	11870. Carboxylesterase 1F
Mm.13036	Cml1	27190. Camello-like 1
Mm.15537	Cyp1a2	788. Cytochrome P450, family 1, subfamily a, polypeptide 2

TABLE 23: CONTINUED

Mm.142581	Cyp2c55	12853. Cytochrome P450, family 2, subfamily c, polypeptide 55
Mm.378235	Dbp	9722. D site albumin promoter binding protein
Mm.236443	Fasn	600. Fatty acid synthase
Mm.281298	Gadd45g	9861. Growth arrest and DNA-damage-inducible 45 gamma
Mm.299	Inmt	17669. Indolethylamine N-methyltransferase
Mm.218561	Keg1	20751. Kidney expressed gene 1
Mm.46561	Lect1	8337. Leukocyte cell derived chemotaxin 1
Mm.37907	Lrit1	16575. Leucine-rich repeat, immunoglobulin-like and transmembrane domains 1
Mm.112365	Mus musculus	49479. Transcribed locus
Mm.25466	Mus musculus	57050. Transcribed locus
Mm.381253	Mus musculus	85232. Transcribed locus
Mm.436775	Mus musculus	39287. Transcribed locus
Mm.442553	Mus musculus	64241. Transcribed locus
Mm.415302	Ppargc1b	4892. Peroxisome proliferative activated receptor, gamma, coactivator 1 beta
Mm.290079	Serpina6	12573. Serine (or cysteine) peptidase inhibitor, clade A, member 6
Mm.103665	Slco1a1	8288. Solute carrier organic anion transporter family, member 1a1
Mm.200370	Upp2	12824. Uridine phosphorylase 2

TABLE 24: GENES INCLUDED INTO THE METAGENE ANALYSIS FOR THE PROCESS OF PROLIFERATION

Proliferation metagene

UniGene-ID	**Symbol**	**Description**
Mm.180363	2610039C10Rik	26517. RIKEN cDNA 2610039C10 gene
Mm.282751	Anln	6119. Anillin, actin binding protein
Mm.248360	Anxa1	1138. Annexin A1
Mm.38469	Apbb1	3502. Amyloid beta (A4) precursor protein-binding, family B, member 1
Mm.277585	App	52. Amyloid beta (A4) precursor protein
Mm.239329	Arhgef2	6165. Rho/rac guanine nucleotide exchange factor (GEF) 2
Mm.22085	Arl3	8439. ADP-ribosylation factor-like 3
Mm.389890	Atf5	13964. Activating transcription factor 5
Mm.2443	Bak1	1105. BCL2-antagonist/killer 1
Mm.8552	Birc5	1439. Baculoviral IAP repeat-containing 5
Mm.2185	Bub1	4377. Budding uninhibited by benzimidazoles 1 homolog (S. cerevisiae)
Mm.285993	Calm1	2303. Calmodulin 1
Mm.288630	Calm3	6639. Calmodulin 3
Mm.194368	Ccdc99	14212. Coiled-coil domain containing 99
Mm.4189	Ccna2	1886. Cyclin A2
Mm.260114	Ccnb1	2082. Cyclin B1
Mm.22592	Ccnb2	7995. Cyclin B2
Mm.273049	Ccnd1	130. Cyclin D1
Mm.27291	Ccnd3	1460. Cyclin D3
Mm.289747	Cdc20	2740. Cell division cycle 20 homolog (S. cerevisiae)

TABLE 24: CONTINUED

Mm.285723	Cdca3	22333. Cell division cycle associated 3
Mm.28038	Cdca8	19026. Cell division cycle associated 8
Mm.281367	Cdk1	1054. Cyclin-dependent kinase 1
Mm.272394	Cdkn3	22330. Cyclin-dependent kinase inhibitor 3
Mm.273502	Cenph	20925. Centromere protein H
Mm.9916	Cep55	17042. Centrosomal protein 55
Mm.45127	Cgref1	26130. Cell growth regulator with EF hand domain 1
Mm.279308	Chek2	3241. Checkpoint kinase 2
Mm.22448	Ckap2	13712. Cytoskeleton associated protein 2
Mm.329078	Cul7	3281. Cullin 7
Mm.292470	Dbf4	13346. DBF4 homolog (S. cerevisiae)
Mm.25410	Dsn1	23140. DSN1, MIND kinetochore complex component, homolog (S. cerevisiae)
Mm.249280	Esco2	14947. Establishment of cohesion 1 homolog 2 (S. cerevisiae)
Mm.197520	Fbxo5	17159. F-box protein 5
Mm.4704	Foxg1	1050. Forkhead box G1
Mm.39293	Haus1	22071. HAUS augmin-like complex, subunit 1
Mm.57223	Hells	2436. Helicase, lymphoid specific
Mm.157190	Hmga2	2932. High mobility group AT-hook 2
Mm.29755	Incenp	7501. Inner centromere protein
Mm.306511	Insl6	24005. Insulin-like 6
Mm.42203	Kif11	2695. Kinesin family member 11
Mm.224306	Klhl13	7688. Kelch-like 13 (Drosophila)
Mm.4964	Lif	280. Leukemia inhibitory factor
Mm.288179	Lig1	2611. Ligase I, DNA, ATP-dependent
Mm.16711	Mcm2	1112. Minichromosome maintenance deficient 2 mitotin (S. cerevisiae)
Mm.378965	Mcm7	1623. Minichromosome maintenance deficient 7 (S. cerevisiae)
Mm.246750	Mnat1	9085. Menage a trois 1
Mm.4619	Msh2	491. MutS homolog 2 (E. coli)
Mm.185800	Mus musculus	38861. Transcribed locus
Mm.254588	Mus musculus	36480. Transcribed locus
Mm.359575	Mus musculus	42964. Transcribed locus, weakly similar to NP_001034869.1 cyclin-I2 [Homo sapiens]
Mm.218233	Myh10	355. Myosin, heavy polypeptide 10, non-muscle
Mm.29786	Ncaph	11665. Non-SMC condensin I complex, subunit H
Mm.288980	Nedd9	5014. Neural precursor cell expressed, developmentally down-regulated gene 9
Mm.29071	Nek9	5029. NIMA (never in mitosis gene a)-related expressed kinase 9
Mm.222184	Nup37	14890. Nucleoporin 37
Mm.299887	Nup43	13615. Nucleoporin 43
Mm.290015	Nusap1	19262. Nucleolar and spindle associated protein 1
Mm.247480	Ofd1	9441. Oral-facial-digital syndrome 1 gene homolog (human)
Mm.246412	Oip5	27136. Opa interacting protein 5
Mm.28659	Pes1	3379. Pescadillo homolog 1, containing BRCT domain (zebrafish)
Mm.3193	Pkia	19495. Protein kinase inhibitor, alpha
Mm.16525	Plk1	1667. Polo-like kinase 1 (Drosophila)
Mm.1237	Pmp22	472. Peripheral myelin protein 22

TABLE 24: CONTINUED

Mm.14501	Ppm1g	6914. Protein phosphatase 1G (formerly 2C), magnesium-dependent, gamma isoform
Mm.227274	Prc1	9981. Protein regulator of cytokinesis 1
Mm.19111	Prkaca	415. Protein kinase, cAMP dependent, catalytic, alpha
Mm.18344	Psmc3ip	14139. Proteasome (prosome, macropain) 26S subunit, ATPase 3, interacting protein
Mm.389499	Psrc1	18606. Proline/serine-rich coiled-coil 1
Mm.273804	Racgap1	4275. Rac GTPase-activating protein 1
Mm.330492	Rad51	1505. RAD51 homolog (S. cerevisiae)
Mm.12091	Rassf1	8632. Ras association (RalGDS/AF-6) domain family member 1
Mm.180734	Rpa1	4185. Replication protein A1
Mm.274399	Sept8	5339. Septin 8
Mm.428571	Sept9	5434. Septin 11
Mm.439776	Sesn3	9125. Sestrin 3
Mm.23298	Smpd3	4579. Sphingomyelin phosphodiesterase 3, neutral
Mm.379024	Tacc3	10608. Transforming, acidic coiled-coil containing protein 3
Mm.18213	Tgfb2	500. Transforming growth factor, beta 2
Mm.206505	Timp2	1683. Tissue inhibitor of metalloproteinase 2
Mm.259893	Topbp1	4830. Topoisomerase (DNA) II binding protein 1
Mm.407737	Tpx2	10171. TPX2, microtubule-associated protein homolog (Xenopus laevis)
Mm.275095	Trip13	7851. Thyroid hormone receptor interactor 13
Mm.151594	Trnp1	27510. TMF1-regulated nuclear protein 1
Mm.273570	Trrap	302. Transformation/transcription domain-associated protein
Mm.335454	Wdr6	6905. WD repeat domain 6
Mm.2806	Xpc	1656. Xeroderma pigmentosum, complementation group C
Mm.335237	Zwilch	14280. Zwilch, kinetochore associated, homolog (Drosophila)

6. LIST OF FIGURES

7. LIST OF TABLES

8. REFERENCES

1. Arias, I., et al., *The Liver: Biology and Pathobiology*. 5 ed. 2009, West Sussex, UK: Willey-Blackwell.
2. Ramadori, G., et al., *Physiology and pathophysiology of liver inflammation, damage and repair.* J Physiol Pharmacol, 2008. **59 Suppl 1**: p. 107-17.
3. Ramadori, G. and B. Christ, *Cytokines and the hepatic acute-phase response.* Semin Liver Dis, 1999. **19**(2): p. 141-55.
4. Taub, R., *Liver regeneration: from myth to mechanism.* Nat Rev Mol Cell Biol, 2004. **5**(10): p. 836-47.
5. Nahmias, Y., F. Berthiaume, and M.L. Yarmush, *Integration of technologies for hepatic tissue engineering.* Adv Biochem Eng Biotechnol, 2007. **103**: p. 309-29.
6. Rappaport, A.M., et al., *Subdivision of hexagonal liver lobules into a structural and functional unit; role in hepatic physiology and pathology.* Anat Rec, 1954. **119**(1): p. 11-33.
7. Ishibashi, H., et al., *Liver architecture, cell function, and disease.* Semin Immunopathol, 2009. **31**(3): p. 399-409.
8. Gebhardt, R., *Metabolic zonation of the liver: regulation and implications for liver function.* Pharmacol Ther, 1992. **53**(3): p. 275-354.
9. Jungermann, K. and N. Katz, *Functional hepatocellular heterogeneity.* Hepatology, 1982. **2**(3): p. 385-95.
10. Rodes, J.B., J-P., et al., *The Textbook of Hepatology: From Basic Science to Clinical Practice*. 3rd ed. 2007, Malden, MA: Wiley-Blackwell Publishing.
11. Christoffels, V.M., et al., *A mechanistic model for the development and maintenance of portocentral gradients in gene expression in the liver.* Hepatology, 1999. **29**(4): p. 1180-92.
12. Jungermann, K. and T. Kietzmann, *Zonation of parenchymal and nonparenchymal metabolism in liver.* Annu Rev Nutr, 1996. **16**: p. 179-203.
13. Kietzmann, T. and K. Jungermann, *Modulation by oxygen of zonal gene expression in liver studied in primary rat hepatocyte cultures.* Cell Biol Toxicol, 1997. **13**(4-5): p. 243-55.
14. Jungermann, K. and T. Kietzmann, *Role of oxygen in the zonation of carbohydrate metabolism and gene expression in liver.* Kidney Int, 1997. **51**(2): p. 402-12.
15. LeCluyse, E.L., et al., *Organotypic liver culture models: meeting current challenges in toxicity testing.* Crit Rev Toxicol, 2012. **42**(6): p. 501-48.
16. Wisse, E., et al., *Structure and function of sinusoidal lining cells in the liver.* Toxicol Pathol, 1996. **24**(1): p. 100-11.
17. Blouin, A., R.P. Bolender, and E.R. Weibel, *Distribution of organelles and membranes between hepatocytes and nonhepatocytes in the rat liver parenchyma. A stereological study.* J Cell Biol, 1977. **72**(2): p. 441-55.
18. Bataller, R. and D.A. Brenner, *Liver fibrosis.* J Clin Invest, 2005. **115**(2): p. 209-18.

19. Friedman, S.L., *Molecular regulation of hepatic fibrosis, an integrated cellular response to tissue injury.* J Biol Chem, 2000. **275**(4): p. 2247-50.

20. Martinez-Hernandez, A. and P.S. Amenta, *The hepatic extracellular matrix. I. Components and distribution in normal liver.* Virchows Arch A Pathol Anat Histopathol, 1993. **423**(1): p. 1-11.

21. Martinez-Hernandez, A. and P.S. Amenta, *The extracellular matrix in hepatic regeneration.* FASEB J, 1995. **9**(14): p. 1401-10.

22. Weibel, E.R., et al., *Correlated morphometric and biochemical studies on the liver cell. I. Morphometric model, stereologic methods, and normal morphometric data for rat liver.* J Cell Biol, 1969. **42**(1): p. 68-91.

23. Hendriks, H.F., et al., *Perisinusoidal fat-storing cells are the main vitamin A storage sites in rat liver.* Exp Cell Res, 1985. **160**(1): p. 138-49.

24. Friedman, S.L., *Hepatic stellate cells: protean, multifunctional, and enigmatic cells of the liver.* Physiol Rev, 2008. **88**(1): p. 125-72.

25. Kmiec, Z., *Cooperation of liver cells in health and disease.* Adv Anat Embryol Cell Biol, 2001. **161**: p. III-XIII, 1-151.

26. Gaudio, E., et al., *New insights into liver stem cells.* Dig Liver Dis, 2009. **41**(7): p. 455-62.

27. Turner, R., et al., *Human hepatic stem cell and maturational liver lineage biology.* Hepatology, 2011. **53**(3): p. 1035-45.

28. Schuppan, D., et al., *Matrix as a modulator of hepatic fibrogenesis.* Semin Liver Dis, 2001. **21**(3): p. 351-72.

29. Martinez-Hernandez, A., *The hepatic extracellular matrix. I. Electron immunohistochemical studies in normal rat liver.* Lab Invest, 1984. **51**(1): p. 57-74.

30. Wang, Y., et al., *Paracrine signals from mesenchymal cell populations govern the expansion and differentiation of human hepatic stem cells to adult liver fates.* Hepatology, 2010. **52**(4): p. 1443-54.

31. Treyer, A. and A. Musch, *Hepatocyte polarity.* Compr Physiol, 2013. **3**(1): p. 243-87.

32. Decaens, C., et al., *Which in vitro models could be best used to study hepatocyte polarity?* Biol Cell, 2008. **100**(7): p. 387-98.

33. Fuller, S.D., R. Bravo, and K. Simons, *An enzymatic assay reveals that proteins destined for the apical or basolateral domains of an epithelial cell line share the same late Golgi compartments.* EMBO J, 1985. **4**(2): p. 297-307.

34. Bohan, A. and J.L. Boyer, *Mechanisms of hepatic transport of drugs: implications for cholestatic drug reactions.* Semin Liver Dis, 2002. **22**(2): p. 123-36.

35. Russell, D.W., *The enzymes, regulation, and genetics of bile acid synthesis.* Annu Rev Biochem, 2003. **72**: p. 137-74.

36. Schwarz, M., et al., *Disruption of cholesterol 7alpha-hydroxylase gene in mice. II. Bile acid deficiency is overcome by induction of oxysterol 7alpha-hydroxylase.* J Biol Chem, 1996. **271**(30): p. 18024-31.

37. Trauner, M. and J.L. Boyer, *Bile salt transporters: molecular characterization, function, and regulation.* Physiol Rev, 2003. **83**(2): p. 633-71.

38. Alrefai, W.A. and R.K. Gill, *Bile acid transporters: structure, function, regulation and pathophysiological implications.* Pharm Res, 2007. **24**(10): p. 1803-23.

39. Boyer, J.L., et al., *Upregulation of a basolateral FXR-dependent bile acid efflux transporter OSTalpha-OSTbeta in cholestasis in humans and rodents.* Am J Physiol Gastrointest Liver Physiol, 2006. **290**(6): p. G1124-30.

40. Donner, M.G. and D. Keppler, *Up-regulation of basolateral multidrug resistance protein 3 (Mrp3) in cholestatic rat liver.* Hepatology, 2001. **34**(2): p. 351-9.

41. Jonker, J.W., et al., *Hepatobiliary ABC transporters: physiology, regulation and implications for disease.* Front Biosci (Landmark Ed), 2009. **14**: p. 4904-20.

42. Brandon, E.F., et al., *An update on in vitro test methods in human hepatic drug biotransformation research: pros and cons.* Toxicol Appl Pharmacol, 2003. **189**(3): p. 233-46.

43. Nebert, D.W. and D.W. Russell, *Clinical importance of the cytochromes P450.* Lancet, 2002. **360**(9340): p. 1155-62.

44. Anzenbacher, P. and E. Anzenbacherova, *Cytochromes P450 and metabolism of xenobiotics.* Cell Mol Life Sci, 2001. **58**(5-6): p. 737-47.

45. Park, B.K., et al., *The role of metabolic activation in drug-induced hepatotoxicity.* Annu Rev Pharmacol Toxicol, 2005. **45**: p. 177-202.

46. Glatt, H., *Sulfotransferases in the bioactivation of xenobiotics.* Chem Biol Interact, 2000. **129**(1-2): p. 141-70.

47. Pauli-Magnus, C. and P.J. Meier, *Pharmacogenetics of hepatocellular transporters.* Pharmacogenetics, 2003. **13**(4): p. 189-98.

48. Omiecinski, C.J., et al., *Xenobiotic metabolism, disposition, and regulation by receptors: from biochemical phenomenon to predictors of major toxicities.* Toxicol Sci, 2011. **120 Suppl 1**: p. S49-75.

49. H., Z., *Hepatotoxicity: the adverse effects of drugs and other chemicals on liver.* 2nd ed. 1999, Philadelphia, USA: Lipponcott, Williams&Wilkins.

50. Kaplowitz, N., *Drug-induced liver disorders: implications for drug development and regulation.* Drug Saf, 2001. **24**(7): p. 483-90.

51. Ostapowicz, G., et al., *Results of a prospective study of acute liver failure at 17 tertiary care centers in the United States.* Ann Intern Med, 2002. **137**(12): p. 947-54.

52. Soldatow, V.Y., et al., *In vitro models for liver toxicity testing.* Toxicol Res (Camb), 2013. **2**(1): p. 23-39.

53. Russell, W.M.S.a.B., R. l., *The Principles of Humane Experimental Technique*, 1959, Methuen: London.

54. DelRaso, N.J., *In vitro methodologies for enhanced toxicity testing.* Toxicol Lett, 1993. **68**(1-2): p. 91-9.

55. Lake, B.G., et al., *In vitro assays for induction of drug metabolism.* Methods Mol Biol, 2009. **481**: p. 47-58.

56. Swift, B., N.D. Pfeifer, and K.L. Brouwer, *Sandwich-cultured hepatocytes: an in vitro model to evaluate hepatobiliary transporter-based drug interactions and hepatotoxicity.* Drug Metab Rev, 2010. **42**(3): p. 446-71.

57. Guguen-Guillouzo, C. and A. Guillouzo, *General review on in vitro hepatocyte models and their applications.* Methods Mol Biol, 2010. **640**: p. 1-40.

58. Jefferson, D.M., et al., *Posttranscriptional modulation of gene expression in cultured rat hepatocytes.* Mol Cell Biol, 1984. **4**(9): p. 1929-34.

59. Ben-Ze'ev, A., et al., *Cell-cell and cell-matrix interactions differentially regulate the expression of hepatic and cytoskeletal genes in primary cultures of rat hepatocytes.* Proc Natl Acad Sci U S A, 1988. **85**(7): p. 2161-5.

60. Mizuguchi, T., et al., *Alteration of expression of liver-enriched transcription factors in the transition between growth and differentiation of primary cultured rat hepatocytes.* J Cell Physiol, 1998. **174**(3): p. 273-84.

61. Elaut, G., et al., *Molecular mechanisms underlying the dedifferentiation process of isolated hepatocytes and their cultures.* Curr Drug Metab, 2006. **7**(6): p. 629-60.

62. Dunn, J.C., et al., *Hepatocyte function and extracellular matrix geometry: long-term culture in a sandwich configuration.* FASEB J, 1989. **3**(2): p. 174-7.

63. Dunn, J.C., R.G. Tompkins, and M.L. Yarmush, *Long-term in vitro function of adult hepatocytes in a collagen sandwich configuration.* Biotechnol Prog, 1991. **7**(3): p. 237-45.

64. Dunn, J.C., R.G. Tompkins, and M.L. Yarmush, *Hepatocytes in collagen sandwich: evidence for transcriptional and translational regulation.* J Cell Biol, 1992. **116**(4): p. 1043-53.

65. LeCluyse, E.L., K.L. Audus, and J.H. Hochman, *Formation of extensive canalicular networks by rat hepatocytes cultured in collagen-sandwich configuration.* Am J Physiol, 1994. **266**(6 Pt 1): p. C1764-74.

66. Liu, X., et al., *Partial maintenance of taurocholate uptake by adult rat hepatocytes cultured in a collagen sandwich configuration.* Pharm Res, 1998. **15**(10): p. 1533-9.

67. Liu, X., et al., *Biliary excretion in primary rat hepatocytes cultured in a collagen-sandwich configuration.* Am J Physiol, 1999. **277**(1 Pt 1): p. G12-21.

68. Tuschl, G. and S.O. Mueller, *Effects of cell culture conditions on primary rat hepatocytes-cell morphology and differential gene expression.* Toxicology, 2006. **218**(2-3): p. 205-15.

69. Mathijs, K., et al., *Assessing the metabolic competence of sandwich-cultured mouse primary hepatocytes.* Drug Metab Dispos, 2009. **37**(6): p. 1305-11.

70. Guguen-Guillouzo, C., et al., *Maintenance and reversibility of active albumin secretion by adult rat hepatocytes co-cultured with another liver epithelial cell type.* Exp Cell Res, 1983. **143**(1): p. 47-54.

71. Peters, S.J., et al., *Co-culture of primary rat hepatocytes with rat liver epithelial cells enhances interleukin-6-induced acute-phase protein response.* Cell Tissue Res, 2010. **340**(3): p. 451-7.

72. Landry, J., et al., *Spheroidal aggregate culture of rat liver cells: histotypic reorganization, biomatrix deposition, and maintenance of functional activities.* J Cell Biol, 1985. **101**(3): p. 914-23.

73. Dilworth, C., et al., *The use of liver spheroids as an in vitro model for studying induction of the stress response as a marker of chemical toxicity.* Toxicol In Vitro, 2000. **14**(2): p. 169-76.

74. Brophy, C.M., et al., *Rat hepatocyte spheroids formed by rocked technique maintain differentiated hepatocyte gene expression and function.* Hepatology, 2009. **49**(2): p. 578-86.

75. Sakai, Y., S. Yamagami, and K. Nakazawa, *Comparative analysis of gene expression in rat liver tissue and monolayer- and spheroid-cultured hepatocytes.* Cells Tissues Organs, 2010. **191**(4): p. 281-8.

76. Uygun, B.E., et al., *Organ reengineering through development of a transplantable recellularized liver graft using decellularized liver matrix.* Nat Med, 2010. **16**(7): p. 814-20.

77. Kidambi, S., et al., *Oxygen-mediated enhancement of primary hepatocyte metabolism, functional polarization, gene expression, and drug clearance.* Proc Natl Acad Sci U S A, 2009. **106**(37): p. 15714-9.

78. Zellmer, S., et al., *Transcription factors ETF, E2F, and SP-1 are involved in cytokine-independent proliferation of murine hepatocytes.* Hepatology, 2010. **52**(6): p. 2127-36.

79. Rippin, S.J., et al., *Cholestatic expression pattern of sinusoidal and canalicular organic anion transport systems in primary cultured rat hepatocytes.* Hepatology, 2001. **33**(4): p. 776-82.

80. Liu, J.K., C.M. DiPersio, and K.S. Zaret, *Extracellular signals that regulate liver transcription factors during hepatic differentiation in vitro.* Mol Cell Biol, 1991. **11**(2): p. 773-84.

81. Rodriguez-Antona, C., et al., *Cytochrome P450 expression in human hepatocytes and hepatoma cell lines: molecular mechanisms that determine lower expression in cultured cells.* Xenobiotica, 2002. **32**(6): p. 505-20.

82. Boyer, J.L., *Nuclear receptor ligands: rational and effective therapy for chronic cholestatic liver disease?* Gastroenterology, 2005. **129**(2): p. 735-40.

83. Redinger, R.N., *Nuclear receptors in cholesterol catabolism: molecular biology of the enterohepatic circulation of bile salts and its role in cholesterol homeostasis.* J Lab Clin Med, 2003. **142**(1): p. 7-20.

84. Cereghini, S., *Liver-enriched transcription factors and hepatocyte differentiation.* FASEB J, 1996. **10**(2): p. 267-82.

85. Crosson, S.M., G.F. Davies, and W.J. Roesler, *Hepatic expression of CCAAT/enhancer binding protein alpha: hormonal and metabolic regulation in rats.* Diabetologia, 1997. **40**(10): p. 1117-24.

86. Yamada, T., et al., *CCAAT/enhancer-binding protein delta gene expression is mediated by APRF/STAT3.* J Biochem, 1997. **121**(4): p. 731-8.

87. Schrem, H., J. Klempnauer, and J. Borlak, *Liver-enriched transcription factors in liver function and development. Part I: the hepatocyte nuclear factor network and liver-specific gene expression.* Pharmacol Rev, 2002. **54**(1): p. 129-58.

88. Maire, P., J. Wuarin, and U. Schibler, *The role of cis-acting promoter elements in tissue-specific albumin gene expression.* Science, 1989. **244**(4902): p. 343-6.

89. Chen, J., A.D. Cooper, and B. Levy-Wilson, *Hepatocyte nuclear factor 1 binds to and transactivates the human but not the rat CYP7A1 promoter.* Biochem Biophys Res Commun, 1999. **260**(3): p. 829-34.

90. Sladek, F.M., et al., *Liver-enriched transcription factor HNF-4 is a novel member of the steroid hormone receptor superfamily.* Genes Dev, 1990. **4**(12B): p. 2353-65.

91. Li, J., G. Ning, and S.A. Duncan, *Mammalian hepatocyte differentiation requires the transcription factor HNF-4alpha.* Genes Dev, 2000. **14**(4): p. 464-74.

92. Wagner, M., G. Zollner, and M. Trauner, *Nuclear receptors in liver disease.* Hepatology, 2011. **53**(3): p. 1023-34.

93. Mangelsdorf, D.J. and R.M. Evans, *The RXR heterodimers and orphan receptors.* Cell, 1995. **83**(6): p. 841-50.

94. Geier, A., et al., *Principles of hepatic organic anion transporter regulation during cholestasis, inflammation and liver regeneration.* Biochim Biophys Acta, 2007. **1773**(3): p. 283-308.

95. Kast, H.R., et al., *Regulation of multidrug resistance-associated protein 2 (ABCC2) by the nuclear receptors pregnane X receptor, farnesoid X-activated receptor, and constitutive androstane receptor.* J Biol Chem, 2002. **277**(4): p. 2908-15.

96. Gerloff, T., et al., *Functional analysis of the rat bile salt export pump gene promoter.* Eur J Biochem, 2002. **269**(14): p. 3495-503.

97. Denson, L.A., et al., *Interleukin-1beta suppresses retinoid transactivation of two hepatic transporter genes involved in bile formation.* J Biol Chem, 2000. **275**(12): p. 8835-43.

98. Karpen, S.J., *Nuclear receptor regulation of hepatic function.* J Hepatol, 2002. **36**(6): p. 832-50.

99. Paraskevas, S., et al., *Modulation of JNK and p38 stress activated protein kinases in isolated islets of Langerhans: insulin as an autocrine survival signal.* Ann Surg, 2001. **233**(1): p. 124-33.

100. Paine, A.J. and E. Andreakos, *Activation of signalling pathways during hepatocyte isolation: relevance to toxicology in vitro.* Toxicol In Vitro, 2004. **18**(2): p. 187-93.

101. Vinken, M., et al., *Involvement of cell junctions in hepatocyte culture functionality.* Crit Rev Toxicol, 2006. **36**(4): p. 299-318.

102. Jarpe, M.B., et al., *Anti-apoptotic versus pro-apoptotic signal transduction: checkpoints and stop signs along the road to death.* Oncogene, 1998. **17**(11 Reviews): p. 1475-82.

103. Kyriakis, J.M. and J. Avruch, *Mammalian mitogen-activated protein kinase signal transduction pathways activated by stress and inflammation.* Physiol Rev, 2001. **81**(2): p. 807-69.

104. Hambleton, J., et al., *Activation of c-Jun N-terminal kinase in bacterial lipopolysaccharide-stimulated macrophages.* Proc Natl Acad Sci U S A, 1996. **93**(7): p. 2774-8.

105. Pearson, G., et al., *Mitogen-activated protein (MAP) kinase pathways: regulation and physiological functions.* Endocr Rev, 2001. **22**(2): p. 153-83.

106. Kyriakis, J.M. and J. Avruch, *Sounding the alarm: protein kinase cascades activated by stress and inflammation.* J Biol Chem, 1996. **271**(40): p. 24313-6.

107. Bogoyevitch, M.A., et al., *Stimulation of the stress-activated mitogen-activated protein kinase subfamilies in perfused heart. p38/RK mitogen-activated protein kinases and c-Jun N-terminal kinases are activated by ischemia/reperfusion.* Circ Res, 1996. **79**(2): p. 162-73.

108. Xia, Z., et al., *Opposing effects of ERK and JNK-p38 MAP kinases on apoptosis.* Science, 1995. **270**(5240): p. 1326-31.

109. Kyriakis, J.M., et al., *The stress-activated protein kinase subfamily of c-Jun kinases.* Nature, 1994. **369**(6476): p. 156-60.

110. Mizukami, Y., et al., *A novel mechanism of JNK1 activation. Nuclear translocation and activation of JNK1 during ischemia and reperfusion.* J Biol Chem, 1997. **272**(26): p. 16657-62.

111. Stravitz, R.T., et al., *Hepatocellular protein kinase C activation by bile acids: implications for regulation of cholesterol 7 alpha-hydroxylase.* Am J Physiol, 1996. **271**(2 Pt 1): p. G293-303.

112. Chen, Z., et al., *MAP kinases.* Chem Rev, 2001. **101**(8): p. 2449-76.

113. Zarubin, T. and J. Han, *Activation and signaling of the p38 MAP kinase pathway.* Cell Res, 2005. **15**(1): p. 11-8.

114. Lewis, T.S., P.S. Shapiro, and N.G. Ahn, *Signal transduction through MAP kinase cascades.* Adv Cancer Res, 1998. **74**: p. 49-139.

115. Godoy, P., et al., *Extracellular matrix modulates sensitivity of hepatocytes to fibroblastoid dedifferentiation and transforming growth factor beta-induced apoptosis.* Hepatology, 2009. **49**(6): p. 2031-43.

116. Hatzis, P., I. Kyrmizi, and I. Talianidis, *Mitogen-activated protein kinase-mediated disruption of enhancer-promoter communication inhibits hepatocyte nuclear factor 4alpha expression.* Mol Cell Biol, 2006. **26**(19): p. 7017-29.

117. Hayden, M.S. and S. Ghosh, *Signaling to NF-kappaB.* Genes Dev, 2004. **18**(18): p. 2195-224.

118. Gilmore, T.D., *Introduction to NF-kappaB: players, pathways, perspectives.* Oncogene, 2006. **25**(51): p. 6680-4.

119. Rawlings, J.S., K.M. Rosler, and D.A. Harrison, *The JAK/STAT signaling pathway.* J Cell Sci, 2004. **117**(Pt 8): p. 1281-3.

120. Darnell, J.E., Jr., *STATs and gene regulation.* Science, 1997. **277**(5332): p. 1630-5.

121. Shuai, K. and B. Liu, *Regulation of JAK-STAT signalling in the immune system.* Nat Rev Immunol, 2003. **3**(11): p. 900-11.

122. Yuan, T.L. and L.C. Cantley, *PI3K pathway alterations in cancer: variations on a theme.* Oncogene, 2008. **27**(41): p. 5497-510.

123. Martelli, A.M., et al., *The phosphatidylinositol 3-kinase/Akt/mTOR signaling network as a therapeutic target in acute myelogenous leukemia patients.* Oncotarget, 2010. **1**(2): p. 89-103.

124. Yart, A., H. Chap, and P. Raynal, *Phosphoinositide 3-kinases in lysophosphatidic acid signaling: regulation and cross-talk with the Ras/mitogen-activated protein kinase pathway.* Biochim Biophys Acta, 2002. **1582**(1-3): p. 107-11.

125. Newton, A.C., *Protein kinase C: structure, function, and regulation.* J Biol Chem, 1995. **270**(48): p. 28495-8.

126. Webb, B.L., S.J. Hirst, and M.A. Giembycz, *Protein kinase C isoenzymes: a review of their structure, regulation and role in regulating airways smooth muscle tone and mitogenesis.* Br J Pharmacol, 2000. **130**(7): p. 1433-52.

127. Liaskou, E., D.V. Wilson, and Y.H. Oo, *Innate immune cells in liver inflammation.* Mediators Inflamm, 2012. **2012**: p. 949157.

128. Akira, S., S. Uematsu, and O. Takeuchi, *Pathogen recognition and innate immunity.* Cell, 2006. **124**(4): p. 783-801.

129. Srinivasan, G., et al., *Lipocalin 2 deficiency dysregulates iron homeostasis and exacerbates endotoxin-induced sepsis.* J Immunol, 2012. **189**(4): p. 1911-9.

130. Flo, T.H., et al., *Lipocalin 2 mediates an innate immune response to bacterial infection by sequestrating iron.* Nature, 2004. **432**(7019): p. 917-21.

131. Koj, A., *Initiation of acute phase response and synthesis of cytokines.* Biochim Biophys Acta, 1996. **1317**(2): p. 84-94.

132. Crawford, J., *Cellular and molecular biology of the inflamed liver.* Curr Opin Gastroenterol, 1997(13): p. 175-185.

133. Poltorak, A., et al., *Defective LPS signaling in C3H/HeJ and C57BL/10ScCr mice: mutations in Tlr4 gene.* Science, 1998. **282**(5396): p. 2085-8.

134. Luster, M.I., et al., *Endotoxin-induced cytokine gene expression and excretion in the liver.* Hepatology, 1994. **19**(2): p. 480-8.

135. Sewnath, M.E., et al., *Interleukin-1 receptor type I gene-deficient bile duct-ligated mice are partially protected against endotoxin.* Hepatology, 2002. **35**(1): p. 149-58.

136. Ceciliani, F., A. Giordano, and V. Spagnolo, *The systemic reaction during inflammation: the acute-phase proteins.* Protein Pept Lett, 2002. **9**(3): p. 211-23.

137. Poli, V., *The role of C/EBP isoforms in the control of inflammatory and native immunity functions.* J Biol Chem, 1998. **273**(45): p. 29279-82.

138. Alam, T., M.R. An, and J. Papaconstantinou, *Differential expression of three C/EBP isoforms in multiple tissues during the acute phase response.* J Biol Chem, 1992. **267**(8): p. 5021-4.

139. Niehof, M., et al., *Autoregulation enables different pathways to control CCAAT/enhancer binding protein beta (C/EBP beta) transcription.* J Mol Biol, 2001. **309**(4): p. 855-68.

140. Weinstein, S.L., et al., *Bacterial lipopolysaccharide induces tyrosine phosphorylation and activation of mitogen-activated protein kinases in macrophages.* J Biol Chem, 1992. **267**(21): p. 14955-62.

141. Han, J., et al., *Endotoxin induces rapid protein tyrosine phosphorylation in 70Z/3 cells expressing CD14.* J Biol Chem, 1993. **268**(33): p. 25009-14.

142. Weber, L.W., M. Boll, and A. Stampfl, *Hepatotoxicity and mechanism of action of haloalkanes: carbon tetrachloride as a toxicological model.* Crit Rev Toxicol, 2003. **33**(2): p. 105-36.

143. Nieto, N., et al., *Rat hepatic stellate cells contribute to the acute-phase response with increased expression of alpha1(I) and alpha1(IV) collagens, tissue inhibitor of metalloproteinase-1, and matrix-metalloproteinase-2 messenger RNAs.* Hepatology, 2001. **33**(3): p. 597-607.

144. Taniguchi, M., et al., *Molecular process in acute liver injury and regeneration induced by carbon tetrachloride.* Life Sci, 2004. **75**(13): p. 1539-49.

145. Michalopoulos, G.K., *Liver regeneration after partial hepatectomy: critical analysis of mechanistic dilemmas.* Am J Pathol, 2010. **176**(1): p. 2-13.

146. Higgins, G.M.A., R. M., *Experimental pathology of the liver. I. Restoration of the liver of the white rat following partial surgical removal.* Arch Pathol. , 1931(12): p. 186–202.

147. Michalopoulos, G.K. and M.C. DeFrances, *Liver regeneration.* Science, 1997. **276**(5309): p. 60-6.

148. Greenbaum, L.E., et al., *Coexistence of C/EBP alpha, beta, growth-induced proteins and DNA synthesis in hepatocytes during liver regeneration. Implications for maintenance of the differentiated state during liver growth.* J Clin Invest, 1995. **96**(3): p. 1351-65.

149. Mischoulon, D., et al., *Growth-dependent inhibition of CCAAT enhancer-binding protein (C/EBP alpha) gene expression during hepatocyte proliferation in the regenerating liver and in culture.* Mol Cell Biol, 1992. **12**(6): p. 2553-60.

150. Crispe, I.N., *The liver as a lymphoid organ.* Annu Rev Immunol, 2009. **27**: p. 147-63.

151. Tacke, F., T. Luedde, and C. Trautwein, *Inflammatory pathways in liver homeostasis and liver injury.* Clin Rev Allergy Immunol, 2009. **36**(1): p. 4-12.

152. Cavaillon, J.M., *Pro- versus anti-inflammatory cytokines: myth or reality.* Cell Mol Biol (Noisy-le-grand), 2001. **47**(4): p. 695-702.

153. Kuiper, J., E. Casteleyn, and T.J. Van Berkel, *Regulation of liver metabolism by intercellular communication.* Adv Enzyme Regul, 1988. **27**: p. 193-208.

154. Trauner, M., P. Fickert, and R.E. Stauber, *Inflammation-induced cholestasis.* J Gastroenterol Hepatol, 1999. **14**(10): p. 946-59.

155. Hartmann, G., A.K. Cheung, and M. Piquette-Miller, *Inflammatory cytokines, but not bile acids, regulate expression of murine hepatic anion transporters in endotoxemia.* J Pharmacol Exp Ther, 2002. **303**(1): p. 273-81.

156. Whiting, J.F., et al., *Tumor necrosis factor-alpha decreases hepatocyte bile salt uptake and mediates endotoxin-induced cholestasis.* Hepatology, 1995. **22**(4 Pt 1): p. 1273-8.

157. Bolder, U., et al., *Hepatocyte transport of bile acids and organic anions in endotoxemic rats: impaired uptake and secretion.* Gastroenterology, 1997. **112**(1): p. 214-25.

158. Roelofsen, H., et al., *Impaired hepatocanalicular organic anion transport in endotoxemic rats.* Am J Physiol, 1995. **269**(3 Pt 1): p. G427-34.

159. Vos, T.A., et al., *Up-regulation of the multidrug resistance genes, Mrp1 and Mdr1b, and down-regulation of the organic anion transporter, Mrp2, and the bile salt transporter, Spgp, in endotoxemic rat liver.* Hepatology, 1998. **28**(6): p. 1637-44.

160. Zhang, F.X., et al., *Bacterial lipopolysaccharide activates nuclear factor-kappaB through interleukin-1 signaling mediators in cultured human dermal endothelial cells and mononuclear phagocytes.* J Biol Chem, 1999. **274**(12): p. 7611-4.

161. Lee, H.Y., et al., *Stress pathway activation induces phosphorylation of retinoid X receptor.* J Biol Chem, 2000. **275**(41): p. 32193-9.

162. Li, D., et al., *Interleukin-1 beta-mediated suppression of RXR:RAR transactivation of the Ntcp promoter is JNK-dependent.* J Biol Chem, 2002. **277**(35): p. 31416-22.

163. Cherrington, N.J., et al., *Lipopolysaccharide-mediated regulation of hepatic transporter mRNA levels in rats.* Drug Metab Dispos, 2004. **32**(7): p. 734-41.

164. Geier, A., et al., *Effects of proinflammatory cytokines on rat organic anion transporters during toxic liver injury and cholestasis.* Hepatology, 2003. **38**(2): p. 345-54.

165. Elferink, M.G., et al., *LPS-induced downregulation of MRP2 and BSEP in human liver is due to a posttranscriptional process.* Am J Physiol Gastrointest Liver Physiol, 2004. **287**(5): p. G1008-16.

166. Vos, T.A., et al., *Regulation of hepatic transport systems involved in bile secretion during liver regeneration in rats.* Hepatology, 1999. **29**(6): p. 1833-9.

167. Gerloff, T., et al., *Differential expression of basolateral and canalicular organic anion transporters during regeneration of rat liver.* Gastroenterology, 1999. **117**(6): p. 1408-15.

168. Geier, A., et al., *Hepatobiliary organic anion transporters are differentially regulated in acute toxic liver injury induced by carbon tetrachloride.* J Hepatol, 2002. **37**(2): p. 198-205.

169. Bruccoleri, A., et al., *Induction of early-immediate genes by tumor necrosis factor alpha contribute to liver repair following chemical-induced hepatotoxicity.* Hepatology, 1997. **25**(1): p. 133-41.

170. Yamada, Y. and N. Fausto, *Deficient liver regeneration after carbon tetrachloride injury in mice lacking type 1 but not type 2 tumor necrosis factor receptor.* Am J Pathol, 1998. **152**(6): p. 1577-89.

171. Godoy, P., et al., *Recent advances in 2D and 3D in vitro systems using primary hepatocytes, alternative hepatocyte sources and non-parenchymal liver cells and their use in investigating mechanisms of hepatotoxicity, cell signaling and ADME.* Arch Toxicol, 2013. **87**(8): p. 1315-530.

172. Lee, S.M., et al., *Isolation of human hepatocytes by a two-step collagenase perfusion procedure.* J Vis Exp, 2013(79).

173. Smedsrod, B., et al., *Functional and morphological characterization of cultures of Kupffer cells and liver endothelial cells prepared by means of density separation in Percoll, and selective substrate adherence.* Cell Tissue Res, 1985. **241**(3): p. 639-49.

174. Hoehme, S., et al., *Prediction and validation of cell alignment along microvessels as order principle to restore tissue architecture in liver regeneration.* Proc Natl Acad Sci U S A, 2010. **107**(23): p. 10371-6.

175. Madrahimov, N., et al., *Marginal hepatectomy in the rat: from anatomy to surgery.* Ann Surg, 2006. **244**(1): p. 89-98.

176. Dahmen, U., et al., *Small-for-size syndrome in the rat: does size or technique matter?* J Surg Res, 2008. **149**(1): p. 15-26.

177. Livak, K.J. and T.D. Schmittgen, *Analysis of relative gene expression data using real-time quantitative PCR and the 2(-Delta Delta C(T)) Method.* Methods, 2001. **25**(4): p. 402-8.

178. Bolstad, B.M., *Low Level Analysis of High-density OligonucleotideArray Data: Background, Normalization and Summarization*. 2004: Berkeley: University of California.

179. Gentleman, R.C., et al., *Bioconductor: open software development for computational biology and bioinformatics.* Genome Biol, 2004. **5**(10): p. R80.

180. Smyth, G.K., *Limma: linear models for microarray data*, in *Bioinformatics and Computational Biology Solutions using R and Bioconductor*, R.C. Gentleman, et al., Editors. 2005, Springer: New York. p. 397-420.

181. RDC, T., *R:A Language and Environment for Statistical Computing.* . 2011, Vienna, Austria: R Foundation for Statistical Computing.

182. Benjamini, Y. and Y. Hochberg, *Controlling the false discovery rate: a practical and powerful approach to multiple testing.* J. R. Stat. Soc. Ser. B 1995. **57 (1)**: p. 289-300.

183. Dai, M., et al., *Evolving gene/transcript definitions significantly alter the interpretation of GeneChip data.* Nucleic Acids Res, 2005. **33**(20): p. e175.

184. Bezdek, J.C. and R.J. Hathaway, *Numerical convergence and interpretation of the fuzzy c-shells clustering algorithm.* IEEE Trans Neural Netw, 1992. **3**(5): p. 787-93.

185. Elkon, R., et al., *Genome-wide in silico identification of transcriptional regulators controlling the cell cycle in human cells.* Genome Res, 2003. **13**(5): p. 773-80.

186. Ulitsky, I., et al., *Expander: from expression microarrays to networks and functions.* Nat Protoc, 2010. **5**(2): p. 303-22.

187. Kalluri, R., *EMT: when epithelial cells decide to become mesenchymal-like cells.* J Clin Invest, 2009. **119**(6): p. 1417-9.

188. Small, J.V., et al., *The lamellipodium: where motility begins.* Trends Cell Biol, 2002. **12**(3): p. 112-20.

189. Ringner, M., *What is principal component analysis?* Nat Biotechnol, 2008. **26**(3): p. 303-4.

190. Borkham-Kamphorst, E., et al., *Protective effects of lipocalin-2 (LCN2) in acute liver injury suggest a novel function in liver homeostasis.* Biochim Biophys Acta, 2013. **1832**(5): p. 660-73.

191. Shashidharamurthy, R., et al., *Differential role of lipocalin 2 during immune complex-mediated acute and chronic inflammation in mice.* Arthritis Rheum, 2013. **65**(4): p. 1064-73.

192. Inoue, K., et al., *Metallothionein as an anti-inflammatory mediator.* Mediators Inflamm, 2009. **2009**: p. 101659.

193. Inoue, K., et al., *Role of metallothionein in lung inflammation induced by ozone exposure in mice.* Free Radic Biol Med, 2008. **45**(12): p. 1714-22.

194. Arlt, A. and H. Schafer, *Role of the immediate early response 3 (IER3) gene in cellular stress response, inflammation and tumorigenesis.* Eur J Cell Biol, 2011. **90**(6-7): p. 545-52.

195. Huang, J.H. and W.S. Liao, *Induction of the mouse serum amyloid A3 gene by cytokines requires both C/EBP family proteins and a novel constitutive nuclear factor.* Mol Cell Biol, 1994. **14**(7): p. 4475-84.

196. Wu, F. and S. Chakravarti, *Differential expression of inflammatory and fibrogenic genes and their regulation by NF-kappaB inhibition in a mouse model of chronic colitis.* J Immunol, 2007. **179**(10): p. 6988-7000.

197. Jeffrey, K.D., et al., *Carboxypeptidase E mediates palmitate-induced beta-cell ER stress and apoptosis.* Proc Natl Acad Sci U S A, 2008. **105**(24): p. 8452-7.

198. Dohi, T. and L.C. Burkly, *The TWEAK/Fn14 pathway as an aggravating and perpetuating factor in inflammatory diseases: focus on inflammatory bowel diseases.* J Leukoc Biol, 2012. **92**(2): p. 265-79.

199. Ratziu, V., et al., *Zf9, a Kruppel-like transcription factor up-regulated in vivo during early hepatic fibrosis.* Proc Natl Acad Sci U S A, 1998. **95**(16): p. 9500-5.

200. Kojima, S., et al., *Transcriptional activation of urokinase by the Kruppel-like factor Zf9/COPEB activates latent TGF-beta1 in vascular endothelial cells.* Blood, 2000. **95**(4): p. 1309-16.

201. Tsukamoto, H., et al., *Annexin A2 regulates a disintegrin and metalloproteinase 17-mediated ectodomain shedding of pro-tumor necrosis factor-alpha in monocytes and colon epithelial cells.* Inflamm Bowel Dis, 2013. **19**(7): p. 1365-73.

202. Zimmermann, N., et al., *Expression and regulation of small proline-rich protein 2 in allergic inflammation.* Am J Respir Cell Mol Biol, 2005. **32**(5): p. 428-35.

203. Schafer, M., et al., *Nrf2 links epidermal barrier function with antioxidant defense.* EMBO Mol Med, 2012. **4**(5): p. 364-79.

204. Cicha, I. and M. Goppelt-Struebe, *Connective tissue growth factor: context-dependent functions and mechanisms of regulation.* Biofactors, 2009. **35**(2): p. 200-8.

205. Kanehisa, M., et al., *The KEGG resource for deciphering the genome.* Nucleic Acids Res, 2004. **32**(Database issue): p. D277-80.

206. Botella, L.M., et al., *Transcriptional activation of endoglin and transforming growth factor-beta signaling components by cooperative interaction between Sp1 and KLF6: their potential role in the response to vascular injury.* Blood, 2002. **100**(12): p. 4001-10.

207. Hewitt, N.J., et al., *Primary hepatocytes: current understanding of the regulation of metabolic enzymes and transporter proteins, and pharmaceutical practice for the use of hepatocytes in metabolism, enzyme induction, transporter, clearance, and hepatotoxicity studies.* Drug Metab Rev, 2007. **39**(1): p. 159-234.

208. Dooley, S., et al., *Hepatocyte-specific Smad7 expression attenuates TGF-beta-mediated fibrogenesis and protects against liver damage.* Gastroenterology, 2008. **135**(2): p. 642-59.

209. Borkham-Kamphorst, E., F. Drews, and R. Weiskirchen, *Induction of lipocalin-2 expression in acute and chronic experimental liver injury moderated by pro-inflammatory cytokines interleukin-1beta through nuclear factor-kappaB activation.* Liver Int, 2011. **31**(5): p. 656-65.

210. Jaeschke, H., *Reactive oxygen and mechanisms of inflammatory liver injury: Present concepts.* J Gastroenterol Hepatol, 2011. **26 Suppl 1**: p. 173-9.

211. Akira, S. and T. Kishimoto, *NF-IL6 and NF-kappa B in cytokine gene regulation.* Adv Immunol, 1997. **65**: p. 1-46.

212. Ramji, D.P. and P. Foka, *CCAAT/enhancer-binding proteins: structure, function and regulation.* Biochem J, 2002. **365**(Pt 3): p. 561-75.

213. Yang, J., et al., *Lipocalin 2 promotes breast cancer progression.* Proc Natl Acad Sci U S A, 2009. **106**(10): p. 3913-8.

214. Costa, D., et al., *Lipocalin-2 controls the expression of SDF-1 and the number of responsive cells in bone.* Cytokine, 2010. **51**(1): p. 47-52.

215. Martinez-Ferrer, M., et al., *Role of nicotinic and estrogen signaling during experimental acute and chronic bladder inflammation.* Am J Pathol, 2008. **172**(1): p. 59-67.

216. Vinuesa, E., et al., *Lipocalin-2-induced renal regeneration depends on cytokines.* Am J Physiol Renal Physiol, 2008. **295**(5): p. F1554-62.

217. Lai, H.S., et al., *Lipocalin-2 gene expression during liver regeneration after partial hepatectomy in rats.* Int J Surg, 2013. **11**(4): p. 314-8.

218. De Minicis, S., et al., *Gene expression profiles during hepatic stellate cell activation in culture and in vivo.* Gastroenterology, 2007. **132**(5): p. 1937-46.

219. Samson, S.L. and N.C. Wong, *Role of Sp1 in insulin regulation of gene expression.* J Mol Endocrinol, 2002. **29**(3): p. 265-79.

220. Black, A.R., J.D. Black, and J. Azizkhan-Clifford, *Sp1 and kruppel-like factor family of transcription factors in cell growth regulation and cancer.* J Cell Physiol, 2001. **188**(2): p. 143-60.

221. Zheng, X.L., et al., *Epidermal growth factor induction of apolipoprotein A-I is mediated by the Ras-MAP kinase cascade and Sp1.* J Biol Chem, 2001. **276**(17): p. 13822-9.

222. Angel, P. and M. Karin, *The role of Jun, Fos and the AP-1 complex in cell-proliferation and transformation.* Biochim Biophys Acta, 1991. **1072**(2-3): p. 129-57.

223. Behrens, A., et al., *Impaired postnatal hepatocyte proliferation and liver regeneration in mice lacking c-jun in the liver.* EMBO J, 2002. **21**(7): p. 1782-90.

224. Eferl, R. and E.F. Wagner, *AP-1: a double-edged sword in tumorigenesis.* Nat Rev Cancer, 2003. **3**(11): p. 859-68.

225. Leppa, S. and D. Bohmann, *Diverse functions of JNK signaling and c-Jun in stress response and apoptosis.* Oncogene, 1999. **18**(45): p. 6158-62.

226. Brigstock, D.R., *Connective tissue growth factor (CCN2, CTGF) and organ fibrosis: lessons from transgenic animals.* J Cell Commun Signal, 2010. **4**(1): p. 1-4.

227. Chen, P.S., et al., *CTGF enhances the motility of breast cancer cells via an integrin-alphavbeta3-ERK1/2-dependent S100A4-upregulated pathway.* J Cell Sci, 2007. **120**(Pt 12): p. 2053-65.

228. Liu, S.C., et al., *CTGF increases IL-6 expression in human synovial fibroblasts through integrin-dependent signaling pathway.* PLoS One, 2012. **7**(12): p. e51097.

229. Deshmane, S.L., et al., *Monocyte chemoattractant protein-1 (MCP-1): an overview.* J Interferon Cytokine Res, 2009. **29**(6): p. 313-26.

230. Zhang, W., et al., *NAD(P)H oxidase-dependent regulation of CCL2 production during retinal inflammation.* Invest Ophthalmol Vis Sci, 2009. **50**(6): p. 3033-40.

231. Renner, F. and M.L. Schmitz, *Autoregulatory feedback loops terminating the NF-kappaB response.* Trends Biochem Sci, 2009. **34**(3): p. 128-35.

232. Garcia, J., et al., *IEX-1: a new ERK substrate involved in both ERK survival activity and ERK activation.* EMBO J, 2002. **21**(19): p. 5151-63.

233. Schneider, A., U. Klingmuller, and M. Schilling, *Short-term information processing, long-term responses: Insights by mathematical modeling of signal transduction. Early activation dynamics of key signaling mediators can be predictive for cell fate decisions.* Bioessays, 2012. **34**(7): p. 542-50.

234. Marshall, C.J., *Specificity of receptor tyrosine kinase signaling: transient versus sustained extracellular signal-regulated kinase activation.* Cell, 1995. **80**(2): p. 179-85.

235. Mosimann, C., G. Hausmann, and K. Basler, *Beta-catenin hits chromatin: regulation of Wnt target gene activation.* Nat Rev Mol Cell Biol, 2009. **10**(4): p. 276-86.

236. Benhamouche, S., et al., *Apc tumor suppressor gene is the "zonation-keeper" of mouse liver.* Dev Cell, 2006. **10**(6): p. 759-70.

237. Baumann, H. and J. Gauldie, *The acute phase response.* Immunol Today, 1994. **15**(2): p. 74-80.

238. Moshage, H., *Cytokines and the hepatic acute phase response.* J Pathol, 1997. **181**(3): p. 257-66.

239. Boess, F., et al., *Gene expression in two hepatic cell lines, cultured primary hepatocytes, and liver slices compared to the in vivo liver gene expression in rats: possible implications for toxicogenomics use of in vitro systems.* Toxicol Sci, 2003. **73**(2): p. 386-402.

240. Chiang, J.Y., *Bile acid regulation of hepatic physiology: III. Bile acids and nuclear receptors.* Am J Physiol Gastrointest Liver Physiol, 2003. **284**(3): p. G349-56.

241. Crestani, M., Sadeghpour, A., Stroup, D., Galli, G., Chiang, J. Y. L., *Transcriptional activation of the cholesterol 7α-hydroxylase gene (CYP7A) by nuclear hormone receptors.* J. Lipid Res, 1998. **39:** 2192–2200.

242. Gupta, S., et al., *Down-regulation of cholesterol 7alpha-hydroxylase (CYP7A1) gene expression by bile acids in primary rat hepatocytes is mediated by the c-Jun N-terminal kinase pathway.* J Biol Chem, 2001. **276**(19): p. 15816-22.

243. Song, K.H., et al., *Hepatocyte growth factor signaling pathway inhibits cholesterol 7alpha-hydroxylase and bile acid synthesis in human hepatocytes.* Hepatology, 2007. **46**(6): p. 1993-2002.

244. De Fabiani, E., et al., *The negative effects of bile acids and tumor necrosis factor-alpha on the transcription of cholesterol 7alpha-hydroxylase gene (CYP7A1) converge to hepatic nuclear factor-4: a novel mechanism of feedback regulation of bile acid synthesis mediated by nuclear receptors.* J Biol Chem, 2001. **276**(33): p. 30708-16.

245. Zhang, L., et al., *Significance and mechanism of CYP7a1 gene regulation during the acute phase of liver regeneration.* Mol Endocrinol, 2009. **23**(2): p. 137-45.

246. Seok, J., et al., *Genomic responses in mouse models poorly mimic human inflammatory diseases.* Proc Natl Acad Sci U S A, 2013. **110**(9): p. 3507-12.

247. Leist, M. and T. Hartung, *Inflammatory findings on species extrapolations: humans are definitely no 70-kg mice.* Arch Toxicol, 2013. **87**(4): p. 563-7.